

Electronic Thesis and Dissertation Repository

11-26-2019 2:30 PM

Synthesis of Polycarbamate–based Nanoassemblies and Previously Inaccessible Polyglyoxylates

Rebecca Yardley, *The University of Western Ontario*

Supervisor: Gillies, Elizabeth R., *The University of Western Ontario*

A thesis submitted in partial fulfillment of the requirements for the Doctor of Philosophy degree in Chemistry

© Rebecca Yardley 2019

Follow this and additional works at: <https://ir.lib.uwo.ca/etd>

 Part of the [Polymer Chemistry Commons](#)

Recommended Citation

Yardley, Rebecca, "Synthesis of Polycarbamate–based Nanoassemblies and Previously Inaccessible Polyglyoxylates" (2019). *Electronic Thesis and Dissertation Repository*. 6770.
<https://ir.lib.uwo.ca/etd/6770>

This Dissertation/Thesis is brought to you for free and open access by Scholarship@Western. It has been accepted for inclusion in Electronic Thesis and Dissertation Repository by an authorized administrator of Scholarship@Western. For more information, please contact wlsadmin@uwo.ca.

Abstract

Self-immolative polymers (SIPs) are a subclass of degradable polymers that can be triggered to depolymerize when exposed to a specific stimulus. The main advantages of SIPs are the controlled and predictable depolymerization pathway, signal amplification, and tunability of the polymer regarding which stimuli it responds to. The work presented in this thesis details the synthesis, characterization, and applications of two different families of SIPs: polycarbamates (PCBs) and polyglyoxylates (PGs). PCBs are known to have depolymerization rates that are sensitive to environmental conditions surrounding them. In efforts to modify the depolymerization, PCB was incorporated into amphiphilic diblock copolymers, first with multi-stimuli-responsive poly(2-(dimethylamino)ethyl methacrylate) (PDMAEMA). Evaluation of the ultraviolet (UV) light-responsive depolymerization behaviour under different pH and temperature conditions indicated that temperature was determining factor driving faster depolymerization. Secondly, PCB was incorporated into a block copolymer with thermo-responsive poly(*N*-isopropylacrylamide) (PNIPAAm), which responds at lower temperatures than PDMAEMA. However, this system appeared to aggregate irreversibly in solution even at lower temperatures, making it problematic in experiments. PGs are one of the newer classes of SIPs. Previously, many glyoxylate monomers were inaccessible because of problems synthesizing the monomers or achieving large volumes of sufficiently pure monomers for polymerization. Overall, only a few new monomers were successfully polymerized, only yielding lower degrees of polymerization compared to PEtG. To expand the usefulness of this family, previously inaccessible PGs were achieved through a transesterification reaction with PEtG. A family of alkyl PGs and functional PGs were created, with the latter being used in further post-transesterification modification. This work represents significant advancements in the synthesis, and applications of SIPs.

Keywords

Self-immolative polymer, stimuli-responsive, degradation, depolymerization, polyglyoxylate, poly(ethyl-glyoxylate), polycarbamate, poly(dimethylaminoethyl methacrylate), poly(*N*-isopropylacrylamide), lower critical solution temperature, amphiphilic block copolymer, self-assembly, micelle, drug delivery, transesterification, post-polymerization modification.

Summary for a Lay Audience

Self-immolative polymers (SIPs) are a type of degradable polymers that can breakdown into their building blocks when exposed to a small amount of a specific stimuli, that could include pH, light, or heat. When exposed to the specific stimulus, the responsive end-group is cleaved, and the polymer quickly breaks down end-to-end, like beads falling off a string. This thesis investigates two different types of SIPs. The first class of SIP was attached to a water-soluble polymer, to create a polymer with two distinct sections (one water soluble, and one insoluble in water). When the polymer is in water, a ball like structure formed with the insoluble SIP on the inside and the water-soluble portion sticking outside the polymer. The percentage of polymer breakdown was monitored at different temperatures and acidities. The second type of SIP was studied to find new ways of creating subclasses of the polymer. There are two methods of forming new polymers. If we think of a polymer as beads on a string we can either create new coloured beads and then put them on the string (referred to as monomer synthesis), or we can take an already existing beaded string and spray paint it to achieve a new colour (referred to as post-polymerization modification). When monomer synthesis failed, new classes of the SIP were achieved through post-polymerization modification, allowing us to achieve previously inaccessible SIPs.

Co-Authorship Statement

The work described in this thesis contains contributions from the author as well as co-worker Dr. Amir Rabiee Kenaree, and my supervisor Prof. Elizabeth R. Gillies.

Chapter 1 is composed of multiple segments. The first segment (1.1-1.3) contains all sections pertaining to degradable and responsive polymers, as well as the section on block copolymer self-assembly and was written by the author and edited by Prof. Elizabeth Gillies. The second segment (1.4) contains excerpts written by the author as part of a review on self-immolative polymers, with the section 1.4.2.2 being written by Dr. Amir Rabiee Kenaree, and all portions were edited by the author, Dr. Amir Rabiee Kenaree and Prof. Elizabeth Gillies. The third section (1.5-1.6) was written by the author and edited by Prof. Elizabeth Gillies.

Chapter 2 describes the synthesis, characterization, aqueous self-assembly, and depolymerization behaviour of a self-immolative amphiphilic block copolymer. All work was completed by the author. The chapter was written by the author and edited by Prof. Elizabeth Gillies.

Chapter 3 describes the synthesis, characterization, aqueous self-assembly, and depolymerization behaviour of a self-immolative amphiphilic block copolymer. All work was completed by the author. The chapter was written by the author and edited by Prof. Elizabeth Gillies.

Chapter 4 describes the synthesis, characterization and depolymerization of a series of post-polymerization functionalized materials. The initial polymerization of the PEG polymers was performed by Dr. Amir Rabiee Kenaree. The chapter was written by the author and edited by Dr. Amir Rabiee Kenaree and Prof. Elizabeth Gillies.

Chapter 5 was written by the author and edited by Prof. Elizabeth Gillies.

Acknowledgments

I first want to express my never-ending gratitude to my supervisor, Prof. Elizabeth Gillies, for allowing me to join her research group. I have learnt many lessons, both personal and professional, since joining the group almost 5 years ago. Through her guidance, I have become a better chemist, communicator, and mentor.

This degree would not have been possible without the amazingly supportive work environment in the Gillies Group. Throughout my 5 years, I have seen many students come and go, and they have all been an essential part of this journey. Special thanks to Dr. Amir Rabiee Kenaree, who taught me many chemical and writing skills, even before he was an official group member. I also want to thank all the friends I made at Western over the years, including everyone from the various *Backside Attack* sports teams, the Beer O'clock and Alibi crews, and especially all the people who became as close as family (a.k.a. the ones that stopped knocking when they came over.)

The Chemistry Department is made up of fantastic staff were always willing to help along the way. Aneta Borecki, is the real M.V.P. for wearing as many hats as she does (Gillies Group, NMR facility and X-Ray facility), and still be willing to talk. Mat Willans was always working to keep the NMR spectrometers functioning. The office staff was always helpful, especially Darlene, who always answered my questions with a smile. The ChemBio Stores staff, Marylou, Monica, Yuhua and Sherrie were always willing to help me, even on my fifth visit of the day.

A special thanks to my committee members for taking the time to read this thesis and providing meaningful feedback.

I cannot forget to thank my parents, Jim and Karen, who have given me so much over the years. Thank you for always believing in me, likely more than I did most days. Our relationship has changed a lot since I moved out to start this Ph.D. adventure, but I feel closer to both of you than ever. During our almost daily conversations, you always listened, even when you had no idea what I was talking about and somehow knew just what to say. I cannot wait to see how our relationship keeps changing as I enter a new chapter in my life.

Colin, thank you for being the best big brother and role model I could ask for! I promise to fulfill your dream of “Dr. Yardley paging Dr. Yardley” someday soon. Also, thank you for getting me the sister I always wanted in Sarah, and two adorable nieces, Vivian and Lydia.

To the Paquette Clan: thank you for welcoming me into the family as lovingly as you have. Bizz and Claude, thanks for letting me steal your son! Michelle, Peekie, and Renee, my new sisters, thanks for teaching me all the ways to deal with Joe.

Lastly, I want to thank my husband, Joe. You have been with me through all the highs and lows of this journey, and I can never accurately tell you how much your never-ending support has meant to me. You made our home a haven from the frustrations of grad school, filled with pizza, love and tequila. Thanks for believing in me. I love you.

Table of Contents

Abstract.....	i
Summary for a Lay Audience.....	iii
Co-Authorship Statement.....	iv
Acknowledgments.....	v
Table of Contents.....	vii
List of Tables.....	xi
List of Figures.....	xii
List of Schemes.....	xix
List of Appendices.....	xxi
List of Abbreviations.....	xxii
Chapter 1.....	1
1 Introduction.....	1
1.1 Polymers: a (brief) history.....	1
1.2 Non-degradable polymers.....	3
1.2.1 Non-degradable stimuli-responsive polymers.....	3
1.2.2 pH-Responsive polymers.....	4
1.2.3 Thermo-responsive polymers.....	6
1.2.4 Light-responsive polymers.....	8
1.2.5 Gas-responsive polymers.....	10
1.3 Stimuli-responsive Degradable polymers.....	11
1.3.1 Acid-degradable polymers.....	12
1.3.2 Redox-degradable polymers.....	14
1.3.3 Photo-degradable polymers.....	15
1.3.4 Limitations of stimuli-responsive degradable polymers.....	17

1.4 Self-immolative polymers.....	17
1.4.1 Irreversible SIPs.....	19
1.4.2 Reversible SIPs.....	24
1.5 Aqueous self-assembly of block copolymers	44
1.6 Scope of thesis	46
1.7 References.....	47
Chapter 2.....	58
2 Multi-stimuli-responsive self-immolative polymer assemblies.....	58
2.1 Introduction.....	58
2.2 Experimental.....	60
2.2.1 General materials and procedures.....	60
2.2.2 Instrumentation	61
2.2.3 Synthetic procedures.....	62
2.2.4 LCST determination.....	66
2.2.5 Block copolymer self-assembly and characterization.....	66
2.2.6 Assembly degradation and depolymerization studies.....	66
2.3 Results and discussion	67
2.3.1 Polymer design and synthesis.....	67
2.3.2 Synthesis of end-caps.....	68
2.3.3 Synthesis of polymers.....	69
2.3.4 Synthesis of block copolymers	70
2.3.5 LCST measurements for PDMAEMA-N ₃	73
2.3.6 Block copolymer self-assembly	73
2.3.7 Depolymerization studies.....	75
2.4 Conclusion	81
2.5 References.....	82

3	Effects of poly(<i>N</i> -isopropylacrylamide) on the depolymerization behaviour of polycarbamate based block co-polymers	87
3.1	Introduction.....	87
3.2	Experimental.....	89
3.2.1	General materials and procedures.....	89
3.2.2	Instrumentation	89
3.2.3	Synthetic procedures.....	90
3.2.4	Block copolymer self-assembly.....	93
3.2.5	Cloud point determination	94
3.2.6	Nile red loading of particles for fluorescence monitoring of assembly degradation.....	94
3.2.7	Assembly degradation studied by small molecule drug release	95
3.2.8	Nanoparticle depolymerization studied by NMR spectroscopy	97
3.3	Results and discussion	97
3.3.1	Polymers design and synthesis.....	97
3.3.2	Cloud point measurements of PNIPAAm.....	105
3.3.3	Block copolymer self-assembly.....	106
3.3.4	Depolymerization studies.....	109
3.4	Conclusions.....	118
3.5	References.....	119
4	Transesterification of poly(ethyl glyoxylate)s: a simple route towards directly-inaccessible polyglyoxylates.....	122
4.1	Introduction.....	122
4.2	Experimental.....	124
4.2.1	General materials and procedures.....	124
4.2.2	Instrumentation	125
4.2.3	Synthetic procedures.....	126

4.2.4	SEC depolymerization study for PEtG _{carbonate} (general procedure).....	130
4.2.5	¹ H NMR depolymerization studies of PEtG _{UV} (general procedure).....	130
4.2.6	Florescence of pyrene	131
4.3	Results and discussion	131
4.3.1	Optimizing the PEtG design for transesterification reactions.....	131
4.3.2	Transesterification reactions	135
4.3.3	Depolymerization studies.....	139
4.3.4	Synthesis and characterization of PGs with functional groups.....	140
4.4	Conclusions.....	143
4.5	Acknowledgments.....	144
4.6	References.....	144
5	Conclusion and future work.....	149
5.1	Polycarbamates	149
5.1.1	Conclusions.....	149
5.1.2	Future work.....	151
5.2	Polyglyoxylates.....	154
5.2.1	Conclusions.....	154
5.2.2	Future work.....	156
5.3	References.....	158
	Appendices.....	160
	Curriculum vitae	244

List of Tables

Table 2.1: Average micelle diameters and PDI from DLS	74
Table 3.1: Summary of molar mass data for all polymers	105
Table 3.2: Average micelle diameters and PDI values from DLS	107
Table 3.3: Drug loading and encapsulation efficiencies for methotrexate and celecoxib incorporated into nanoassemblies of PCB_{UV}-PNIPAAm and PCB_{CON}-PNIPAAm	112
Table 4.1: SEC characterization data and reaction conversions for PGs.	137

List of Figures

Figure 1.1: Global resin production in metric tonnes from 1950 to 2015. ⁵	2
Figure 1.2: Synthetic polymer classification.....	2
Figure 1.3: Chemical structures of common non-degradable polymers.	3
Figure 1.4: Chemical structures of weak polyacids and polybases, with their associated pKa values, that have pH responsive behaviour.....	5
Figure 1.5: Structures of a) P2VP-QD and b) PAA-QD; c) schematic illustration of the conformation and behaviour of these polymers grafted to graphene-oxide and the associated colours over a pH range of 1-7. (Adapted with permission from reference 8. Copyright American Chemical Society.)	6
Figure 1.6: Phase diagrams from polymer compounds containing a) UCST, b) LCST or both (c) and d).....	7
Figure 1.7: Chemical structures of common thermo-responsive polymers.	8
Figure 1.8: Photographs showing the reversible sol-gel transition of a PDMAEMA- <i>ran</i> -PMMA copolymer. (Reproduced from reference 14 with permission from The Royal Society of Chemistry.)	8
Figure 1.9: Chemical structure of PNIPAM and modified spiropyran containing polymer, and the associated thermo-responsive colour changes visible when irradiated with UV-light. (Reproduced with permission from reference 22. Copyright 2009 American Chemical Society.)	10
Figure 1.10: Schematic representation of PDMAEMA functionalized cellulose nanofibers aerogels and the associated oil/water operations in the presence of an inert environment or CO ₂ . (Reproduced with permission from reference 29. Copyright 2019 American Chemical Society.)	11

Figure 1.11: a) Synthesis of a estradiol-polyketal conjugate and the release of estradiol from various microparticle assemblies at pH 7.4 (unless otherwise indicated). (Reproduced with permission from reference 37. Copyright 2016 American Chemical Society.).....	14
Figure 1.12: Chemical structure of a reduction-sensitive L-cysteine based polymer and the mechanism for its incorporation into nanoparticles and subsequent depolymerization on contact with a reducing agent. (Reproduced with permission from reference 43. Copyright 2015 Wiley-VCH Verlag GmbH & Co. KGaA, Weinheim.).....	15
Figure 1.13: Schematic showing the photo-degradable behaviour of <i>o</i> -nitrobenzyl modified PLA and PLGA. (Reproduced with permission from reference 46. Copyright 2015 American Chemical Society.).....	17
Figure 1.14: Depolymerization can be triggered by (a) end-cap cleavage; (b) backbone cleavage of a linear polymer; (c) backbone cleavage of a cyclic polymer. After the initial cleavage, the arrows represent a cascade of sequential reactions leading to depolymerization.	18
Figure 1.15: After end-cap or backbone cleavage, SIPs can (a) irreversibly depolymerize to molecules different from the original polymerization monomers or (b) reversibly depolymerize back to monomers.	19
Figure 1.16: Separation of solid PBE (U) from solid polyethylene (P) and polypropylene (S) by selective depolymerization induced by DBU. (Adapted from reference 73 with permission from The Royal Society of Chemistry.	26
Figure 1.17: Block and random cyclic copolymers of <i>o</i> -PA can be prepared by a reversible opening and closing of the cyclic PPA backbone. (Reproduced from reference 87. Copyright 2013, American Chemical Society.).....	30
Figure 1.18: Acid release and destruction of PPA-based transistor arrays due to (a) the activity of a photoacid generator after irradiation with UV light and (b) melting an acid microdroplet-containing wax within the PPA. Adapted with permission from reference 95 (a) and reference 96 (b). Copyright 2014, John Wiley and Sons.....	32

Figure 1.19: Composites composed of carbon fiber and PPA (left) can be fully disintegrated to the starting carbon fiber (right, bottom) and <i>o</i> -PA (right, top) before the reproduction of the composite. Adapted with permission from reference 102. Copyright 2019, American Chemical Society.....	33
Figure 1.20: Scanning electron micrograph of a nanoscale pattern prepared by t-SPL of a PPA film followed by transfer to a silicon substrate by RIE. Adapted with permission from reference 114. Copyright 2010, John Wiley and Sons.	35
Figure 1.21: Visual ion sensors based on PPAb (red triangles, blue circles, and yellow grids are Pd(0), fluoride ion, and non-responsive PPAs respectively. Adapted with permission from reference 109. Copyright 2015, John Wiley and Sons.....	36
Figure 1.22: TEM images of assemblies formed from thermo-responsive PEG-PEtG-PEG triblock copolymers (a) micelles; (b) vesicles; (c) IONP-loaded micelles. Adapted from reference 125 with permission from The Royal Society of Chemistry.	40
Figure 1.23: Influence of the interfacial curvature on the available morphologies of amphiphilic block copolymers, and representative morphologies.....	45
Figure 2.1: a) Schematic of PCB block breakdown and b) Initially proposed behaviour of PCB-PDMAEMA block copolymer assemblies.....	60
Figure 2.2 Chemical structure of target polymers PCB_{UV}-PDMAEMA and PCB_{CON}-PDMAEMA	68
Figure 2.3: Characterization of PCB_{UV}-PDMAEMA : a) ¹ H NMR spectroscopy (600 MHz, CDCl ₃); b) DMF SEC traces (refractive index detection); c) IR Spectra.	72
Figure 2.4: Transmittance of a 10 mg/mL solution/suspension of PDMAEMA-N₃ or PCB_{UV}-PDMAEMA versus temperature in 100 mM pH 7.0 or 8.0 phosphate buffer.....	73
Figure 2.5: TEM images of assemblies formed from a) PCB_{UV}-PDMAEMA via DMF into water; b) PCB_{UV}-PDMAEMA via water into DMF; c) PCB_{CON}-PDMAEMA via DMF into water; d) PCB_{CON}-PDMAEMA via water into DMF.....	75

Figure 2.6: Change in the fluorescence of Nile red encapsulated in PCB_{UV}-PDMAEMA or PCB_{CON}-PDMAEMA assemblies following irradiation with UV light at a) pH 7.0 and b) pH 8.0 (100 μ M phosphate buffer).	77
Figure 2.7: Change in DLS count rate for PCB_{UV}-PDMAEMA or PCB_{CON}-PDMAEMA assemblies following irradiation with UV light at a) pH 7.0 and b) pH 8.0 (100 μ M phosphate buffer).	79
Figure 2.8: Percent depolymerization measured by ¹ H NMR spectroscopy for the PCB blocks of PCB_{UV}-PDMAEMA and PCB_{CON}-PDMAEMA after irradiation and incubation in 100 mM, pH 8.0 phosphate buffered D ₂ O at either 20 or 65 °C.....	80
Figure 2.9: Out of the three stimuli investigated (pH, UV and temperature) the elevated temperature dominated the depolymerization behaviour, masking any other environmental factors.....	82
Figure 3.1: Initially proposed behaviour of PCB-PNIPAAm block copolymer assemblies..	88
Figure 3.2: Chemical structures of target polymers PCB_{UV}-PNIPAAm , PCB_{CON}-PNIPAAm , PCB_{UV}-PEG , and PCB_{CON}-PEG	98
Figure 3.3: Chemical structures of UV-responsive end-cap 3.1 and control end-cap 3.2	98
Figure 3.4: Schematics of the CuAAC reactions for the coupling of PNIPAAm-N₃ with propargyl alcohol and their corresponding IR spectra showing complete loss of peaks corresponding to the azide stretches at 2100 cm ⁻¹ : a) CuSO ₄ /sodium ascorbate conditions and b) CuBr/PMDETA conditions.	101
Figure 3.5: Characterization of PCB_{UV}-PNIPAAm : a) ¹ H NMR spectra (600 MHz, CDCl ₃); b) IR spectra; c) DMF SEC traces (refractive index detection. The ¹ H NMR spectrum of PCB_{UV}-PNIPAAm has peaks from both blocks after purification and the SEC trace of PCB_{UV}-PNIPAAm has a decreased retention time, indicating an increase in molar mass and no peaks corresponding to the original homopolymers were observed. The azide stretch at 2100 cm ⁻¹ is absent post CuAAC, indicating no free PNIPAAm-N₃ is present.	103

Figure 3.6: Characterization of **PCB_{CON}-PNIPAAm**: a) ¹H NMR spectra (600 MHz, CDCl₃); b) IR spectra; c) DMF SEC traces (refractive index detection. The ¹H NMR spectrum of **PCB_{CON}-PNIPAAm** has peaks from both blocks after purification and the SEC trace of **PCB_{CON}-PNIPAAm** has a decreased retention time, indicating an increase in molar mass and no peaks corresponding to the original homopolymers were observed. The azide stretch at 2100 cm⁻¹ is absent post CuAAC, indicating no free **PNIPAAm-N₃** is present. 104

Figure 3.7: Transmission of **PNIPAAm-N₃** solutions as a function of temperature in a) ultrapure deionized water, b) 100 mM pH 7.4 sodium phosphate buffer and c) 500 mM, pH 7.4 sodium phosphate buffer..... 106

Figure 3.8: TEM images of a) **PCB_{UV}-PNIPAAm** nanoassemblies and b) **PCB_{CON}-PNIPAAm** nanoassemblies. Both assemblies were formed by dropping the DMF/polymer mixture into ultrapure water. Each scale bar represents 50 nm. 108

Figure 3.9: Transmission of a 0.8 mg/ml suspension of **PCB_{UV}-PNIPAAm**, **PCB_{CON}-PNIPAAm**, **PCB_{UV}-PEG**, and **PCB_{CON}-PEG** versus temperature in a 100 mM sodium phosphate buffer at pH 7.4. **PCB_{UV}-PEG**, and **PCB_{CON}-PEG** show high transmission over the entire temperature window whereas **PCB_{UV}-PNIPAAm** and **PCB_{CON}-PNIPAAm** show cloud points..... 109

Figure 3.10: Relative fluorescence versus emission wavelength for Nile red dissolved in pH 7.4, 100 mM sodium phosphate buffer, Nile red with **PCB_{UV}-PNIPAAm** in pH 7.4, 100 mM sodium phosphate buffer and Nile red with **PCB_{UV}-PDMAEMA** (from Chapter 2). Samples were excited at 540 nm. The Nile red concentration was 2 wt% of the polymer and the polymer concentration was 0.8 mg/mL..... 110

Figure 3.11: Absorbance versus wavelength for pure **PCB_{UV}-PNIPAAm** and **PCB_{CON}-PNIPAAm** and their drug loaded versions for a) methotrexate (16 µg/mL) and b) celecoxib (8 µg/mL) in methanol. Polymer assemblies were prepared in buffer as previously described to yield 2 mL of assemblies and then dried and dissolved in 2 mL of methanol. Drug content was determined by comparing to drug calibration curves in methanol (**Figure A3.11** for methotrexate and **Figure A3.12** for celecoxib). 112

Figure 3.12: Percent methotrexate release from **PCB_{UV}-PNIPAAm** and **PCB_{CON}-PNIPAAm** nanoassemblies incubated at 25 °C or 45 °C over 96 hours..... 114

Figure 3.13: a) Depolymerization scheme for the PCB blocks of **PCB_{UV}-PNIPAAm**; b) **PCB_{UV}-PNIPAAm** (left) and **PCB_{CON}-PNIPAAm** (right) ¹H NMR spectroscopy samples incubated at 25 °C after 1 week showing signs of aggregation as the sample precipitated out, coating the NMR tubes; ¹H NMR spectra at different time points for **PCB_{UV}-PNIPAAm** after irradiation and incubation in 100 mM, pH 7.4 sodium phosphate buffered D₂O at c) 25 °C or d) 45 °C showing a small degree of polymer degradation as indicated by peaks d and e corresponding to the cyclic urea degradation product. 116

Figure 3.14: a) Methotrexate loaded **PCB_{UV}-PNIPAAm** nanoassemblies incubated at 25 °C after 2 weeks showing signs of aggregation as the sample had precipitated out (red circle) and b) DLS trace of **PCB_{UV}-PNIPAAm** nanoassemblies immediately after preparation and DLS of the same sample after three days at room temperature, showing an increase in particle size and PDI, suggesting particle aggregation. 117

Figure 4.1: SEC traces recorded during the stability tests of (a) **PEtG_{carbonate}**, (b) **PEtG_{ether}**, and (c) **PEtG_{UV}**. Black, red, blue, green, and brown colors were used for depicting traces recorded at 0, 1, 3, 6, and 24 h, respectively..... 133

Figure 4.2: (a) SEC, (b) TGA, and (c) UV-degradation study results for **PnPrG**, **PiPrG**, **PnBuG**, **PPenG**, **PHexG**, **POctG**, and **PBnG**, results for UV-light exposed and kept in dark samples are depicted using solid and broken lines, respectively. Note: depolymerization% were calculated relative to the depolymerization amount observed for the parent **PEtG_{UV}** in 24 h, **PnPrG**, **PiPrG**, **PnBuG**, **PPenG**, and **PBnG** were studied in a 9/1 mixture of CD₃CN/D₂O and **PHexG** and **POctG** were studied in a 9/1 mixture of acetone-*d*₆/D₂O..... 138

Figure 4.3: (a) Alkyne region of the FTIR spectra recorded for **PPG** and **PPG_{pyr}** showing the loss of a **H-C=C** stretch after CuAAC reaction (b) SEC traces for **PPG** and **PPG_{pyr}**, (c) emission spectra of **PPG_{pyr}** before/after UV-light exposure recorded in MeCN/H₂O: 9/1 (irradiation at 341 nm), and (d) **PPG_{pyr}** sample used for emission spectroscopy..... 143

Figure 5.1: Graphical summary of Chapter 2. Out of the three stimuli investigated (pH, UV, and temperature) the elevated temperature dominated the depolymerization behaviour, masking any other environmental factors.	150
Figure 5.2: Schematic representation of the inter-micellar and intra-micellar crosslinking for a) AB diblock copolymer and (b) ABC triblock copolymer micelles at high copolymer concentrations. Reproduced with permission from reference 5. Copyright 2007 the Royal Society of Chemistry.....	152
Figure 5.3: Schematic of the self-assembly of ABC triblock copolymer PEG-PMAA-PCB_{UV} and subsequent crosslinking by EDC coupling with 2,2-(ethylenedioxy)bis(ethylamine) to yield SCMPs.	154
Figure 5.4: Graphical summary of Chapter 4. The transesterification reaction of PEtG with TBD has lead to the development of previously inaccessible PGs.....	156
Figure 5.5: Possible reactions that could be performed on the available functional handles including CuAAC and Sonogashira cross-couplings on the propargyl, thiolene click chemistry on the allyl, and cycloaddition reactions to the furan.	157
Figure 5.6: a) synthetic strategy for making water-soluble, crosslinkable PGs and b) schematic representing their use as fast-gelling injectable-hydrogels at pH 7.4.	158

List of Schemes

- Scheme 1.1:** Representative molecules found in light-responsive polymers: 1) azobenzene undergoing a *cis-trans* isomerization and b) hydrophobic spiropyran converting to hydrophilic merocyanine. 9
- Scheme 1.2:** Chemical structures and hydrolysis products of generic a) acetal/ketals, b) imines, and c) hydrazones. 13
- Scheme 1.3:** Chemical structures of light sensitive moieties and their irreversible decomposition: a) *o*-nitrobenzyl, b) coumarin, and c) 2-diazo-1,2-naphthoquinones. 16
- Scheme 1.4:** Synthesis and depolymerization PBCs having different pendant groups and end-caps. 20
- Scheme 1.5:** (a) Synthesis and depolymerization of a polycarbamate based on 4-hydroxybenzyl alcohol and DMED (**PBC-L**); (b) Chemical structures of related analogues containing 2-methylaminoethanol (**PBC-L2**) or mercaptoethanol (**PC-L**) spacers. 22
- Scheme 1.6:** Synthesis and depolymerization of PBEs with different pendant groups and end-caps. 25
- Scheme 1.7:** $\text{BF}_3 \cdot \text{OEt}_2$ catalyzed polymerization of *o*-PA and its derivatives to give PPAs. Cleavage of the backbone leads to depolymerization to the corresponding monomers. 29
- Scheme 1.8:** Anionic polymerization of PAs using phosphazene and various responsive end-caps. 34
- Scheme 1.9:** (a) Synthesis of PEtGs with different end-caps, its depolymerization back to monomer, and eventual monomer hydration and hydrolysis to afford GAH; (b) Synthesis of different glyoxylates from their fumaric or maleic acid esters. 37
- Scheme 1.10:** Synthesis of PGAMs with different pendant groups starting from PEtG with a MMT end-cap. 43

Scheme 2.1: Synthesis of linker end-caps: a) UV-responsive end-cap 2.2 and b) control end-cap 2.4	69
Scheme 2.2: Polymerization of PCB_{UV} and PCB_{CON}	69
Scheme 2.3: Synthesis of PDMAEMA-N₃ using an azide-functionalized ATRP initiator...	70
Scheme 2.4: Synthesis of PCB_{UV}-PDMAEMA and PCB_{CON}-PDMAEMA diblock copolymers using CuAAC.....	71
Scheme 3.1: Polymerization of PCB_{UV} and PCB_{CON}	99
Scheme 3.2: a) Synthesis of PEG-N₃ and b) polymerization of PNIPAAm-N₃ using an azide functionalized ATRP initiator.....	100
Scheme 3.3: Synthesis of PCB_{UV}-PNIPAAm , PCB_{CON}-PNIPAAm , PCB_{UV}-PEG , and PCB_{CON}-PEG using CuAAC.	102
Scheme 4.1: (a) Preparation of PEtG_{carbonate} using benzyl chloroformate (b) possible pathways for the reaction of alcohols with PEtG_{carbonate} , (c) preparation of PEtG_{ether} and (d) testing the stability of PEtG_{ether} under the transesterification reaction conditions.....	132
Scheme 4.2: (a) Preparation of PEtG_{UV} and (b) transesterification of PEtG_{ether} using different alcohols.	135
Scheme 4.3: UV-light depolymerization of PEtG_{UV}	140
Scheme 4.4: Click reaction of PPG with Pyr-N₃	141
Scheme 5.1: a) Synthesis of PEG macroinitiator for ATRP; b) synthesis of diblock copolymer PEG-PMAA-Br via ATRP and the subsequent conversion of the bromine end-group to an azide, PEG-PMAA-N₃ ; and c) the synthesis of ABC triblock copolymer PEG-PMAA-PCB_{UV} by CuAAC.	153

List of Appendices

Appendix 1 – Permission to reuse copyrighted material	160
Appendix 2 – Supporting information for Chapter 2.....	178
Appendix 3 – Supporting Information for Chapter 3.....	192
Appendix 4 – Supporting information for Chapter 4.....	201

List of Abbreviations

(TMS) ₂ NLi	bis(trimethylsilyl)amide
Δ	change
°C	degrees Celsius
μL	microliter
¹³ C	carbon-thirteen
¹ H	proton
4H2B	4-hydroxy-2-butanone
A	absorbance
a.u.	arbitrary units
AB	aryl boronic ester
Ac	acetate
AC	allyl carbonate
AcOH	acetic acid
AE	allyl ether
ATR	attenuated total reflectance
ATRP	atom transfer radical polymerization
<i>b</i>	block copolymer
BCE	before the common era
BEHP	bis(2-ethylhexyl) phthalate
Bn	benzyl
BOC	<i>tert</i> -butyloxycarbonyl
BOMCl	chloromethyl benzyl ether
br	broad
Bu	butyl
<i>ca.</i>	approximately
CAC	critical aggregation concentration

CCPM	core-crosslinked polymeric micelles
CE	common era
cm	centimeter
cm ⁻¹	wavenumber
<i>co</i>	copolymer
CON	control
cPPA	cyclic polyphthalaldehyde
CuAAC	copper(I)-catalyzed azide-alkyne cycloaddition reaction
d	doublet
<i>D</i>	dispersity
DBU	1,8-diazabicyclo[5.4.0]undec-7-ene
dd	doublet of doublets
DI	deionized water
DLS	dynamic light scattering
DMAEMA	2-dimethylaminoethyl methacrylate
DMAP	4-(dimethylamine)pyridine
DMED	<i>N,N'</i> -dimethylethylenediamine
DMF	dimethylformamide
DMSO	dimethylsulfoxide
DMT	dimethoxytrityl
DOX	doxorubicin
DP _n	degree of polymerization
DS	disulfide
DSC	differential scanning calorimetry
DTT	dithiothreitol
EDC	1-ethyl-3-(3-dimethylaminopropyl)carbodiimide
EI	electron-impact ionization
Et	ethyl
Et ₂ O	diethyl ether

EtG	ethyl glyoxylate
EtOAc	ethyl acetate
EtOH	ethanol
Fmoc	fluorenylmethyloxycarbonyl
FTIR	Fourier transform infrared spectroscopy
FW	formula weight
g	grams
G	Gibb's free energy
GAH	glycolic acid hydrate
GPa	gigapascal
h	hours
H	enthalpy
HMTETA	1,1,4,7,10,10-hexamethyltriethylenetetraamine
Hz	Hertz
<i>i</i>	iso
IONP	iron oxide nanoparticle
IR	infrared
<i>J</i>	NMR coupling constant
kg	kilograms
LCST	lower critical solution temperature
m	multiplet
Me	methyl
MeOH	methanol
MFH	magnetic field hyperthermia
mg	milligram
min	minute
mL	milliliter
mM	millimolar
mm	millimeter

mmol	millimole
MMT	monomethoxytrityl
M_n	number average molecular weight
mol	moles
mol%	mole percent
MPa	megapascal
MS	mass spectrometry
Mt	megatonnes
M_w	weight average molecular weight
MW	molecular weight
MWCO	molecular weight cutoff
n	open-chain
NB	2-nitrobenzyl
NEt ₃	triethylamine
NIPAm	<i>N</i> -isopropylacrylamide
nm	nanometers
NMR	nuclear magnetic resonance
NVOC	6-nitroveratryl carbonate
<i>o</i>	ortho
<i>o</i> -PA	<i>ortho</i> -phthalaldehyde
P _{2-<i>t</i>} -Bu	1- <i>tert</i> -butyl-2,2,4,4,4-pentakis(dimethylamino)-2λ ⁵ ,4λ ⁵ -catenadi(phosphazene)
P2VP	poly(2-vinylpyridine)
P3M	perylene-3-ylmethyl
PAA	poly(acrylic acid)
PAG	photoacid generator
PBC	poly(benzyl carbamate)
PBE	Poly(benzyl ether)
PC	polycarbonate
PCB	polycarbamate

PDI	polydispersity index
PDMAEMA	poly(2-dimethylaminoethyl methacrylate)
PDMA-SS	Poly(<i>N,N</i> ,-dimethylacrylamide)-functionalized disulfide
PE	polyethylene
PEG	poly(ethylene glycol)
PEGMA	poly(ethylene glycol methacrylate)
PEtG	poly(ethyl glyoxylate)
PG	polyglyoxylate
PGAm	polyglyoxylamide
PLA	poly(lactic acid)
PLGA	poly(lactic- <i>co</i> -glycolic acid)
PMDETA	<i>N,N,N',N'',N''</i> -pentamethyldiethylenetriamine
PMeG	poly(methyl glyoxylate)
PMMA	poly(methyl methacrylate)
PNIPAAm	poly(<i>N</i> -isopropylacrylamide)
PP	polypropylene
PPA	polyphthalaldehyde
ppm	parts per million
Pr	propyl
PS	polystyrene
PSSA	poly(4-styrenesulfonic acid)
PTFE	polytetrafluoroethylene
PTI	Photon Technology International
PVC	poly(vinyl chloride)
QD	quantum dot
r.t.	room temperature
<i>ran</i>	random copolymer
RI	refractive index
RPM	rotations per minute

s	singlet
S	entropy
SCPM	shell-crosslinked polymeric micelles
SEC	size exclusion chromatography
SIP	self-immolative polymer
<i>t</i>	tertiary
TBD	1,5,7-triazabicyclo[4.4.0]dec-5-ene
TBS	<i>tert</i> -butyldimethylsilane
T _c	ceiling temperature
T _c (bulk)	ceiling temperature for undiluted monomer
T _c (<i>c</i> ^o)	ceiling temperature for an initial monomer concentration of 1 M
TEM	transmission electron microscopy
TFA	trifluoroacetic acid
T _g	glass transition temperature
TGA	thermal gravimetric analysis
THF	tetrahydrofuran
TMS	tetramethylsilane
T _o	onset degradation temperature
Trit	trityl
UCST	upper critical solution temperature
UV	ultraviolet
UV-vis	ultraviolet-visible
v/v	volume-to-volume ratio
wt%	weight percent
δ	chemical shift
ε	molar absorptivity
λ	wavelength

Chapter 1

1 Introduction

Portions of the introduction have been adapted from:

R. E. Yardley, A. Rabiee Kenaree, E. R. Gillies. Triggering Depolymerization: Progress and Opportunities for Self-Immolative Polymers. *Macromolecules*, **2019**, ASAP.

1.1 Polymers: a (brief) history

Humanity has been using polymeric materials for centuries, with known records of ancient Mesoamerican cultures processing natural rubber to create balls and statues as far back as 1600 BCE.¹ Flash forward to 1869 CE when John Wesley Hyatt created the first industrially produced polymer, celluloid, as a substitute for ivory.² Celluloid is modified cellulose and was widely praised for saving the dwindling elephant and tortoise populations. This was the beginning of the polymer revolution, as humanity was no longer constrained by the scarcity of natural resources.

But what defines a polymer?

The word *polymer* means “of many parts,” and the modern definition of a polymer is a macromolecule made up of many repeating units called monomers. As these long strings of connected repeating units increase in molecular weight, their physical, chemical, and optical properties will change relative to the properties of the starting monomer. The change in properties is caused by chain entanglement, which occurs after a critical molecular mass is achieved. Many of the original synthetic polymers were strong, lightweight, and flexible, which is why synthetic polymers are often referred to as *plastic* which means “pliable and easily shaped.”

Since the first fully synthetic polymer, Bakelite, was created in 1907 by Leo Baekaland, there have been numerous advances in the field of polymer chemistry.³ World War II led to many developments, including nylon,⁴ as natural resources were incapable to keep up

with the demands of war. Plastic production has continued to increase on an almost exponential scale since the ending of the war, with over 350 million tonnes of plastic resin being produced in 2015 (**Figure 1.1**).⁵ With the sheer amount of plastic being produced every year, there has been a constant effort to create new polymers.

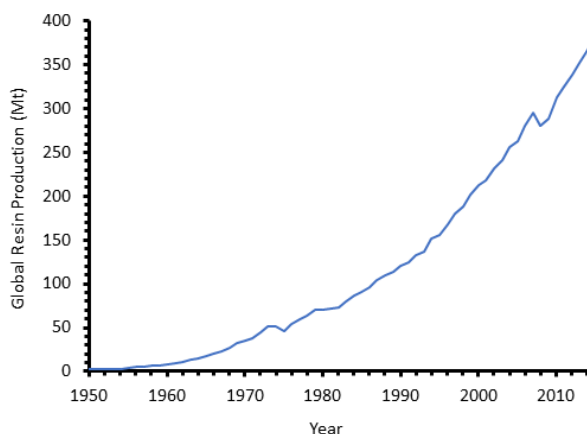


Figure 1.1: Global resin production in metric tonnes from 1950 to 2015.⁵

There are many ways to classify polymers depending on which characteristics are being evaluated. For the purpose of this thesis, polymers will be broadly classified into degradable and non-degradable polymers (**Figure 1.2**).

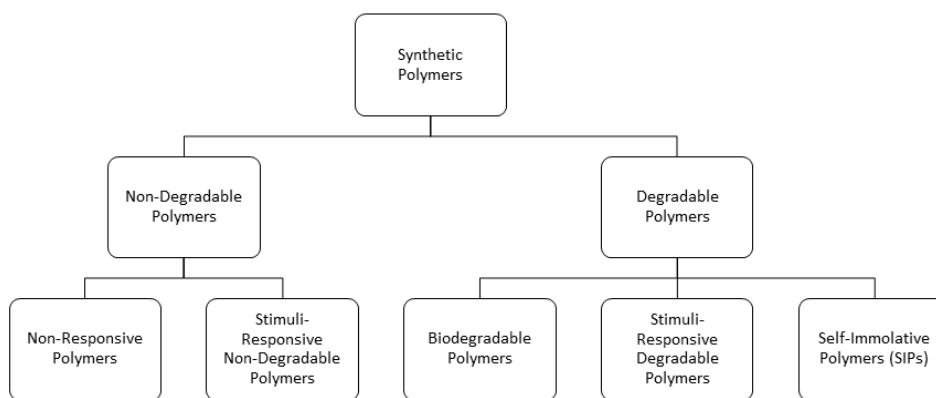


Figure 1.2: Synthetic polymer classification.

1.2 Non-degradable polymers

No polymer is non-degradable given enough time or exposure to environmental conditions. Non-degradable polymers can be loosely defined as polymers that will not completely breakdown until well after their commercial lifespan under common environmental conditions. For example, consumers rely on plastic beverage packaging to retain its structure and impermeability under a wide range of conditions and polyethylene used in joint replacements should resist degradation in the human body over a period of decades. These polymers often have backbones composed entirely of strong carbon-carbon bonds that withstand many chemical, biological, mechanical, thermal, and photochemical conditions. Some commonly used non-degradable polymers include polyethylene (PE), polypropylene (PP), polystyrene (PS), poly(vinyl chloride) (PVC), and polytetrafluoroethylene (PTFE) (**Figure 1.3**). These polymers are relatively inert, and do not respond to outside stimuli.

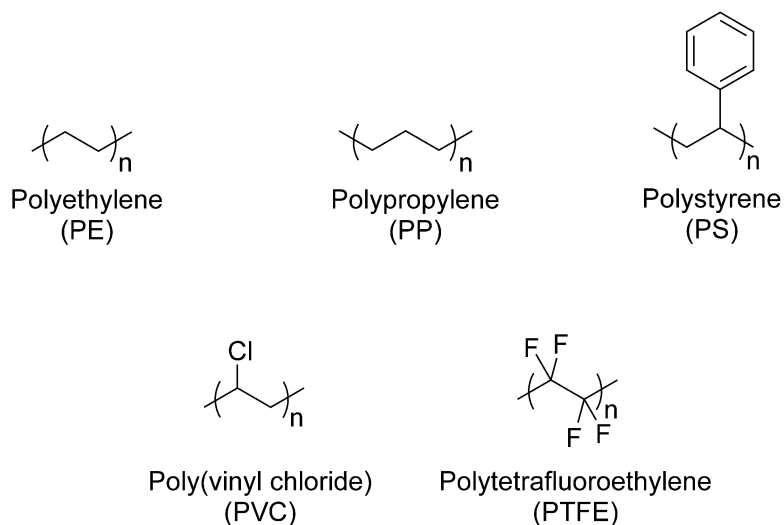


Figure 1.3: Chemical structures of common non-degradable polymers.

1.2.1 Non-degradable stimuli-responsive polymers

Non-degradable stimuli-responsive polymers are polymers that can detect and respond to external stimuli by changes in the physical properties such as shape, solubility, and colour.⁶

These changes in physical properties can be triggered by a variety of stimuli, including changes in pH, heat, light, and specific chemicals or gases. Depending on the specific application and environment of use, each stimulus has inherent advantages and disadvantages. For example, light and heat are great stimuli for closed systems, as they can be applied externally.

1.2.2 pH-Responsive polymers

By changing the pH of an aqueous system, pH-responsive polymers can be triggered to undergo reversible physical changes relating to their solubility, volume, configuration, and conformation.⁷ Polymers that are pH-responsive contain either acidic or basic functional groups, such as organic acids, pyridines, and amines on the polymeric side chains. Weak polyacids and polybases are protonated at low pH and deprotonated at neutral or high pH.⁷ Whether a polymeric side chain is in its protonated or deprotonated state will affect the charge and consequently the solubility of the polymer in aqueous media. The solubility is affected by altering the ionic interactions, hydrogen bonding, or hydrophobic interactions. Some examples of pH-responsive polymers include poly(acrylic acid) (PAA), poly(4-styrenesulfonic acid) (PSSA), poly(2-vinylpyridine) (P2VP), and poly(2-*N,N'*-dimethylaminoethyl methacrylate) (PDMAEMA) (**Figure 1.4**). pH-Responsive polymers have been used as pH sensors,⁸ as switches for adhesive to antifouling surfaces,⁹ as ionic purification/separation materials,¹⁰ and in various supramolecular assemblies, including drug and gene delivery systems.¹¹⁻¹² The design of polymers responsive to changes in pH represents an important advancement for drug delivery, as several areas in the body, including the gastrointestinal tract, mucus membranes, and tumors are mildly acidic (*i.e.* pH 5.8–7.4).¹¹

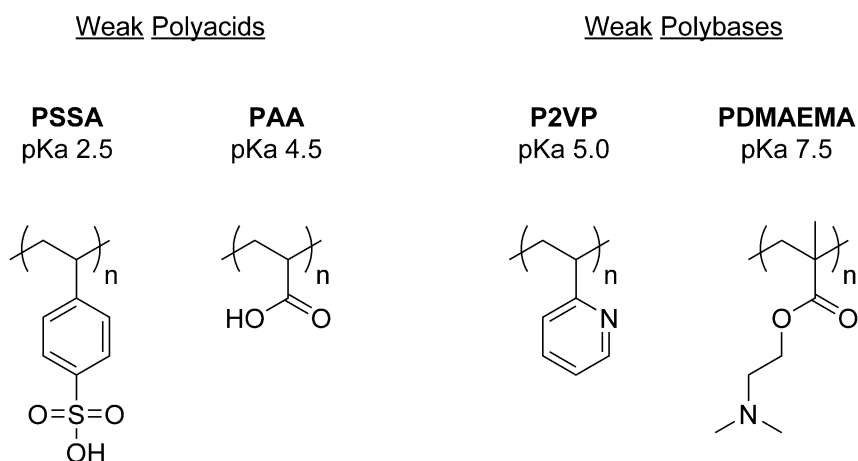


Figure 1.4: Chemical structures of weak polyacids and polybases, with their associated pKa values, that have pH responsive behaviour.

In 2014, the incorporation of two pH-responsive polymers, PAA and P2VP, along with quantum dots (QDs) allowed for the creation of a pH sensor.⁸ The pH sensor was highly stable and could detect pH in the range from pH 1–7. P2VP chains were grafted to orange QDs (cadmium selenide/zinc sulfide) and PAA was grafted to blue QDs (cadmium sulfide/zinc sulfide). Through π - π interactions, the polymers were deposited in a single layer on to a sheet of graphene oxide. At low pH (< 3) the P2VP is protonated leading to swelling and chain extension, whereas the protonation of PAA causes insolubility. At a pH higher than 4.5, both polymers are deprotonated causing the reverse, where P2VP is insoluble and PAA is soluble. Depending on the pH of the system, the polymer that is extended and the associated QD will determine the colour of the system (**Figure 1.5**).

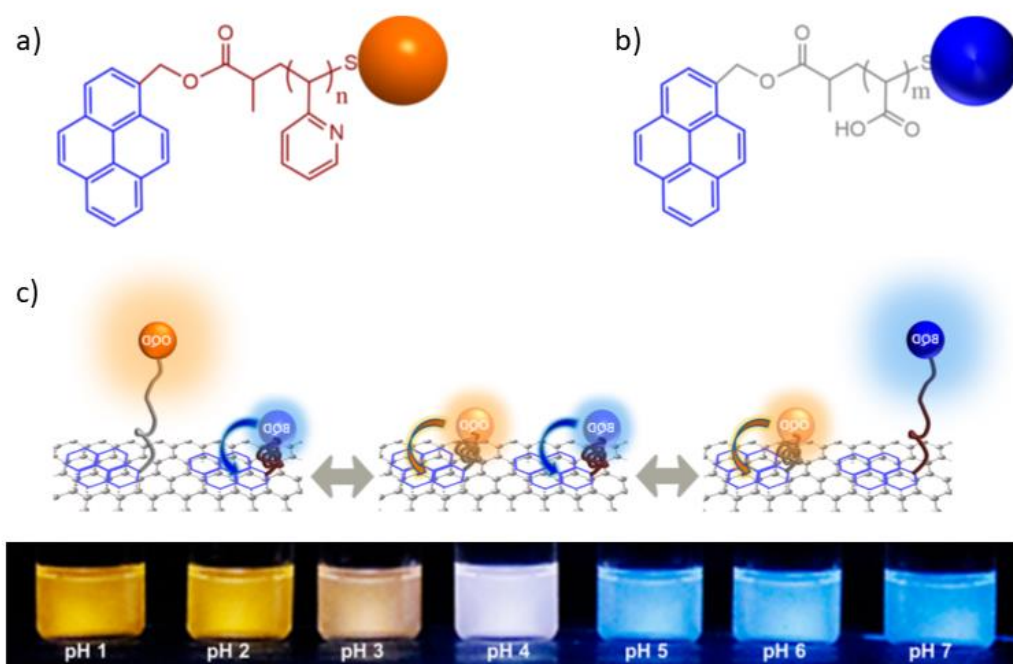


Figure 1.5: Structures of a) P2VP-QD and b) PAA-QD; c) schematic illustration of the conformation and behaviour of these polymers grafted to graphene-oxide and the associated colours over a pH range of 1-7. (Adapted with permission from reference 8. Copyright American Chemical Society.)

1.2.3 Thermo-responsive polymers

One of the best studied and well understood stimuli in terms of polymers and their response is temperature. It has been extensively studied because it can be readily applied to closed systems.¹³ Research in the area of thermo-responsive polymers mainly focuses on polymers in aqueous solutions that show a miscibility gap (area where the mixture becomes heterogeneous) in their phase diagrams. Depending where the miscibility gap is found, the system may have an upper critical solution temperature (UCST) or a lower critical solution temperature (LCST). The UCST is an upper bound temperature, below which the polymer will be insoluble at all concentrations. The LCST is a lower bound temperature, above which the polymer will be insoluble for all concentrations based on entropically driven demixing. Factors that affect LCST include polymer chain length, pH, salt concentration,

and polymer concentration.¹¹ Some polymer systems may experience both an LCST and UCST (**Figure 1.6**) depending on their composition.

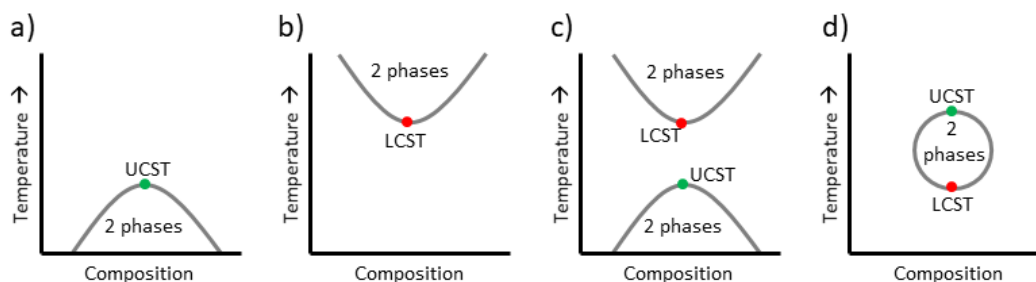


Figure 1.6: Phase diagrams from polymer compounds containing a a) UCST, b) LCST or both (c) and d).

One of the most widely studied polymers that exhibits LCST behavior is poly(*N*-isopropylacrylamide) (PNIPAAm). PNIPAAm has an LCST of ~ 32 °C, which is close to physiological temperature, making it ideal for many biomedical applications. As the solution temperature rises above the LCST, the PNIPAAm chains undergo a transition from the extended (solvated) random coil to a compact (desolvated) globular conformation. The entropically driven demixing is driven by the hydrogen bonds that form between the polymer chains and water. The mixing of the system possesses a negative entropy, and therefore the mixing is temperature dependent, with low temperatures producing a negative Gibbs free energy.

Biomedical applications of PNIPAAm are based on the principle that a polymer-drug complex is formed at room temperature when the polymer is soluble. After injection into the body, the polymer will warm, allowing the coil-globule transition to occur, and the drug contents are released. More recently, other polymers have been investigated for use in the biomedical field such as PDMAEMA and poly(ethylene glycol methacrylate) (PEGMA) (**Figure 1.7**).

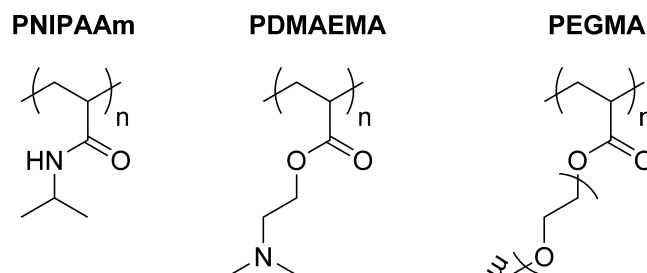


Figure 1.7: Chemical structures of common thermo-responsive polymers.

Temperature-responsive systems can be used as thermo-gelling polymers, which are temperature-sensitive physical hydrogels. Loh and coworkers synthesized a random copolymer of PDMAEMA and poly(methyl methacrylate) (PMMA), PDMAEMA-*ran*-PMMA.¹⁴ The addition of the 12 mol% PMMA caused a decrease in the LCST of up to 5 °C from pure PDMAEMA of the same molecular weight. Below the LCST of the polymer, the solution was clear and free flowing, however above the LCST (~26-38 °C depending on concentration and polymer composition) it became and opaque gel (**Figure 1.8**).

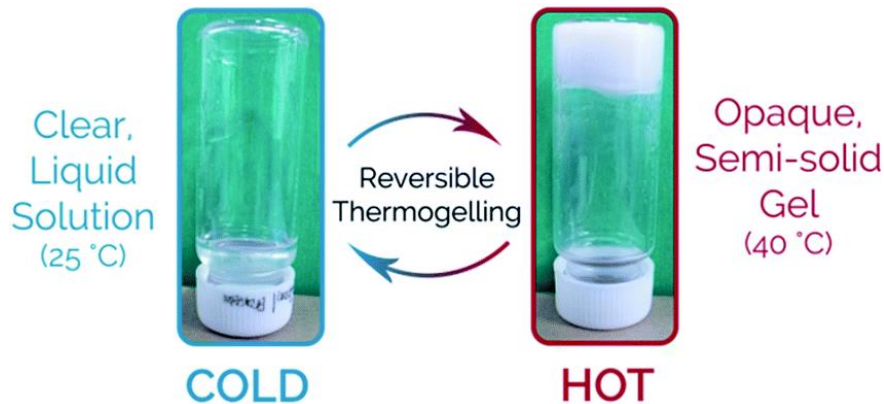
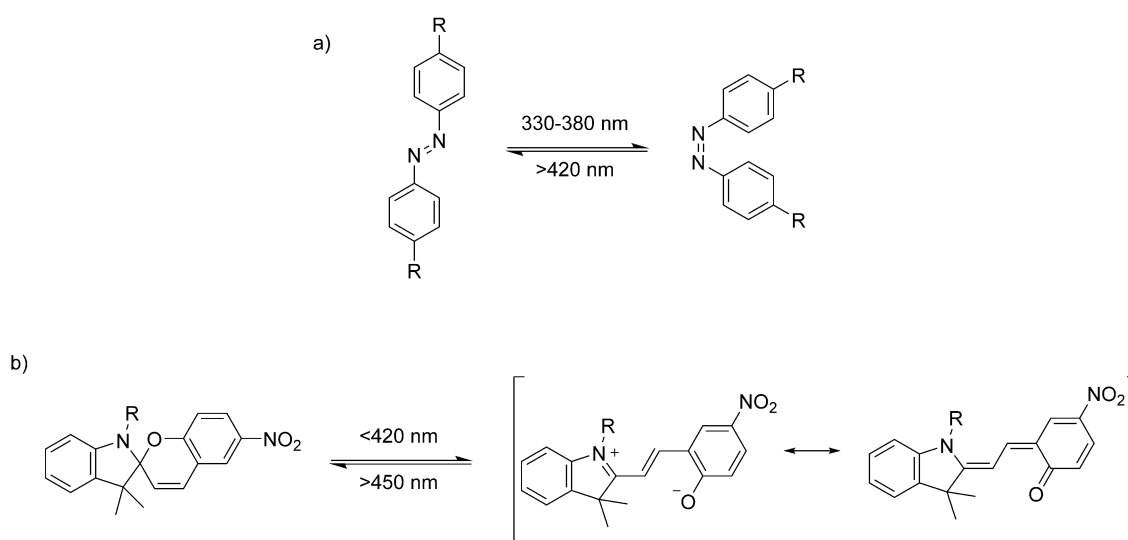


Figure 1.8: Photographs showing the reversible sol-gel transition of a PDMAEMA-*ran*-PMMA copolymer. (Reproduced from reference 14 with permission from The Royal Society of Chemistry.)

1.2.4 Light-responsive polymers

Light-responsive polymers have also been extensively studied because light can be applied externally to a closed system, similarly to temperature. Other advantages include the ability

to precisely target a location, and to apply very narrow wavelength bands of light.¹⁵⁻¹⁷ Over the years, many functional groups have been used including azobenzenes and spiropyran which have a reversible response to light irradiation (**Scheme 1.1**).¹⁸⁻²² Azobenzenes undergo a *trans-cis* isomerization from irradiation with 330-380 nm light, and undergo the reverse *cis-trans* isomerization when irradiated with >420 nm light.²³ Another reversible light-responsive moiety is a hydrophobic spiropyran which can isomerize to a hydrophilic merocyanine upon irradiation with 420 nm light.²⁰ Often, these transitions are accompanied with a colour change.



Scheme 1.1: Representative molecules found in light-responsive polymers: 1) azobenzene undergoing a *cis-trans* isomerization and b) hydrophobic spiropyran converting to hydrophilic merocyanine.

A block copolymer composed of PNIPAM and modified spiropyran was used as a temperature sensor.²² When irradiated, the colourless spiropyran results in a colourless solution, but upon irradiation and consequent isomerization to the merocyanine, the solution becomes coloured. A bathochromic/hypsochromic shift of the absorption spectrum within a wide temperature range will then occur (**Scheme 1.1**). The heat-induced bathochromic shift could be explained by the formation of a less polar domain by polymer aggregation when the polymer changed from a coiled to a globular structure at the LCST.

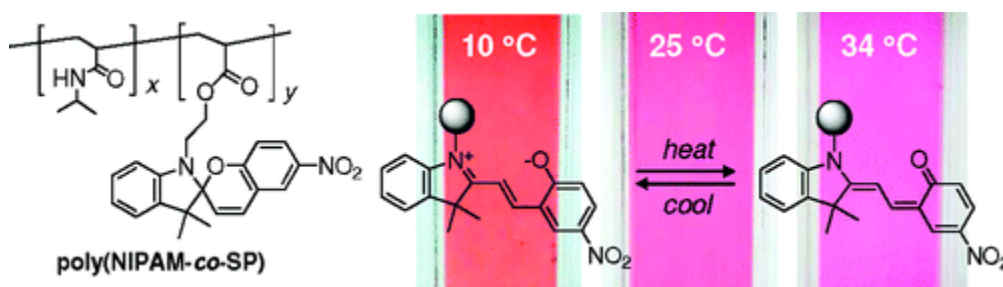


Figure 1.9: Chemical structure of PNIPAM and modified spiropyran containing polymer, and the associated thermo-responsive colour changes visible when irradiated with UV-light. (Reproduced with permission from reference 22. Copyright 2009 American Chemical Society.)

1.2.5 Gas-responsive polymers

Small molecules, such as gases, can be easily removed or added to a system, especially when dealing with large volumes that may be common in industry. Several gaseous triggers have been reported in the literature, including work studying CO_2 ,²⁴⁻²⁵ CO ,²⁶ and NO .²⁷ Gas-responsive polymers have been used in applications as drug delivery vehicles, cell signaling systems, microgels, and nanoreactors.²⁸

CO_2 has been the most widely studied trigger for gas-responsive polymers as it is a naturally-abundant and non-toxic gas.²⁸ Functional groups that respond to CO_2 include tertiary amines, guanadines, and imidazoles.²⁴ Many of these polymers are used in aqueous systems, and changes in pH occur in the system as CO_2 is introduced. Therefore, compounds with tertiary amines, that possess pKa values in the appropriate range (pKa from 6.5-8.1) have been extensively explored. Bubbling CO_2 through a system results in the protonation of the polymer, and the deprotonation of the polymer is triggered by sparging the system with inert gas such as Ar or N_2 . These systems are much desired as the stimuli is non-toxic and aqueous environments are tenants of green chemistry.

Recently, Tam and co-workers synthesized grafted PDMAEMA onto cellulose nanofibers to create CO_2 responsive aerogels (**Figure 1.10**).²⁹ In the presence of CO_2 the surface of the aerogel switches from hydrophobic to hydrophilic in nature. When in ambient environments (pH of 7 and temperature of 25 °C), the surface of the aerogel was

hydrophobic, and when used as a filter could separate oil from an oil-water mixture. After exposure to CO_2 for 15 min, the surface of the aerogel changed from hydrophobic to hydrophilic and the separation process was completely reversed (**Figure 1.10**). This was shown to be stable for multiple cycles.

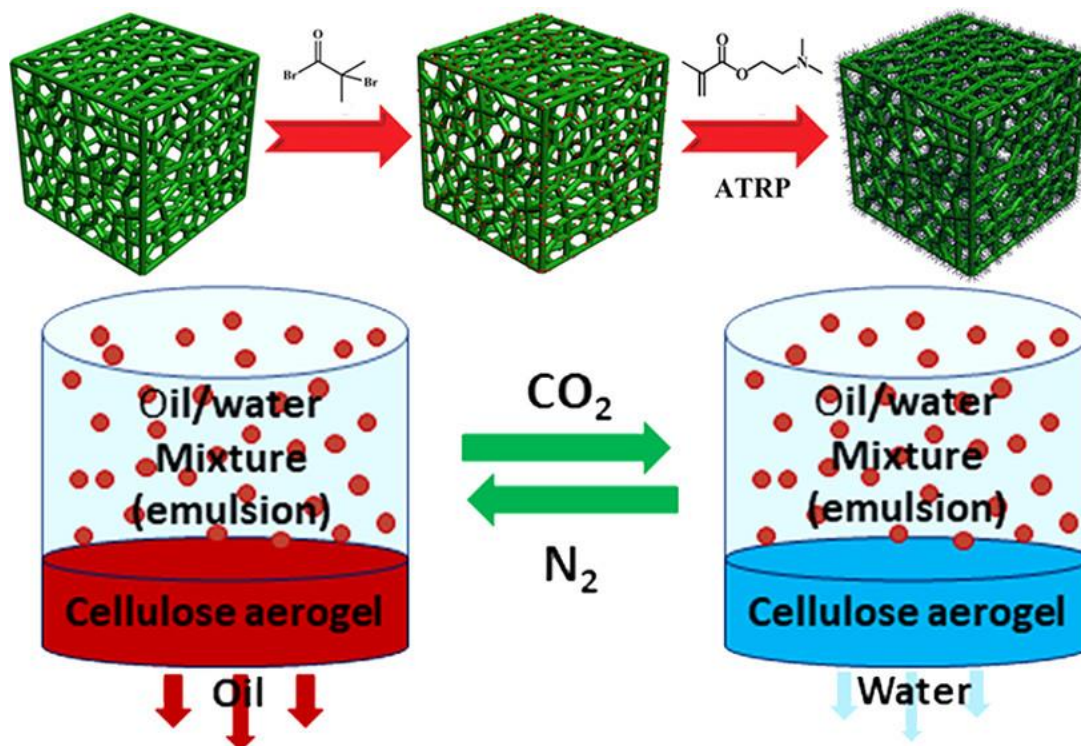


Figure 1.10: Schematic representation of PDMAEMA functionalized cellulose nanofibers aerogels and the associated oil/water operations in the presence of an inert environment or CO_2 . (Reproduced with permission from reference 29. Copyright 2019 American Chemical Society.)

1.3 Stimuli-responsive Degradable polymers

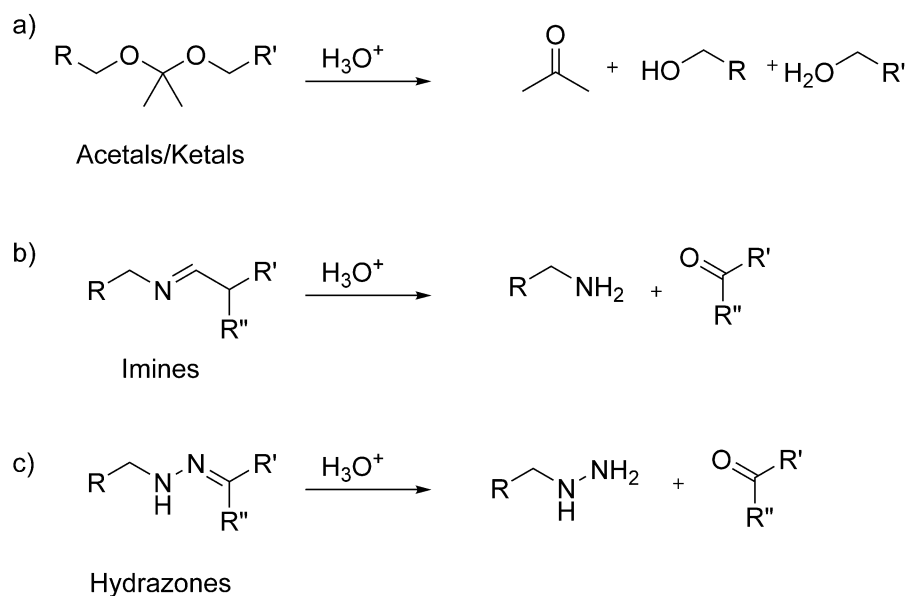
Many traditional applications of polymers have relied on their long-term stability, as previously discussed. In recent years, however, there has been increased interest in polymers that can be readily degraded. This interest is on the one hand motivated by increasing attention to the global problem of plastic pollution.³⁰⁻³¹ However, degradable polymers are of significant interest for the growing biomedical fields of drug delivery³² and tissue engineering.³³

Degradable polymers may be naturally occurring (*e.g.* polysaccharides and proteins) or produced synthetically. Both natural and synthetic versions tend to share common characteristics in their architecture, often being composed of ester, amide, and/or ether bonds. These polymers typically undergo a gradual degradation, either *in vivo* or in the environment, often assisted by microbes. Much attention in the area of degradable polymers has focused on polysaccharides³⁴ and polyesters.³⁵⁻³⁶ In many cases, a polymer would ideally remain highly stable while being used in its application, and then would degrade rapidly on demand under specified conditions.

While the concept of triggered degradation is not new, over the last decade there has been a resurgence of interest in controlling polymer degradation. In particular, significant progress has been made in the ability to trigger degradation with specific stimuli and in demonstrating its application in smart materials and devices. In general, there are three main classes of stimuli-responsive degradable polymers: acid-, redox-, and photo-degradable polymers.

1.3.1 Acid-degradable polymers

Acid-degradable polymers are usually created by the incorporation of acid-sensitive functional groups, including acetals, ketals, imines, and hydrozones (**Scheme 1.2**). These functional groups are stable in neutral environments but undergo rapid degradation in acidic environments.



Scheme 1.2: Chemical structures and hydrolysis products of generic a) acetal/ketals, b) imines, and c) hydrazones.

The degradation of acetal and ketals has been the subject of interest because they are charge-neutral and undergo hydrolysis at a rate proportional to the hydronium concentration of the local environment. This makes them ideal for biomedical applications as they remain stable under physiological conditions but can break down upon exposure to the more acidic medium encountered within a tumor cell (pH 5.7-7.8), triggering polymer degradation and release of the drug, for example.

Polymers were prepared from estradiol-polyketal conjugates, by incorporating estradiol into the polymer backbone (**Figure 1.11a**).³⁷ These polymers were then incorporated into microparticles that showed prolonged release that was pH responsive, as the faster drug release occurred at low pH (**Figure 1.11b**).

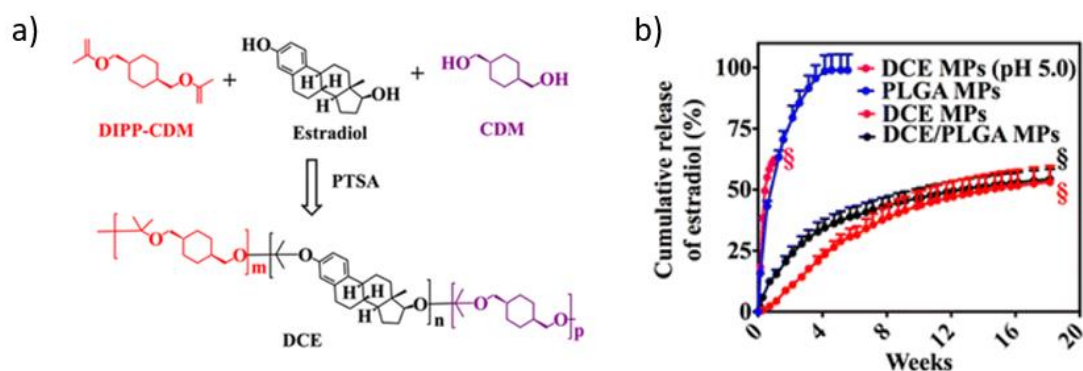


Figure 1.11: a) Synthesis of a estradiol-polyketal conjugate and the release of estradiol from various microparticle assemblies at pH 7.4 (unless otherwise indicated). (Reproduced with permission from reference 37. Copyright 2016 American Chemical Society.)

1.3.2 Redox-degradable polymers

Another class of biologically relevant stimuli are reducing and oxidizing reagents as diseased tissues are known to have higher concentrations of redox-active species.³⁸ For example, cancer cells have up to 10 times the concentrations of reducing glutathione compared to healthy cells. One method of utilizing this property is to synthesize polymers with disulfide linkages built into their backbones (polydisulfides), as they can be cleaved by reducing agents such as dithiothreitol (DTT) or glutathione.³⁹⁻⁴²

Over the years there has been a number of degradable disulfide-based systems used in the biomedical field for drug delivery.^{13, 42} These systems had limitations, however, such as complicated syntheses, lack of tunable properties, and a lack of acceptable host response. Recently, Farokhzad reported the development of a biodegradable and biocompatible poly(disulfide amine) that is prepared in one-step, in under 10 minutes, via a polycondensation reaction between fatty diacids and L-cysteine esters (**Figure 1.12**).⁴³ These were incorporated into nanoparticles for drug delivery and were shown to completely disassemble in the presence of reducing agents DTT or glutathione. It was also shown that increasing the chain length of the hydrophobic fatty acid caused an increase in the retention time for hydrophobic molecules, such as Nile red, allowing for tunable drug retention.

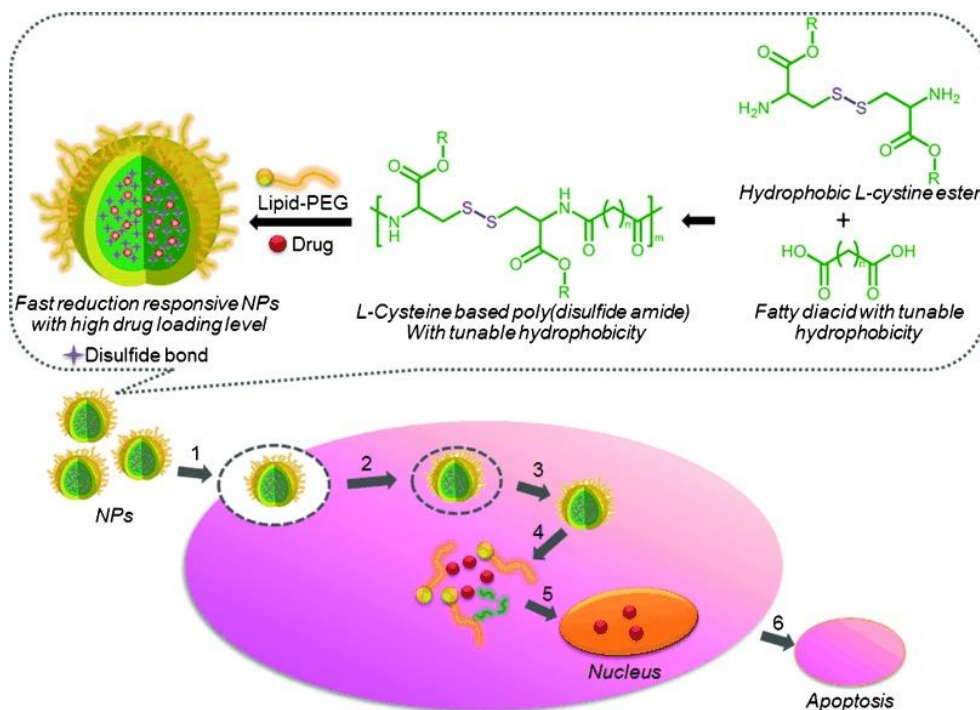
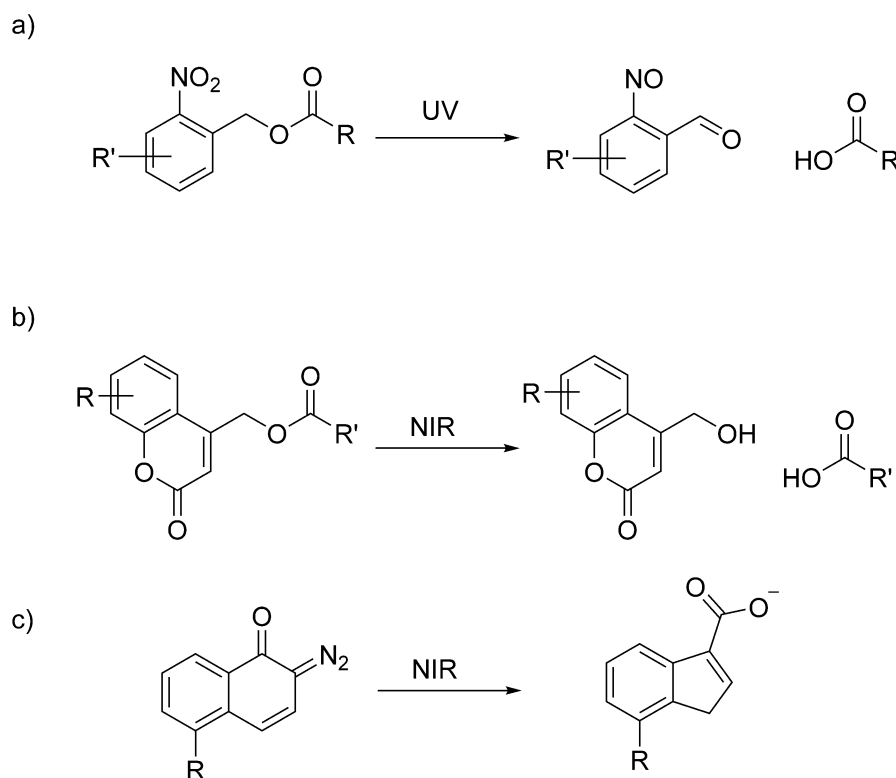


Figure 1.12: Chemical structure of a reduction-sensitive L-cysteine based polymer and the the mechanism for its incorporation into nanoparticles and subsequent depolymerization on contact with a reducing agent. (Reproduced with permission from reference 43. Copyright 2015 Wiley-VCH Verlag GmbH & Co. KGa, Weinheim.)

1.3.3 Photo-degradable polymers

As discussed previously, light is a convenient stimulus as it can be controlled in both temporal and spatial dimensions. Photo-degradable polymers differ from the previously discussed photo-responsive polymers because they incorporate units that undergo irreversible changes upon exposure to stimuli. These polymers often include photocleavable linkers such as coumarin dimers,^{17, 44} *o*-nitrobenzyl esters and carbonates,⁴⁵⁻⁴⁶ and 2-diazo-1,2-naphthoquinones⁴⁷ (**Scheme 1.3**).



Scheme 1.3: Chemical structures of light sensitive moieties and their irreversible decomposition: a) *o*-nitrobenzyl, b) coumarin, and c) 2-diazo-1,2-naphthoquinones.

Photocleavable moieties are extensively used as protecting groups because they have many of the following characteristics: 1) strong absorption at wavelengths above 300 nm, 2) high quantum yield, 3) stable in media prior to irradiation, 4) soluble in various media, 5) photochemical by-products do not absorb in the same range, 6) biocompatible, and 7) the cleavage event is rapid.⁴⁸ The most used family of photocleavable groups is the nitrobenzyl family. This is because the cleavage event is rapid, and therefore not the rate determining step for most systems.⁴⁸ The nitrobenzyl group absorbs a photon, allowing for the cleavage of the N=O π -bond via a Norrish Type II reaction.⁴⁹ This brings the molecule into a diradical excited state, which then abstracts a proton from the benzylic carbon. A five-member ring is formed followed by cleavage of the 2-nitrosobenzaldehyde group. This system has also been extensively studied over the years leading to variations that work in a variety of wavelengths and media.⁴⁸

Two common degradable polymers are poly(lactic acid) (PLA) and poly(lactic-*co*-glycolic acid) (PLGA) which degrade based on their hydrolytic cleavage, which is a slow and uncontrolled process. Almutairi and coworkers incorporated a UV-responsive modified *o*-nitrobenzyl group.⁴⁶ Upon UV cleavage of this photolabile group, an internal cyclization reaction occurred to produce a 5-membered ring. After successive cleavages, complete degradation of the polymer was achieved.

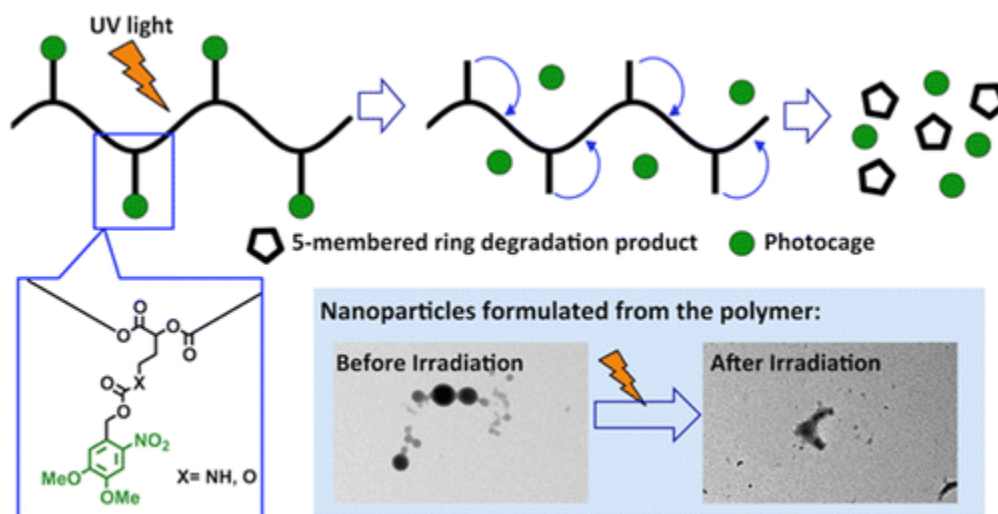


Figure 1.13: Schematic showing the photo-degradable behaviour of *o*-nitrobenzyl modified PLA and PLGA. (Reproduced with permission from reference 46. Copyright 2015 American Chemical Society.)

1.3.4 Limitations of stimuli-responsive degradable polymers

Stimuli-responsive degradable polymers break down in response to external stimuli but need multiple stimuli-mediated events to achieve complete depolymerization. These levels may be easy to achieve in laboratory conditions, however, can be difficult to achieve in natural or *in vivo* environments.

1.4 Self-immolative polymers

Inspired by the notion of self-destruction, polymers that depolymerize end-to-end upon triggering have often referred to as self-immolative polymers (SIPs).⁵⁰ Other naming conventions including continuous head-to-tail depolymerization⁵¹ and cascade

depolymerization⁵² have also been used. A defining feature of SIPs is their ability to undergo complete end-to-end depolymerization following a single bond cleavage event by a stimulus. This provides an amplified response to the stimulus, as many molecules are released from a single stimulus event. End-to-end depolymerization can occur following the stimulus-mediated cleavage of a polymer end-cap (**Figure 1.14a**), or backbone bond of either a linear (**Figure 1.14b**) or cyclic SIP (**Figure 1.14c**).

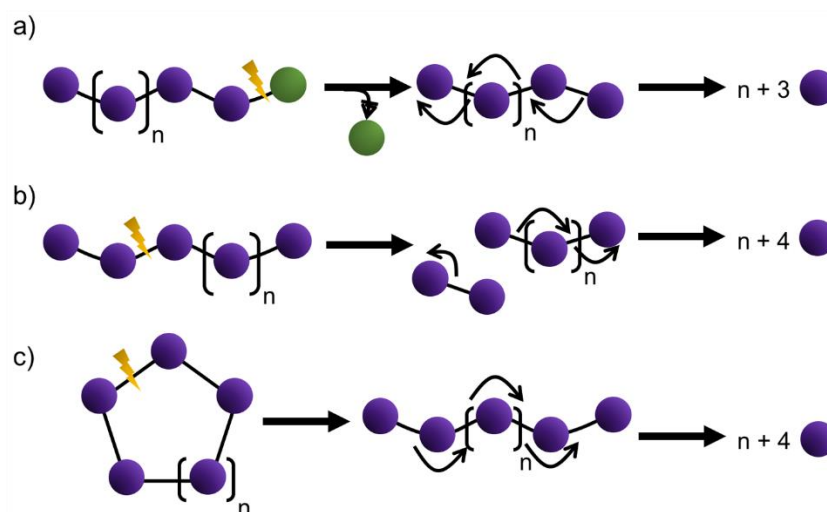


Figure 1.14: Depolymerization can be triggered by (a) end-cap cleavage; (b) backbone cleavage of a linear polymer; (c) backbone cleavage of a cyclic polymer. After the initial cleavage, the arrows represent a cascade of sequential reactions leading to depolymerization.

Depolymerizable SIP backbones can be categorized as either irreversible or reversible. Irreversible SIPs degrade to products that differ from the monomers from which they were synthesized, and therefore they cannot be repolymerized (**Figure 1.15a**). In contrast, reversible SIPs depolymerize to the monomers from which they were synthesized, making repolymerization possible, at least in principle (**Figure 1.15b**). The different SIP backbones and their derivatives vary widely in terms of their depolymerization rates, triggering chemistry, degradation products, as well as their thermal and mechanical properties. Therefore, they must be carefully selected and tuned according to the target application. Several comprehensive reviews on SIPs have been published over the years.^{51,}

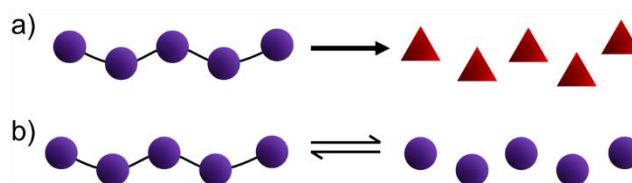


Figure 1.15: After end-cap or backbone cleavage, SIPs can (a) irreversibly depolymerize to molecules different from the original polymerization monomers or (b) reversibly depolymerize back to monomers.

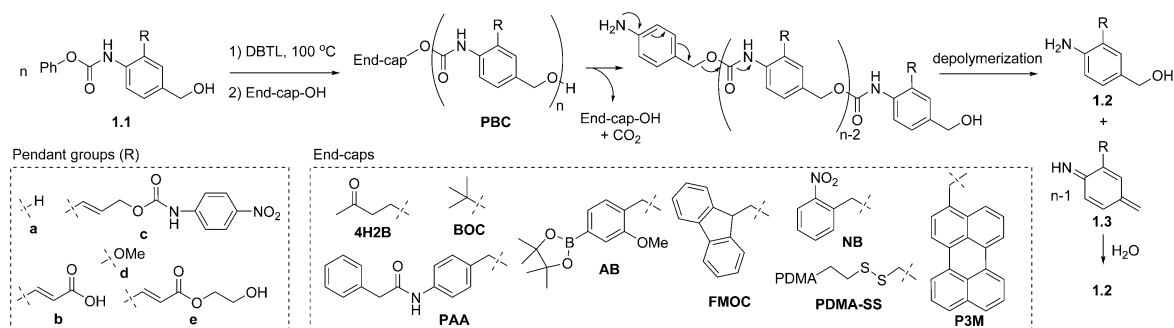
1.4.1 Irreversible SIPs

The first reported irreversible linear SIPs were inspired by self-immolative dendrimers.⁵⁶⁻⁵⁸ Unlike the step-wise synthesis of dendrimers, the polymers were prepared in one-step reactions. Irreversible SIPs have been prepared by step-growth polymerizations and depolymerize by elimination and/or cyclization reactions. Poly(benzyl carbamate)s (PBCs) derived from 4-aminobenzyl alcohol have been the most widely used irreversible SIPs. Polycarbonates and variations incorporating different linkers have also been introduced to tune the depolymerization rate and to introduce new properties and functions. Proof of concept studies with these polymers in different applications such as sensors and drug delivery vehicles have been performed.

1.4.1.1 Poly(benzyl carbamates) (PBCs)

The first PBC SIP was introduced by Shabat and coworkers in 2008.⁵⁰ A phenyl carbamate (**1.1**) was polymerized using dibutyltin dilaurate (DBTL) as a catalyst at 100 °C with an alcohol end-capping agent to afford **PBCa** (**Scheme 1.4**). The polymerization reaction is quite versatile and a variety of functional monomers as well as different end-caps have been incorporated. PBCs have also been incorporated as depolymerizable side chains on bottlebrush polymers.⁵⁹ However, the degree of polymerization (DP_n) has typically been limited to < 20 , and the step-growth polymerization mechanism results in relatively broad dispersities (D) ranging from ~ 1.4 – 2.0 . Following end-cap cleavage to reveal a terminal aniline, the depolymerization of PBCs is based on a 1,6-elimination-decarboxylation cascade.⁶⁰ The released azaquinone methides (**1.3**) react with water or other nucleophiles

to generate 4-aminobenzyl alcohol or its derivatives (**1.2**). In the presence of water, the depolymerization is relatively rapid, reaching completion over several hours.⁵⁰ However, in less polar media the depolymerization reaction is very slow,⁶¹⁻⁶³ often requiring days. Phillips and coworkers accelerated the depolymerization rate of PBC oligomers through the introduction of electron-donating methoxy groups or by reduction of the aromatic character of the repeat units using naphthalene derivatives.⁶⁴ Both of these approaches lowered the energetic costs of dearomatization involved in the depolymerization.



Scheme 1.4: Synthesis and depolymerization PBCs having different pendant groups and end-caps.

PBCs have been incorporated into a number of different sensor designs. Shabat and coworkers incorporated *ortho*-acrylate substituents onto a PBC and 4-hydroxy-2-butanone as an end-cap, resulting in the water soluble SIP **PBCb-4H2B**.⁵⁰ While the polymers were not fluorescent, cleavage of the end-cap by bovine serum albumin resulted in depolymerization to the corresponding aniline derivative, which fluoresced at 510 nm. Alternatively, 4-nitroaniline carbamates were incorporated as pendant groups, along with *ortho*-acrylates and a phenylacetamide end-cap (**Scheme 1.4 PBCb/c-PAA**).⁶³ Cleavage of the end-cap by penicillin-G amidase triggered the backbone depolymerization by the 1,6-elimination-decarboxylation cascade and release of 4-nitroaniline reporters by an analogous pendant group fragmentation.

PBC-based materials have also been explored for encapsulation and release applications. The ability to achieve high degrees of payload release in response to subtle chemical stimuli can provide advantages over traditional stimuli-responsive polymers. For example,

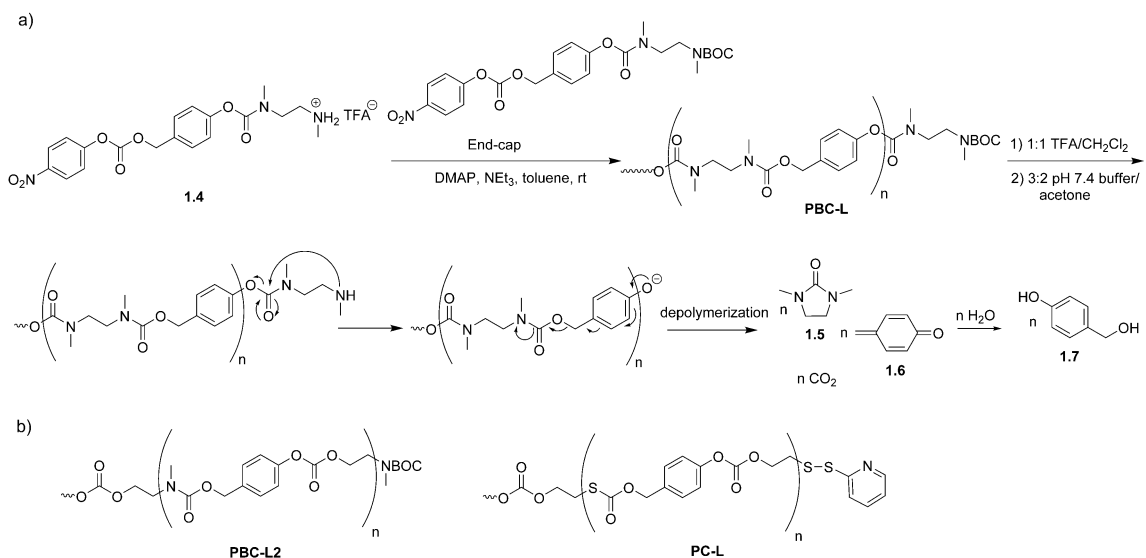
Moore and coworkers prepared microcapsules from PBCs (**Scheme 1, PBCe-BOC and PBCe-FMOC**).⁶⁵ The hydroxyl pendant groups of the PBCs were activated with 2,4-toluene diisocyanate, then microcapsules were prepared using an emulsion process with butanediol as a chain extender. The capsules prepared from BOC and FMOC end-capped polymers released their payload over 24 – 48 h using HCl and piperidine as stimuli respectively. Liu and coworkers also explored this concept by combining PBCs with hydrophilic poly(*N,N*-dimethylacrylamide) (PDMA) to afford amphiphilic block copolymers that self-assembled to form vesicles.⁶⁶ End-caps including perylen-3-ylmethyl carbamate (**P3M**), 2-nitrobenzyl carbamate (**NB**), and a PDMA-functionalized disulfide carbamate (**PDMA-SS**) were incorporated to enable triggering with visible light, UV light, and thiols respectively. Thiols in particular are biologically relevant stimuli as the reducing peptide glutathione is known to be present at higher concentrations in hypoxic tumors and also within cells compared to the extracellular environment.³⁸ Stimuli-triggered depolymerization of the SIP block and consequent vesicle disintegration resulted in the release of various payloads such as doxorubicin (DOX), camptothecin, and enzymes.

Most recently, Shabat and coworkers also developed poly(benzyl carbonate)s that depolymerized to release quinone methides.⁶⁷ Schaap's adamantylidene-dioxetane turn-ON chemiluminescence probe was incorporated into each monomer unit such that trapping of the quinone methide by water generated a phenolate-dioxetane, which spontaneously decomposed by a chemically initiated electron-exchange process to generate an excited state benzoate and adamantanone. Emission of blue light (499 nm) occurred as the benzoate decayed to the ground state. In all of the above examples, a key characteristic was the release of multiple reporter molecules in response to one end-cap cleavage, exemplifying the key amplification feature of SIPs. Signal amplification is particularly important for the fabrication of sensors as higher sensitivities provide better detection limits.⁶⁸

1.4.1.2 Polycarbamates containing linkers

Cyclization spacers have been incorporated into SIPs to modulate their properties and depolymerization rates. In the early days of SIP development, our group began working on

PBCs without pendant functional groups. They were poorly soluble in most solvents, which hindered our efforts to study their depolymerization. While Shabat and coworkers introduced pendant solubilizing groups, based on the known favorable cyclization of *N,N'*-dimethylethylenediamine (DMED) derivatives to *N,N'*-dimethylimidazolidinones,⁶⁹ we inserted DMED spacers to improve the solubility.⁵² The target SIP was synthesized from monomer **1.4**, containing a protonated amine (**Scheme 1.5a**). The addition of 4-dimethylaminopyridine (DMAP), NEt₃, and BOC-protected monomer as an end-cap, afforded the BOC end-capped polycarbamate **PBC-L** with a DP_n of ~16 and *D* of 1.6. Depolymerization was triggered by cleavage of the BOC group with trifluoroacetic acid (TFA) then immersion in pH 7.4 phosphate buffer:acetone (3:2). It occurred by a cascade of cyclization-1,6-elimination-decarboxylation reactions, requiring about 3 days to reach completion.



Scheme 1.5: (a) Synthesis and depolymerization of a polycarbamate based on 4-hydroxybenzyl alcohol and DMED (**PBC-L**); (b) Chemical structures of related analogues containing 2-methylaminoethanol (**PBC-L2**) or mercaptoethanol (**PC-L**) spacers.

We also incorporated different cyclization spacers (**Scheme 1.5b**).⁷⁰ For example, the replacement of DMED with 2-methylaminoethanol in **PBC-L2** or the mercaptoethanol spacer in **PC-L** resulted in more rapid cyclization reactions. While **PBC-L** required 7 h to

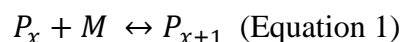
reach 50% depolymerization after triggering, **PBC-L2** was 50% degraded in 1 h, and polymer **PC-L** was 50% degraded in less than 30 min. Thus, the insertion of cyclization spacers allowed tuning of the depolymerization rate. However, a limitation of all of these backbones is the tendency to form cyclic oligomers during the polymerization (~20 wt%). These cyclic species are difficult to separate from the desired linear polymers and do not depolymerize upon end-cap cleavage as they do not possess end-caps. Cyclic species have not been reported for PBCs (**Scheme 1.4**), likely because their more rigid structures make intramolecular cyclization less favorable.

Polycarbamates with linkers were the first SIPs incorporated into block copolymers and used in encapsulation and release studies.⁵² For example, we prepared an amphiphilic block copolymer by conjugating a hydrophilic PEG block to the end-cap of the hydrophobic SIP block. The resulting block copolymer **PBC-PEG (Figure 3a)** was self-assembled to form nanoparticles. Hydrolysis of the ester linkage between PEG and the SIP block resulted in the depolymerization of the SIP and degradation of the nanoparticles. Nile red, a hydrophobic dye molecule, was encapsulated into the SIP nanoparticles and was released as the nanoparticles degraded.

Almutairi and coworkers incorporated end-caps responsive to UV and near-infrared (NIR) light onto **PBC-L** and prepared nanoparticles from the resulting polymers using an emulsion process.⁷¹ The nanoparticles were degraded using UV or NIR light and released Nile red in response to these stimuli. The cytotoxicity of the polymers and their degradation products were also explored. The materials were found to be as well tolerated as poly(lactic-*co*-glycolic) acid, which is approved in certain clinical applications. Nevertheless, like the poly(benzyl carbamate)s described above, this class of polycarbamates releases azaquinone methides during their depolymerization and further investigations of potential toxicity are required.

1.4.2 Reversible SIPs

Reversible SIPs are typically based on polymers with low (i.e., below room temperature) ceiling temperatures (T_c), where T_c is defined as the temperature above which, polymer of high molar mass is not formed in a given chain polymerization:⁷²

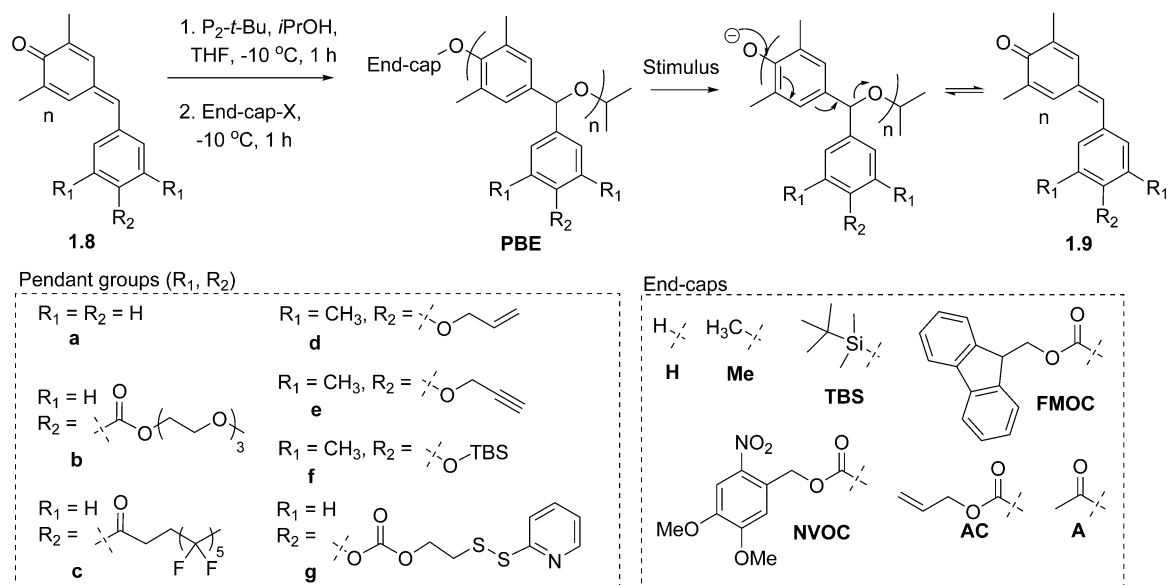


where P_x is the growing chain with DP of x and M is a monomer. By definition, at the ceiling temperature $\Delta G = 0$ for Equation 1, and consequently $T_c = \Delta H/\Delta S$. Thus, the ceiling temperature for a given polymerization depends on both enthalpic and entropic contributions. T_c also depends on the initial monomer concentration, and $T_c(c^0)$ denotes the ceiling temperature for an initial monomer concentration of 1 M, while $T_c(\text{bulk})$ denotes the ceiling temperature for undiluted monomer. Polymers can be synthesized below the T_c , but above the T_c , depolymerization occurs spontaneously. Capping or cyclization of the polymer below its T_c prevents the depolymerization, but when the end-cap or backbone is cleaved at room temperature, depolymerization can occur. Many of the reversible SIP backbones have actually been known for decades, but in the past decade, there have been significant developments in the introduction of stimuli-responsive end-caps that enable depolymerization to be triggered by a wide range of stimuli. This has facilitated the application of triggered depolymerization in diverse fields ranging from smart composites to drug delivery. Their depolymerization back to the monomers from which they were initially synthesized also endows reversible SIPs with the potential to be recycled through depolymerization and subsequent repolymerization. The most important classes of reversible SIPs are poly(benzyl ether)s, polyphthalaldehydes, polyglyoxylates, and polyglyoxylamides

1.4.2.1 Poly(benzyl ether)s (PBEs)

Inspired by the work of McGrath and coworkers on PBE dendrimers,⁵⁸ as well as prior work on the anionic polymerization of quinone methides,⁷³ Phillips and coworkers introduced depolymerizable PBEs.⁷⁴ They polymerized 2,6-dimethyl-7-phenyl-1,4-

benzoquinone (**1.8a**) using **1-tert-butyl-2,2,4,4,4-pentakis(dimethylamino)-2 λ^5 ,4 λ^5 -catenadi(phosphazene)** (P_2 -*t*-Bu) and an alcohol initiator at low temperatures (-10 to -20 °C) to afford polymer **PBEa** with high DP_{ns} , up to 2300 and D of 1.3–1.5 (**Scheme 1.6**). The methyl groups on monomer **1.8a** were incorporated to prevent the uncontrolled polymerization⁷³ and the phenyl moiety was incorporated to make depolymerization more favorable, as extended conjugation stabilizes the initial quinone methide depolymerization product compared to the (aza)quinone methides generated in the depolymerization of the polycarbamates and polycarbonates described above. End-capping was performed using chloroformates or alkyl or silyl chlorides to afford the corresponding PBEs responsive to light, fluoride, acidic environments and redox reactions.



Scheme 1.6: Synthesis and depolymerization of PBEs with different pendant groups and end-caps.

The ether backbone imparted higher stability to PBEs compared with other backbones such as PBCs when exposed to base, acid, and heat. However, they depolymerized by 1,6-elimination reactions (**Scheme 1.6**) in less than 1 h when exposed to stimuli, even in organic solvents. Different groups such as tri(ethylene glycol)s,⁷⁵ fluoroalkyl chains,⁷⁵ alkenes for thiol-ene reactions,⁷⁶⁻⁷⁷ alkynes for CuAAC,⁷⁸ and masked self-immolative moieties,⁷⁹ were incorporated onto the pendant phenyl ring of PBEs (**Scheme 1.6, PBEb-**

f). Furthermore, Zhang and coworkers prepared bottlebrush PBEs by grafting PEG or polystyrene (PS) side chains.⁷⁸ Interestingly, the PS-grafted polymer depolymerized more slowly, which was attributed to conformational constraints that made it more difficult for the backbone to attain the ideal geometry for the 1,6-elimination reaction.

Phillips and coworkers explored the triggered depolymerization of PBEs in the solid state. They combined hydrogen-terminated PBEs (**PBEb-H** and **PBEc-H**) with other polymers such as PS, polyethylene, and polypropylene, resulting in mixtures of plastics that could not be separated based on properties such as solubility.⁷⁵ Addition of the base 1,8-diazabicyclo[5.4.0]undec-7-ene (DBU) resulted in selective depolymerization of the PBE in about 2 h at 23 °C (**Figure 1.16**). After recovering the monomers by extraction, they were repolymerized to afford PBE in 83% yield, compared to 87% yield for the original polymerization. Optimization of aspects such as cost and efficiency of monomer recovery would be required, but this was an interesting proof of concept for the use of SIPs in mixed plastic recycling.

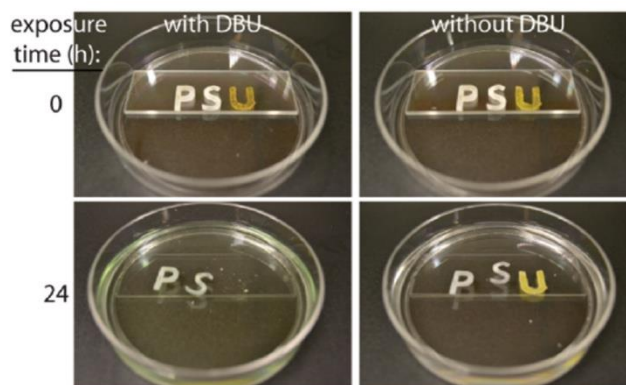


Figure 1.16: Separation of solid **PBE** (U) from solid polyethylene (P) and polypropylene (S) by selective depolymerization induced by DBU. (Adapted from reference 73 with permission from The Royal Society of Chemistry.

While depolymerization occurred for the hydrogen-capped PBE in 2 h with DBU,⁷⁵ Phillips and coworkers also noted that the depolymerization of most PBEs was very slow in the solid state.⁷⁹ They attributed this to a lack of accessible end-caps at the solid-liquid interface, and therefore incorporated stimuli-responsive triggers, such as TBS-protected

phenols, on each backbone repeat unit (e.g., **PBEf-A**, **Scheme 1.6**). Cleavage of these moieties resulted in 1,6-elimination reactions of the resulting phenols, cleaving the backbone. Rigid polymer disks prepared from polymer **PBEf-A** were depolymerized to soluble products in less than 5 h in the presence of fluoride ions at 23 °C. In a related approach, Zhang and coworkers reported PBEs with pendant disulfide groups (**PBEg-TBS**, **Scheme 1.6**).⁸⁰ Conjugation of PEG-SH *via* disulfide exchange led to graft copolymers, while reaction with HS-PEG-SH led to gels. The materials were degraded by a reducing agent (DTT), as the released thiol cyclized onto the carbonate group, releasing the phenol, which underwent a 1,6-elimination to initiate the depolymerization. In these latter two examples, the cleavage of the PBE through the pendant groups resulted in one fragment terminated with a phenol, that depolymerized, and another fragment terminated with a benzylic alcohol, which did not immediately depolymerize. In this sense, PBEs differ from polyaldehydes where backbone cleavage results in two unstable fragments as described in the next sections.

Ergene and Palermo explored cationic PBEs as potential antibacterial polymers.⁷⁶⁻⁷⁷ They grafted primary and tertiary amines as well as quaternary ammonium groups onto alkene-functionalized PBEs using thiol-ene chemistry (**PBEd-TBS**, **Scheme 1.6**). The primary amine-functionalized PBEs had the highest activities. The tertiary amine-functionalized PBEs were much less active, and the quaternary ammonium systems had intermediate activities. Hemolysis, the lysis of red blood cells, often serves as an initial indicator of toxicity to mammalian cells. The primary and tertiary amine-functionalized PBEs were highly hemolytic, but the quaternary ammonium-functionalized PBE was much less hemolytic. Depolymerization of the primary ammonium-functionalized polymer, induced by fluoride, greatly reduced its hemolytic toxicity, while retaining high antibacterial activity. In a follow-up work, Ergene and Palermo grafted varying ratios of PEG and primary amines to **PBEd-TBS** to modulate their hydrophobic-hydrophilic balance.⁸¹ With 25–50 mol% of 800 g/mol PEG, high antibacterial activities were retained while reducing hemolytic activities, and only minor changes in these activities were observed upon depolymerization. In contrast, grafting of 2000 g/mol PEG resulted in similar decreases in

antibacterial and hemolytic activities. Overall, this work demonstrates a potential role for depolymerization in modulating the behavior of antibacterial polymers. Further work will be needed to determine the toxicity of the PBEs and their depolymerization products. The authors also noted the potential for SIPs in the development of antibiofilm coatings with a triggerable self-cleaning characteristic. Some initial efforts towards this approach were recently reported by Lienkamp and coworkers in collaboration with our group using UV light-sensitive PEtG as a sheddable coating layer.⁸²

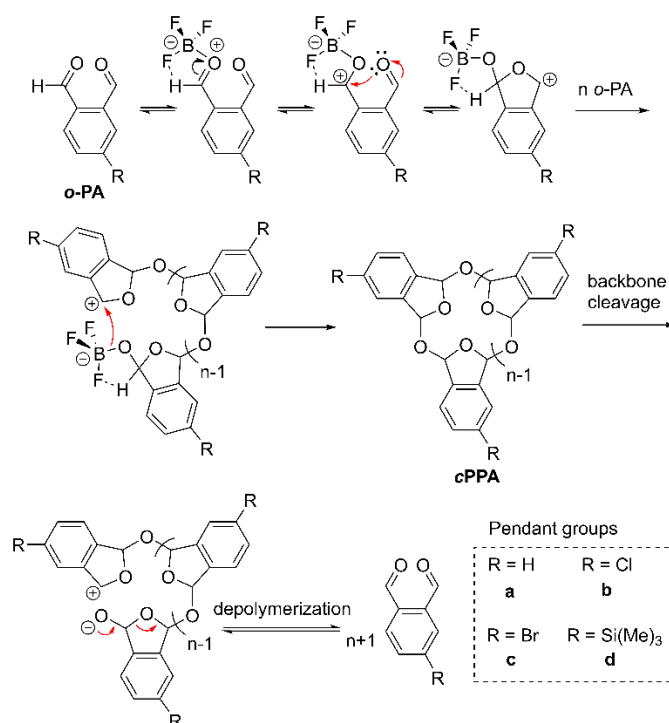
1.4.2.2 Polyphthalaldehydes (PPAs)

PPAs are polyacetals composed of *o*-phthalaldehyde (*o*-PA) or its derivatives.⁸³ Because of the relatively small enthalpy change associated with the conversion of the aldehyde's carbon-oxygen double bond to two carbon-oxygen single bonds in the polymer, the entropy gained through depolymerization overrides the enthalpic cost of depolymerization at relatively low temperatures, leading to low T_c values (e.g., -40 °C for *o*-PPA).⁸⁴ Metastable PPAs can be prepared *via* cyclization or end-capping reactions, but when terminal hemiacetal moieties are revealed through either a backbone or end-cap cleavage, they rapidly depolymerize to the monomers at ambient temperatures. Significant advancements have been made in both the synthesis and application of PPAs over the past decade.

1.4.2.2.1 Cyclic polyphthalaldehydes (cPPA)

In 1960s, Aso and Tagami studied different acid catalysts for the polymerization of *o*-PA, including $\text{BF}_3 \cdot \text{OEt}_2$ (**Scheme 1.7**), TiCl_4 , SnCl_4 , and $[\text{Ph}_3\text{C}][\text{BF}_4]$ at -78 °C and suggested cyclic structures of the polymers (**cPPAa**).⁸⁵⁻⁸⁶ The polymerizations were rapid (less than 1 h) but they could not control the DP_n of the isolated PPAs. Ito and coworkers used $\text{BF}_3 \cdot \text{OEt}_2$ for the polymerization of *o*-PA derivatives including 4-chlorophthalaldehyde, 4-bromophthalaldehyde, and 4-trimethylsilylphthalaldehyde affording **cPPAb-d**.⁸⁷ The electron-withdrawing groups made the backbones less susceptible to cleavage. Moore and coworkers finally confirmed the cyclic structures of cationically synthesized PPAs *via* end-group analysis using NMR spectroscopy and mass spectrometry.⁸⁸ They also discovered that under cationic conditions, the cyclic polyacetal backbone of PPAs could reversibly

cleave to release or incorporate monomers before backbiting and forming the final cyclic polymers. Taking advantage of this scrambling mechanism, they prepared random and multi-block copolymers by simply mixing PPAs with different derivatives of *o*-PA (**Figure 1.17**).⁸⁹ Kohl and coworkers later suggested that the $\text{BF}_3 \cdot \text{OEt}_2$ mediated synthesis of PPAs involves zwitterionic intermediates and that the interactions of two chain ends with opposite charges allows the ring formation events.⁹⁰



Scheme 1.7: $\text{BF}_3 \cdot \text{OEt}_2$ catalyzed polymerization of *o*-PA and its derivatives to give PPAs. Cleavage of the backbone leads to depolymerization to the corresponding monomers.

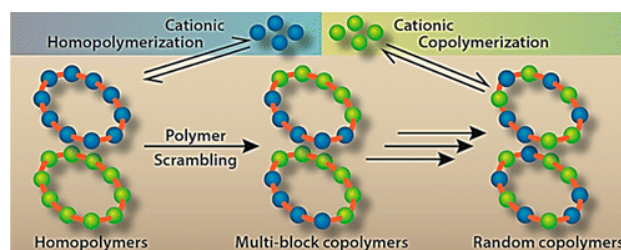


Figure 1.17: Block and random cyclic copolymers of *o*-PA can be prepared by a reversible opening and closing of the cyclic PPA backbone. (Reproduced from reference 87. Copyright 2013, American Chemical Society.)

Kohl and coworkers also recently employed $\text{BF}_3 \cdot \text{OEt}_2$ to copolymerize *o*-PA with a series of aliphatic aldehydes.⁹¹ The copolymerization yield and average molar mass decreased by increasing the aliphatic aldehyde feed percentage. However, the mechanical properties of the lower molar mass copolymers were enhanced by crosslinking using radiation-induced thiol–ene click chemistry. These results were important as pure PPAs are highly brittle, and the copolymerization strategy provided access to a range of PPA-based copolymers with varying mechanical properties and also functional groups. As for many commercial plastics, the properties of PPA have also been tuned through the incorporation of additives. For example, Sottos and coworkers showed that remaining solvents, such as CHCl_3 , CH_2Cl_2 , or dioxane, from a solvent-casting process could serve as plasticizers and change the mechanical properties of PPA films.⁹² For example, depending on the solvent, they found different elastic moduli (2.5–3 GPa), tensile strengths (25–35 MPa), failure strains (1–1.5%), and T_g values (64–95 °C). The additive strategy was also explored by Kohl and coworkers through the incorporation of ionic-liquid and ether-ester plasticizers.⁹³ Their study showed that plasticizers changed the thermal stability and mechanical properties. For example, 20 parts per hundred bis(2-ethylhexyl) phthalate (BEHP) reduced the storage modulus to *ca.* 1.2 MPa, which is about half that of pure *o*-PPA. In addition, the additives lowered the melting point of the degradation products from 54.3 °C (pure *o*-PA) to 37.5 °C (for formulated mixtures), which enabled the degradation products to better maintain the liquid state. This can potentially improve the transient nature of PPA devices by allowing them to be more readily absorbed into the environment.

Cyclic PPAs are metastable solids due to their susceptibility to backbone cleavage and depolymerization. This feature has garnered interest for a number of applications. Early work focused on lithography applications, wherein a resist was patterned using a depolymerization-inducing beam to dry-develop a pattern. Ito and Willson initially exploited the pH-sensitivity of PPA's acetal backbone by combining the polymer with photoacid generators (PAGs).⁹⁴ In their early studies using linear PPAs, good light sensitivity and pattern development were observed.⁹⁵⁻⁹⁶ However, the required formulations were too sensitive and the depolymerization product *o*-PA contaminated the expensive optics. They also investigated the more stable halogenated derivatives **cPPAb** and **cPPAc**.⁸⁷ However, they were not able to self-develop at temperatures below 100 °C and required a postbaking step.

More recently, the groups of White, Rogers, and Moore fabricated transient electronics based on cyclic PPAs.⁹⁷ They combined PPA with a PAG to create substrates for free-standing transistor arrays. Upon exposure to a UV light (379 nm), acid-triggered depolymerization led to disintegration of the array (**Figure 1.18a**). They also prepared thermally-triggerable transient electronics based on PPAs layered with an acid microdroplet-containing wax.⁹⁸ Melting the wax released the acid, resulting in rapid device destruction (**Figure 1.18**). Kohl and coworkers also explored strategies for the fabrication of PPA-based electronics.⁹⁹ For example, they prepared materials by layering PAG-free PPA with a thin layer of PPA/PAG blend and showed that this method improved the shelf life of the materials.¹⁰⁰ Building on this work, they investigated the application of different polynuclear aromatic hydrocarbons as PAGs and showed that the combination of a pentacene-based sensitizer with PPAs afforded a transient material able to depolymerize after 1 min in direct sunlight.¹⁰¹

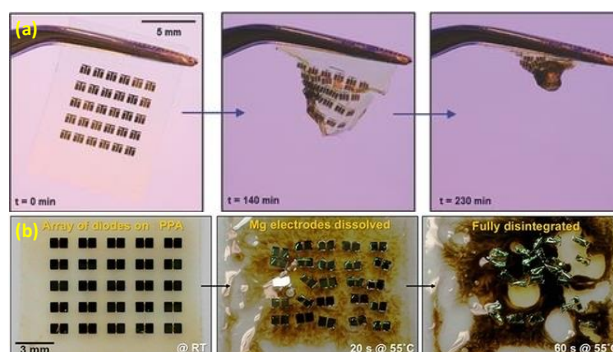


Figure 1.18: Acid release and destruction of PPA-based transistor arrays due to (a) the activity of a photoacid generator after irradiation with UV light and (b) melting an acid microdroplet-containing wax within the PPA. Adapted with permission from reference 95 (a) and reference 96 (b). Copyright 2014, John Wiley and Sons.

Mechanically-triggered depolymerization of cyclic PPA has also been investigated by the Moore and Boydston, groups.¹⁰² Their study showed that for PPA above a critical molar mass of about 30 kg/mol, mechanical forces applied using pulsed ultrasound induced heterolytic chain scission, created hemiacetate and oxocarbenium chain ends, leading to subsequent depolymerization. Exploiting the potentially reversible depolymerization back to monomer, they recycled 67% of the resulting *o*-PA and repolymerized it to produce high molar mass PPA.

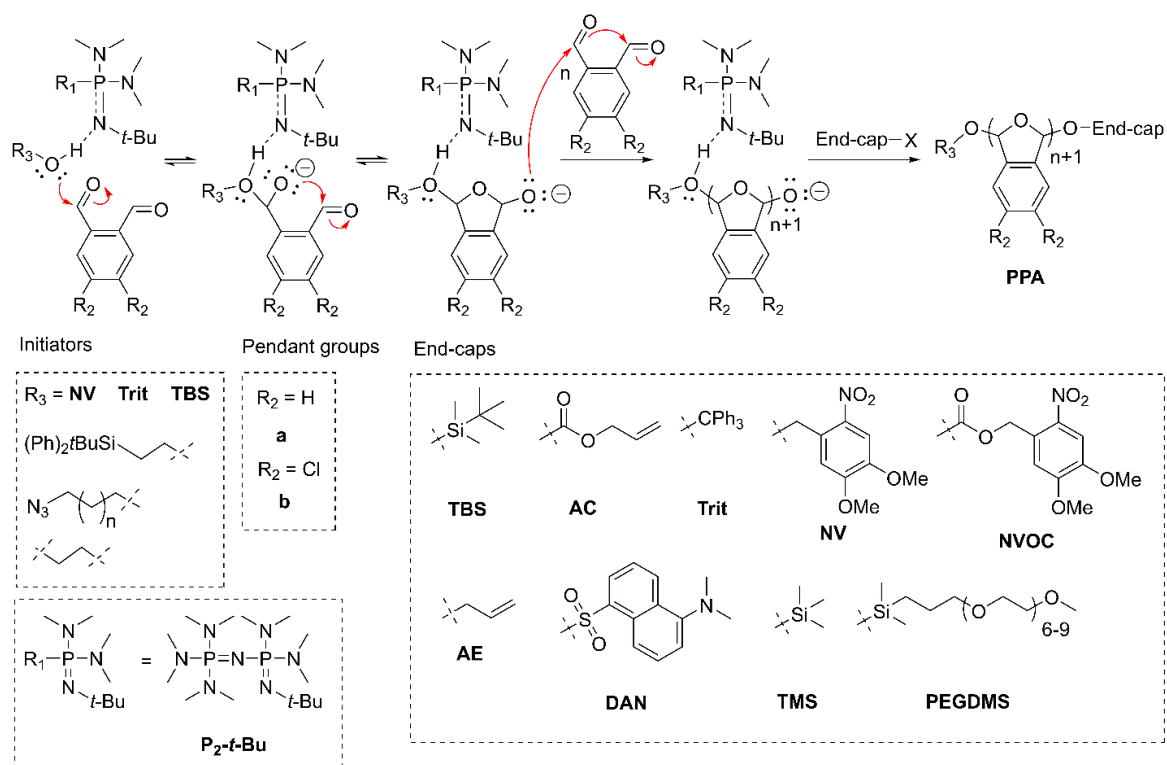
Moore and coworkers used cyclic PPAs for ion-triggered release of payloads from microcapsules.¹⁰³ The core-shell microcapsules were prepared by emulsification followed by rapid solvent evaporation, and were then suspended in acidic solutions with or without coactivating salts such as LiCl. The microcapsules selectively depolymerized in the presence of specific ions and released their contents due to a specific ion coactivation effect. Moore and coworkers also recently reported *o*-PPA-based composites which can be quantitatively recycled.¹⁰⁴ As PPAs are not thermally stable, a 14 min heat treatment at 120 °C was sufficient to fully disintegrate the composite and yield the monomer in addition to the reinforcing materials before reusing them to reproduce the identical composites (**Figure 1.19**). Even after three full cycles of depolymerization and repolymerization, the composites retained the same moduli (4.5 GPa) and tensile strengths (30 MPa).



Figure 1.19: Composites composed of carbon fiber and PPA (left) can be fully disintegrated to the starting carbon fiber (right, bottom) and *o*-PA (right, top) before the reproduction of the composite. Adapted with permission from reference 102. Copyright 2019, American Chemical Society.

1.4.2.2.2 Linear polyphthalaldehydes

Linear PPAs can be produced by anionic polymerization methods as the propagating species have only one charged terminus and thus the chance of cyclization by backbiting onto the other neutral terminus is negligible. In an early work, Aso and Tagami used anionic initiators including *t*-BuOLi, Na with naphthalene, and Na with benzophenone to prepare linear PPAs.¹⁰⁵ End-capping was performed with reagents such as acetic anhydride. Similar to *c*PPA, the backbones of linear PPAs can be cleaved using heat, acid, or mechanical force. To enable PPA cleavage using different stimuli, Phillips and coworkers incorporated different end-caps. Using an *n*-BuLi-initiated *o*-PA polymerization, they introduced fluoride ion-responsive *t*-butyldimethylsilyl (TBS) and Pd(0)-responsive allyl carbonate (AC) end-caps.¹⁰⁶ However, the polymerization reactions were slow (3–12 days) and showed a negative deviation from the targeted DP_n values. Building on a work by Hedrick, Knoll, and Coulembier, showing that phosphazene superbases served as suitable initiators for rapid and well-controlled polymerization of *o*-PA,¹⁰⁷⁻¹⁰⁸ Phillips and coworkers used P₂-*t*-Bu with functional alcohol initiators to successfully polymerize *o*-PA in 3 h, and directly installed stimuli-responsive end-caps (**Scheme 1.8**).¹⁰⁹⁻¹¹⁰ Depolymerization was successfully triggered using stimuli corresponding to the specific end-caps.



Scheme 1.8: Anionic polymerization of PAs using phosphazene and various responsive end-caps.

As the synthesis of different *o*-PA derivatives is tedious, a limited number of linear PPA derivatives have been reported. Phillips and coworkers used the phosphazene/alcohol initiated polymerization method to prepare poly(4,5-dichlorophthalaldehyde)s (**PPAb**, **Scheme 1.8**).¹¹¹ Post-polymerization modification is an alternative approach to modify the structure and properties of PPAs. Moore and coworkers used the phosphazene/alcohol initiated polymerization to copolymerize benzaldehyde derivatives with *o*-PA, resulting in random copolymers with functional groups for post-polymerization reactions.¹¹²⁻¹¹³ Pendant nitrophenyl, bromophenyl, aldehyde, alkene, alkyne, imine, and hydroxyl groups were then used for the formation of nanoparticles, networks, and graft copolymers.

As noted above, linear PPAs were investigated in early lithography applications with PAGs due to the intrinsic acid-sensitivity of their polyacetal backbones.⁹⁵⁻⁹⁶ More recently, Knoll and coworkers exploited their intrinsic thermo-sensitivity in thermal scanning probe

nanolithography (t-SPL).¹¹⁴⁻¹¹⁵ In this method, a cantilever, resting at *ca.* 300 nm above the surface, was heated to 700 °C and created a 3-D pattern by the thermal depolymerization of a PPA film. The pattern could also be transferred to the silicon substrate by reactive ion etching (RIE) (**Figure 1.20**).^{107, 116} Taking advantage of the high precision of t-SPL, a PPA pattern was created for a sorting device that separated 60- and 100-nm particles in opposing directions in seconds.¹¹⁷

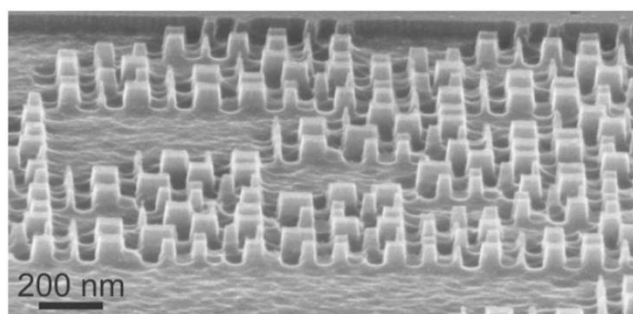


Figure 1.20:. Scanning electron micrograph of a nanoscale pattern prepared by t-SPL of a PPA film followed by transfer to a silicon substrate by RIE. Adapted with permission from reference 114. Copyright 2010, John Wiley and Sons.

Phillips and coworkers have employed PPA end-cap cleavage in their applications. In their early work, they prepared stimuli-responsive plastics *via* patterning of a TBS end-capped PPA within a control allyl ether (AE)-capped PPA (**PPAa-TBS** and **PPAa-AE**, **Scheme 1.8**).¹⁰⁶ The depolymerization of **PPAa-TBS** was induced with fluoride ion, and resulted in a cylindrical hole. Using **PPAa-TBS**, they also prepared microcapsules with aqueous cores containing fluorescein-labeled dextran.¹¹⁰ Exposure to fluoride ion resulted in holes in the capsule wall, causing release of the dextran. Exploiting its high stability, Phillips and coworkers later created multi-layered macroscopic patterns composed of **PPAb** with different stimuli-responsive end-caps.¹¹¹ Different layers were selectively degraded in the presence of specific stimuli such as Pd(0) and fluoride ion (**Figure 1.21**). They have also fabricated self-powered microscale pumps which generated flow based on the depolymerization of **PPAa-TBS** to soluble monomers in the presence of fluoride ions.¹¹⁸

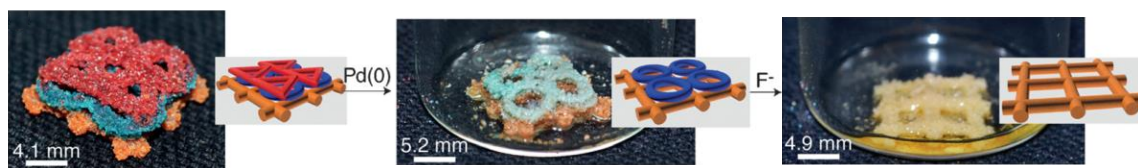


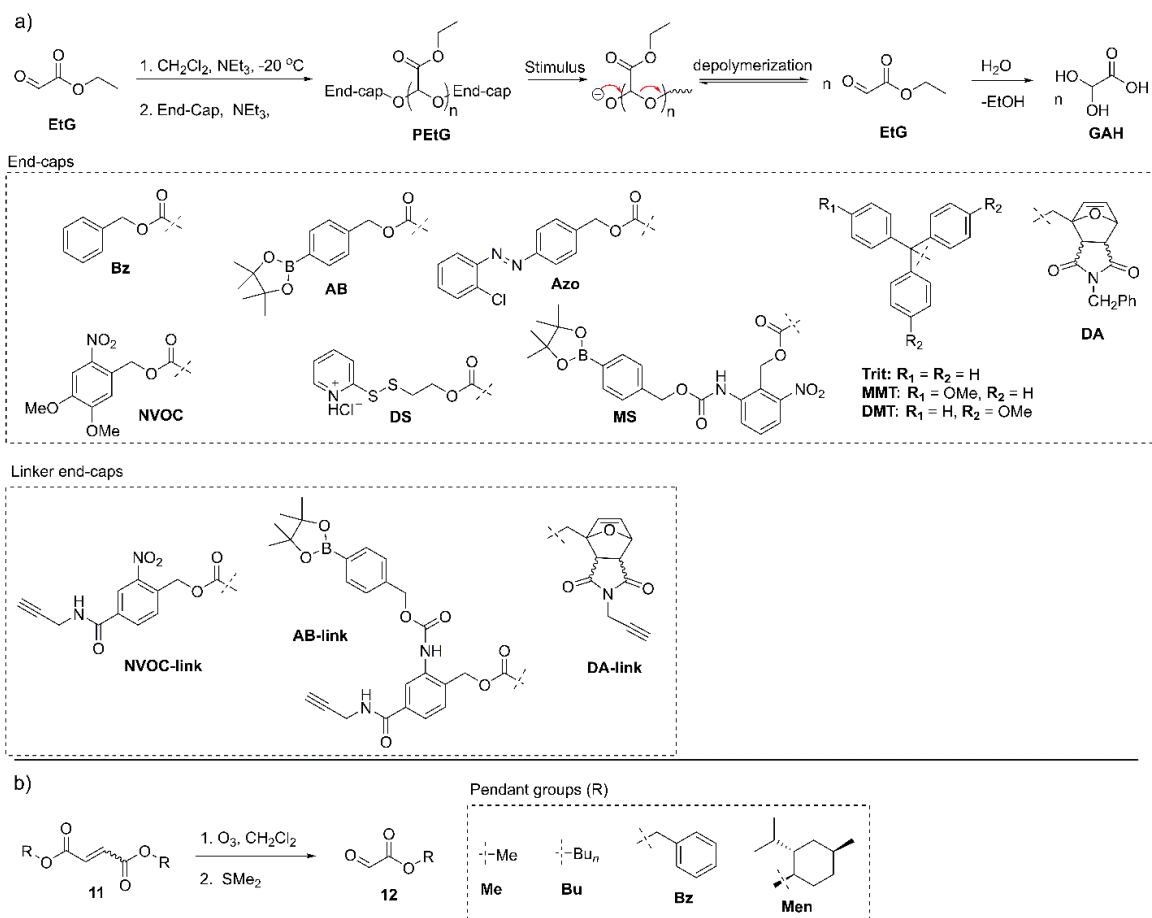
Figure 1.21: Visual ion sensors based on **PPAb** (red triangles, blue circles, and yellow grids are Pd(0), fluoride ion, and non-responsive PPAs respectively). Adapted with permission from reference 109. Copyright 2015, John Wiley and Sons.

1.4.2.3 Polyglyoxylates (PGs).

PGs are another class of polyaldehydes that exhibit low T_c , and consequently undergo depolymerization following an end-cap or backbone cleavage. Poly(ethyl glyoxylate) (PEtG),¹¹⁹ poly(methyl glyoxylate) (PMeG),¹²⁰ and poly(glyoxylic acid) salts¹²¹ were reported over the past few decades and were initially stabilized through end-capping with isocyanates or vinyl ethers. With these end-caps, PGs degraded gradually by the hydrolysis of the pendant esters, backbone acetal cleavage, and backbone depolymerization, leading to the corresponding alcohols and glyoxylic acid hydrate (GAH).¹²² The conversion of GAH to CO₂ occurs through the glyoxylic acid cycle, an anaerobic variant of the Krebs's cycle, which occurs in bacteria, plants, and protists. The degradation products of PEtG were found to be non-toxic to plants and also in an invertebrate model.¹²³ GAH is also a metabolic intermediate that can be processed in the human liver, so it is anticipated to be nontoxic at low concentrations.¹²⁴

In 2014, our group introduced stimuli-responsive end-caps to PGs to allow their triggered end-to-end depolymerization.¹²⁵ We polymerized ethyl glyoxylate (EtG) in CH₂Cl₂ using catalytic NEt₃ at -20 °C to afford **PEtG (Scheme 1.9a)**. Rigorous purification of the commercial EtG, through distillation over P₄O₁₀, was critical to depolymerize oligomers, and dehydrate the EtG hydrate. Based on size exclusion chromatography and end-group analysis using NMR spectroscopy, the polymerization is initiated by trace EtG hydrate. Thus, the molar mass of PGs is strongly dependent on the monomer purity. We have reported PEtGs with M_n values between ~5–250 kg/mol and D of 1.4–2.1. Initially, 6-nitroveratryl carbonate (**NVOC**) was introduced as a stimuli-responsive end-cap, allowing

depolymerization to be induced by UV light.¹²⁵ It was later expanded to other stimuli including reducing thiols (**DS**, **Azo**), H₂O₂ (**AB**), acid (**Trit**, **MMT**, **DMT**), heat (**DA**), and multiple stimuli (light, reducing agents, and H₂O₂; **MS**) (**Scheme 1.9a**).¹²⁶⁻¹²⁸



Scheme 1.9: (a) Synthesis of PETGs with different end-caps, its depolymerization back to monomer, and eventual monomer hydration and hydrolysis to afford GAH; (b) Synthesis of different glyoxylates from their fumaric or maleic acid esters.

In addition to **EtG**, other glyoxylate monomers were synthesized and polymerized. We prepared methyl glyoxylate (**MeG**), *n*-butyl glyoxylate (**BuG**), benzyl glyoxylate (**BzG**) and L-menthyl glyoxylate (**MenG**) from their corresponding maleic or fumaric diesters (**11**) by ozonolysis under reducing conditions (**Scheme 1.9**).^{125, 129} So far, a key criterion for obtaining pure monomer has been the ability to purify the glyoxylate by distillation over P₄O₁₀, at less than 165 °C, as the P₄O₁₀ drying byproduct H₃PO₄

contaminates the distillate at higher temperatures. Other drying agents such as CaH₂ resulted in slow cracking of oligomers and impure product.¹³⁰ In addition, the monomer precursors must be stable to ozonolysis, preventing the incorporation of double and triple bonds as pendant groups, as they would undesirably be cleaved by ozonolysis. We polymerized **MeG**, **BuG**, **BzG**, and **MenG**, and copolymerized them with **EtG**.^{125, 129} The homopolymers had low M_n (2.1–3.8 kg/mol), which can in some cases be attributed to steric hindrance (e.g., **BuG**, **MenG**). However, it has also been challenging to achieve purities as high as we achieved for EtG. With further optimization of the monomer distillation process, higher DP_n s will likely be achieved. In contrast, copolymers of the different glyoxylates with EtG typically had relatively high DP_n s (M_n ranging from 30–40 kg/mol), suggesting that this approach mitigates issues of monomer purity and steric hindrance.

In addition to the NEt₃-mediated polymerization method, anionic polymerization of glyoxylates has also been investigated. Moore and coworkers used *n*-BuLi as an initiator for EtG polymerization and end-capped the resulting polymer with phenyl isocyanate.¹³¹ However, the fact that the resulting polymer had two end-caps, based on NMR spectroscopy, suggested that the polymerization was not directly initiated from *n*-BuLi. Instead, EtG hydrate quickly quenched the *n*-BuLi, producing hydrate-based initiators that grew bidirectionally, resulting in two polymer termini that were later end-capped. To address this, we developed and reported a rigorous purification procedure for EtG and re-explored its anionic polymerization.¹³⁰ Initiation with *n*-BuLi at 20 °C, followed by cooling to -20 °C for 10 min, led to good dispersity values ($D \sim 1.5$) and good control over DP_n up to ~200 repeating units ($M_n \sim 20$ kg/mol). Beyond this, the concentration of added initiator became so low that even trace hydrate initiators became significant and the DP_n deviated from the expected value. Up to a DP_n of 200, the end-group fidelity was greater than 90%, dropping to 71% at a targeted DP_n of 400. Different alkyl-lithium reagents and alkoxides were also effective initiators.

Moore and coworkers have also investigated the cationic polymerization of EtG using different initiators such as $\text{BF}_3 \cdot \text{OEt}_2$, SnCl_4 , and Ph_3CBF_4 .¹³¹ No end groups were found on cationically synthesized PEtG, suggesting a cyclic structure. Based on mass spectrometry results, Lewis acid initiators and high monomer concentrations led to backbiting of the growing PEtG chain on a pendant ester, leading to loss of an ethyl group. On the other hand, lower concentrations and carbocationic initiators led to backbiting on the backbone acetal. Both cyclic and lariat-shaped polymers were formed. Cationic copolymerization of EtG and *o*-PA was used to reduce the brittleness of PPA and increase its thermal stability.¹³¹ The T_g and decomposition temperatures varied according to the ratio of monomers, with higher EtG leading to lower T_g and increased decomposition temperature.

PGs are attractive for biomedical applications as they eventually degrade to GAH, a metabolic intermediate. We prepared PEG-PEtG-PEG block copolymers by first introducing a linker end-cap containing both a photo-responsive moiety and a terminal alkyne (**Scheme 1.9a**, **NVOC-link**), and then attaching the PEG blocks using copper-assisted azide-alkyne cycloaddition (CuAAC).¹²⁵ The resulting amphiphilic block copolymers were self-assembled to form micelles in aqueous solutions. Irradiation with UV light led to the depolymerization and disintegration of the micelles in less than 1 hour. The approach was also extended to linker end-caps such as **DS** and **AB-link** (**Scheme 1.9a**), which are responsive to reducing thiols and H_2O_2 respectively.¹³² These stimuli are intrinsically present in the body and are associated with inflammation and cancer. Conjugation of PEG *via* disulfide exchange or CuAAC led to triblock copolymers that could also be self-assembled to form micelles. Treatment with the appropriate stimulus led to rapid depolymerization and micelle disintegration. The micelles were used to encapsulate Nile red, Dox, and curcumin. All payloads were rapidly released in the presence of low concentrations of stimuli, suggesting an amplification effect.

In the course of the work on PEG-PEtG-PEG micelles, we found that not all of the drugs we investigated could be encapsulated at high loadings into the PEtG micelle core. This

was addressed by changing the pendant groups on the PG block.¹²⁹ By incorporating **BuG**, **MenG**, or chloral (non-glyoxylate aldehyde), we tuned the hydrophobicity of the micelle core and its compatibility with the drug celecoxib. Cytotoxicity studies were performed on the micelles in MDA-MB-231 human breast cancer cells. The different glyoxylate systems had different effects on cell metabolic activity and the degraded (triggered) micelles had different effects than the intact micelles. However, caution must be used in interpreting the results of these studies, as it is known that degradation products such as glyoxylate and ethanol can be metabolized in the liver but not in MDA-MB-231 cells.¹²⁴

Using a thermally-triggerable PEG-PEtG-PEG triblock copolymer that was prepared using the **DA-link** end-cap (**Scheme 1.9a**), capable of undergoing a retro-Diels-Alder-elimination cascade, we also investigated the indirect triggering of nanoassemblies in collaboration with the Sandre group.¹²⁷ A 63 kg/mol PEtG block was coupled to either 750 or 5000 g/mol PEG, leading to vesicle and micellar assemblies respectively (**Figure 1.22a,b**). Direct triggering of PEtG was achieved by heating the assemblies at 75 °C. For indirect triggering, we encapsulated iron oxide nanoparticles (IONPs) into the micelle cores (**Figure 1.22c**). Oscillating magnetic fields are known to induce localized heating around IONPs, an effect termed magnetic field hyperthermia (MFH).¹³³ MFH led to a rapid increase in particle diameter and decrease in DLS count rate for the IONP-loaded micelles, which was attributed to their depolymerization followed by aggregation and sedimentation of the released hydrophobic IONPs.

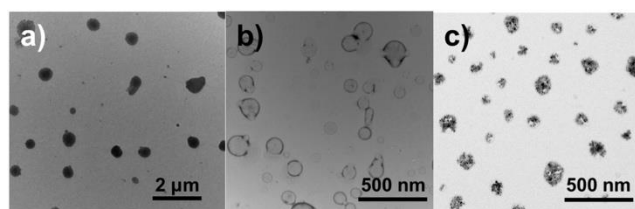


Figure 1.22: TEM images of assemblies formed from thermo-responsive PEG-PEtG-PEG triblock copolymers (a) micelles; (b) vesicles; (c) IONP-loaded micelles. Adapted from reference 125 with permission from The Royal Society of Chemistry.

We also prepared PEtG-based particles for drug delivery applications by using an emulsion process.¹³⁴ We blended PEtG with PLA to achieve a two-stage release process, where a portion of loaded drug was released through an initial triggered depolymerization of PEtG, and a slower second-stage release occurred through the gradual degradation of PLA. Both **NVOC** and **DS** end-capped PEtG were used and gave particles with diameters of 130–150 nm. The particles were loaded with Nile red as a probe and with the drug celecoxib. In each case, the extent of release following triggering with the stimulus (UV light or DTT) increased with an increasing PEtG:PLA ratio, showing in principle that the extent of initial release could be tuned according to the particle composition. However, in cytotoxicity studies with MDA-MB-231 cells we found that the sodium cholate surfactant was relatively toxic. Thus, less toxic surfactant should be used in future studies.

While the above work involved PG-based assemblies in solution, we also investigated the solid state depolymerization of PEtG. For example, **PEtG-NVOC** (**Scheme 1.9**) films were immersed in aqueous buffer solutions at pH 3 to 8.¹²⁸ For irradiated films, the percent degradation depended on the pH, with pH 5 being the fastest, consistent with a hemiacetal fragmentation mechanism. The degradation time was also dependent on the film thickness. For instance, a 25 μm thick film required 3 days for complete erosion and increasing the film thickness to 150 μm increased the time to 10 days. Another determining factor was the temperature as much faster erosion was observed at 30 °C compared to that at 20 °C. We also found that the percent degradation was not dependent on the presence of water, and complete depolymerization was observed in the dry solid state.¹²⁸ In the absence of water, the monomer remains unhydrated. With a boiling point of 110 °C, EtG can readily evaporate from the surface. We used this feature to demonstrate single step micropatterning as well as a depolymerization-repolymerization sequence.

While **PEtG-NVOC** films are very stable in the absence of UV light, we observed that trityl end-capped PEtGs such as **PEtG-MMT** and **PEtG-DMT** (**Scheme 1.7a**) were surprisingly unstable in the solid state.¹³⁵ For example, films of **PEtG-DMT** were stable for more than 30 days at 6 °C, but completely degraded in less than 5 days at 30 °C. **PEtG-**

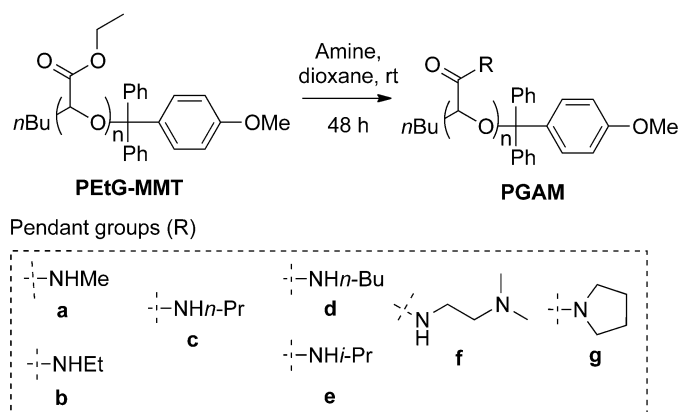
MMT films were more stable, requiring more than 30 days for complete depolymerization at 30 °C. We attributed this behavior to an equilibrium between the capped and uncapped polymer, the position of which depends on the stability of the corresponding trityl cation. In the uncapped state, depolymerization occurs and is irreversible due to evaporation of monomer from the surface. To demonstrate the potential application of the system as a thermal history sensor, we incorporated Nile red and IR-780 dyes into the films. Depolymerization led to aggregation of the dyes and changed the colour of the films. We envision that these materials can potentially be used for smart packaging applications.

PEtG is an amorphous polymer with low T_g of about -10 °C. Therefore, it forms tacky and rubbery coatings at ambient temperatures. To improve its properties, we recently blended **PEtG-NVOC** with polyesters including polycaprolactone (PCL), poly(lactic acid) and poly(R-3-hydroxybutyrate).¹³⁶ We found that PEtG exhibited micro-scale phase separation with the polyesters, resulting in glassy or crystalline polyester domains. The mechanical properties of the blends were intermediate between those of the corresponding homopolymers, indicating that it was possible to tune the physical properties of the films through blending and to achieve non-tacky films. For example, while PCL had a Young's modulus of 490 MPa and tensile strength of 13 MPa, the 50:50 PCL:PEtG blend has values of 192 MPa and 5 MPa respectively. Mass loss studies and SEM images of the films showed that light-triggered degradation of the PEtG blocks was achieved, leaving a porous matrix of polyester that eroded more slowly. These coatings may be useful for the controlled release of drugs or fertilizers, as the payload may be released through the porous eroded film.

1.4.2.4 Polyglyoxylamides (PGAMs)

We recently reported PGAMs as a new class of SIPs with the aim of removing the hydrolytically labile pendant esters of PGs and enabling further structure-property tuning.¹²⁶ The PGAMs were synthesized by the reaction of PEtG with different amines at ambient temperatures for 48 hours (**Scheme 1.10**). High (> 95%) conversions of the esters to amides were obtained with a variety of primary amines, and with the secondary amine

pyrrolidine. Other secondary amines led to lower conversions, suggesting steric hindrance impeded the reaction. Another consideration is that the PEtG end-cap must be stable under the amidation conditions. For example, the carbonate-based end-caps were cleaved during the amidation, leading to depolymerization, while trityl end-caps were stable. The depolymerization mechanism for PGAMs is the same as that of the polyglyoxylates, involving hemiacetal degradation, and produces the corresponding glyoxylamide hydrates as depolymerization products.



Scheme 1.10: Synthesis of PGAMs with different pendant groups starting from PEtG with a MMT end-cap.

The PGAMs had very different properties than their corresponding esters. For example, PMeG and PEtG have T_g values of 25 and -9 °C respectively,¹²⁵ whereas poly(methyl glyoxylamide) (**PGAMa**) and poly(ethyl glyoxylamide) (**PGAMB**) have T_g values of 90 and 85 °C respectively.¹²⁶ These differences can be attributed to the abilities of the PGAMs to form hydrogen bonds. Some PGAMs (**PGAMa,f,g**) were soluble in water, opening opportunities for applications requiring water solubility. For example, in collaboration with Ree and Kelland we reported the study of PGAMs as kinetic hydrate inhibitors for the prevention of gas hydrate plugging in oil and gas lines.¹³⁷ Overall, there are many potential applications of PGAMs that remain unexplored. However, the limited availability of end-caps that are stable to the amidation reaction, yet undergo stimuli-selective cleavage is an ongoing challenge that must be addressed to fully exploit the PGAMs.

1.5 Aqueous self-assembly of block copolymers

Blends of different polymers with different physical properties can undergo phase separation. Phase separation of polymers is driven by thermodynamically-favourable interactions between polymers of the same identity and unfavourable interactions between different polymers, and often leads to macrophase separation of polymer mixtures.¹³⁸ When two polymers with different physical properties are covalently joined to create block copolymers they are now unable to undergo macrophase separation, but will undergo microphase separation.¹³⁹ Given the appropriate conditions, the polymers will achieve the most thermodynamically favourable arrangement.¹⁴⁰ This self-assembly behaviour has been extensively studied and can occur in either the solid state or in a solution. Aqueous self-assembly will be discussed as it pertains to this thesis.

Block copolymers that undergo self-assembly in solution are referred to as amphiphilic, as they typically have a distinct hydrophobic and hydrophilic region.¹³⁸ A driving factor of aqueous self-assembly is that one of the blocks is soluble in water (hydrophilic) and will orient its self on the periphery of the self-assembled structure, while the other block is insoluble (hydrophobic) and will be on the inside of the structure.¹⁴⁰ This thesis will discuss self-assembly in aqueous environments, but any solvent could potentially be used to induce self-assembly. A less common situation is when double-hydrophilic block copolymers undergo self-assembly by modifying conditions such as temperature,¹⁴¹⁻¹⁴² pH,¹⁴³ ionic strength, or the addition of a complexation additive.¹⁴⁴ This is how self-assembly occurs for some PDMAEMA and PNIPAAm block copolymers.

For block copolymers to aggregate in solution, they must first achieve a minimum concentration, called the critical aggregation concentration (CAC).¹³⁸ Below the CAC, the polymer will be molecularly dissolved in solution, and above the CAC, assemblies will begin to form, with an equilibrium existing between polymers both in and outside of the assemblies. The main factor determining the CAC in aqueous solution is the length of the hydrophobic block in an amphiphilic block copolymer, as the interactions between the hydrophobic block drive core formation and associated self-assembly architecture.^{138, 140}

Once the CAC has been achieved, there are a number of morphologies that can be obtained. The self-assembly of block copolymers in solution is largely controlled by three factors: packing of the core forming block, the interfacial energy between the core and the solvent, and the packing interactions of the coronal chains.¹⁴⁰ Which morphology is formed is predominantly determined by the hydrophilic volume fraction, and how it relates to the curvature of the surface. This relationship has been extensively studied by Eisenberg and coworkers on block copolymers of polystyrene-*b*-poly(acrylic acid) (PS-*b*-PAA).¹⁴⁰ The longer the hydrophilic block (PAA), the larger the hydrophilic volume fraction, the larger the curvature of the surface which will encourage the formation of lower order morphologies, such as micelles. In contrast, the smaller the PAA block, the more likely higher order morphologies (*e.g.* rod-like micelles, vesicles, and lamella structures) will occur, which can be attributed to the lower interfacial curvature caused by the smaller coronal interactions (**Figure 1.17**). The interfacial energy between the core and the solvent will influence the morphologies in the early stages of formations. As water is added, the energy of the packing of the core chains is minimized through arrangement into particles with different morphologies, if the core chains are effectively swelled by a non-selective solvent.

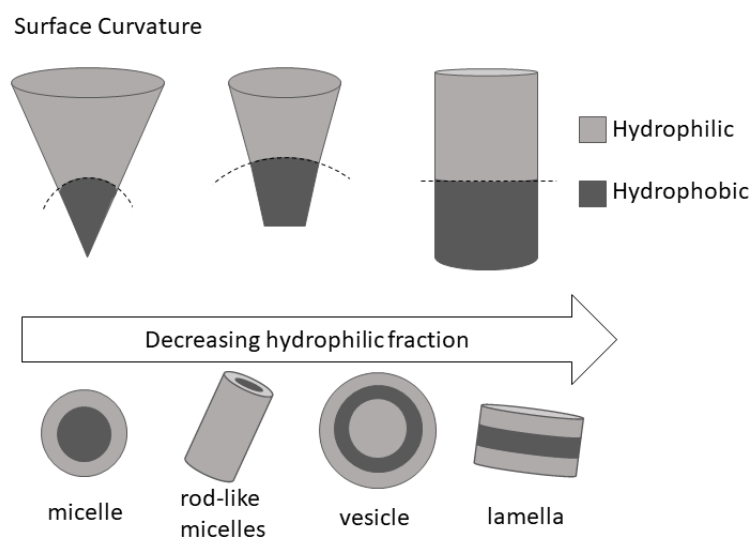


Figure 1.23: Influence of the interfacial curvature on the available morphologies of amphiphilic block copolymers, and representative morphologies.

1.6 Scope of thesis

This thesis will focus on improvements to two of the major SIP classes: polycarbamates and polyglyoxylates.

Studies combining SIPs with other stimuli-responsive blocks to create amphiphilic block copolymers had not been reported. Although work has been reported on tuning the depolymerization behavior of polycarbamates by adding cyclizing spacers, preparing multi-stimuli-responsive SIPs to study the properties of these systems and understand how one triggering event could affect another, and possibly control the percent depolymerization, was of interest. The motivation behind this work was foundational proof of concept. In addition, while polyglyoxylates had been reported, they had limited structural diversity due to the requirement to prepare and polymerize different monomers. The aim of one project in this thesis was to access synthetic diversity in a more efficient manner using transesterification. The motivation behind this work was to develop a universal method of creating previously inaccessible polyglyoxylates with unique chemical and physical properties. This would allow for the creation of new polyglyoxylates in the future with unique properties that could be used in more applications than currently available to poly(ethyl glyoxylate).

Chapter 2 will focus on the synthesis of multi-stimuli-responsive amphiphilic block copolymers and their self-assembly. The block copolymer is composed of a hydrophobic polycarbamate block and a pH- and thermo-responsive PDMAEMA as the hydrophilic block. Added stimuli-responsive behaviour was introduced by the synthesis and subsequent incorporation of a novel UV-responsive linker or a non-responsive control linker between the blocks. The effects of pH, temperature, and UV light on the depolymerization behaviour of the SIP block were evaluated, with a focus on how the chain-collapse of PDMAEMA above its LCST affected the depolymerization behaviour.

Chapter 3 is an extension of Chapter 2 and explores the effect of thermo-responsive PNIPAAm as the hydrophilic block in a block copolymer with a hydrophobic

polycarbamate. As PNIPAAm has a lower LCST than the previously discussed PDMAEMA, the effects of chain-collapse on this SIP depolymerization were studied at lower temperatures.

Chapter 4 explores the transesterification of poly(ethyl glyoxylate) with a guanidine base catalyst 1,5,7-triazabicyclo[4.4.0]dec-5-ene (TBD). Transesterification was only possible due to novel end-capping and synthetic methods for poly(ethyl glyoxylate). Transesterification eliminated issues with the purification of monomers discussed in Chapter 4 and allowed the creation of functionalized polyglyoxylates that could undergo further modification using click reactions. It also allowed for the elucidation of trends in the thermal properties of polyglyoxylate systems.

1.7 References

1. Hosler, D.; Burkett, S. L.; Tarkanian, M. J., Prehistoric Polymers: Rubber Processing in Ancient Mesoamerica. *Science* **1999**, *284*, 1988–1991.
2. Hyatt, J. W., Address of Acceptance. *J. Ind. Eng. Chem.* **1914**, *6*, 158–161.
3. Baekeland, L. H., The Synthesis, Constitution, and Uses of Bakelite. *J. Ind. Eng. Chem.* **1909**, *1*, 149–161.
4. Bolton, E. K., Chemical Industry Medal. Development of Nylon. *Ind. Eng. Chem.* **1942**, *34*, 53–58.
5. Geyer, R.; Jambeck, J. R.; Law, K. L., Production, Use, and Fate of All Plastics Ever Made. *Sci. Adv.* **2017**, *3*, e1700782.
6. Wei, M.; Gao, Y.; Li, X.; Serpe, M. J., Stimuli-Responsive Polymers and Their Applications. *Polym. Chem.* **2017**, *8*, 127–143.
7. Kocak, G.; Tuncer, C.; Bütün, V., pH-Responsive Polymers. *Polym. Chem.* **2017**, *8*, 144–176.
8. Paek, K.; Yang, H.; Lee, J.; Park, J.; Kim, B. J., Efficient Colorimetric pH Sensor Based on Responsive Polymer–Quantum Dot Integrated Graphene Oxide. *ACS Nano* **2014**, *8*, 2848–2856.
9. Seok Lee, K.; In, I.; Young Park, S., pH and Redox Responsive Polymer For Antifouling Surface Coating. *Appl. Surf. Sci.* **2014**, *313*, 532–536.

10. Brunsen, A.; Díaz, C.; Pietrasanta, L. I.; Yameen, B.; Ceolín, M.; Soler-Illia, G. J. A. A.; Azzaroni, O., Proton and Calcium-Gated Ionic Mesochannels: Phosphate-Bearing Polymer Brushes Hosted in Mesoporous Thin Films As Biomimetic Interfacial Architectures. *Langmuir* **2012**, *28*, 3583–3592.
11. Schmaljohann, D., Thermo- and pH-Responsive Polymers in Drug Delivery. *Adv. Drug Deliv. Rev.* **2006**, *58*, 1655–1670.
12. Deirram, N.; Zhang, C.; Kermaniyan, S. S.; Johnston, A. P. R.; Such, G. K., pH-Responsive Polymer Nanoparticles for Drug Delivery. *Macromol. Rapid Commun.* **2019**, *40*, 1800917.
13. Alarcón, C. d. I. H.; Pennadam, S.; Alexander, C., Stimuli Responsive Polymers for Biomedical Applications. *Chem. Soc. Rev.* **2005**, *34*, 276–285.
14. Zheng, J. Y.; Tan, M. J.; Thoniyot, P.; Loh, X. J., Unusual Thermogelling Behaviour of Poly[2-(imethylamino)ethyl methacrylate] (PDMAEMA)-Based Polymers Polymerized in Bulk. *RSC Adv.* **2015**, *5*, 62314–62318.
15. Bertrand, O.; Gohy, J.-F., Photo-Responsive Polymers: Synthesis and Applications. *Polym. Chem.* **2017**, *8*, 52–73.
16. Jochum, F. D.; Theato, P., Temperature- and Light-Responsive Smart Polymer Materials. *Chem. Soc. Rev.* **2013**, *42*, 7468–7483.
17. Kumar, S.; Allard, J.-F.; Morris, D.; Dory, Y. L.; Lepage, M.; Zhao, Y., Near-Infrared Light Sensitive Polypeptide Block Copolymer Micelles for Drug Delivery. *J. Mater. Chem.* **2012**, *22*, 7252–7257.
18. Kumar, G. S.; Neckers, D. C., Photochemistry of azobenzene-containing polymers. *Chem. Rev.* **1989**, *89*, 1915–1925.
19. Wang, K.; Yin, L.; Miu, T.; Liu, M.; Zhao, Y.; Chen, Y.; Zhou, N.; Zhang, W.; Zhu, X., Design and Synthesis of a Novel Azobenzene-Containing Polymer Both in the Main- and Side-Chain Toward Unique Photocontrolled Isomerization Properties. *Mater. Chem. Front.* **2018**, *2*, 1112–1118.
20. Klajn, R., Spiropyran-Based Dynamic Materials. *Chem. Soc. Rev.* **2014**, *43*, 148–184.
21. Achilleos, D. S.; Vamvakaki, M., Multiresponsive Spiropyran-Based Copolymers Synthesized by Atom Transfer Radical Polymerization. *Macromolecules* **2010**, *43*, 7073–7081.

22. Shiraishi, Y.; Miyamoto, R.; Hirai, T., Spiropyran-Conjugated Thermoresponsive Copolymer as a Colorimetric Thermometer with Linear and Reversible Color Change. *Org. Lett.* **2009**, *11*, 1571–1574.
23. Cembran, A.; Bernardi, F.; Garavelli, M.; Gagliardi, L.; Orlandi, G., On the Mechanism of the cis–trans Isomerization in the Lowest Electronic States of Azobenzene: S0, S1, and T1. *J. Am. Chem. Soc.* **2004**, *126*, 3234–3243.
24. Lin, S.; Theato, P., CO₂-Responsive Polymers. *Macromol. Rapid Commun.* **2013**, *34*, 1118–1133.
25. Hu, L.; Zhang, Q.; Li, X.; Serpe, M. J., Stimuli-Responsive Polymers for Sensing and Actuation. *Mater. Horiz.* **2019**.
26. Xu, M.; Liu, L.; Hu, J.; Zhao, Y.; Yan, Q., CO-Signaling Molecule-Responsive Nanoparticles Formed from Palladium-Containing Block Copolymers. *ACS Macro Lett.* **2017**, *6*, 458–462.
27. Xu, M.-M.; Liu, R.-J.; Yan, Q., Biological Stimuli-Responsive Polymer Systems: Design, Construction and Controlled Self-assembly. *Chin. J. Polym. Sci.* **2018**, *36*, 347–365.
28. Zhang, Q.; Lei, L.; Zhu, S., Gas-Responsive Polymers. *ACS Macro Lett.* **2017**, *6*, 515–522.
29. Li, Y.; Zhu, L.; Grishkewich, N.; Tam, K. C.; Yuan, J.; Mao, Z.; Sui, X., CO₂-Responsive Cellulose Nanofibers Aerogels for Switchable Oil–Water Separation. *ACS Appl. Mater. Interfaces* **2019**, *11*, 9367–9373.
30. Haward, M., Plastic Pollution of the World’s Seas and Oceans as a Contemporary Challenge in Ocean Governance. *Nat. Commun.* **2018**, *9*, 667.
31. Rochman, C. M., Microplastics Research—From Sink to Source. *Science* **2018**, *360*, 28–29.
32. Nicolas, J.; Mura, S.; Brambilla, D.; Mackiewicz, N.; Couvreur, P., Design, Functionalization Strategies and Biomedical Applications of Targeted Biodegradable/Biocompatible Polymer-Based Nanocarriers for Drug Delivery. *Chem. Soc. Rev.* **2013**, *42*, 1147–1235.
33. Langer, R.; Vacanti, J., Advances in Tissue Engineering. *J. Pediatr. Surg.* **2016**, *51*, 8–12.
34. Pushpamalar, J.; Veeramachineni, A. K.; Owh, C.; Loh, X. J., Biodegradable Polysaccharides for Controlled Drug Delivery. *ChemPlusChem* **2016**, *81*, 504–514.

35. Tyler, B.; Gullotti, D.; Mangraviti, A.; Utsuki, T.; Brem, H., Polylactic Acid (PLA) Controlled Delivery Carriers for Biomedical Applications. *Adv. Drug Deliv. Rev.* **2016**, *107*, 163–175.
36. Pitt, G. G.; Gratzl, M. M.; Kimmel, G. L.; Surles, J.; Sohindler, A., Aliphatic Polyesters II. The Degradation of Poly (DL-lactide), Poly (ϵ -caprolactone), and Their Copolymers In Vivo. *Biomaterials* **1981**, *2*, 215–220.
37. Guo, S.; Nakagawa, Y.; Barhoumi, A.; Wang, W.; Zhan, C.; Tong, R.; Santamaria, C.; Kohane, D. S., Extended Release of Native Drug Conjugated in Polyketal Microparticles. *J. Am. Chem. Soc.* **2016**, *138*, 6127–6130.
38. Kuppusamy, P.; Li, H.; Ilangovan, G.; Cardounel, A. J.; Zweier, J. L.; Yamada, K.; Krishna, M. C.; Mitchell, J. B., Noninvasive Imaging of Tumor Redox Status and Its Modification by Tissue Glutathione Levels. *Cancer Res.* **2002**, *62*, 307–312.
39. Emilriti, E.; Ranucci, E.; Ferruti, P., New Poly(amidoamine)s Containing Disulfide Linkages in Their Main Chain. *J. Polym. Sci., Part A: Polym. Chem.* **2005**, *43*, 1404–1416.
40. Tsarevsky, N. V.; Matyjaszewski, K., Reversible Redox Cleavage/Coupling of Polystyrene with Disulfide or Thiol Groups Prepared by Atom Transfer Radical Polymerization. *Macromolecules* **2002**, *35*, 9009–9014.
41. Li, C.; Madsen, J.; Armes, S. P.; Lewis, A. L., A New Class of Biochemically Degradable, Stimulus-Responsive Triblock Copolymer Gelators. *Angew. Chem. Int. Ed.* **2006**, *45*, 3510–3513.
42. Quinn, J. F.; Whittaker, M. R.; Davis, T. P., Glutathione Responsive Polymers and Their Application in Drug Delivery Systems. *Polym. Chem.* **2017**, *8*, 97–126.
43. Wu, J.; Zhao, L.; Xu, X.; Bertrand, N.; Choi, W. I.; Yameen, B.; Shi, J.; Shah, V.; Mulvale, M.; MacLean, J. L.; Farokhzad, O. C., Hydrophobic Cysteine Poly(disulfide)-Based Redox-Hypersensitive Nanoparticle Platform for Cancer Theranostics. *Angew. Chem. Int. Ed.* **2015**, *54*, 9218–9223.
44. Honda, S.; Tanaka, N.; Toyota, T., Synthesis of Star-Shaped Poly(n-butyl acrylate) Oligomers with Coumarin End Groups and their Networks for a UV-Tunable Viscoelastic Material. *J. Polym. Sci., Part A: Polym. Chem.* **2018**, *56*, 9–15.
45. Zhao, H.; Sterner, E. S.; Coughlin, E. B.; Theato, P., o-Nitrobenzyl Alcohol Derivatives: Opportunities in Polymer and Materials Science. *Macromolecules* **2012**, *45*, 1723–1736.
46. Olejniczak, J.; Chan, M.; Almutairi, A., Light-Triggered Intramolecular Cyclization in Poly(lactic-co-glycolic acid)-Based Polymers for Controlled Degradation. *Macromolecules* **2015**, *48*, 3166–3172.

47. Goodwin, A. P.; Mynar, J. L.; Ma, Y.; Fleming, G. R.; Fréchet, J. M. J., Synthetic Micelle Sensitive to IR Light via a Two-Photon Process. *J. Am. Chem. Soc.* **2005**, *127*, 9952–9953.
48. Klán, P.; Šolomek, T.; Bochet, C. G.; Blanc, A.; Givens, R.; Rubina, M.; Popik, V.; Kostikov, A.; Wirz, J., Photoremovable Protecting Groups in Chemistry and Biology: Reaction Mechanisms and Efficacy. *Chem. Rev.* **2013**, *113*, 119-191.
49. Bamford, C. H.; Norrish, R. G. W., 359. Primary photochemical reactions. Part VII. Photochemical decomposition of isovaleraldehyde and di-n-propyl ketone. *Journal of the Chemical Society (Resumed)* **1935**, 1504-1511.
50. Sagi, A.; Weinstain, R.; Karton, N.; Shabat, D., Self-Immolative Polymers. *J. Am. Chem. Soc.* **2008**, *130*, 5434–5435.
51. Phillips, S. T.; DiLauro, A. M., Continuous Head-to-Tail Depolymerization: An Emerging Concept for Imparting Amplified Responses to Stimuli-Responsive Materials. *ACS Macro Lett.* **2014**, *3*, 298–304.
52. DeWit, M. A.; Gillies, E. R., A Cascade Biodegradable Polymer Based on Alternating Cyclization and Elimination Reactions. *J. Am. Chem. Soc.* **2009**, *131*, 18327–18334.
53. Roth, M. E.; Green, O.; Gnaim, S.; Shabat, D., Dendritic, Oligomeric, and Polymeric Self-Immolative Molecular Amplification. *Chem. Rev.* **2016**, *116*, 1309–1352.
54. Wong, A. D.; DeWit, M. A.; Gillies, E. R., Amplified Release Through the Stimulus Triggered Degradation of Self-immolative Oligomers, Dendrimers, and Linear Polymers. *Adv. Drug Deliv. Rev.* **2012**, *64*, 1031–1045.
55. Peterson, G. I.; Larsen, M. B.; Boydston, A. J., Controlled Depolymerization: Stimuli-Responsive Self-Immolative Polymers. *Macromolecules* **2012**, *45*, 7317–7328.
56. Amir, R. J.; Pessah, N.; Shamis, M.; Shabat, D., Self-Immolative Dendrimers. *Angew. Chem. Int. Ed.* **2003**, *42*, 4494–4499.
57. de Groot, F. M. H.; Albrecht, C.; Koekkoek, R.; Beusker, P. H.; Scheeren, H. W., "Cascade-Release Dendrimers" Liberate All End Groups Upon a Single Triggering Event in the Dendritic Core. *Angew. Chem. Int. Ed.* **2003**, *42*, 4490–4494.
58. Li, S.; Szalai, M. L.; Kevitch, R. M.; McGrath, D. V., Dendrimer Disassembly by Benzyl Ether Depolymerization. *J. Am. Chem. Soc.* **2003**, *125*, 10516–10517.
59. Wu, Y.; Zhang, L.; Zhang, M.; Liu, Z.; Zhu, W.; Zhang, K., Bottlebrush Polymers With Self-Immolative Side Chains. *Polym. Chem.* **2018**, *9*, 1799–1806.

60. Carl, P. L.; Chakravarty, P. K.; Katzenellenbogen, J. A., A Novel Connector Linkage Applicable in Prodrug Design. *J. Med. Chem.* **1981**, *24*, 479–480.
61. Peterson, G. I.; Church, D. C.; Yakelis, N.; Boydston, A., 1,2-Oxazine Linker as a Thermal Trigger for Self-Immolative Polymers. *Polymer* **2014**, *55*, 5980–5985.
62. Wong, A. D.; Güngör, T. M.; Gillies, E. R., Multiresponsive Azobenzene End-Cap for Self-Immolative Polymers. *ACS Macro Lett.* **2014**, *3*, 1191–1195.
63. Weinstain, R.; Sagi, A.; Karton, N.; Shabat, D., Self-Immolative Comb-Polymers: Multiple-Release of Side-Reporters by a Single Stimulus Event. *Chem. - Eur. J.* **2008**, *14*, 6857–6861.
64. Robbins, J. S.; Schmid, K. M.; Phillips, S. T., Effects of Electronics, Aromaticity, and Solvent Polarity on the Rate of Azaquinone–Methide-Mediated Depolymerization of Aromatic Carbamate Oligomers. *J. Org. Chem.* **2013**, *78*, 3159–3169.
65. Esser-Kahn, A. P.; Sottos, N. R.; White, S. R.; Moore, J. S., Programmable Microcapsules from Self-Immolative Polymers. *J. Am. Chem. Soc.* **2010**, *132*, 10266–10268.
66. Liu, G.; Wang, X.; Hu, J.; Zhang, G.; Liu, S., Self-Immolative Polymersomes for High-Efficiency Triggered Release and Programmed Enzymatic Reactions. *J. Am. Chem. Soc.* **2014**, *136*, 7492–7497.
67. Gnaim, S.; Shabat, D., Self-Immolative Chemiluminescence Polymers: Innate Assimilation of Chemiexcitation in a Domino-like Depolymerization. *J. Am. Chem. Soc.* **2017**, *139*, 10002–10008.
68. Scrimin, P.; Prins, L. J., Sensing Through Signal Amplification. *Chem. Soc. Rev.* **2011**, *40*, 4488–4505.
69. Saari, W. S.; Schwering, J. E.; Lyle, P. A.; Smith, S. J.; Engelhardt, E. L., Cyclization-Activated Prodrugs. Basic Carbamates of 4-Hydroxyanisole. *J. Med. Chem.* **1990**, *33*, 97–101.
70. Chen, E. K. Y.; McBride, R. A.; Gillies, E. R., Self-Immolative Polymers Containing Rapidly Cyclizing Spacers: Toward Rapid Depolymerization Rates. *Macromolecules* **2012**, *45*, 7364–7374.
71. de Gracia Lux, C.; McFearin, C. L.; Joshi-Barr, S.; Sankaranarayanan, J.; Fomina, N.; Almutairi, A., Single UV or Near IR Triggering Event Leads to Polymer Degradation into Small Molecules. *ACS Macro Lett.* **2012**, *1*, 922–926.
72. Penczek, S.; Load, G., Glossary of Terms Related to Kinetics, Thermodynamics, and Mechanisms of Polymerization. *Pure Appl. Chem.* **2008**, *80*, 2163–2193.

73. Uno, T.; Minari, M.; Kubo, M.; Itoh, T., Asymmetric Anionic Polymerization of 2,6-Dimethyl-7-phenyl-1,4-benzoquinone Methide. *J. Polym. Sci. A Polym. Chem.* **2004**, *42*, 4548–4555.
74. Olah, M. G.; Robbins, J. S.; Baker, M. S.; Phillips, S. T., End-Capped Poly(benzyl ethers): Acid and Base Stable Polymers That Depolymerize Rapidly from Head-to-Tail in Response to Specific Applied Signals. *Macromolecules* **2013**, *46*, 5924–5928.
75. Baker, M. S.; Kim, H.; Olah, M. G.; Lewis, G. G.; Phillips, S. T., Depolymerizable Poly(benzyl ether)-Based Materials for Selective Room Temperature Recycling. *Green Chem.* **2015**, *17*, 4541–4545.
76. Ergene, C.; Palermo, E. F., Self-Immolative Polymers With Potent and Selective Antibacterial Activity by Hydrophilic Side Chain Grafting. *J. Mater. Chem. B* **2018**, *6*, 7217–7229.
77. Ergene, C.; Palermo, E. F., Cationic Poly(benzyl ether)s as Self-Immolative Antimicrobial Polymers. *Biomacromolecules* **2017**, *18*, 3400–3409.
78. Xiao, Y.; Li, H.; Zhang, B.; Cheng, Z.; Li, Y.; Tan, X.; Zhang, K., Modulating the Depolymerization of Self-Immolative Brush Polymers with Poly(benzyl ether) Backbones. *Macromolecules* **2018**, *51*, 2899–2905.
79. Yeung, K.; Kim, H.; Mohapatra, H.; Phillips, S. T., Surface-Accessible Detection Units in Self-Immolative Polymers Enable Translation of Selective Molecular Detection Events into Amplified Responses in Macroscopic, Solid-State Plastics. *J. Am. Chem. Soc.* **2015**, *137*, 5324–5327.
80. Xiao, Y.; Li, Y.; Zhang, B.; Li, H.; Cheng, Z.; Shi, J.; Xiong, J.; Bai, Y.; Zhang, K., Functionalizable, Side Chain-Immolative Poly(benzyl ether)s. *ACS Macro Lett.* **2019**, *8*, 399–402.
81. Palermo, E. F.; Lienkamp, K.; Gillies, E. R.; Ragona, P. J., Antibacterial Activity of Polymers: Discussions on the Nature of Amphiphilic Balance. *Angew. Chem.* **2019**, *131*, 3728–3731.
82. Riga, E. K.; Gillies, E.; Lienkamp, K., Self-Regenerating Antimicrobial Polymer Surfaces via Multilayer-Design—Sequential and Triggered Layer Shedding under Physiological Conditions. *Adv. Mater. Interfaces* **2019**, *6*, 1802049.
83. Wang, F.; Diesendruck, C. E., Polyphthalaldehyde: Synthesis, Derivatives, and Applications. *Macromol. Rapid Commun.* **2018**, *39*, 1700519.
84. Schwartz, J. M.; Engler, A.; Phillips, O.; Lee, J.; Kohl, P. A., Determination of Ceiling Temperature and Thermodynamic Properties of Low Ceiling Temperature Polyaldehydes. *J. Polym. Sci., Part A: Polym. Chem.* **2018**, *56*, 221–228.

85. Tagami, S.; Kagiya, T.; Aso, C., Polymerization of Aromatic Aldehydes. VII. Cyclopolymerization of *o*-Formylphenylacetaldehyde and Formation of a Cyclic Trimer. *Polym. J.* **1971**, *2*, 101.
86. Aso, C.; Tagami, S., Cyclopolymerization of *o*-Phthalaldehyde. *J. Polym. Sci., Part B: Polym. Phys.* **1967**, *5*, 217–220.
87. Ito, H.; Schwalm, R., Thermally Developable, Positive Resist Systems with High Sensitivity. *J. Electrochem. Soc.* **1989**, *136*, 241–245.
88. Kaitz, J. A.; Diesendruck, C. E.; Moore, J. S., End Group Characterization of Poly(phthalaldehyde): Surprising Discovery of a Reversible, Cationic Macrocyclization Mechanism. *J. Am. Chem. Soc.* **2013**, *135*, 12755–12761.
89. Kaitz, J. A.; Diesendruck, C. E.; Moore, J. S., Dynamic Covalent Macrocyclic Poly(phthalaldehyde)s: Scrambling Cyclic Homopolymer Mixtures Produces Multi-Block and Random Cyclic Copolymers. *Macromolecules* **2013**, *46*, 8121–8128.
90. Schwartz, J. M.; Phillips, O.; Engler, A.; Sutlief, A.; Lee, J.; Kohl, P. A., Stable, High-Molecular-Weight Poly(phthalaldehyde). *J. Polym. Sci. A Polym. Chem.* **2017**, *55*, 1166–1172.
91. Engler, A.; Phillips, O.; Miller, R. C.; Tobin, C.; Kohl, P. A., Cationic Copolymerization of *o*-Phthalaldehyde and Functional Aliphatic Aldehydes. *Macromolecules* **2019**, *52*, 4020–4029.
92. Lopez Hernandez, H.; Takekuma, S. K.; Mejia, E. B.; Plantz, C. L.; Sottos, N. R.; Moore, J. S.; White, S. R., Processing-Dependent Mechanical Properties of Solvent Cast Cyclic Polyphthalaldehyde. *Polymer* **2019**, *162*, 29–34.
93. Jiang, J.; Warner, M.; Phillips, O.; Engler, A.; Kohl, P. A., Tunable Transient and Mechanical Properties of Photodegradable Poly(phthalaldehyde). *Polymer* **2019**, *176*, 206–212.
94. Ito, H.; Willson, C. G., Chemical Amplification in the Design of Dry Developing Resist Materials. *Polym. Eng. Sci.* **1983**, *23*, 1012–1018.
95. Ito, H.; England, W. P.; Ueda, M., Chemical Amplification Based on Acid-Catalyzed Depolymerization. *J. Photopolym. Sci. Tec.* **1990**, *3*, 219–233.
96. Ito, H.; Ueda, M.; Schwalm, R., Highly Sensitive Thermally Developable Positive Resist Systems. *J. Vac. Sci. Technol.* **1988**, *6*, 2259–2263.
97. Hernandez, H. L.; Kang, S.-K.; Lee, O. P.; Hwang, S.-W.; Kaitz, J. A.; Inci, B.; Park, C. W.; Chung, S.; Sottos, N. R.; Moore, J. S.; Rogers, J. A.; White, S. R., Triggered

Transience of Metastable Poly(phthalaldehyde) for Transient Electronics. *Adv. Mater.* **2014**, *26*, 7637–7642.

98. Park, C. W.; Kang, S.-K.; Lopez Hernandez, H.; Kaitz, J. A.; Wie, D. S.; Shin, J.; Lee, O. P.; Sottos, N. R.; Moore, J. S.; Rogers, J. A.; White, S. R., Thermally Triggered Degradation of Transient Electronic Devices. *Adv. Mater.* **2015**, *27*, 3783–3788.

99. Lee, K. M.; Phillips, O.; Engler, A.; Kohl, P. A.; Rand, B. P., Phototriggered Depolymerization of Flexible Poly(phthalaldehyde) Substrates by Integrated Organic Light-Emitting Diodes. *ACS Appl. Mater. Interfaces* **2018**, *10*, 28062–28068.

100. Jiang, J.; Phillips, O.; Engler, A.; Vong, M. H.; Kohl, P. A., Photodegradable Transient Bilayered Poly(phthalaldehyde) with Improved Shelf Life. *Polym. Adv. Technol.* **2019**, *30*, 1198–1204.

101. Phillips, O.; Engler, A.; Schwartz, J. M.; Jiang, J.; Tobin, C.; Guta, Y. A.; Kohl, P. A., Sunlight Photodepolymerization of Transient Polymers. *J. Appl. Polym. Sci.* **2019**, *136*, 47141.

102. Diesendruck, C. E.; Peterson, G. I.; Kulik, H. J.; Kaitz, J. A.; Mar, B. D.; May, P. A.; White, S. R.; Martínez, T. J.; Boydston, A. J.; Moore, J. S., Mechanically Triggered Heterolytic Unzipping of a Low-Ceiling-Temperature Polymer. *Nat. Chem.* **2014**, *6*, 623.

103. Tang, S.; Tang, L.; Lu, X.; Liu, H.; Moore, J. S., Programmable Payload Release from Transient Polymer Microcapsules Triggered by a Specific Ion Coactivation Effect. *J. Am. Chem. Soc.* **2018**, *140*, 94–97.

104. Lloyd, E. M.; Lopez Hernandez, H.; Feinberg, A. M.; Yourdkhani, M.; Zen, E. K.; Mejia, E. B.; Sottos, N. R.; Moore, J. S.; White, S. R., Fully Recyclable Metastable Polymers and Composites. *Chem. Mater.* **2019**, *31*, 398–406.

105. Aso, C.; Tagami, S., Polymerization of Aromatic Aldehydes. III. The Cyclopolymerization of Phthalaldehyde and the Structure of the Polymer. *Macromolecules* **1969**, *2*, 414–419.

106. Seo, W.; Phillips, S. T., Patterned Plastics That Change Physical Structure in Response to Applied Chemical Signals. *J. Am. Chem. Soc.* **2010**, *132*, 9234–9235.

107. Coulembier, O.; Knoll, A.; Pires, D.; Gotsmann, B.; Duerig, U.; Frommer, J.; Miller, R. D.; Dubois, P.; Hedrick, J. L., Probe-Based Nanolithography: Self-Amplified Depolymerization Media for Dry Lithography. *Macromolecules* **2010**, *43*, 572–574.

108. Schwesinger, R.; Schlemper, H., Peralkylated Polyaminophosphazenes—Extremely Strong, Neutral Nitrogen Bases. *Angew. Chem. Int. Ed.* **1987**, *26*, 1167–1169.

109. DiLauro, A. M.; Robbins, J. S.; Phillips, S. T., Reproducible and Scalable Synthesis of End-Cap-Functionalized Depolymerizable Poly(phthalaldehydes). *Macromolecules* **2013**, *46*, 2963–2968.
110. DiLauro, A. M.; Abbaspourrad, A.; Weitz, D. A.; Phillips, S. T., Stimuli-Responsive Core–Shell Microcapsules with Tunable Rates of Release by Using a Depolymerizable Poly(phthalaldehyde) Membrane. *Macromolecules* **2013**, *46*, 3309–3313.
111. DiLauro, A. M.; Lewis, G. G.; Phillips, S. T., Self-Immolative Poly(4,5-dichlorophthalaldehyde) and its Applications in Multi-Stimuli-Responsive Macroscopic Plastics. *Angew. Chem. Int. Ed.* **2015**, *127*, 6298–6303.
112. Kaitz, J. A.; Possanza, C. M.; Song, Y.; Diesendruck, C. E.; Spiering, A. J. H.; Meijer, E. W.; Moore, J. S., Depolymerizable, Adaptive Supramolecular Polymer Nanoparticles and Networks. *Polym. Chem.* **2014**, *5*, 3788–3794.
113. Kaitz, J. A.; Moore, J. S., Functional Phthalaldehyde Polymers by Copolymerization with Substituted Benzaldehydes. *Macromolecules* **2013**, *46*, 608–612.
114. de Marneffe, J.-F.; Chan, B. T.; Spieser, M.; Vereecke, G.; Naumov, S.; Vanhaeren, D.; Wolf, H.; Knoll, A. W., Conversion of a Patterned Organic Resist into a High Performance Inorganic Hard Mask for High Resolution Pattern Transfer. *ACS Nano* **2018**, *12*, 11152–11160.
115. Cheong, L. L.; Paul, P.; Holzner, F.; Despont, M.; Coady, D. J.; Hedrick, J. L.; Allen, R.; Knoll, A. W.; Duerig, U., Thermal Probe Maskless Lithography for 27.5 nm Half-Pitch Si Technology. *Nano Lett.* **2013**, *13*, 4485–4491.
116. Knoll, A. W.; Pires, D.; Coulembier, O.; Dubois, P.; Hedrick, J. L.; Frommer, J.; Duerig, U., Probe-Based 3-D Nanolithography Using Self-Amplified Depolymerization Polymers. *Adv. Mater.* **2010**, *22*, 3361–3365.
117. Skaug, M. J.; Schwemmer, C.; Fringes, S.; Rawlings, C. D.; Knoll, A. W., Nanofluidic Rocking Brownian Motors. *Science* **2018**, *359*, 1505–1508.
118. Zhang, H.; Yeung, K.; Robbins, J. S.; Pavlick, R. A.; Wu, M.; Liu, R.; Sen, A.; Phillips, S. T., Self-Powered Microscale Pumps Based on Analyte-Initiated Depolymerization Reactions. *Angew. Chem. Int. Ed.* **2012**, *51*, 2400–2404.
119. Burel, F.; Rossignol, L.; Pontvianne, P.; Hartman, J.; Couesnon, N.; Bunel, C., Synthesis and Characterization of Poly(ethyl glyoxylate) – a New Potentially Biodegradable Polymer. *e-Polym.* **2003**, *3*, 31.
120. Brachais, C. H.; Huguet, J.; Bunel, C., Synthesis, Characterization and Stabilization of Poly(methyl glyoxylate). *Polymer* **1997**, *38*, 4959–4964.

121. Crutchfield, M. M.; Papanu, V. D.; Warren, C. B. Polymeric Acetal Carboxylates. 1977.
122. Belloncle, B.; Burel, F.; Oulyadi, H.; Bunel, C., Study of the In Vitro Degradation of Poly(ethyl glyoxylate). *Polym. Degrad. Stab.* **2008**, *93*, 1151–1157.
123. Belloncle, B.; Bunel, C.; Menu-Bouaouiche, L.; Lesouhaitier, O.; Burel, F., Study of the Degradation of Poly(ethyl glyoxylate): Biodegradation, Toxicity and Ecotoxicity Assays. *J. Polym. Environ.* **2012**, *20*, 726–731.
124. Baker, P. R. S.; Cramer, S. D.; Kennedy, M.; Assimos, D. G.; Holmes, R. P., Glycolate and Glyoxylate Metabolism in HepG2 Cells. *Am. J. Physiol.: Cell Physiol.* **2004**, *287*, C1359–C1365.
125. Fan, B.; Trant, J. F.; Wong, A. D.; Gillies, E. R., Polyglyoxylates: A Versatile Class of Triggerable Self-Immolative Polymers from Readily Accessible Monomers. *J. Am. Chem. Soc.* **2014**, *136*, 10116–10123.
126. Sirianni, Q. E. A.; Rabiee Kenaree, A.; Gillies, E. R., Polyglyoxylamides: Tuning Structure and Properties of Self-Immolative Polymers. *Macromolecules* **2019**, *52*, 262–270.
127. Fan, B.; Trant, J. F.; Hemery, G.; Sandre, O.; Gillies, E. R., Thermo-Responsive Self-Immolative Nanoassemblies: Direct and Indirect triggering. *Chem. Commun.* **2017**, *53*, 12068–12071.
128. Fan, B.; Trant, J. F.; Yardley, R. E.; Pickering, A. J.; Lagugné-Labarthe, F.; Gillies, E. R., Photocontrolled Degradation of Stimuli-Responsive Poly(ethyl glyoxylate): Differentiating Features and Traceless Ambient Depolymerization. *Macromolecules* **2016**, *49*, 7196–7203.
129. Fan, B.; Yardley, R. E.; Trant, J. F.; Borecki, A.; Gillies, E. R., Tuning the Hydrophobic Cores of Self-Immolative Polyglyoxylate Assemblies. *Polym. Chem.* **2018**, *9*, 2601–2610.
130. Rabiee Kenaree, A.; Gillies, E. R., Controlled Polymerization of Ethyl Glyoxylate Using Alkylolithium and Alkoxide Initiators. *Macromolecules* **2018**, *51*, 5501–5510.
131. Kaitz, J. A.; Diesendruck, C. E.; Moore, J. S., Divergent Macrocyclization Mechanisms in the Cationic Initiated Polymerization of Ethyl Glyoxylate. *Macromolecules* **2014**, *47*, 3603–3607.
132. Fan, B.; Gillies, E. R., Poly(ethyl glyoxylate)-Poly(ethylene oxide) Nanoparticles: Stimuli-Responsive Drug Release via End-to-End Polyglyoxylate Depolymerization. *Mol. Pharm.* **2017**, *14*, 2548–2559.

133. Périgo, E. A.; Hemery, G.; Sandre, O.; Ortega, D.; Garaio, E.; Plazaola, F.; Teran, F. J., Fundamentals and Advances in Magnetic Hyperthermia. *Appl. Phys. Rev.* **2015**, *2*, 041302.
134. Gambles, M. T.; Fan, B.; Borecki, A.; Gillies, E. R., Hybrid Polyester Self-Immolative Polymer Nanoparticles for Controlled Drug Release. *ACS Omega* **2018**, *3*, 5002–5011.
135. Fan, B.; Salazar, R.; Gillies, E. R., Depolymerization of Trityl End-Capped Poly(Ethyl Glyoxylate): Potential Applications in Smart Packaging. *Macromol. Rapid Commun.* **2018**, *39*, 1800173.
136. Heuchan, S. M.; MacDonald, J. P.; Bauman, L. A.; Fan, B.; Henry, H. A. L.; Gillies, E. R., Photoinduced Degradation of Polymer Films Using Polyglyoxylate–Polyester Blends and Copolymers. *ACS Omega* **2018**, *3*, 18603–18612.
137. Ree, L. H. S.; Sirianni, Q. E. A.; Gillies, E. R.; Kelland, M. A., Systematic Study of Polyglyoxylamides as Powerful, High-Cloud-Point Kinetic Hydrate Inhibitors. *Energy Fuels* **2019**, *33*, 2067–2075.
138. Hamley, I. W., *Introduction to Soft matter: Synthetic and Biological Self-Assembling Materials*. Revised Edition ed.; John Wiley & Sons, Ltd.: West Sussex, England, 2007.
139. Bates, F. S., Polymer-Polymer Phase Behavior. *Science* **1991**, *251*, 898–905.
140. Mai, Y.; Eisenberg, A., Self-Assembly of Block Copolymers. *Chem. Soc. Rev.* **2012**, *41*, 5969–5985.
141. Casse, O.; Shkilnyy, A.; Linders, J.; Mayer, C.; Häussinger, D.; Völkel, A.; Thünemann, A. F.; Dimova, R.; Cölfen, H.; Meier, W.; Schlaad, H.; Taubert, A., Solution Behavior of Double-Hydrophilic Block Copolymers in Dilute Aqueous Solution. *Macromolecules* **2012**, *45*, 4772–4777.
142. Ge, Z.; Xie, D.; Chen, D.; Jiang, X.; Zhang, Y.; Liu, H.; Liu, S., Stimuli-Responsive Double Hydrophilic Block Copolymer Micelles with Switchable Catalytic Activity. *Macromolecules* **2007**, *40*, 3538–3546.
143. Mountrichas, G.; Pispas, S., Synthesis and pH Responsive Self-Assembly of New Double Hydrophilic Block Copolymers. *Macromolecules* **2006**, *39*, 4767–4774.
144. Cölfen, H., Double-Hydrophilic Block Copolymers: Synthesis and Application as Novel Surfactants and Crystal Growth Modifiers. *Macromol. Rapid Commun.* **2001**, *22*, 219–252.

Chapter 2

2 Multi-stimuli-responsive self-immolative polymer assemblies

Adapted from:

R. E. Yardley, E. R. Gillies. Multi-Stimuli-Responsive Self-Immolative Polymer Assemblies *J. Polym. Sci. A. Polym. Chem.*, **2018**, *56*, 1868–1877.

2.1 Introduction

Over the past few decades, there has been significant interest in degradable polymers such as poly(lactic acid),¹⁻⁴ poly(glycolic acid)⁵⁻⁶ and polycaprolactone^{4, 7} for a wide range of applications from nanomedicine to compostable consumer products. The degradation rates of these polymers can be controlled to some extent by modifying their chemical structures or chain lengths, but it occurs gradually under all aqueous conditions and may be slower or faster than desired for a given application. To address this limitation, stimuli-responsive polymers that degrade in response to external stimuli have been developed. Stimuli-responsive units or linkages have been incorporated into the polymer backbone and later cleaved in response to stimuli causing a breakdown of the polymer. For example, acid-labile acetals and ketals,⁸⁻¹⁰ reduction-sensitive disulfide linkages¹¹⁻¹⁴ or photochemically-sensitive units such as coumarin dimers,¹⁵⁻¹⁶ *o*-nitrobenzyl esters and carbonates,¹⁷⁻¹⁸ and 2-diazo-1,2-naphthoquinones¹⁹ have been used. However, many stimuli-mediated reactions must occur in these systems in order to completely degrade the polymers.

Self-immolative polymers (SIPs), which depolymerize end-to-end in response to the cleavage of stimuli-responsive end-caps at the polymer termini, were introduced to provide amplified responses to stimuli.²⁰⁻²² The stimulus to which they respond can be easily modified by simply switching the end-cap, while retaining the structure of the polymer backbone. Cleavage of end-caps in response to stimuli such as acid,²³ reducing agents,²⁴⁻²⁵ heat,²⁶ or light^{24, 27-28} has been shown to trigger depolymerization. Various SIP backbones

have been developed. Polyphthalaldehydes^{22, 29-32} and polyglyoxylates^{27, 33-34} rely on low ceiling temperatures, which allow them to undergo reversible loss of monomers after end-cap cleavage. Systems such as polycarbamates,³⁵⁻⁴⁰ poly(benzyl ether)s,⁴¹ and poly(carbamate-thiocarbamate)s²⁵ undergo cyclization and/or elimination reactions that result in their depolymerization to products that are different from the monomers from which they were prepared. The degradation rate of this latter class of SIPs is generally quite sensitive to environmental factors such as pH and solvent.^{36, 38-39}

Another class of stimuli-responsive polymers is thermo-responsive polymers, which undergo changes in their physical properties when exposed to changes in temperature. For example, poly(*N*-isopropylacrylamide) (PNIPAAm) exhibits a lower critical solution temperature (LCST).⁴²⁻⁴³ Below the LCST, the polymer chains are soluble, but above the LCST an entropically driven phase separation occurs. Another well-studied polymer that has an LCST is poly(2-(dimethylamino)ethyl methacrylate) (PDMAEMA).⁴⁴⁻⁴⁵ It differs from PNIPAAm in that it is responsive to both pH and temperature. The LCST of PDMAEMA is only observed when the pH of the solution is above the pKa of the polymer (~7.5). Both PNIPAAm and PDMAEMA have been used in recent years in the preparation of thermo-responsive nanomaterials.⁴⁶

The synthesis of block copolymers is an approach that allows for the combination of two known polymers to create a new polymer with unique properties. Amphiphilic block copolymers can self-assemble in aqueous solution to form a wide variety of morphologies including spherical micelles, vesicles and bilayers.⁴⁷ Previous work has investigated the self-assembly of amphiphilic block copolymers that were prepared by combining a hydrophobic SIP block with a simple non-responsive hydrophilic block such as poly(ethylene glycol) (PEG) and poly(*N,N*-dimethylacrylamide).^{24, 34, 36, 48} These copolymers self-assembled to form nanoparticles and vesicles that degraded upon application of the stimulus and depolymerization of the hydrophobic SIP block. To the best of our knowledge, the use of hydrophilic blocks that are also responsive to stimuli has not yet been investigated.

Herein we report the synthesis, self-assembly, and stimuli-responsive depolymerization of block copolymers composed of a hydrophobic self-immolative polycarbamate (PCB)³⁶ and a hydrophilic PDMAEMA block, conjugated by a UV light-responsive linker. It was proposed that irradiation should result in depolymerization of the hydrophobic polycarbamate block, leading to disintegration of the copolymer assemblies. Concomitantly, the PDMAEMA block should exhibit responsiveness to pH and temperature. As the depolymerization of the polycarbamate SIP block is sensitive to its environment, it was hypothesized that collapse of the PDMAEMA chains around the assembly cores might hinder water access to the cores, thereby modulating the amount of the polycarbamate depolymerization (**Figure 2.1**).

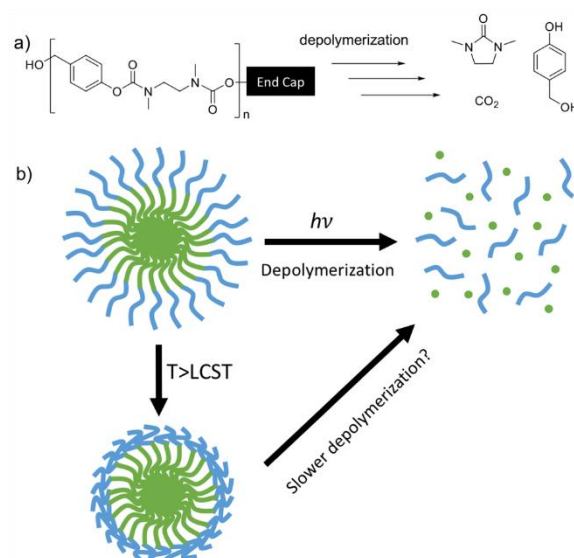


Figure 2.1: a) Schematic of PCB block breakdown and b) Initially proposed behaviour of PCB-PDMAEMA block copolymer assemblies.

2.2 Experimental

2.2.1 General materials and procedures

Compounds **2.1**,²⁷ and **2.3**⁴⁹ from **Scheme 2.1** and **2.5**³⁶ (**Scheme 2.2**) and **2.6**⁵⁰ (**Scheme 2.3**) were prepared as previously reported. 3-Bromo-1-propanol, 2-bromo-2-methylpropionyl bromide and 4-nitrophenol chloroformate were purchased from AK

Scientific. 1,1,4,7,10,10-Hexamethyltriethylenetetramine (HMTETA) was purchased from Alfa Aesar. Copper (I) bromide, sodium azide and 2-(dimethylamino)ethyl methacrylate were purchased from Sigma-Aldrich and used without further purification unless otherwise noted. Anhydrous dimethylformamide (DMF) was obtained from a solvent purification system equipped with aluminum oxide columns. Pyridine, NEt_3 and CH_2Cl_2 were distilled from CaH_2 (particle size 0-2mm). Column chromatography was performed using silica gel (0.063-0.200 mm particle size, 70-230 mesh). Ultrapure deionized water was obtained from the Barnstead EASYpure II system.

Unless otherwise stated, all reactions were performed under a N_2 atmosphere using flame or oven dried glassware. Dialyses were performed using Spectra/Por regenerated cellulose membranes.

2.2.2 Instrumentation

^1H NMR spectra were obtained at 600 MHz or 400 MHz using Varian INOVA spectrometers. ^{13}C NMR spectra were obtained at 150 MHz using a Varian Inova spectrometer. NMR spectra were referenced relative using tetramethylsilane (TMS) using the residual solvent signals of CHCl_3 (7.26 ppm), $(\text{CH}_3)_2\text{CO}$ (2.05 ppm), and CH_3CN (1.94 ppm) as internal standards. A Thermo Scientific DFS (Double Focusing Sector) mass spectrometer, utilizing a reversed Nier Johnson geometry was used for high resolution mass spectrometry. Size exclusion chromatography (SEC) was carried out at a flow rate of 1 mL/min in DMF with 10 mM LiBr and 1% (v/v) NEt_3 at 85 °C using a Waters 515 HPLC pump and Waters Temperature Control Module II equipped with a Wyatt Optilab T-rEX refractometer and two PLgel 5 μm mixed-D (300 mm \times 7.5 mm) columns from Polymer Laboratories by Varian connected in series. The calibration was performed using poly(methyl methacrylate standards) (PMMA) standards. Infrared (IR) spectra were obtained on a PerkinElmer Spectrum Two FTIR Spectrometer using the attenuated total reflectance accessory. Dynamic light scattering (DLS) was performed using a Zetasizer Nano ZS instrument from Malvern Instruments at 25 °C at a concentration of 0.8 mg/mL of polymer assemblies. Transmission electron microscopy (TEM) imaging was performed

using a Phillips CM10 Microscope operating at an acceleration voltage of 80 kV. 10 μ L of micelle suspension (0.8 mg/mL) was placed onto a copper grid. After 5 min, the resulting liquid was wicked away using strips of Fisherbrand™ Qualitative-Grade Filter Paper Circles and allowed to air-dry for 2 hours. Fluorescence spectra were obtained using a QM-4 SE spectrometer from Photon Technology International (PTI) equipped with both excitation and emission monochromators. UV-visible spectra were obtained on a Varian UV/vis Cary 300 spectrophotometer equipped with a Varian Cary 8453 Temperature Controller. Infrared (IR) spectra were obtained on a PerkinElmer Spectrum Two FTIR Spectrometer using the attenuated total reflectance accessory.

2.2.3 Synthetic procedures

Synthesis of end-cap 2.2

Compound **2.1**²⁷ (1.20 g, 5.12 mmol, 1.00 equiv.) was dissolved in dry pyridine (1.30 mL, 15.9 mmol, 3.10 equiv.) and dry THF (25 mL). 4-Nitrophenyl chloroformate (2.07 g, 10.3 mmol, 2.00 equiv.) was added and the reaction was stirred for 3 hours. The volatiles were removed *in vacuo* and the resulting residue was dissolved in ethyl acetate (EtOAc) (50 mL). The solution was then washed with 1 M HCl (50 mL) then the aqueous layer was extracted with EtOAc (3 x 50 mL). The organic layers were combined and dried with MgSO₄ and concentrated. The product was purified using silica gel chromatography with 1:1 hexanes:EtOAc as the eluent to yield a pale yellow solid (1.64 g). Yield: 81%. ¹H NMR (600 MHz, CD₃CN, δ , ppm): 8.55 (s, 1H), 8.30 (d, J = 9.2 Hz, 2H), 8.18 (d, J = 6.0 Hz, 1H), 7.87 (d, J = 7.8 Hz, 1H), 7.61 (br s, 1H), 7.48 (d, J = 9.2, 2H), 5.71 (s, 2H), 4.16 (d, J = 6.0 Hz 2H), 2.13 (s, 1H). ¹³C NMR (150 MHz, acetonitrile-D₃, δ , ppm): 169.4, 160.8, 157.5, 152.7, 151.1, 140.5, 139.1, 137.7, 134.9, 130.8, 129.3, 127.6, 85.2, 76.5, 72.2, 34.2. IR (cm⁻¹): 3277, 3114, 3081, 2920, 2852, 2129, 1749, 1613, 1588, 1517. MS (m/z): calcd for C₁₈H₁₃N₃O₈, 399.07026; found, 399.06970 [M]⁺.

Synthesis of end-cap 2.4

In a dry round bottom flask, compound **2.3**⁴⁹ (1.17 g, 7.20 mmol, 1.00 equiv.), pyridine (2.30 mL, 28.8 mmol, 4.00 equiv.) and dry CH₂Cl₂ (50 mL) were combined and stirred for 10 min. 4-Nitrophenyl chloroformate (2.90 g, 14.4 mmol, 2.00 equiv.) was added and the reaction was stirred for 2 hours. The mixture was then filtered to remove solids. The filtrate was washed with 1 M HCl (50 mL) and water (2 x 50 mL), dried with MgSO₄, and concentrated. The crude product was dissolved in CH₂Cl₂ (20 mL) and imidazole (1.63 g, 21.6 mmol, 3.00 equiv.) was added. The resulting mixture was stirred for 30 min, then passed through a silica plug. The filtrate was concentrated to yield white crystals (2.12 g). Yield: 94%. ¹H NMR (600 MHz, CDCl₃, δ, ppm): 8.27 (d, *J* = 10.8 Hz, 2H), 7.41-7.36 (m, 4H) 7.01 (d, *J* = 8.9 Hz, 2H), 5.24 (s, 2H), 4.72 (s, 2H), 2.53 (s, 1H). ¹³C NMR (150 MHz, CDCl₃, δ, ppm): 158.6, 155.9, 152.9, 145.8, 131.1, 127.7, 125.7, 122.2, 115.6, 78.7, 76.2, 71.2, 56.3. IR (cm⁻¹): 3380, 3304, 3126, 3080, 2949, 1776, 1645, 1521 cm⁻¹. MS (*m/z*): calcd for C₁₈H₁₃N₃O₈, 327.07429; found, 327.07498 [M]⁺.

Synthesis of PCB_{UV} and general procedure for synthesis of the self-immolative block

Monomer precursor **2.5**³⁶ (2.04 g, 4.04 mmol, 1.00 equiv.) was dissolved in 1:1 TFA:CH₂Cl₂ (dry) and the reaction mixture was stirred at room temperature under Ar for 2 hours. The solvent was removed via a stream of Ar gas. Additional dry CH₂Cl₂ (5 mL) was added and removed again to ensure all TFA has been removed. The flask was then placed under vacuum to remove all residual solvent. The resulting monomer was dissolved in 1:3 dry THF:Toluene (24 mL) and the solution was cooled to 0 °C. End-cap **2.2** was added (79.8 mg, 0.2 mmol, 0.05 equiv.), followed by NEt₃ (7.04 mL, 50.5 mmol, 12.5 equiv.) and 4-(dimethylamino)pyridine (DMAP). The reaction was warmed to room temperature and stirred for 24 hours. The solution was then diluted with CH₂Cl₂ (50 mL), washed with 1 M HCl (50 mL) and 10% Na₂CO₃ (2 x 50 mL). The organic layer was dried over MgSO₄ and the volatiles were removed *in vacuo* to provide a yellow solid. The crude polymer was further purified by dialysis using a 3.5 kg/mol molecular weight cutoff (MWCO) membrane against DMF followed by ultrapure deionized water over 24 hours. The sample was lyophilized to afford the product as a white powder (979 mg). Yield: 49%.

^1H NMR (600 MHz, CDCl_3 , δ , ppm): 8.50 (s, 1H), 8.18-7.87 (m, 2H), 7.38-7.24 (m, 40 H), 7.11-7.04 (m, 35 H), 5.56 (s, 2H), 5.13-5.08 (m, 37 H), 4.17 (s, 2H), 3.69-3.40 (m, 76 H), 3.12-2.88 (m, 135 H), 2.28 (s, 1H). IR (cm^{-1}): 2962, 1694, 1505. SEC: $M_n = 4.64$ kg/mol, $M_w = 10.70$ kg/mol, $D = 2.31$.

Synthesis of PCB_{CON}

This polymer was synthesized by the same procedure as described above for PCB_{UV} except that end-cap **2.4** was used (65.4 mg, 0.2 mmol, 0.05 equiv.). The product was obtained as a white powder (1.04 g). Yield: 51%. ^1H NMR (600 MHz, CDCl_3 , δ , ppm): 7.38-7.25 (m, 52 H), 7.11-7.04 (m, 39 H), 7.05-7.03 (m, 2H), 5.13-5.08 (m, 40 H), 4.69 (s, 2H), 3.69-3.40 (m, 79 H), 3.12-2.88 (m, 154 H), 2.54 (s, 1H). IR (cm^{-1}): 2961, 1690, 1510. SEC: $M_n = 5.40$ kg/mol, $M_w = 11.3$ kg/mol, $D = 2.11$.

Synthesis of PDMAEMA-N₃

2-(Dimethylamino)ethyl methacrylate (DMAEMA) was passed through a neutral alumina plug to remove the inhibitor. In a Schlenk flask, DMAEMA (5.00 g, 31.8 mmol, 40.0 equiv.), HMTETA (0.44 mL, 0.80 mmol, 1 equiv.) and CuBr (114 mg, 0.80 mmol, 1 equiv.) were dissolved in 1,3-dichlorobenzene (4 mL) and degassed by bubbling N_2 through the system for 30 min. In a separate flask, a 0.8 M (200 mg/mL) solution of initiator **2.6** in 1,3-dichlorobenzene was prepared and degassed for 30 min. The Schlenk flask was heated to 50 °C. The initiator solution (1.0 mL, 0.80 mmol, 1.0 equiv.) was added to the Schlenk flask via a degassed syringe once 50 °C was achieved and the reaction was stirred for 55 min. The flask was then cooled to -78 °C, the stopper was removed, and air was bubbled through the solution to quench the polymerization. The volatiles were removed *in vacuo*, then the product was redissolved in THF and passed through a neutral alumina plug to remove copper. The polymer was then precipitated from THF into hexanes three times to yield the pure final product, a clear, colourless solid (3.43 g). Yield: 67%. ^1H NMR (600 MHz, CDCl_3 , δ , ppm): 4.26 (t, $J = 5.85$ Hz, 2 H), 4.07 (m, 69 H), 3.39 (t, $J = 6.79$ Hz, 2 H), 2.75-2.59 (m, 98 H), 2.39-2.25 (m, 200 H), 2.01-1.82 (m, 64 H), 1.14-0.87 (m, 100 H).

IR (cm⁻¹): 2948, 2863, 2821, 2769, 2098, 1723, 1517. SEC: $M_n = 5.31$ kg/mol, $M_w = 6.17$ kg/mol, $D = 1.16$.

Synthesis of PCB_{UV}-PDMAEMA and general procedure for the Cu(I)-assisted azide-alkyne cycloaddition (CuAAC) of self-immolative block and PDMAEMA

In a Schlenk flask, **PCB_{UV}** (170 mg, 0.02 mmol, 1.0 equiv.), **PDMAEMA-N₃** (175 mg, 0.03 mmol, 1.2 equiv.), and HMTETA (46 mg, 0.20 mmol, 10 equiv.) were dissolved in DMF (10 mL). 3 cycles of freeze-pump-thaw were performed. CuBr (15 mg, 0.1 mmol, 5.0 equiv.) was then added and the reaction mixture was heated at 50 °C for 17 hours. The solution was then cooled to room temperature and passed through a neutral alumina plug to remove most of the copper. The product was then dialyzed using a 10 kg/mol MWCO membrane against DMF, water with EDTA (1.0 g/L, adjusted to pH 8.0 by the addition of NaOH pellets), and finally ultrapure deionized water. The product was then lyophilized to provide a white solid (251 mg). Yield: 76%. ¹H NMR (600 MHz, CDCl₃, δ, ppm): 7.37-7.23 (m, 42 H), 7.12-7.04 (m, 40 H), 5.11-5.04 (m, 43 H), 4.67 (m, 2 H), 4.19 (s, 2H), 4.15-3.87 (m, 145 H), 3.69-3.40 (m, 91 H), 3.12-2.88 (m, 173 H), 2.57 (m, 147 H), 2.29 (m, 440 H), 2.01-1.73 (m, 240 H), 1.14-0.89 (m, 229 H). IR (cm⁻¹): 2963, 2881, 2846, 2785, 1718, 1701, 1687, 1513. SEC: $M_n = 9.42$ kg/mol, $M_w = 16.4$ kg/mol, $D = 1.74$.

Synthesis of PCB_{CON}-PDMAEMA

This polymer was synthesized by the same procedure as described above for **PCB_{UV}-PDMAEMA** except that **PCB_{CON}** (250 mg, 0.2 mmol, 1.0 equiv.) was used. The product was obtained as a white powder (380 mg). Yield: 74%. ¹H NMR (600 MHz, CDCl₃, δ, ppm): 7.38-7.24 (m, 36 H), 7.11-7.04 (m, 37 H), 5.13-5.04 (m, 38 H), 4.41 (s, 2H), 4.10-3.90 (m, 96 H), 3.69-3.40 (m, 77 H), 3.1-2.78 (m, 149 H), 2.62-2.46 (m, 94 H), 2.29-2.15 (m, 290 H), 2.01-1.56 (m, 140 H), 1.28-0.85 (m, 151 H). IR (cm⁻¹): 2962, 2879, 2785, 1716, 1689, 1509. SEC: $M_n = 10.2$ kg/mol, $M_w = 18.9$ kg/mol, $D = 1.85$.

2.2.4 LCST determination

10 mg of polymer was dissolved in 1.0 mL of 100 mM, pH 7.0 or pH 8.0 potassium phosphate buffer. The transmittance was then monitored at 500 nm using a UV-visible spectrometer as the solution was heated at 2 °C/min. This measurement was repeated in triplicate.

2.2.5 Block copolymer self-assembly and characterization

Self-assembly was performed using a nanoprecipitation method.⁵¹ 8 mg of the block copolymer was dissolved in 1.0 mL of DMF with stirring overnight. Then, 0.1 mL of the polymer solution was rapidly injected into 0.9 mL of ultrapure deionized water while stirring at 700 rpm. Alternatively, 0.9 mL of ultrapure deionized water was injected dropwise over one min into 0.1 mL of polymer solution with stirring. After stirring overnight, the suspensions were dialyzed using a 2 kg/mol MWCO membrane against ultrapure deionized water (500 mL, 24 h, water changed once at ~12 h). Each system was prepared in triplicate.

2.2.6 Assembly degradation and depolymerization studies

The assemblies and depolymerization were monitored via Nile red fluorescence encapsulation, dynamic light scattering (DLS) count rate, and NMR Spectroscopy.

2.2.6.1 Assembly degradation studied by Nile red fluorescence

In a vial, 30 μ L of 0.1 mg/mL solution of Nile red in CH_2Cl_2 was added and then the solvent was evaporated. Next, 8 mg of the copolymer was added and then dissolved in 1.0 mL of DMF. Assemblies were then prepared as described above but dialyzed against 100 mM potassium phosphate buffers of pH 7.0 or 8.0. The samples were incubated at 20 or 65 °C. After 30 min, the fluorescence of each system was measured using an excitation wavelength of 540 nm and recording the emission at 600 nm. The samples, in a quartz cuvet, were then irradiated with UV light using an ACE Glass photochemistry cabinet containing a mercury light source (450 W bulb, 2.8 mW/cm² of UVA radiation) for 30 min.

The samples were again incubated at 20 or 65 °C in the dark. The emission intensity at 600 nm was measured at select time points over 168 hours.

2.2.6.2 Assembly degradation studied by DLS

Assemblies were prepared as described above for the Nile red studies, except that no dye was used. The samples were incubated at either 20 or 65 °C. After 30 min, the count rate was measured by DLS, with the attenuator fixed at 9 to obtain the $t = 0$ count rate. The samples were then irradiated with UV light as described for the Nile red study and incubated at either 20 or 65 °C in the dark. The count rate was measured at selected time points over 168 hours.

2.2.6.3 Nanoparticle depolymerization studied by NMR spectroscopy

In a small vial, 40 mg of the copolymer was dissolved in 1.4 mL of 100 mM, pH 8.0 potassium phosphate buffered D₂O and stirred for 30 min. The sample was then split between two NMR tubes with one being incubated at 20 °C and the other at 65 °C. After 30 min, ¹H NMR spectra of the suspensions were obtained. The samples were then irradiated with UV light as described for the Nile red study, and incubated at either 20 or 65 °C in the dark. ¹H NMR spectra were obtained at select time points over 30 days. The integration of emerging peaks associated with the formation of PCB degradation products was compared to that of the PDMAEMA peaks, which remained constant to the over the 28 days.

2.3 Results and discussion

2.3.1 Polymer design and synthesis

To investigate the influence of PDMAEMA on the depolymerization of the PCB block, two target polymers were designed (**Figure 2.2**). The first polymer PCB_{UV}-PDMAEMA contains a UV-responsive *o*-nitrobenzyl carbonate linker between the polycarbamate and PDMAEMA blocks, while the second (control) polymer PCB_{CON}-PDMAEMA contains a non-stimuli-responsive benzyl carbonate.

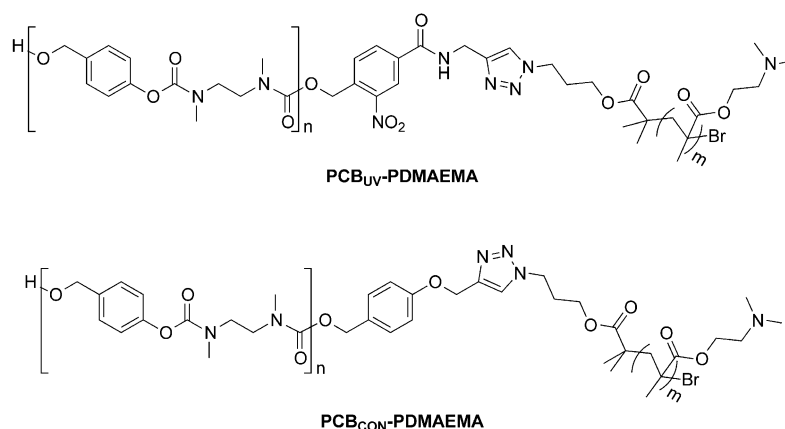
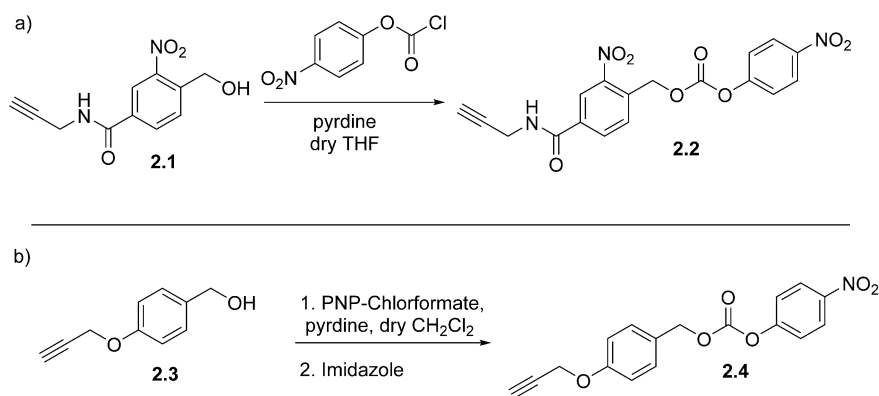


Figure 2.2 Chemical structure of target polymers **PCB_{UV}-PDMAEMA** and **PCB_{CON}-PDMAEMA**.

2.3.2 Synthesis of end-caps

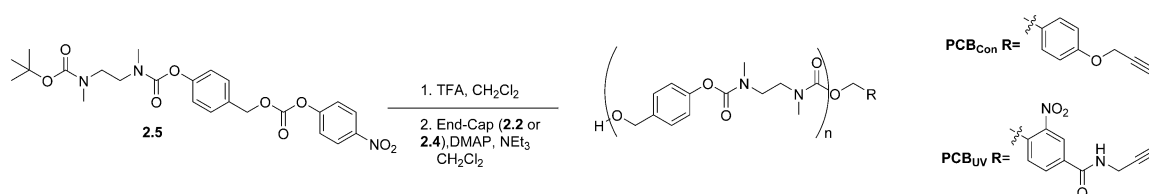
To prepare the two target polymers, two linker end-caps were synthesized, one being sensitive to UV light and the other being not responsive to stimuli. Both end-caps contained alkynes for the conjugation of the PDMAEMA block using a Cu(I)-assisted azide-alkyne cycloaddition (CuAAC). The light-responsive moiety was an *o*-nitrobenzyl derivative cleavable at the benzylic site to release uncapped PCB SIP. The un-activated form of the end cap (compound **2.1**) was synthesized in two steps from commercially available 4-(bromomethyl)-3-nitrobenzoic acid and has been previously reported.²⁷ The alcohol on **1** was activated with 4-nitrophenyl chloroformate to yield end-cap **2** (**Scheme 2.1a**). For the control end-cap, the propargyl ether-functionalized benzyl alcohol **3**⁴⁹ was activated with 4-nitrophenyl chloroformate for afford end-cap **4** (**Scheme 2.1b**).



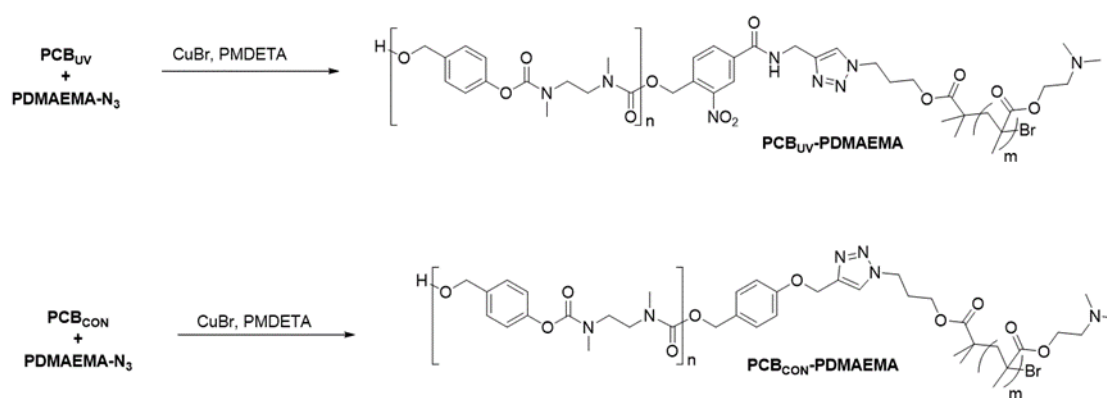
Scheme 2.1: Synthesis of linker end-caps: a) UV-responsive end-cap **2.2** and b) control end-cap **2.4**.

2.3.3 Synthesis of polymers

To prepare the PCB blocks, our previously reported monomer precursor **2.5**³⁶ was first deprotected by being treated with 1:1 CH₂Cl₂:TFA to cleave the *t*-butyloxycarbonyl protecting group (**Scheme 2.2**). This monomer was then immediately immersed in CH₂Cl₂ in the presence of DMAP, NEt₃, and 0.05 equiv. of either end-cap **2** or **4**. After 24 h, the resulting polymers were isolated by extraction followed by dialysis to afford **PCB_{UV}** (from end-cap **2**) and **PCB_{CON}** (from end-cap **4**). ¹H NMR spectroscopy indicated that **PCB_{UV}** and **PCB_{CON}** had M_n values of 4752 g mol⁻¹ and 5280 g mol⁻¹ respectively based on integration of the end-cap peaks relative to those of the backbone repeat units (**Figure A2.5-6**). Size exclusion chromatography in DMF relative to PMMA standards provided an M_n of 4640 g/mol and *D* of 2.31 for **PCB_{UV}** and a M_n of 5400 g/mol and *D* of 2.11 for **PCB_{CON}**. These SEC values are in good agreement with those obtained from NMR spectroscopy.



Scheme 2.2: Polymerization of **PCB_{UV}** and **PCB_{CON}**.



Scheme 2.4: Synthesis of **PCB_{UV}-PDMAEMA** and **PCB_{CON}-PDMAEMA** diblock copolymers using CuAAC.

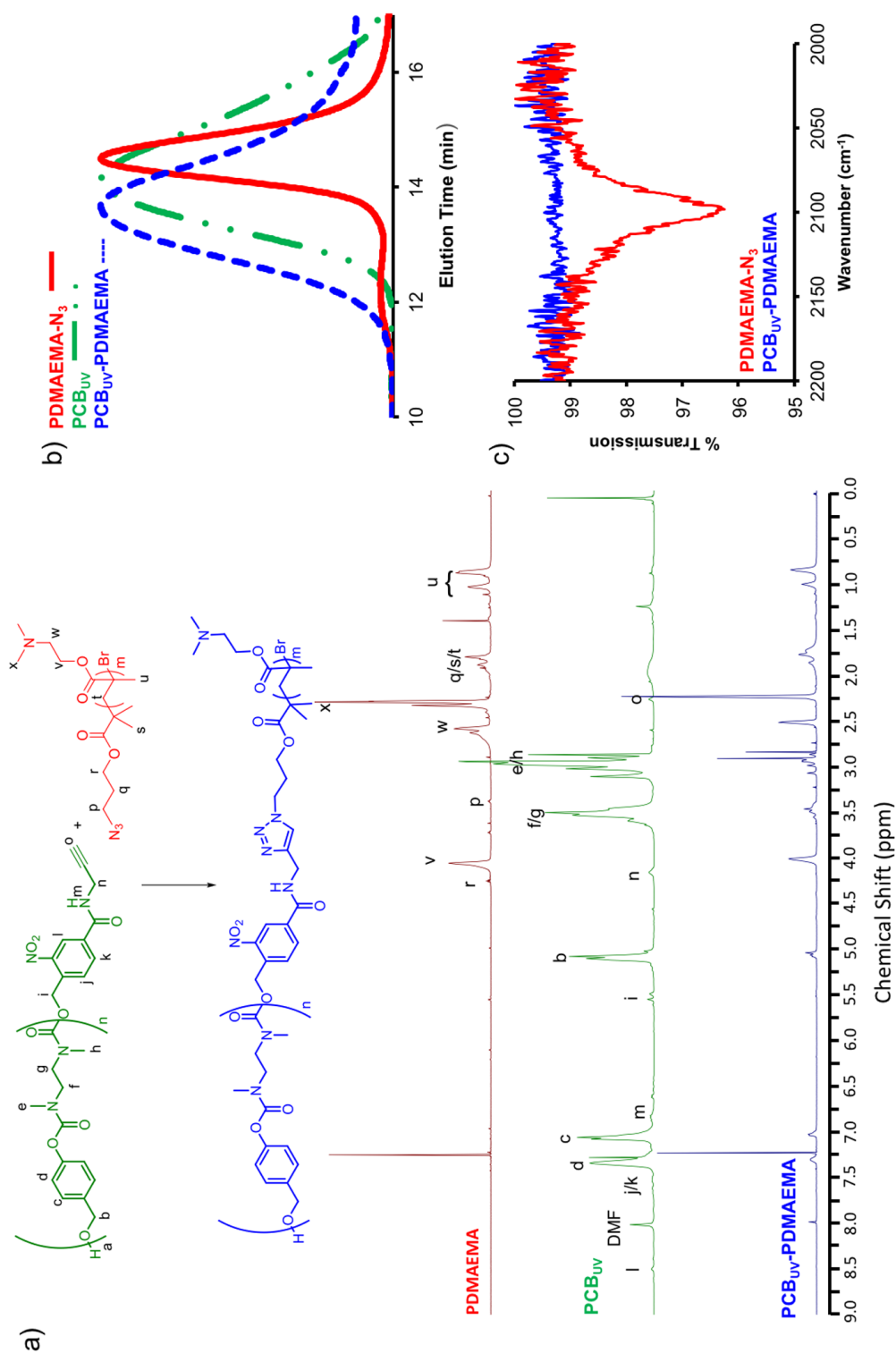


Figure 2.3: Characterization of $\text{PCB}_{\text{UV}}\text{-PDMAEMA}$: a) ^1H NMR spectroscopy (600 MHz, CDCl_3); b) DMF SEC traces (refractive index detection); c) IR Spectra.

2.3.5 LCST measurements for PDMAEMA-N₃

PDMAEMA is known to exhibit LCST behaviour when above its pKa.⁴⁴⁻⁴⁵ The pKa of **PDMAEMA-N₃** was determined to be 7.2 by performing a titration with 0.5 M KOH on a solution of PDMAEMA in water (**Figure A2.11**). The cloud point of 10 mg/mL **PDMAEMA-N₃** was then evaluated in 100 mM pH 8.0 phosphate buffer by measuring the transmittance at 500 nm, while increasing the temperature from 20 to 70 °C at a rate of ~1 °C per minute. The cloud point, corresponding to a large sharp drop in transmittance, was found to be ~58 °C (**Figure 2.4**). In contrast, at a concentration of 10 mg/mL in 100 mM pH 7.0 phosphate buffer, no cloud point was observed. The cloud point at a range of pH and buffer concentrations were also determined, but have been left out for brevity.

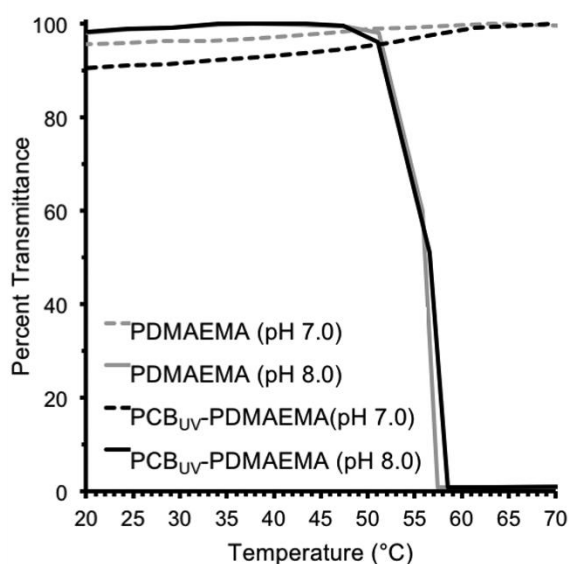


Figure 2.4: Transmittance of a 10 mg/mL solution/suspension of **PDMAEMA-N₃** or **PCB_{UV}-PDMAEMA** versus temperature in 100 mM pH 7.0 or 8.0 phosphate buffer.

2.3.6 Block copolymer self-assembly

The self-assembly of the amphiphilic diblock copolymers **PCB_{UV}-PDMAEMA** and **PCB_{CON}-PDMAEMA** was performed by nanoprecipitation, involving either the addition of a DMF solution of the polymer into water or the addition of water into the DMF polymer solution. DMF was then removed by dialysis. The resulting assemblies were first

characterized by DLS and TEM. Assemblies with diameters ranging from 68 – 95 nm and polydispersity indices (PDI) of 0.16 – 0.27 were obtained based on DLS (**Table 2.1**). TEM showed that the assemblies were solid particles with diameters ranging from ~20 - 50 nm (**Figure 2.5**). The smaller diameters observed by TEM can be attributed to the dried state of the particles versus the hydrated state measured by DLS. For subsequent studies, the water into DMF method was chosen because of the more similar diameters observed for the two copolymers and their lower PDI values.

The cloud point of the **PCB_{UV}-PDMAEMA** assemblies was measured using the same method described above for **PDMAEMA-N₃**. The cloud point at pH 8.0 was ~58 °C, the same temperature determined for **PDMAEMA-N₃**, and no cloud point was detected at pH 7.0.

Table 2.1: Average micelle diameters and PDI from DLS

	DMF into Water		Water into DMF	
	Diameter (nm)	PDI	Diameter (nm)	PDI
PCB_{UV}-PDMAEMA	95 ± 8	0.27	68 ±0.6	0.19
PCB_{CON}-PDMAEMA	71 ± 7	0.21	68 ±0.5	0.16

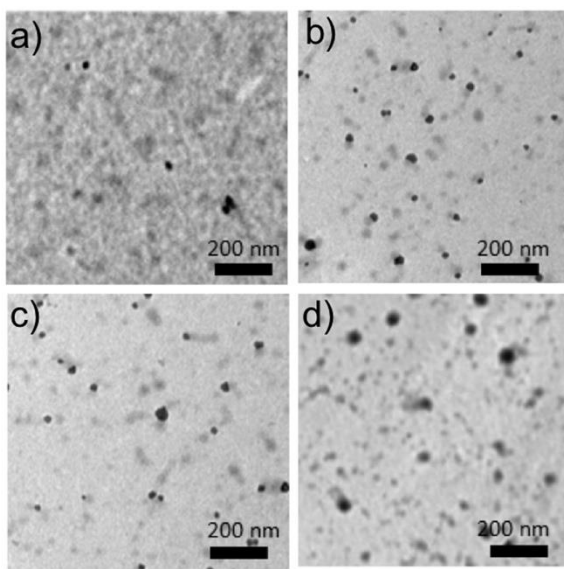


Figure 2.5: TEM images of assemblies formed from a) **PCB_{UV}-PDMAEMA** via DMF into water; b) **PCB_{UV}-PDMAEMA** via water into DMF; c) **PCB_{CON}-PDMAEMA** via DMF into water; d) **PCB_{CON}-PDMAEMA** via water into DMF.

2.3.7 Depolymerization studies

First, the depolymerization of the assemblies was investigated by fluorescence spectroscopy using Nile red as an encapsulated probe molecule. Nile red fluoresces strongly in the hydrophobic cores of particles, but undergoes extensive aggregation and quenching in water.⁵²⁻⁵³ Thus, a decrease in Nile red fluorescence can correspond to its release from particles into the aqueous environment as they degrade. The micelles were prepared by the water into DMF nanoprecipitation method with the addition of 2 wt% Nile red relative to polymer in the DMF. The resulting assemblies were dialyzed against a 100 mM phosphate buffer of pH 7.0 or 8.0. Before the stimulus was applied, a sample of each system was equilibrated at room temperature (20 °C) or above the LCST (65 °C) and the initial Nile red fluorescence was measured. UV light was then applied to both the **PCB_{UV}-PDMAEMA** and **PCB_{CON}-PDMAEMA** assemblies and they were incubated at either 20 or 65 °C. The fluorescence was measured at various time points over a period of 168 h (7 days).

Comparing the **PCB_{UV}-PDMAEMA** and **PCB_{CON}-PDMAEMA** at 20 °C, the stimuli-responsive polymer exhibited a decrease in fluorescence of ~30 % at pH 7.0 and ~20% at pH 8.0, whereas the control exhibited only a negligible decrease (< 10%) (**Figure 2.6**). This result suggests that stimuli-responsive depolymerization occurred and that background degradation of the control was minimal. At 65 °C, the decrease in Nile red fluorescence was also greater for **PCB_{UV}-PDMAEMA** than **PCB_{CON}-PDMAEMA** at both pH 7.0 and 8.0 for most time points. This suggests that stimuli-responsive depolymerization was still occurring at this temperature. Comparing pH 7.0 and pH 8.0 at 65 °C for **PCB_{UV}-PDMAEMA**, it appears that the release was faster at pH 7.0 over the first ~75 hours. As the cyclization and elimination reactions involved in depolymerization should normally be faster at pH 8.0 than 7.0,³⁶ this suggests a possible slowing of the amount of depolymerization due to PDMAEMA chain collapse at pH 8.0 and 65 °C. However, by 100 h, the systems at the two pHs were very similar with ~60% decrease in Nile red fluorescence. It was also noted above that the fluorescence decrease was slightly more at pH 7.0 even at 20 °C, so this might relate to the overall hydrophilicity of the PDMAEMA and resulting water access to the particle cores as opposed to chain collapse specifically. The decrease in fluorescence for **PCB_{CON}-PDMAEMA** was ~40% over 168 h at both pHs, indicating that background degradation of the assemblies also occurred at 65 °C. This degradation can likely be attributed to cleavage of the carbonate linkage on the end-cap linker or cleavage of backbone carbamate bonds in the PCB block. Either of these cleavages would result in depolymerization of PCB, thereby amplifying the non-specific degradation. In addition, it is clear that for each system the release of Nile red was faster at 65 °C, suggesting that acceleration of depolymerization was resulting from the temperature increase dominated over the environmental effects associated with **PDMAEMA** chain collapse.

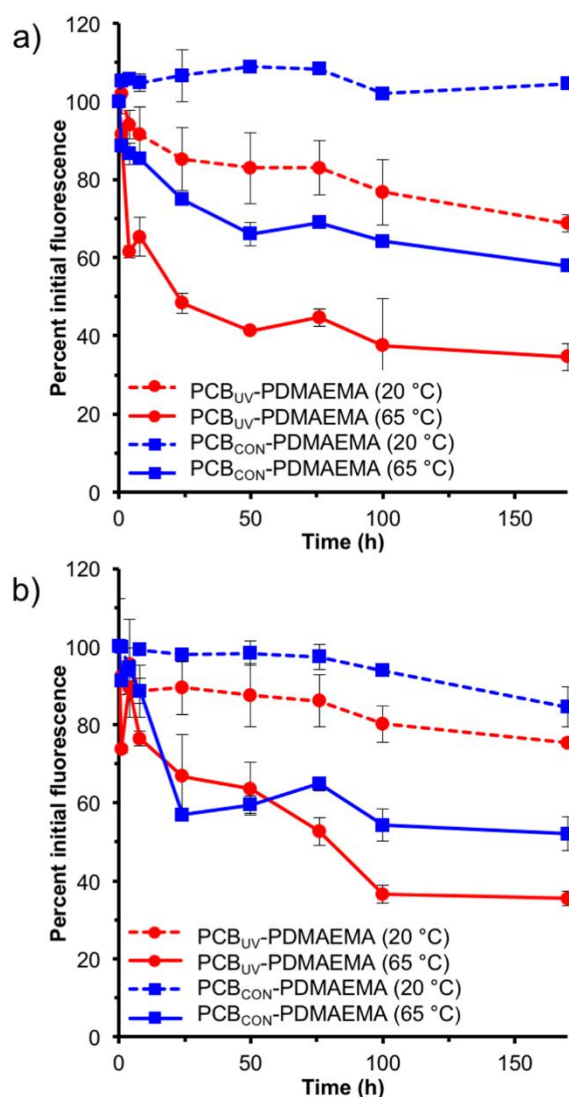


Figure 2.6: Change in the fluorescence of Nile red encapsulated in $\text{PCB}_{\text{UV}}\text{-PDMAEMA}$ or $\text{PCB}_{\text{CON}}\text{-PDMAEMA}$ assemblies following irradiation with UV light at a) pH 7.0 and b) pH 8.0 (100 μM phosphate buffer).

DLS can also provide an indication of assembly degradation because the scattered light intensity, measured as the mean count rate, is proportional to the number of scattering species and their masses. Depolymerization of the assemblies was expected to result in a decrease in the mean count rate over time. The particles were again assembled as they were in the fluorescence study, but without Nile red, at pH 7.0 or 8.0. They were then irradiated with UV light and incubated at either 20 or 65 °C. At 20 °C, a minimal change in count

rate was observed over 180 h for **PCB_{UV}-PDMAEMA** and **PCB_{CON}-PDMAEMA** at both pH values (**Figure 2.7**). While depolymerization was expected to result in a decrease in count rate due to disintegration of the assemblies, the situation may be more complicated. Upon cleavage of the soluble PDMAEMA blocks from the assembly coronas, the resulting hydrophobic particles can aggregate at the same time as depolymerizing, which may result in a net negligible effect on the count rate. In contrast, at 65 °C, all assemblies underwent a significant decrease in scattering count rate of 30-60%. At pH 7.0, where the PDMAEMA should remain soluble, **PCB_{UV}-PDMAEMA** underwent a larger decrease than **PCB_{CON}-PDMAEMA**, indicative of the specific triggering that was observed for the Nile red study. In contrast, at pH 8.0, where the PDMAEMA exhibits an LCST, the count rate was erratic for both systems. This can likely be attributed to aggregation of the PDMAEMA with itself and with the remaining PCB cores as they were depolymerizing. This aggregation would contribute to an increase in count rate, while depolymerization would contribute to a decrease. Thus, there is an effect arising from the PDMAEMA LCST, but it is difficult to elucidate. Overall, the accelerated reactions at 65 °C resulted in more rapid degradation of the assemblies.

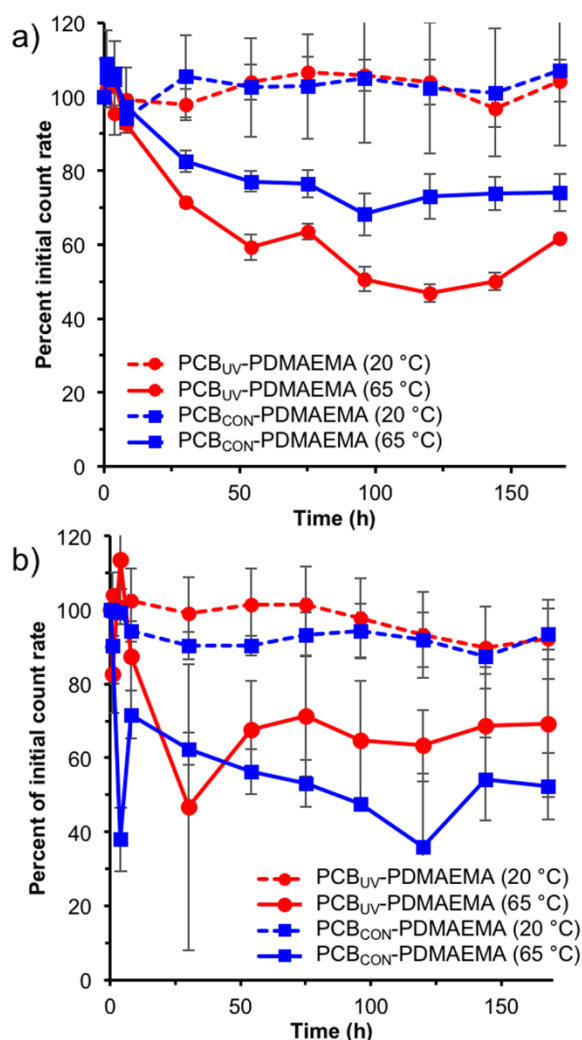


Figure 2.7: Change in DLS count rate for **PCB_{UV}-PDMAEMA** or **PCB_{CON}-PDMAEMA** assemblies following irradiation with UV light at a) pH 7.0 and b) pH 8.0 (100 μ M phosphate buffer).

^1H NMR spectroscopy was used to confirm the depolymerization of the SIP block at pH 8.0 (where the LCST was observed) to support data from the Nile red and DLS studies. For this, assemblies were obtained by sonication of the **PCB_{UV}-PDMAEMA** or **PCB_{CON}-PDMAEMA** in 100 mM, pH 8.0 phosphate buffered D_2O . Initial spectra were obtained, and only peaks corresponding to the PDMAEMA blocks were observed. Peaks corresponding to the PCB block were attenuated as this polymer was packed into the assembly core, resulting in long proton relaxation times (**Figures A2.14-A2.17**). Samples

were then irradiated with UV light and incubated at either 20 or 65 °C. Upon depolymerization, peaks corresponding to the depolymerization products emerged (Figures A2.14-A2.17). The emerging peaks at 2.63 ppm and 3.26 ppm from the cyclic urea formed by the depolymerization of the PCB block were integrated against the peak corresponding to the CH₂ adjacent to the ester on the PDMAEMA block. Over 4 weeks at 20 °C, more rapid depolymerization was observed for **PCB_{UV}-PDMAEMA** than for **PCB_{CON}-PDMAEMA**, confirming that it occurred in a stimuli-responsive manner (Figure 2.8). However, at 65 °C there was less difference between the behavior of the two polymers, indicating that the elevated temperatures needed to be above PDMAEMA's LCST resulted in a high level of background depolymerization. This result was consistent with those of the Nile red and DLS studies.

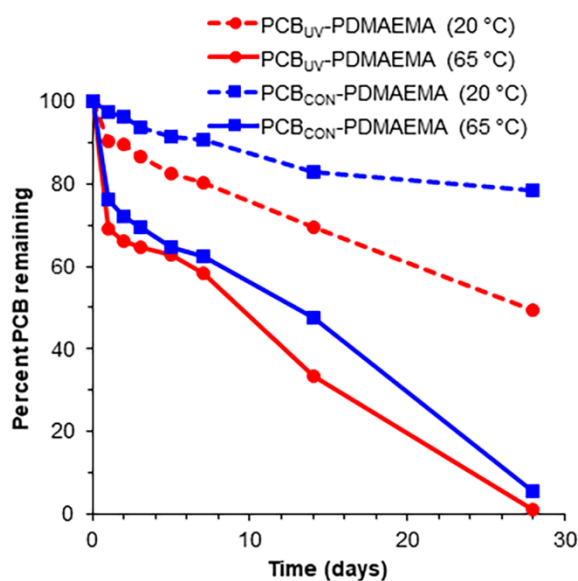


Figure 2.8: Percent depolymerization measured by ¹H NMR spectroscopy for the PCB blocks of **PCB_{UV}-PDMAEMA** and **PCB_{CON}-PDMAEMA** after irradiation and incubation in 100 mM, pH 8.0 phosphate buffered D₂O at either 20 or 65 °C.

2.4 Conclusion

In conclusion, we successfully synthesized PCB-PDMAEMA block copolymers containing a hydrophobic SIP block and a pH- and thermo-responsive hydrophilic block. Both a UV light-responsive system **PCB_{UV}-PDMAEMA** and a control system **PCB_{CON}-PDMAEMA** were prepared and studied. Both block copolymers were self-assembled via nanoprecipitation to afford solid particles with diameters of ~70 nm. The assemblies had an LCST at the same temperature (~58 °C) as the **PDMAEMA-N₃** homopolymer. Depolymerization of the assemblies in response to UV light irradiation was studied using Nile red as a fluorescent probe, and by DLS and NMR spectroscopy. In each case, stimuli-responsive degradation was observed at 20 °C. A possible effect of PDMAEMA solubility change or chain collapse on the amount of depolymerization was suggested by the Nile red data at pH 8.0, but at 65 °C there was significant background degradation of the PCB, reducing the differences in the behavior of **PCB_{UV}-PDMAEMA** and **PCB_{CON}-PDMAEMA**, and masking this effect. In addition, as the effects of elevated reaction rates dominated over any environmental effects from PDMAEMA chain collapse above the LCST, the depolymerizations were always faster at higher temperatures (**Figure 2.9**). In the future, it may be possible to observe the effects of chain collapse more clearly by using an SIP lacking non-specific degradation pathways or by using a thermo-responsive polymer with a lower LCST so that depolymerization can be studied with chain collapse at lower temperatures.

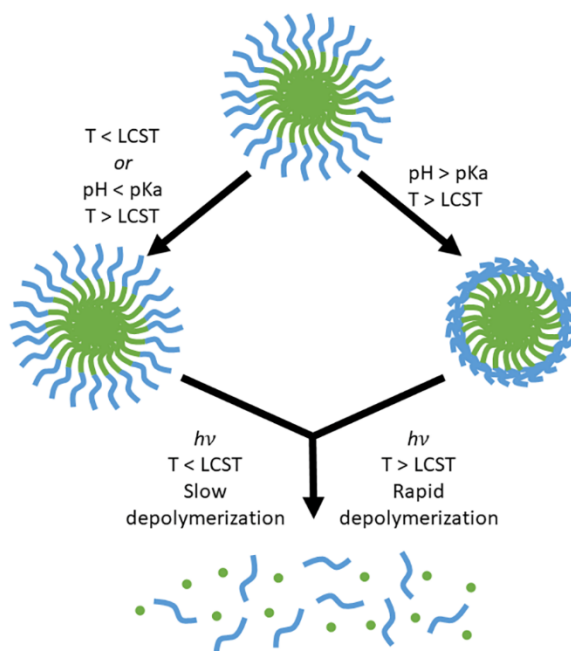


Figure 2.9: Out of the three stimuli investigated (pH, UV and temperature) the elevated temperature dominated the depolymerization behaviour, masking any other environmental factors.

2.5 References

1. Langer, R.; Vacanti, J. P., Tissue engineering. *Science* **1993**, 260, 920.
2. Vert, M.; Schwach, G.; Engel, R.; Coudane, J., Something New in the Field of PLA/GA Bioresorbable Polymers? *J. Control. Release* **1998**, 53, 85–92.
3. Tyler, B.; Gullotti, D.; Mangraviti, A.; Utsuki, T.; Brem, H., Polylactic acid (PLA) controlled delivery carriers for biomedical applications. *Adv. Drug Delivery Rev.* **2016**, 107, 163-175.
4. Pitt, G. G.; Gratzl, M. M.; Kimmel, G. L.; Surles, J.; Sohindler, A., Aliphatic Polyesters II. The Degradation of Poly (DL-lactide), Poly (ϵ -caprolactone), and Their Copolymers In Vivo. *Biomaterials* **1981**, 2, 215–220.
5. Bala, I.; Hariharan, S.; Kumar, M. N. V. R., PLGA Nanoparticles in Drug Delivery: The State of the Art. **2004**, 21, 36.
6. Astete, C. E.; Sabliov, C. M., Synthesis and Characterization of PLGA Nanoparticles. *J. Biomat. Sci.-Polym. E.* **2006**, 17, 247–289.

7. Bezwada, R. S.; Jamiolkowski, D. D.; Lee, I.-Y.; Agarwal, V.; Persivale, J.; Trenka-Benthin, S.; Ernetta, M.; Suryadevara, J.; Yang, A.; Liu, S., Monocryl® Suture, a New Ultra-Pliable Absorbable Monofilament Suture. *Biomaterials* **1995**, *16*, 1141–1148.
8. Heffernan, M. J.; Murthy, N., Polyketal Nanoparticles: A New pH-Sensitive Biodegradable Drug Delivery Vehicle. *Bioconjugate Chem.* **2005**, *16*, 1340–1342.
9. Yang, S. C.; Bhide, M.; Crispe, I. N.; Pierce, R. H.; Murthy, N., Polyketal Copolymers: A New Acid-Sensitive Delivery Vehicle for Treating Acute Inflammatory Diseases. *Bioconjugate Chem.* **2008**, *19*, 1164–1169.
10. Duan, X.; Wu, Y. L.; Ma, M. S.; Du, J. J.; Zhang, S.; Chen, H.; Kong, J., Amphiphilic polymer-drug conjugates based on acid-sensitive 100% hyperbranched polyacetals for cancer therapy. *J. Mater. Sci.* **2017**, *52*, 9430-9440.
11. Emilritri, E.; Ranucci, E.; Ferruti, P., New Poly(amidoamine)s Containing Disulfide Linkages in Their Main Chain. *J. Polym. Sci., Part A: Polym. Chem.* **2005**, *43*, 1404–1416.
12. Tsarevsky, N. V.; Matyjaszewski, K., Reversible Redox Cleavage/Coupling of Polystyrene with Disulfide or Thiol Groups Prepared by Atom Transfer Radical Polymerization. *Macromolecules* **2002**, *35*, 9009–9014.
13. Li, C.; Madsen, J.; Armes, S. P.; Lewis, A. L., A New Class of Biochemically Degradable, Stimulus-Responsive Triblock Copolymer Gelators. *Angew. Chem. Int. Ed.* **2006**, *45*, 3510–3513.
14. Quinn, J. F.; Whittaker, M. R.; Davis, T. P., Glutathione Responsive Polymers and Their Application in Drug Delivery Systems. *Polym. Chem.* **2017**, *8*, 97–126.
15. Kumar, S.; Allard, J.-F.; Morris, D.; Dory, Y. L.; Lepage, M.; Zhao, Y., Near-Infrared Light Sensitive Polypeptide Block Copolymer Micelles for Drug Delivery. *J. Mater. Chem.* **2012**, *22*, 7252–7257.
16. Honda, S.; Tanaka, N.; Toyota, T., Synthesis of Star-Shaped Poly(n-butyl acrylate) Oligomers with Coumarin End Groups and their Networks for a UV-Tunable Viscoelastic Material. *J. Polym. Sci., Part A: Polym. Chem.* **2018**, *56*, 9–15.
17. Zhao, H.; Sterner, E. S.; Coughlin, E. B.; Theato, P., o-Nitrobenzyl Alcohol Derivatives: Opportunities in Polymer and Materials Science. *Macromolecules* **2012**, *45*, 1723–1736.
18. Olejniczak, J.; Chan, M.; Almutairi, A., Light-Triggered Intramolecular Cyclization in Poly(lactic-co-glycolic acid)-Based Polymers for Controlled Degradation. *Macromolecules* **2015**, *48*, 3166–3172.

19. Goodwin, A. P.; Mynar, J. L.; Ma, Y.; Fleming, G. R.; Fréchet, J. M. J., Synthetic Micelle Sensitive to IR Light via a Two-Photon Process. *J. Am. Chem. Soc.* **2005**, *127*, 9952–9953.
20. Roth, M. E.; Green, O.; Gnaim, S.; Shabat, D., Dendritic, oligomeric, and polymeric self-immolative molecular amplification. *Chem. Rev.* **2016**, *116*, 1309-1352.
21. Wong, A. D.; DeWit, M. A.; Gillies, E. R., Amplified Release Through the Stimulus Triggered Degradation of Self-Immolative Dendrimers, Oligomers, and Linear Polymers. *Adv. Drug Delivery Rev.* **2012**, *64*, 1031-1045.
22. Phillips, S. T.; DiLauro, A. M., Continuous Head-to-Tail Depolymerization: An Emerging Concept for Imparting Amplified Responses to Stimuli-Responsive Materials. *ACS Macro Lett.* **2014**, *3*, 298–304.
23. Fan, B.; Trant, J. F.; Gillies, E. R., End-capping strategies for triggering the end-to-end depolymerization of polyglyoxylates. *Macromolecules* **2016**, *49*, 9309-9319.
24. Liu, G.; Wang, X.; Hu, J.; Zhang, G.; Liu, S., Self-immolative polymersomes for high-efficiency triggered release and programmed enzymatic reactions. *J. Am. Chem. Soc.* **2014**, *136*, 7492-7497.
25. Dewit, M. A.; Beaton, A.; Gillies, E. R., A reduction sensitive cascade biodegradable linear polymer. *J. Polym. Sci. Part A: Polym. Chem.* **2010**, *48*, 3977-3985.
26. Fan, B.; Trant, J. F.; Hemery, G.; Sandre, O.; Gillies, E. R., Thermo-responsive self-immolative nanoassemblies: direct and indirect triggering. *Chem. Commun.* **2017**, *53*, 12068-12071.
27. Fan, B.; Trant, J. F.; Wong, A. D.; Gillies, E. R., Polyglyoxylates: A Versatile Class of Triggerable Self-Immolative Polymers from Readily Accessible Monomers. *J. Am. Chem. Soc.* **2014**, *136*, 10116–10123.
28. de Gracia Lux, C.; McFearin, C. L.; Joshi-Barr, S.; Sankaranarayanan, J.; Fomina, N.; Almutairi, A., Single UV or Near IR triggering event leads to polymer degradation into small molecules. *ACS Macro Lett.* **2012**, *1*, 922-926.
29. DiLauro, A. M.; Zhang, H.; Baker, M. S.; Wong, F.; Sen, A.; Phillips, S. T., Accessibility of Responsive End-Caps in Films Composed of Stimuli-Responsive, Depolymerizable Poly(phthalaldehydes). *Macromolecules* **2013**, *46*, 7257–7265.
30. Kaitz, J. A.; Diesendruck, C. E.; Moore, J. S., End Group Characterization of Poly(phthalaldehyde): Surprising Discovery of a Reversible, Cationic Macrocyclization Mechanism. *J. Am. Chem. Soc.* **2013**, *135*, 12755–12761.

31. Kaitz, J. A.; Moore, J. S., Functional Phthalaldehyde Polymers by Copolymerization with Substituted Benzaldehydes. *Macromolecules* **2013**, *46*, 608–612.
32. Tang, S.; Tang, L.; Lu, X.; Liu, H.; Moore, J. S., Programmable Payload Release from Transient Polymer Microcapsules Triggered by a Specific Ion Coactivation Effect. *J. Am. Chem. Soc.* **2018**, *140*, 94–97.
33. Fan, B.; Trant, J. F.; Yardley, R. E.; Pickering, A. J.; Lagugné-Labarthe, F.; Gillies, E. R., Photocontrolled Degradation of Stimuli-Responsive Poly(ethyl glyoxylate): Differentiating Features and Traceless Ambient Depolymerization. *Macromolecules* **2016**, *49*, 7196–7203.
34. Fan, B.; Gillies, E. R., Poly(ethyl glyoxylate)-Poly(ethylene oxide) Nanoparticles: Stimuli-Responsive Drug Release via End-to-End Polyglyoxylate Depolymerization. *Mol. Pharmaceutics* **2017**, *14*, 2548-2559.
35. Sagi, A.; Weinstain, R.; Karton, N.; Shabat, D., Self-Immolative Polymers. *J. Am. Chem. Soc.* **2008**, *130*, 5434–5435.
36. DeWit, M. A.; Gillies, E. R., A Cascade Biodegradable Polymer Based on Alternating Cyclization and Elimination Reactions. *J. Am. Chem. Soc.* **2009**, *131*, 18327–18334.
37. Lewis, G. G.; Robbins, J. S.; Phillips, S. T., Phase-Switching Depolymerizable Poly(carbamate) Oligomers for Signal Amplification in Quantitative Time-Based Assays. *Macromolecules* **2013**, *46*, 5177–5183.
38. Robbins, J. S.; Schmid, K. M.; Phillips, S. T., Effects of Electronics, Aromaticity, and Solvent Polarity on the Rate of Azaquinone–Methide-Mediated Depolymerization of Aromatic Carbamate Oligomers. *J. Org. Chem.* **2013**, *78*, 3159–3169.
39. McBride, R. A.; Gillies, E. R., Kinetics of Self-Immolative Degradation in a Linear Polymeric System: Demonstrating the Effect of Chain Length. *Macromolecules* **2013**, *46*, 5157–5166.
40. Wong, A. D.; Gungör, T. M.; Gillies, E. R., Multiresponsive Azobenzene End-Cap for Self-Immolative Polymers. *ACS Macro Lett.* **2014**, *3*, 1191–1195.
41. Olah, M. G.; Robbins, J. S.; Baker, M. S.; Phillips, S. T., End-Capped Poly(benzyl ethers): Acid and Base Stable Polymers That Depolymerize Rapidly from Head-to-Tail in Response to Specific Applied Signals. *Macromolecules* **2013**, *46*, 5924–5928.
42. Heskins, M.; Guillet, J. E., Solution Properties of Poly(N-isopropylacrylamide). *J. Macromol. Sci. A* **1968**, *2*, 1441–1455.

43. Schild, H. G., Poly(N-isopropylacrylamide): Experiment, Theory and Application. *Prog. Polym. Sci.* **1992**, *17*, 163–249.
44. Plamper, F. A.; Ruppel, M.; Schmalz, A.; Borisov, O.; Ballauff, M.; Müller, A. H. E., Tuning the thermoresponsive properties of weak polyelectrolytes: aqueous solutions of star-shaped and linear poly (N, N-dimethylaminoethyl methacrylate). *Macromolecules* **2007**, *40*, 8361-8366.
45. Niskanen, J.; Wu, C.; Ostrowski, M.; Fuller, G. G.; Hietala, S.; Tenhu, H., Thermoresponsiveness of PDMAEMA. Electrostatic and stereochemical effects. *Macromolecules* **2013**, *46*, 2331-2340.
46. Hu, Y.; Darcos, V.; Monge, S.; Li, S.; Zhou, Y.; Su, F., Thermo-Responsive Release of Curcumin from Micelles Prepared by Self-Assembly of Amphiphilic P(NIPAAm-co-DMAAm)-b-PLLA-b-P(NIPAAm-co-DMAAm) Triblock Copolymers. *Int. J. Pharm.* **2014**, *476*, 31–40.
47. Mai, Y.; Eisenberg, A., Self-Assembly of Block Copolymers. *Chem. Soc. Rev.* **2012**, *41*, 5969–5985.
48. Liu, G.; Zhang, G.; Hu, J.; Wang, X.; Zhu, M.; Liu, S., Hyperbranched Self-Immolative Polymers (hSIPs) for Programmed Payload Delivery and Ultrasensitive Detection. *J. Am. Chem. Soc.* **2015**, *137*, 11645–11655.
49. Rubio-Ruiz, B.; Weiss, J. T.; Unciti-Broceta, A., Efficient Palladium-Triggered Release of Vorinostat from a Bioorthogonal Precursor. *J. Med. Chem.* **2016**, *59*, 9974-9980.
50. Wu, L.; Glebe, U.; Böker, A., Synthesis of Polystyrene and Poly(4-vinylpyridine) Mixed Grafted Silica Nanoparticles via a Combination of ATRP and CuI-Catalyzed Azide-Alkyne Click Chemistry. *Macromol. Rapid Commun.* **2017**, *38*, 1600475.
51. Lepeltier, E.; Bourgaux, C.; Couvreur, P., Nanoprecipitation and the "Ouzo effect": Application to drug delivery devices. *Adv. Drug Delivery Rev.* **2014**, *71*, 86-97.
52. Greenspan, P.; Mayer, E. P.; Fowler, S. D., Nile red: a selective fluorescent stain for intracellular lipid droplets. *J. Cell Biol.* **1985**, *100*, 965-973.
53. Krishna, M. M. G., Excited-state kinetics of the hydrophobic probe Nile Red in membranes and micelles. *J. Phys. Chem. A* **1999**, *103*, 3589-3595.

3 Effects of poly(*N*-isopropylacrylamide) on the depolymerization behaviour of polycarbamate based block co-polymers

3.1 Introduction

Self-immolative polymers (SIPs) are a class of stimuli-responsive polymers that depolymerize end-to-end in response to the cleavage of stimuli-responsive end-caps at the polymer termini. Their design allows for amplified responses to stimuli,¹⁻³ and end-caps can be incorporated that respond to stimuli such as acid,⁴ reducing agents,⁵⁻⁶ heat,⁷ or light.^{5, 8-9} The stimulus to which they respond can be easily modified by simply switching the end-cap, while retaining the structure of the polymer backbone. Various SIP backbones have been developed in the last decade, although this chapter will be focusing on a polycarbamate (PCB) system,¹⁰⁻¹⁴ which depolymerizes irreversibly *via* a series of cyclization and elimination reactions. In previous work it has been found that the depolymerization rate of this class of SIPs is generally quite sensitive to environmental factors such as pH and solvent.^{11, 13, 15}

Another class of stimuli-responsive polymers are thermo-responsive polymers, which undergo changes in their physical properties when exposed to changes in temperature. For example, poly(*N*-isopropylacrylamide) (PNIPAAm) exhibits a lower critical solution temperature (LCST).¹⁶⁻¹⁷ Below the LCST, the polymer chains are soluble, but above the LCST an entropically driven phase separation occurs. Unlike the previously studied thermo-responsive polymer, poly(2-(dimethylamino)ethyl methacrylate) (PDMAEMA),¹⁸⁻¹⁹ PNIPAAm is not pH-responsive. Both PNIPAAm and PDMAEMA have been used in recent years for the preparation of thermo-responsive nanomaterials.²⁰

Amphiphilic block copolymers can self-assemble in aqueous solution to form a wide variety of morphologies including spherical micelles, vesicles, and bilayers.²¹ Building on our previous efforts to control the depolymerization behaviour of self-immolative PCBs, the PCB block will be incorporated into amphiphilic block copolymers. The PCB block

will act as the hydrophobic block and will be attached to either a thermo-responsive hydrophilic PNIPAAm block, or a non-thermo-responsive hydrophilic polyethylene glycol (PEG) block. It was proposed that irradiation should cause depolymerization of the hydrophobic polycarbamate block, leading to disintegration of the copolymer assemblies. Concomitantly, the PNIPAAm block should exhibit thermo-responsive behaviour. As the depolymerization of the polycarbamate SIP block is sensitive to its environment, it was hypothesized that the collapse of the PNIPAAm chains around the assembly cores might hinder water from accessing the cores. This would hopefully reduce the amount of the polycarbamate depolymerization when compared to a nanoassembly with an extended corona at the same time point (**Figure 3.1**).

In the previous chapter, PDMAEMA was used as the thermo-responsive block, but the high temperature ($\sim 58\text{ }^{\circ}\text{C}$) needed to induce the chain collapse of the corona allowed significant background degradation of the PCB. This background degradation masked the possible effect PDMAEMA chain collapse had on the depolymerization. The use of a hydrophilic block with a lower LCST such as PNIPAAm should minimize this background degradation. Herein, we report the synthesis, self-assembly, and stimuli-responsive depolymerization of block copolymers composed of a hydrophobic self-immolative PCB¹¹ and a hydrophilic PNIPAAm or PEG block, conjugated by a UV light-responsive linker.

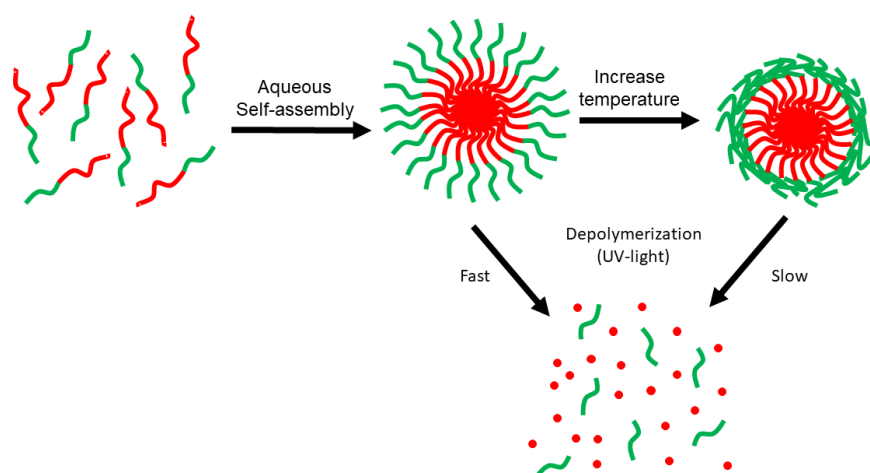


Figure 3.1: Initially proposed behaviour of PCB-PNIPAAm block copolymer assemblies.

3.2 Experimental

3.2.1 General materials and procedures

Compounds **3.1**,²² and **3.2**²² as shown in **Figure 3.3**, **3.3**¹¹ (**Scheme 3.1**), and **3.4**²³ (**Scheme 3.2**) were prepared as previously reported. 4-Nitrophenyl chloroformate, tris[2-(dimethylamino)ethyl]amine (Me₆TREN), and, *N*-isopropylacrylamide (NIPAAm), were purchased from AK Scientific. Copper(II) sulfate was purchased from Alfa Aesar. Copper(I) bromide, and (+)-sodium L-ascorbate were purchased from Sigma-Aldrich and used without further purification unless otherwise noted. Anhydrous DMF was obtained from a solvent purification system equipped with aluminum oxide columns. Pyridine, NEt₃ and CH₂Cl₂ were distilled from CaH₂ (particle size 0-2mm). Column chromatography was performed using silica gel (0.063-0.200 mm particle size, 70-230 mesh). Ultrapure deionized water was obtained from the Barnstead EASYpure II system. Unless otherwise stated, all reactions were performed under a N₂ atmosphere using flame or oven dried glassware. Dialyses were performed using Spectra/Por regenerated cellulose membranes.

3.2.2 Instrumentation

¹H NMR spectra were obtained at 600 MHz or 400 MHz using Varian INOVA spectrometers. NMR spectra were referenced relative using tetramethylsilane (TMS) using the residual solvent signals of CHCl₃ (7.26 ppm), (CH₃)₂CO (2.05 ppm), and CH₃CN (1.94 ppm) as internal standards. Size exclusion chromatography (SEC) was carried out at a flow rate of 1 mL/min in DMF with 10 mM LiBr and 1% (v/v) NEt₃ at 85 °C using a Waters 515 HPLC pump and Waters Temperature Control Module II equipped with a Wyatt Optilab T-rEX refractometer and two PLgel 5 μm mixed-D (300 mm × 7.5 mm) columns from Polymer Laboratories by Varian connected in series. The calibration was performed using poly(methyl methacrylate) (PMMA) standards. Infrared (IR) spectra were obtained on a PerkinElmer Spectrum Two FTIR Spectrometer using the attenuated total reflectance accessory. Dynamic light scattering (DLS) was performed using a Zetasizer Nano ZS instrument from Malvern Instruments at 25 °C at a concentration of 0.8 mg/mL of polymer

assemblies. Transmission electron microscopy (TEM) imaging was performed using a Phillips CM10 Microscope operating at an acceleration voltage of 80 kV. 10 μL of micelle suspension (0.8 mg/mL) was placed onto a copper grid. After 5 min, the resulting liquid was wicked away using strips of Fisherbrand™ Qualitative-Grade Filter Paper Circles and the grid was allowed to air-dry for 2 hours. Fluorescence spectra were obtained using a QM-4 SE spectrometer from Photon Technology International (PTI) equipped with both excitation and emission monochromators. Samples were excited at 540 nm with a slit width of 5 nm. UV-visible spectra were obtained on a Varian UV/vis Cary 300 spectrophotometer equipped with a Varian Cary 8453 Temperature Controller.

3.2.3 Synthetic procedures

Synthesis of PCB_{UV} and general procedure for synthesis of the self-immolative block

Monomer precursor **3.3** (2.04 g, 4.04 mmol, 1.00 equiv.) was dissolved in 1:1 TFA:CH₂Cl₂ (dry) and the reaction mixture was stirred at room temperature under N₂ for 2 hours. The solvent was removed via a stream of N₂ gas. Additional dry CH₂Cl₂ (5 mL) was added and removed again to ensure all TFA was removed. The flask was then placed under vacuum to remove all residual solvent. The resulting monomer was dissolved in 1:3 dry THF:toluene (24 mL) and the solution was cooled to 0 °C. End-cap **3.1** was added (79.8 mg, 0.2 mmol, 0.05 equiv.), followed by NEt₃ (7.04 mL, 50.5 mmol, 12.5 equiv.) and 4-(dimethylamino)pyridine (DMAP). The reaction was warmed to room temperature and stirred for 24 hours. The solution was then diluted with CH₂Cl₂ (50 mL), washed with 1 M HCl (50 mL) followed by 10% Na₂CO₃ (2 x 50 mL). The organic layer was dried over MgSO₄ and volatiles were removed *in vacuo* to provide a yellow solid. The crude polymer was further purified by dialysis using a 2 kg/mol molecular weight cut-off (MWCO) membrane against DMF followed by ultrapure deionized water over 24 hours. The sample was lyophilized to afford the product as a white powder (979 mg). Yield: 49%. ¹H NMR (600 MHz, CDCl₃, δ , ppm): 7.38-7.25 (m, 40 H), 7.11-7.04 (m, 01 H), 5.13-5.08 (m, 42 H), 4.17 (s, 2H), 3.60-3.46 (m, 85 H), 3.12-2.88 (m, 127 H), 2.54 (s, 1H). IR (cm⁻¹): 2962, 1694, 1505. SEC: M_n = 4.59 kg/mol, M_w = 10.0 kg/mol, *D* = 2.19.

Synthesis of PCB_{CON}

The polymer was synthesized using the same procedure as described above for PCB_{UV} except that endcap **3.2** was used (65.4 mg, 0.20 mmol, 0.05 equiv.). The product was obtained as a white powder (1.04 g). Yield: 51%. ¹H NMR (600 MHz, CDCl₃, δ, ppm): 7.38-7.24 (m, 44 H), 7.11-7.04 (m, 41 H), 6.94 (s, 2H), 5.12-5.08 (m, 44 H), 4.67 (s, 2H), 3.6-3.46 (m, 86 H), 3.12-2.88 (m, 137 H), 2.51 (s, 1H). IR (cm⁻¹): 2961, 1690, 1510. SEC: M_n = 4.10 kg/mol, M_w = 10.5 kg/mol, Đ = 2.51.

Synthesis of PNIPAAm-N₃

The procedure was adapted from a previously reported procedure.²⁴ The monomer *N*-isopropylacrylamide (NIPAAm) was purified by two successive recrystallizations in hexanes, and then dried *in vacuo* for 4 hours. In a Schlenk tube, purified NIPAAm (2.00 g, 17.7 mmol, 50 equiv.), CuBr (100 mg, 0.71 mmol, 2 equiv.), and isopropanol (16.7 mL) were combined and degassed for 15 min. by bubbling N₂ gas through the mixture. The ligand tris[2-(dimethylamino)ethyl]amine (Me₆TREN) was added to the flask and the mixture was subjected to three freeze-pump-thaw cycles. In a separate flask, 174 mg of atom transfer radical polymerization (ATRP) initiator **3.5** was dissolved in isopropanol (2.00 mL) and underwent three freeze-pump-thaw cycles. Using a degassed needle, 1.00 mL of the **3.5** initiator solution (1.00 mL = 87 mg, 0.35 mmol, 1.0 equiv.) was transferred to the main flask, achieving an overall monomer concentration of 1.0 M. The solution was stirred at room temperature for 2 hours. The solution was then filtered through a silica plug and concentrated *in vacuo*. The crude polymer was then dissolved in THF (2 mL) and precipitated into pentane (40 mL) three times to yield a white powder (1.21 g). Yield: 60%. ¹H NMR (600 MHz, CDCl₃, δ, ppm): 6.92-6.13 (m, 63 H), 4.14-3.84 (m, 89 H), 3.38 (bs, 2 H), 2.42-1.36 (m, 447 H), 1.12 (544 H). IR (cm⁻¹): 3281, 3063, 2964, 2876, 2103, 1642, 1539, 1456. SEC: M_n = 4.92 kg/mol, M_w = 7.42 kg/mol, Đ = 1.51.

Synthesis of **PCB_{UV}-PNIPAAm** and general procedure for the **Cu(I)**-assisted azide-alkyne cycloaddition (**CuAAC**) of the self-immolative block and **PNIPAAm**

In a Schlenk flask, **PCB_{UV}** (84 mg, 0.017 mmol, 1.0 equiv.), **PNIPAAm-N₃** (100 mg, 0.020 mmol, 1.2 equiv.), **CuSO₄** (10 mg, 0.063 mmol, 3.7 equiv.), and (+)-sodium L-ascorbate (10 mg, 0.050 mmol, 3.0 equiv.) were combined and underwent three vacuum/N₂ cycles. Dry DMF (10 mL) was added to the flask and the resulting solution was sparged with N₂ for 30 min. The samples were heated to 25 °C and stirred for 17 hours. The DMF and other volatiles were removed *in vacuo*, and the crude polymer mixture was redissolved in THF and passed through a silica plug. The polymer was purified by dialysis (6 kg/mol MWCO) with two cycles of DMF and two cycles of ultrapure deionized water over 24 hours. The sample was lyophilized to afford the product as a white powder (138 mg). Yield: 82%. ¹H NMR (600 MHz, CDCl₃, δ, ppm): 7.36-7.28 (m, 40 H), 7.11-6.96 (m, 40 H), 6.25 (bs, 19 H), 5.11-5.02 (m, 39 H), 4.11-3.85 (m, 43 H), 3.63-3.34 (m, 81 H), 3.10-2.89 (m, 122 H), 2.27-1.03 (m, 533 H). IR (cm⁻¹): 3061, 2960, 2874, 1695, 1504 SEC: M_n = 8.90 kg/mol, M_w = 17.2 kg/mol, *D* = 1.92.

Synthesis of **PCB_{CON}-PNIPAAm**

This polymer was synthesized by the same procedure as described above for **PCB_{UV}-PNIPAAm** except that **PCB_{CON}** (70 mg, 0.014 mmol, 1.0 equiv.) was used. The product was obtained as a white powder (112 mg). Yield: 80%. ¹H NMR (600 MHz, CDCl₃, δ, ppm): 7.36-7.28 (m, 39 H), 7.11-6.96 (m, 46 H), 6.25 (bs, 38 H), 5.11-5.02 (m, 44 H), 4.11-3.85 (m, 51 H), 3.63-3.34 (m, 84 H), 3.10-2.89 (m, 129 H), 2.27-1.03 (m, 570 H). IR (cm⁻¹): 3063, 2963, 2876, 1693, 1642, 1539, 1456. SEC: M_n = 8.64 kg/mol, M_w = 17.0 kg/mol, *D* = 1.96.

Synthesis of PCB_{UV}-PEG

This polymer was synthesized by the same procedure as described above for PCB_{UV}-PNIPAAm except that PCB_{UV} (100 mg, 0.020 mmol, 1.0 equiv.) and PEG-N₃ (110 mg, 0.022 mmol, 1.1 equiv.) was used. The product was obtained as a white powder (163 mg). Yield: 81%. ¹H NMR (600 MHz, CDCl₃, δ , ppm): 7.33-7.27 (m, 36 H), 7.07-6.90 (m, 44 H), 5.14-5.04 (m, 41 H), 3.88-3.37 (m, 785 H), 3.11-2.89 (116 H). IR (cm⁻¹): 2970, 2874, 1692, 1503 SEC: M_n = 17.9 kg/mol, M_w = 22.1 kg/mol, D = 1.23.

Synthesis of PCB_{CON}-PEG

This polymer was synthesized by the same procedure as described above for PCB_{UV}-PNIPAAm except that PCB_{CON} (70 mg, 0.014 mmol, 1.0 equiv.) and PEG-N₃ (75 mg, 0.015 mmol, 1.1 equiv.) were used. The product was obtained as a white powder (123 mg). Yield: 88%. ¹H NMR (600 MHz, CDCl₃, δ , ppm): 7.36-7.28 (m, 41 H), 7.06-6.98 (m, 43 H), 5.16-4.90 (m, 46 H), 4.56 (s, 2 H), 3.76-3.39 (m, 837 H), 3.10-2.90 (m, 122 H). IR (cm⁻¹): 2961, 2876, 1690, 1510 SEC: M_n = 15.9 kg/mol, M_w = 20.7 kg/mol, D = 1.31.

3.2.4 Block copolymer self-assembly

Self-assembly was performed using a nanoprecipitation method. Each block copolymer (8 mg) was dissolved in 1.0 mL DMF and stirred overnight. The block copolymer solution was filtered using a 0.2 μ m syringe filter and then 0.1 mL of the polymer solution was rapidly injected into 0.9 mL of ultrapure deionized water while stirring at 700 rpm. Alternatively, 0.9 mL of ultrapure deionized water was injected dropwise over one min into 0.1 mL of the polymer solution with stirring. After stirring overnight, the suspensions were dialyzed using a 2 kg/mol MWCO membrane against ultrapure deionized water (500 mL, 24 h, water changed once at ~12 h). Each system was prepared in triplicate.

3.2.5 Cloud point determination

Cloud point measurement for PNIPAAm-N₃

The polymer (3×5 mg) was dissolved in 1.0 mL each of ultrapure deionized water, 100 mM pH 7.4 potassium phosphate buffer, or 500 μ M pH 7.4 potassium phosphate buffer. The transmittance of each solution was monitored at 500 nm using a UV-visible spectrometer as the solution was heated at 2 °C/min. These solutions were then diluted to 2.5 mg/mL, the measurements were repeated, followed by a dilution to 0.6 mg/mL with the measurements repeated a third time.

Cloud point measurement for the block copolymers

Self-assembly was performed on each diblock copolymer using a nanoprecipitation method. Each block copolymer (4 mg) was dissolved in 0.5 mL DMF and stirred overnight. The block copolymer solution was filtered using 0.2 μ m syringe filter and then 0.1 mL of the polymer solution was rapidly injected into 0.9 mL of ultrapure deionized water while stirring at 700 rpm. After stirring overnight, the suspensions were dialyzed using a 2 kg/mol MWCO membrane against 100 mM pH 7.4 potassium phosphate buffer (500 mL, 24 h, water changed once at ~12 h). The transmittance was then monitored at 500 nm using a UV-visible spectrometer as the solution was heated at 2 °C/min.

3.2.6 Nile red loading of particles for fluorescence monitoring of assembly degradation

In a vial, 30 μ L of a 0.1 mg/mL solution of Nile red in CH₂Cl₂ was added and the solvent was removed. Next, 8 mg of the copolymer was added to the same vial and then dissolved in 1.0 mL of DMF. Assemblies were then prepared as described above but dialyzed against 100 mM potassium phosphate buffer at pH 7.4 (500 mL, 24 h, water changed once at ~12 h). The fluorescence of each system was measured using an excitation wavelength of 540 nm and the emission was recorded at 600 nm.

3.2.7 Assembly degradation studied by small molecule drug release

3.2.7.1 Drug calibration curves

Methotrexate calibration curve and general procedure

A concentrated stock solution of methotrexate was prepared by dissolving 10.2 mg of methotrexate into 10.00 mL of methanol in a volumetric flask. Serial dilutions were performed by removing 5.00 mL of this solution and diluting with methanol to 10.00 mL in a 10 mL volumetric flask. This was continued until 10 different concentrations were achieved. The absorbances of the samples were measured using UV-vis spectroscopy from 200 - 800 nm. The absorbance at 298 nm was plotted against concentration and a linear correlation was established.

Celecoxib calibration curve

A concentrated stock solution of celecoxib was prepared by dissolving 10.2 mg of celecoxib into 10.00 mL methanol in a 10 mL volumetric flask. The procedure was then the same as described above for methotrexate except that the absorbance was recorded at 252 nm.

3.2.7.2 Drug loading efficiency

To determine the drug loading efficiency of the block copolymer assemblies, the block copolymer was dissolved with 30 wt% of the target drug (relative to polymer) in DMF and stirred for 4 hours. The assemblies were then prepared using the DMF into water nanoprecipitation method as described in the block copolymer self-assembly section but dialyzed against 100 mM potassium phosphate buffer at pH 7.4 (500 mL, 12 h, water changed once at ~6 h). The samples were lyophilized to remove water and yielded a white powder. The dry samples were dissolved in methanol (2.0 mL) and the UV-vis absorbance spectra were obtained from 200 - 800 nm. The absorbance at 298 nm for methotrexate and 252 nm for celecoxib was measured and compared to the previously made calibration curve to give a final drug concentration.

Methotrexate

In a small vial, **PCB_{UV}-PNIPAAm** (3.9 mg) and methotrexate (1.4 mg) were dissolved in DMF (0.5 mL). This yielded a micelle with 4.1 wt% methotrexate loading and an encapsulation efficiency of 38%.

In a small vial, **PCB_{CON}-PNIPAAm** (4.2 mg) and methotrexate (1.6 mg) were dissolved in DMF (0.5 mL). This yielded a micelle with 6.9 wt% methotrexate loading and an encapsulation efficiency of 36%.

Celecoxib

In a small vial, **PCB_{UV}-PNIPAAm** (4.2 mg) and celecoxib (1.4 mg) were dissolved in DMF (0.5 mL). This yielded a micelle with 9.2 wt% celecoxib loading and an encapsulation efficiency of 43%.

In a small vial, **PCB_{CON}-PNIPAAm** (4.1 mg) and celecoxib (1.3 mg) were dissolved in DMF (0.5 mL). This yielded a micelle with 11 wt% celecoxib loading and an encapsulation efficiency of 34%.

3.2.7.3 Assembly degradation probed based on methotrexate release

The assemblies were prepared as described above for the drug loading efficiency trials using methotrexate for two block copolymers (**PCB_{UV}-PNIPAAm** and **PCB_{CON}-PNIPAAm**) to yield 4 mL of assemblies in 100 mM potassium phosphate buffer at pH 7.4. Each sample was divided into 2 x 2 mL, where one vial was incubated at 25 °C and another at 45 °C for 30 min. All quartz vials were then irradiated with UV light using an ACE Glass photochemistry cabinet containing a mercury light source (450 W bulb, 2.8 mW/cm² of UVA radiation at the sample) for 1 hours. Each sample was then transferred to 1 kg/mol MWCO dialysis tubing and placed in 20 mL of 100 mM potassium phosphate buffer at pH 7.4. It was then incubated at the previously described temperatures. At specified time points

over a 96 h period, the a UV-vis absorbance spectrum was taken on 2 mL of the dialysate, before being returned to the initial vial.

3.2.8 Nanoparticle depolymerization studied by NMR spectroscopy

In a small vial, 20 mg of the copolymer was dissolved in 1.4 mL of 100 mM, pH 7.4 potassium phosphate buffered D₂O and stirred for 30 min. The sample was then split between two quartz NMR tubes with one being incubated at 25 °C and the other at 45 °C. After 30 min, ¹H NMR spectra of the suspensions were obtained for the 0 h time point. The samples were then irradiated with UV light using an ACE Glass photochemistry cabinet containing a mercury light source (450 W bulb, 2.8 mW/cm² of UVA radiation at the sample) for 30 min and then incubated at either 25 or 45 °C in the dark. ¹H NMR spectra were obtained at select time points over 14 days. The integrations of emerging peaks associated with the formation of PCB degradation products were compared to those of the **PNIPAAm** peaks, which remained constant over the 14 days.

3.3 Results and discussion

3.3.1 Polymers design and synthesis

To investigate the influence of PNIPAAm on the depolymerization of the PCB block, two target polymers were designed (**Figure 3.2**). The first polymer **PCB_{UV}-PNIPAAm** contains a UV light-responsive *o*-nitroveratryl carbonate linker between the PCB and PNIPAAm blocks, while the second (control) polymer **PCB_{CON}-PNIPAAm** contains a non-stimuli-responsive benzyl carbonate. Both polymers are thermally responsive; however, polymers that have similar structures, without being thermally responsive were desired. To achieve this, another two target polymers were designed. These include the UV light-responsive **PCB_{UV}-PEG** and control **PCB_{CON}-PEG**, which both have PEG hydrophilic chains that do not exhibit any LCST behaviour over the same temperature window as PNIPAAm. This provided a set of polymers that respond only to UV light (**PCB_{UV}-PEG**) and to neither heat or light (**PCB_{CON}-PEG**) over the temperature range of 25 - 45 °C. Comparing the PEG and PNIPAAm versions at the higher temperatures, where

only micelles with PNIPAAm will experience a collapse of the corona, should provide insight to determine if the collapsing corona affects amount of depolymerization.

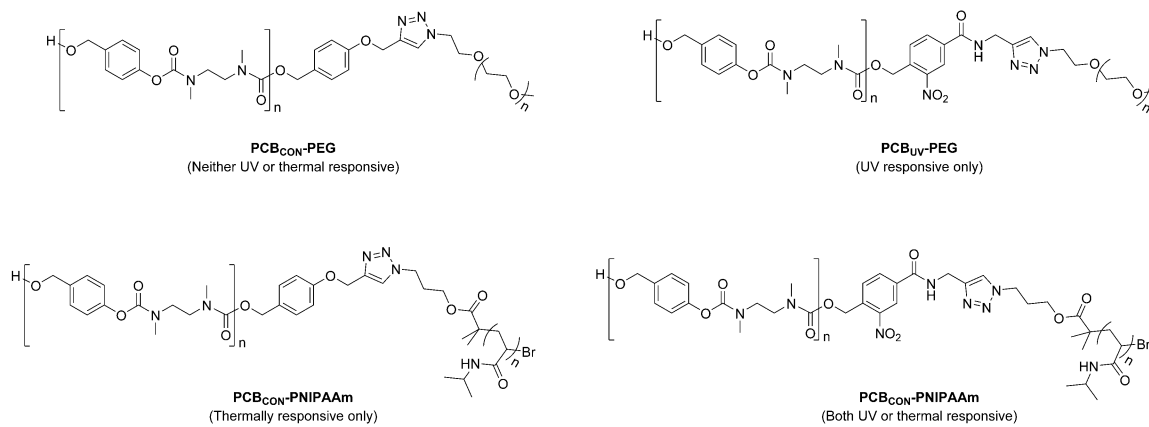


Figure 3.2: Chemical structures of target polymers **PCB_{UV}-PNIPAAm**, **PCB_{CON}-PNIPAAm**, **PCB_{UV}-PEG**, and **PCB_{CON}-PEG**.

To synthesize these four block copolymers, the individual blocks were synthesized and were then coupled together using a CuAAC. The synthetic approach involved the incorporation of alkyne termini on the PCB blocks, which was achieved by using the previously reported UV-responsive end-cap **3.1**²² and non-UV responsive end-cap **3.2**²² (**Figure 3.3**). The light-responsive moiety was an *o*-nitrobenzyl derivative, designed to cleave at the benzylic site when irradiated with UV light, to release an uncapped PCB SIP polymer that should depolymerize. The control end-cap had a similar aromatic motif but lacked the nitro group that imparted responsiveness to UV light.

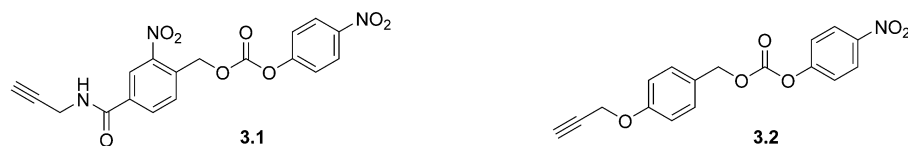
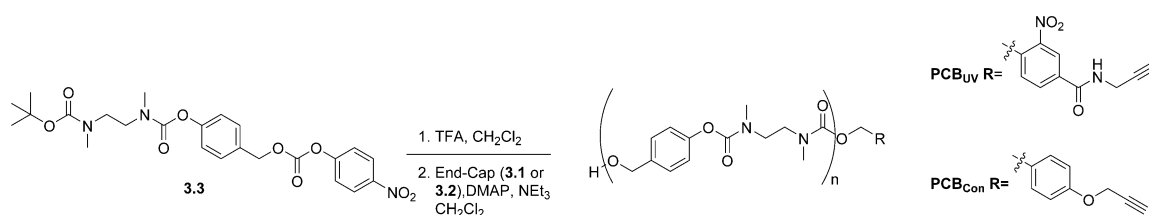


Figure 3.3: Chemical structures of UV-responsive end-cap **3.1** and control end-cap **3.2**

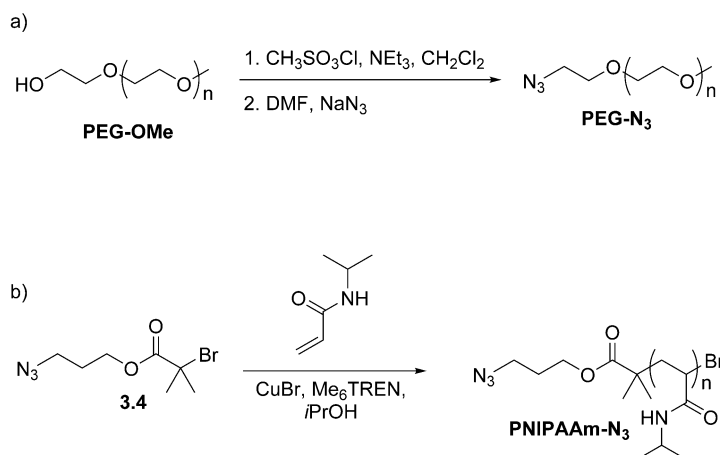
To prepare the PCB blocks, our previously reported activated monomer **3.3**¹¹ was deprotected by treatment with 1:1 CH₂Cl₂:TFA to cleave the *t*-butyloxycarbonyl protecting group, then immediately immersed in CH₂Cl₂ in the presence of DMAP, NEt₃, and 0.05

equiv. of either end-cap **3.1** or **3.2** (**Scheme 3.1**). After 24 h, the resulting polymers were isolated by extraction followed by dialysis to afford **PCB_{UV}** (from end-cap **3.1**) and **PCB_{CON}** (from end-cap **3.2**). ¹H NMR spectroscopy indicated that **PCB_{UV}** and **PCB_{CON}** had M_n values of 5.28 kg/mol and 4.48 kg/mol respectively based on integration of the end-cap peaks relative to those of the backbone repeat units. SEC in DMF relative to PMMA standards provided an M_n of 4.59 kg/mol and D of 2.19 for **PCB_{UV}** and a M_n of 4.10 kg/mol and D of 2.51 for **PCB_{CON}**. These SEC values are in good agreement with those obtained from NMR spectroscopy.



Scheme 3.1: Polymerization of **PCB_{UV}** and **PCB_{CON}**.

Azide moieties were incorporated in the PEG and PNIPAAm blocks to complement the PCB block and allow for a CuAAC to occur. The **PEG-N₃** was synthesized as previously reported from 5K-PEG monomethyl ether (**PEG-OMe**, **Scheme 3.2a**).²⁵ The reaction yielded a polymer with a M_n of 6.62 kg/mol and a D of 1.15 as determined by SEC in DMF relative to PMMA standards. An azide was also incorporated into the terminus of the PNIPAAm block by first synthesizing a modified ATRP initiator (**3.4**) with an azide moiety as previously reported, and then initiating polymerization from this azide. The purified NIPAAm monomer at a concentration of 1 M in dry isopropanol was combined with the initiator in a ratio of 50:1, in the presence of CuBr and ligand Me₆TREN (**Scheme 3.2b**). The polymerization yielded **PNIPAAm-N₃** with a M_n of 4.92 kg/mol and D of 1.53 as determined in DMF relative to PMMA standards, which agreed with NMR data.



Scheme 3.2: a) Synthesis of **PEG- N_3** and b) polymerization of **PNIPAAm- N_3** using and azide functionalized ATRP initiator

Previous work involving the coupling of PDMAEMA to a PCB SIP using CuAAC had limitations regarding what conditions could be used.²² It was suspected that the tertiary amine pendant groups on the PDMAEMA could ligate copper, preventing the copper from catalyzing the CuAAC reaction. To circumvent this, a strong ligand, 1,1,4,7,10,10-hexamethyltriethylenetetramine (HMTETA), and CuBr were complexed before the reaction in a separate solution. This method was successful, however HMTETA is expensive, so more economical CuAAC conditions were developed for use with **PNIPAAm- N_3** . To evaluate reaction conditions, the CuAAC was performed on **PNIPAAm- N_3** with commercially available propargyl alcohol using two common reagent conditions for a PNIPAAm click reactions,²⁶ and the reaction was monitored based on the loss of the azide peak in the IR spectrum post reaction (**Figure 3.4**). Use of both Cu(I)/PMDETA and Cu(II)/sodium ascorbate systems resulted in successful CuAAC reactions based on these experiments, suggesting the either system could be used. Based on ease of use and cost, the Cu(II)/sodium ascorbate system was chosen to complete all four cross coupling reactions.

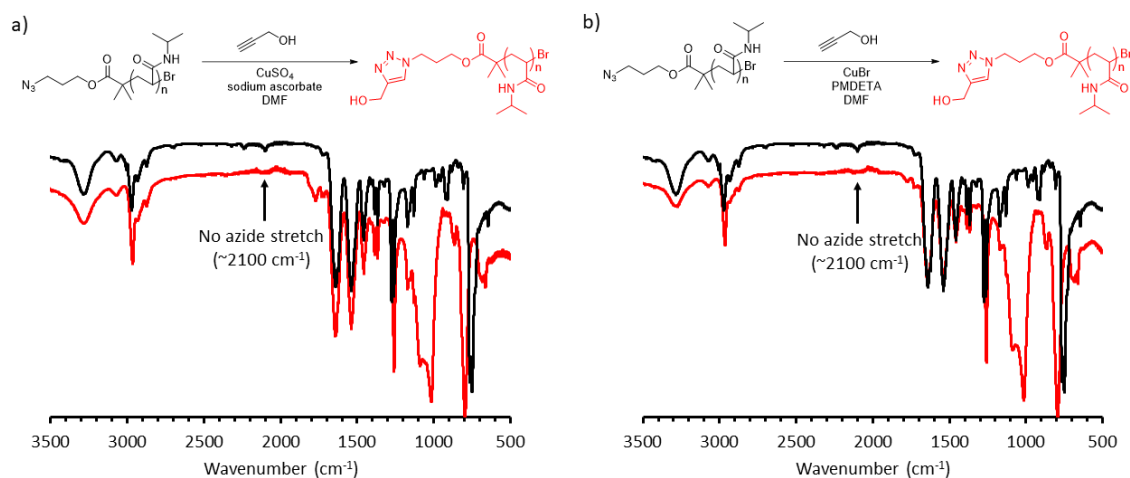
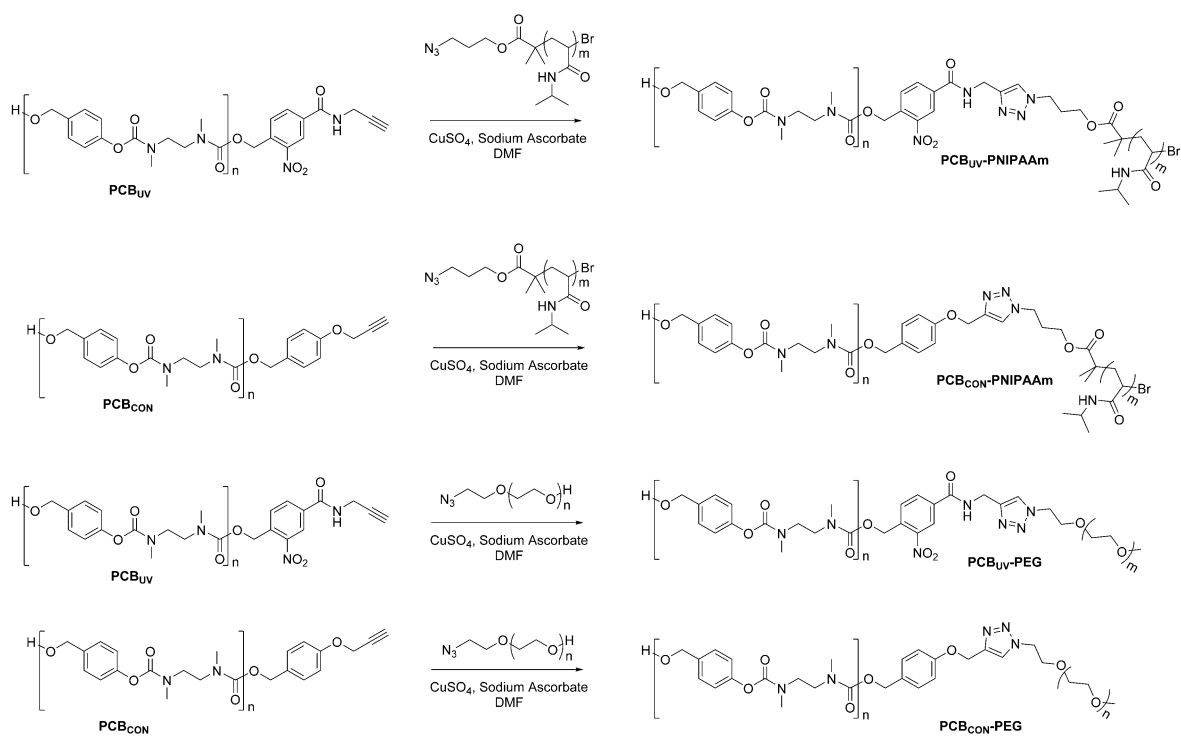


Figure 3.4: Schematics of the CuAAC reactions for the coupling of **PNIPAAm-N₃** with propargyl alcohol and their corresponding IR spectra showing complete loss of peaks corresponding to the azide stretches at 2100 cm⁻¹: a) CuSO₄/sodium ascorbate conditions and b) CuBr/PMDETA conditions.

The PCB and PNIPAAm or PEG blocks were conjugated using CuSO₄ and sodium ascorbate to produce the four target block copolymers: **PCB_{UV}-PNIPAAm**, **PCB_{CON}-PNIPAAm**, **PCB_{UV}-PEG**, and **PCB_{CON}-PEG** (Scheme 3.3). The polymers were purified by dialysis against DMF and then deionized water. To confirm that the polymers were successfully coupled, they were analyzed via ¹H NMR spectroscopy, SEC, and IR spectroscopy. ¹H NMR spectroscopy showed that the product polymers had peaks corresponding to both PCB and the associated hydrophilic blocks (Figures 3.5a, 3.6a, A3.9a, A3.10a). SEC showed an increase in the hydrodynamic volumes of the block copolymers relative to the individual blocks with an M_n of 8.90 kg/mol and a *D* of 1.92 for **PCB_{UV}-PNIPAAm**, M_n of 8.64 kg/mol and a *D* of 1.96 for **PCB_{CON}-PNIPAAm**, M_n of 17.9 kg/mol and a *D* of 1.23 for **PCB_{UV}-PEG**, and M_n of 15.9 kg/mol and a *D* of 1.31 for **PCB_{CON}-PEG** (Figures 3.5c, 3.6c, A3.9c, A3.10c). There was no evidence of contamination by homopolymers based on the single peaks observed in SEC, and lack of peaks corresponding to the elution times of the uncoupled blocks. Finally, IR spectroscopy showed the disappearance of the peak at ~2100 cm⁻¹ that corresponded to an azide stretch (3.5b, 3.6b, A3.9b, A3.10b).



Scheme 3.3: Synthesis of $\text{PCB}_{\text{UV}}\text{-PNIPAAm}$, $\text{PCB}_{\text{CON}}\text{-PNIPAAm}$, $\text{PCB}_{\text{UV}}\text{-PEG}$, and $\text{PCB}_{\text{CON}}\text{-PEG}$ using CuAAC.

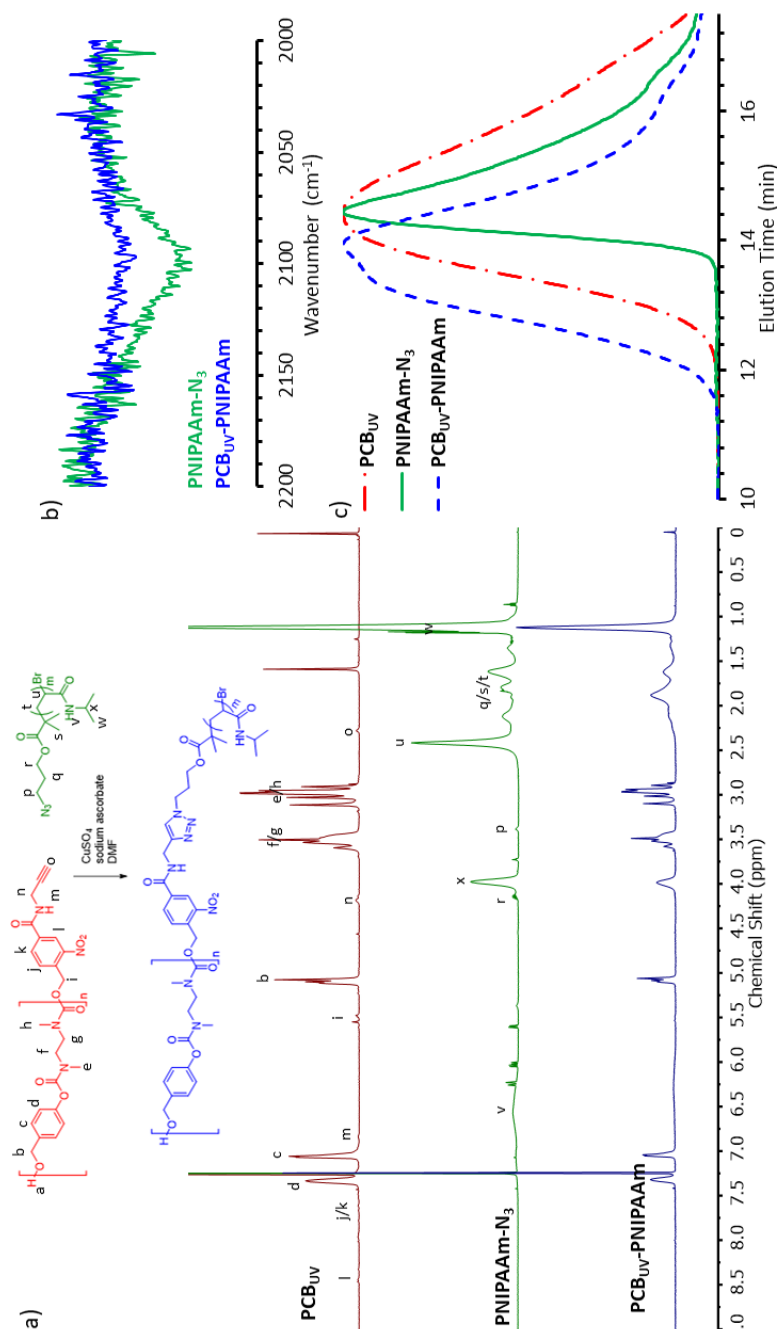


Figure 3.5: Characterization of **PCB_{UV}-PNIPAAm**: a) ¹H NMR spectra (600 MHz, CDCl₃); b) IR spectra; c) DMF SEC traces (refractive index detection). The ¹H NMR spectrum of **PCB_{UV}-PNIPAAm** has peaks from both blocks after purification and the SEC trace of **PCB_{UV}-PNIPAAm** has a decreased retention time, indicating an increase in molar mass and no peaks corresponding to the original homopolymers were observed. The azide stretch at 2100 cm⁻¹ is absent post CuAAC, indicating no free **PNIPAAm-N₃** is present.

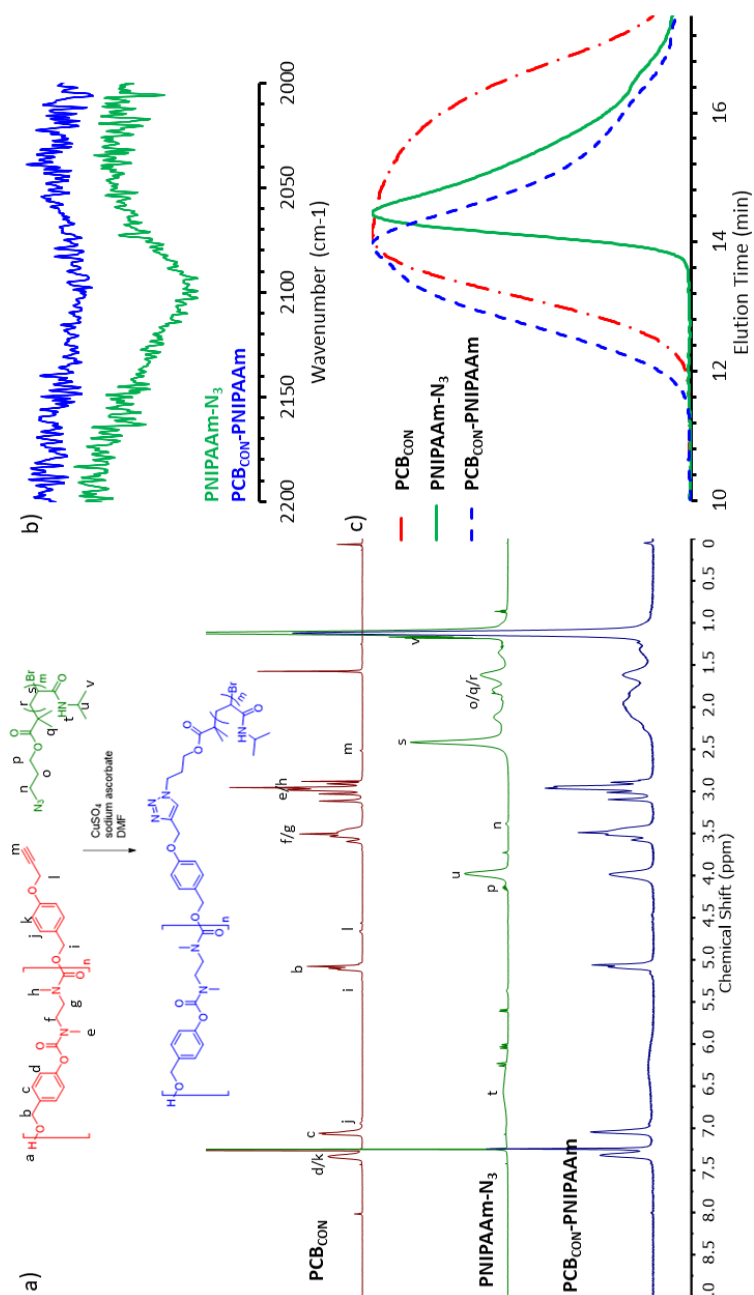


Figure 3.6: Characterization of **PCB_{CON}-PNIPAAm**: a) ¹H NMR spectra (600 MHz, CDCl₃); b) IR spectra; c) DMF SEC traces (refractive index detection). The ¹H NMR spectrum of **PCB_{CON}-PNIPAAm** has peaks from both blocks after purification and the SEC trace of **PCB_{CON}-PNIPAAm** has a decreased retention time, indicating an increase in molar mass and no peaks corresponding to the original homopolymers were observed. The azide stretch at 2100 cm⁻¹ is absent post CuAAC, indicating no free **PNIPAAm-N₃** is present.

Table 3.1: Summary of molar mass data for all polymers

	DMF Size Exclusion Chromatography			¹ H NMR spectroscopy
	M _n (kg/mol)	M _w (kg/mol)	Đ	M _n (kg/mol)
PCB_{UV}	4.59	10.0	2.19	5.28
PCB_{CON}	4.10	10.5	2.51	4.49
PNIPAAm-N₃	4.92	7.42	1.51	6.70
5K-PEG-N₃	6.62	7.60	1.15	-
PCB_{UV}-PNIPAAm	8.90	17.2	1.92	-
PCB_{CON}-PNIPAAm	8.64	17.0	1.96	-
PCB_{UV}-PEG	17.9	22.1	1.23	-
PCB_{CON}-PEG	15.9	20.7	1.31	-

3.3.2 Cloud point measurements of PNIPAAm

PNIPAAm is known to exhibit LCST behaviour, and several factors can affect the temperature at which the cloud point occurs, including chain length, polymer concentration, and salt concentration of the solution. The cloud point of **PNIPAAm-N₃** was monitored for various polymer concentrations from 5.0 mg/mL to 0.6 mg/mL. In pure water, the cloud point for 5.0 mg/mL polymer was determined to be 42 °C (**Figure 3.7a**), which is much higher than the previously reported LCST of PNIPAAm (32 °C).²⁷ The higher cloud point might result from the relatively low molar mass compared to previously reported systems. Since a chain length of around 5 kg/mol was already established for the PNIPAAm block, the effect of different concentrations of sodium phosphate buffer at pH 7.4 on the cloud point was explored. Buffer concentrations of 100 mM (**Figure 3.7b**) and 500 mM (**Figure 3.7c**) were tested. Adding the buffer resulted in a decrease in the LCST at all concentrations, with 500 mM having the largest impact, lowering the cloud point to

25 °C for the 5 mg concentrations. Although the 500 mM buffer solution decreased the cloud point the most (from 42°C to 25 °C at 5.0 mg/mL), 100 mM was chosen for subsequent experiments. The first reason is that I wanted the cloud point at least 10 °C above room temperature (~ 25 °C) which would allow for incubation of the polymer systems both above and below room temperature, eliminating the risk of accidentally exposing a system to a temperature that would trigger the cloud point behavior. The second reason is that although the overall polymer concentration would be close to 0.8 mg/mL, the local concentration of PNIPAAm in a self-assembled nanoassembly would be much higher, which was predicted to allow the PNIPAAm to behave as a more concentrated sample. Therefore for the following studies a sodium phosphate buffer solution of 100 mM at pH 7.4 was used. The cloud points were determined to be 38 °C, 43 °C, and 56 °C for 5.0 mg/mL, 2.5 mg/mL, and 0.6 mg/mL concentrations of **PNIPAAm-N₃** respectively.

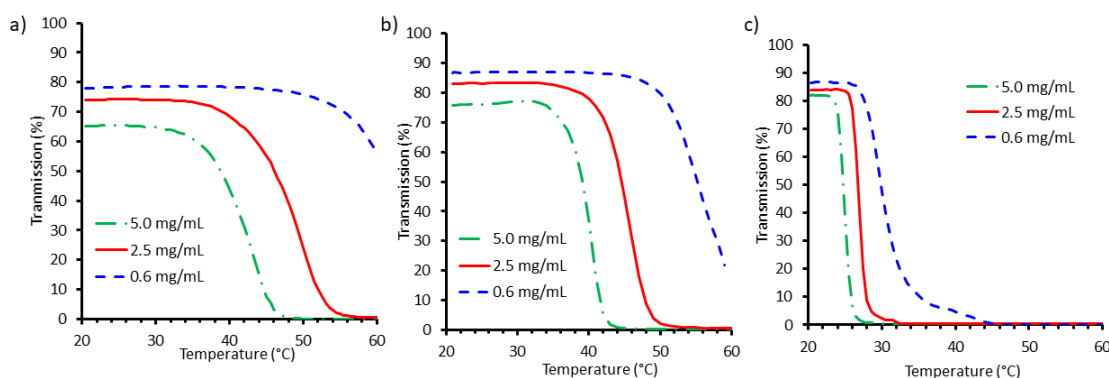


Figure 3.7: Transmission of **PNIPAAm-N₃** solutions as a function of temperature in a) ultrapure deionized water, b) 100 mM pH 7.4 sodium phosphate buffer and c) 500 mM, pH 7.4 sodium phosphate buffer.

3.3.3 Block copolymer self-assembly

The self-assembly of the four amphiphilic diblock copolymers was performed via nanoprecipitation. This procedure involved the addition of either a solution of the polymer in DMF into ultrapure deionized water, or the opposite, where water was added into the solution of DMF. The DMF was then removed by dialysis against ultrapure water. The resulting assemblies were characterized by DLS, indicating that nanoparticles with

diameters ranging from 50 to 260 nm had been formed (**Table 3.2**). Attempts were made to characterize the samples by TEM and confirm the nanoparticle size as well as the structural type, although only images for **PCB_{UV}-PNIPAAm** and **PCB_{CON}-PNIPAAm** were obtained. TEM showed that the assemblies were solid spherical particles with diameters ranging from ~50 to 90 nm (**Figure 3.8**). The smaller diameters observed by TEM can be attributed to the dried state of the particles versus the hydrated state measured by DLS as well as the influence of aggregates on the diameter measured by DLS. The DMF into water method yielded similarly sized assemblies when comparing all diblock copolymers (50-84 nm). The assemblies resulting from this method also had smaller polydispersity index (PDI) values and the diameters were reproducible; therefore this method was chosen as the method for all subsequent studies.

Table 3.2: Average micelle diameters and PDI values from DLS

	DMF into Water		Water into DMF	
	Diameter (nm)	PDI	Diameter (nm)	PDI
PCB_{UV}-PNIPAAm	61.9 ± 19	0.23	149 ± 9	0.34
PCB_{CON}-PNIPAAm	84 ± 4	0.16	260 ± 56	0.72
PCB_{UV}-PEG	50 ± 1	0.28	93 ± 20	0.23
PCB_{CON}-PEG	59 ± 14	0.26	81 ± 5	0.26

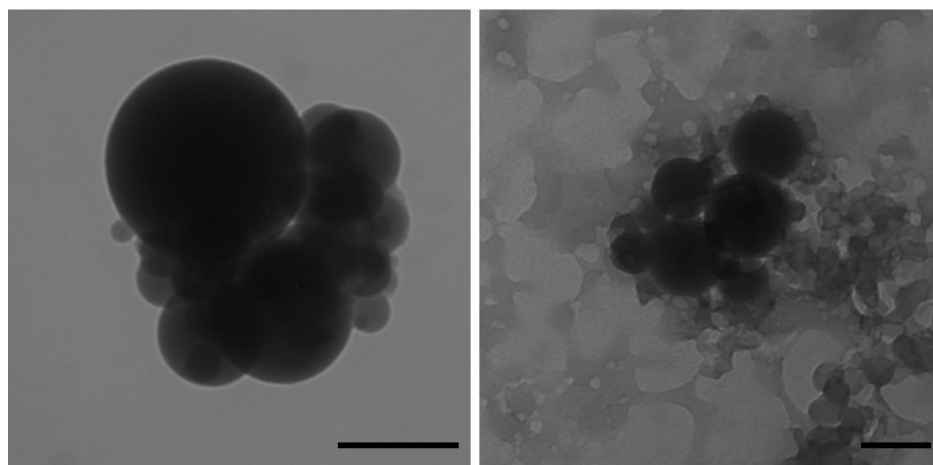


Figure 3.8: TEM images of a) **PCB_{UV}-PNIPAAm** nanoassemblies and b) **PCB_{CON}-PNIPAAm** nanoassemblies. Both assemblies were formed by dropping the DMF/polymer mixture into ultrapure water. Each scale bar represents 50 nm.

The LCST behaviour of the polymer assemblies was evaluated by preparing the nanoassemblies as described above, and then dialyzing the resulting assemblies against 100 mM, pH 7.4 sodium phosphate buffer instead of water. The cloud points of the nanoassemblies were determined using the same method described above. The cloud point of **PCB_{UV}-PNIPAAm** was determined to be 36 °C, and the cloud point of **PCB_{CON}-PNIPAAm** was 38 °C (Figure 3.9). The cloud point was the temperature at which percent transmission dropped to 50%. These cloud point temperatures were lower than those of the free **PNIPAAm-N₃** at these concentrations, suggesting that the increased local concentration of PNIPAAm in the nanoassemblies causes a depression of the cloud point. On the other hand, the control polymers, **PCB_{UV}-PEG** and **PCB_{CON}-PEG** did not show any cloud point over the evaluated temperature range of 25 - 45 °C. The two temperatures chosen for the next experiments were 25 °C for the below cloud point measurements and 45 °C for the above cloud point measurements.

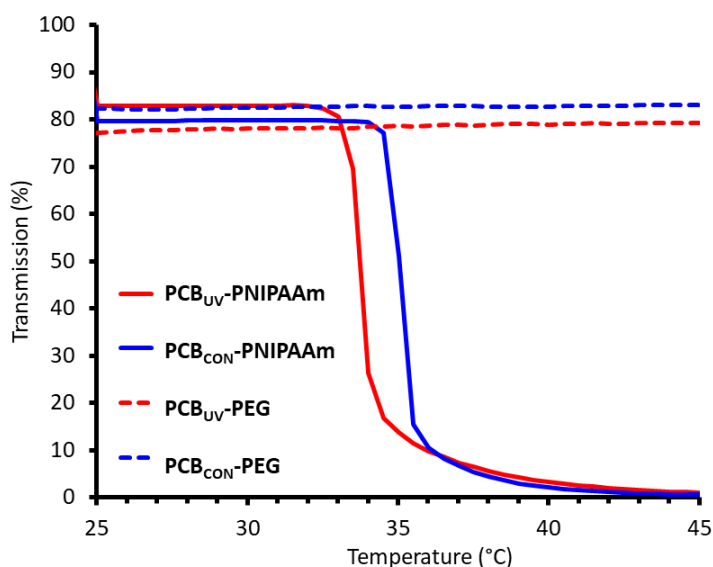


Figure 3.9: Transmission of a 0.8 mg/ml suspension of **PCB_{UV}-PNIPAAm**, **PCB_{CON}-PNIPAAm**, **PCB_{UV}-PEG**, and **PCB_{CON}-PEG** versus temperature in a 100 mM sodium phosphate buffer at pH 7.4. **PCB_{UV}-PEG**, and **PCB_{CON}-PEG** show high transmission over the entire temperature window whereas **PCB_{UV}-PNIPAAm** and **PCB_{CON}-PNIPAAm** show cloud points.

3.3.4 Depolymerization studies

3.3.4.1 Nile red loading

Depolymerization of nanoassemblies can be probed by fluorescence spectroscopy using a fluorescence probe, such as Nile red.^{22, 28} Nile red fluoresces strongly in the hydrophobic cores of particles, but when in a hydrophilic environment it experiences quenching caused by aggregation.²⁹⁻³⁰ A decrease in the fluorescence of Nile red can signify its aggregation as a result of its release into the surrounding environment, suggesting degradation of the nanoassemblies. Nanoassemblies were prepared using the DMF into water nanoprecipitation method, with 2 wt% Nile red relative to the polymer added to the DMF solution. The resulting assemblies were dialyzed against a 100 mM sodium phosphate buffer at pH 7.4. Before applying either the thermal or UV light stimuli to the system, the Nile red fluorescence of the assemblies was assessed to ensure a significant difference between the particles and free Nile red in solution fluorescence. As shown in **Figure 3.10**,

the fluorescence of the **PCB_{UV}-PNIPAAm** nanoassemblies loaded with Nile red exhibited only a slight increase relative to pure Nile red in the buffer solution without any polymer present. In contrast, a fluorescence spectrum of Nile red in **PCB_{UV}-PDMAEMA** assemblies had showed a 7-fold increase in florescence compared to the **PCB_{UV}-PNIPAAm** assemblies.²² The low initial florescence of the Nile red-loaded **PCB_{UV}-PNIPAAm** assemblies compared to Nile red in water, which may arise from poor incorporation of the dye into the nanoassemblies, indicated that it would not be easy to detect its release into water. Therefore, Nile red would not be an ideal probe for monitoring the degradation of these nanoassemblies.

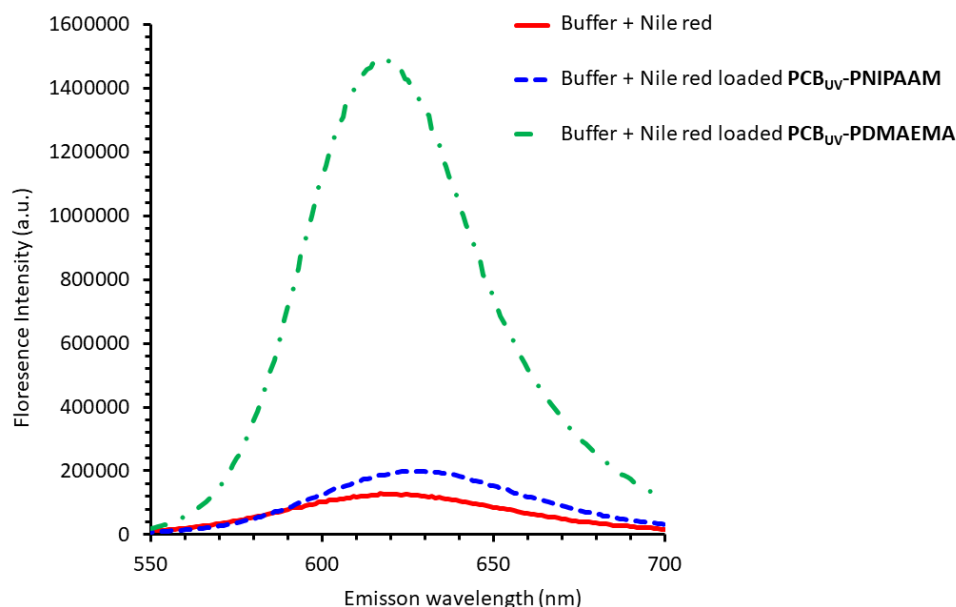


Figure 3.10: Relative fluorescence versus emission wavelength for Nile red dissolved in pH 7.4, 100 mM sodium phosphate buffer, Nile red with **PCB_{UV}-PNIPAAm** in pH 7.4, 100 mM sodium phosphate buffer and Nile red with **PCB_{UV}-PDMAEMA** (from Chapter 2). Samples were excited at 540 nm. The Nile red concentration was 2 wt% of the polymer and the polymer concentration was 0.8 mg/mL.

3.3.4.2 Drug loading

An alternative to Nile red as a small molecule probe is a UV absorbent probe, such as methotrexate or celecoxib, which are a chemotherapeutic agent and NSAID respectively. The nanoassemblies were prepared using the DMF into water nanoprecipitation method, with 30 wt% of the UV active compound relative to the polymer added to the DMF solution. The resulting assemblies were dialyzed against a 100 mM sodium phosphate buffer at pH 7.4 to remove non-encapsulated drug. The samples were then lyophilized. The entire samples were then dissolved in 2.0 mL of methanol and analyzed by UV-Vis spectroscopy. The amount of drug encapsulated into the nanoassemblies was determined by comparing the absorbance of the polymer-drug solutions in methanol at a specified wavelength (302 nm for methotrexate and 252 nm for celecoxib) to calibration curves for solutions of the drug in methanol. From the amount of drug in the final sample, a weight percent compared to the polymer, as well as the total encapsulation efficiency compared to the original amount of drug used in the loading procedure were calculated. Encapsulation efficiency is an important measure for how much of the drug is being used versus washed away during production. Drug loading determines the amount of drug in each particle and is important for dosage levels. Ideal scenarios will have a high encapsulation efficiency (less drug is being wasted) and high drug loading (more drug per weight or volume of nanoassemblies). For **PCB_{UV}-PNIPAAm**, methotrexate had a drug loading of 4.1 wt% and an encapsulation efficiency of 38% and celecoxib had a drug loading of 6.9 wt% and an encapsulation efficiency of 36%. For **PCB_{CON}-PNIPAAm** methotrexate had a drug loading of 9.2 wt% and an encapsulation efficiency of 43% and celecoxib had a drug loading of 11 wt% and an encapsulation efficiency of 34%. Although methotrexate had lower drug loading than celecoxib, the absorbance peak monitored at 302 nm for methotrexate did not overlap with the absorbance of either the polymers or the PCB degradation products. This made methotrexate the suitable probe as the absorbance data would not be affected by absorbance of the polymers or their depolymerization products.

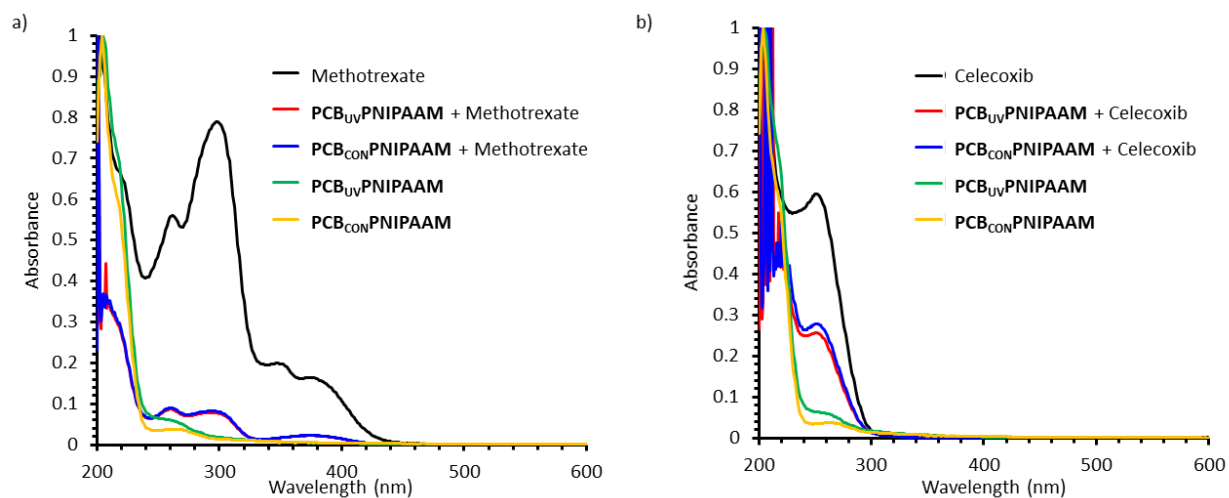


Figure 3.11: Absorbance versus wavelength for pure **PCB_{UV}-PNIPAAm** and **PCB_{CON}-PNIPAAm** and their drug loaded versions for a) methotrexate (16 $\mu\text{g/mL}$) and b) celecoxib (8 $\mu\text{g/mL}$) in methanol. Polymer assemblies were prepared in buffer as previously described to yield 2 mL of assemblies and then dried and dissolved in 2 mL of methanol. Drug content was determined by comparing to drug calibration curves in methanol (**Figure A3.11** for methotrexate and **Figure A3.12** for celecoxib).

Table 3.3: Drug loading and encapsulation efficiencies for methotrexate and celecoxib incorporated into nanoassemblies of **PCB_{UV}-PNIPAAm** and **PCB_{CON}-PNIPAAm**

	Methotrexate		Celecoxib	
	Drug Loading (wt%)	Encapsulation Efficiency (%)	Drug Loading (wt%)	Encapsulation Efficiency (%)
PCB_{UV}-PNIPAAm	4.1	38	9.2	43
PCB_{CON}-PNIPAAm	6.9	36	11	34

Polymer assemblies were prepared using the DMF into water nanoprecipitation method, with 30 wt% methotrexate relative to the polymer, to create 4 mL of drug-loaded nanoassembly solution. These solutions were then split (2 x 2 mL) and loaded into dialysis bags and each bag was placed in 20 mL of buffer. For each polymer, one set up was

incubated at 25 °C and the other at 45 °C. At regular time intervals, 1 mL of each of the buffer solutions were removed, their UV-vis absorbance spectra were obtained, and then the absorbance values were compared to the calibration curve of methotrexate in water (**Figure A3.13**). Methotrexate has an absorbance peak at 370 nm in aqueous media. This procedure allowed determination of the amount of methotrexate that had been released from the nanoassemblies, by comparing the amount of drug in the dialysate to the amount that was loaded into the particles (**Table 3.3**).

For the nanoassemblies of **PCB_{UV}-PNIPAAm** and **PCB_{CON}-PNIPAAm**, rapid release of methotrexate over the first hour after irradiation was observed (**Figure 3.12**). The samples incubated at 45 °C had *ca.* 50% release and samples incubated at 25 °C had *ca.* 75% release over the first hour, but all samples had *ca.* 80% release after 24 hours. After 48 h, the amount of methotrexate present in the dialysate plateaued for all the samples, suggesting that all the methotrexate had been released. Since there was no significant difference between the percent methotrexate release between **PCB_{UV}-PNIPAAm** and **PCB_{CON}-PNIPAAm** nanoassemblies, it was suspected that the drug was being released by a method other than the disappearance of nanoassemblies caused by the depolymerization of the SIP block. This is also supported by previous work on PCB assemblies that suggested the polymer takes days to completely depolymerize, not hours.^{11,22}

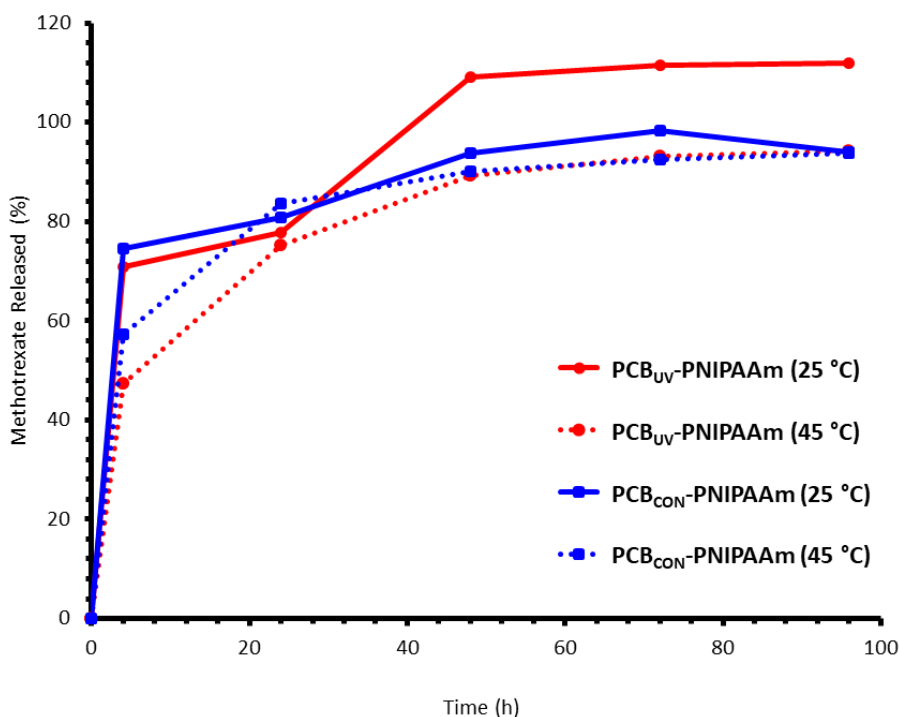


Figure 3.12: Percent methotrexate release from **PCB_{UV}-PNIPAAm** and **PCB_{CON}-PNIPAAm** nanoassemblies incubated at 25 °C or 45 °C over 96 hours.

3.3.4.3 NMR spectroscopy study to probe depolymerization of the PCB block

¹H NMR spectroscopy was used to investigate the depolymerization of the SIP blocks at both 25 °C (below cloud point) and 45 °C (above cloud point) for both **PCB_{UV}-PNIPAAm** and **PCB_{CON}-PNIPAAm**. For this experiment, assemblies were obtained by sonicating the diblock copolymers in 100 mM, pH 7.4 sodium phosphate buffered D₂O. In the initial spectra, only peaks corresponding to the PNIPAAm block were observed, because the peaks corresponding to the SIP blocks were packed into the assembly core, resulting in longer relaxation times. Samples were then irradiated with UV light and incubated at either 25 °C and 45 °C. Upon depolymerization, peaks corresponding to the depolymerization products began to emerge. The main peak monitored was the emerging peak at 3.26 ppm produced by the formation of a cyclic urea species, which was compared to the peak at 3.75 ppm on the PNIPAAm block. Over a two-week period, the control **PCB_{CON}-**

PNIPAAm nanoassemblies underwent no depolymerization at either temperature. The UV-responsive **PCB_{UV}-PNIPAAm** assemblies underwent only 12%, and 14% depolymerization for samples incubated at 25 °C and 45 °C respectively (**Figure 3.13c** and **d**). This showed selective depolymerization based on UV light depending on the end-cap present. Although the extent of depolymerization was slightly higher for the sample incubated above the cloud point, the difference was not significant based on the known errors associated with peak integrations in NMR spectroscopy. In addition, during the ¹H NMR spectroscopy studies, the nanoassemblies appeared to be precipitating out of solution, regardless of what temperature at which they were incubated (**Figure 3.13b**). This observation suggests that the nanoassemblies may have been unstable over the time frame of the experiment, possibly resulting in lack of stable integration of the control peak corresponding to the PNIPAAm block throughout the experiment. Therefore, the amount of depolymerization could not be reliably determined using ¹H NMR spectroscopy.

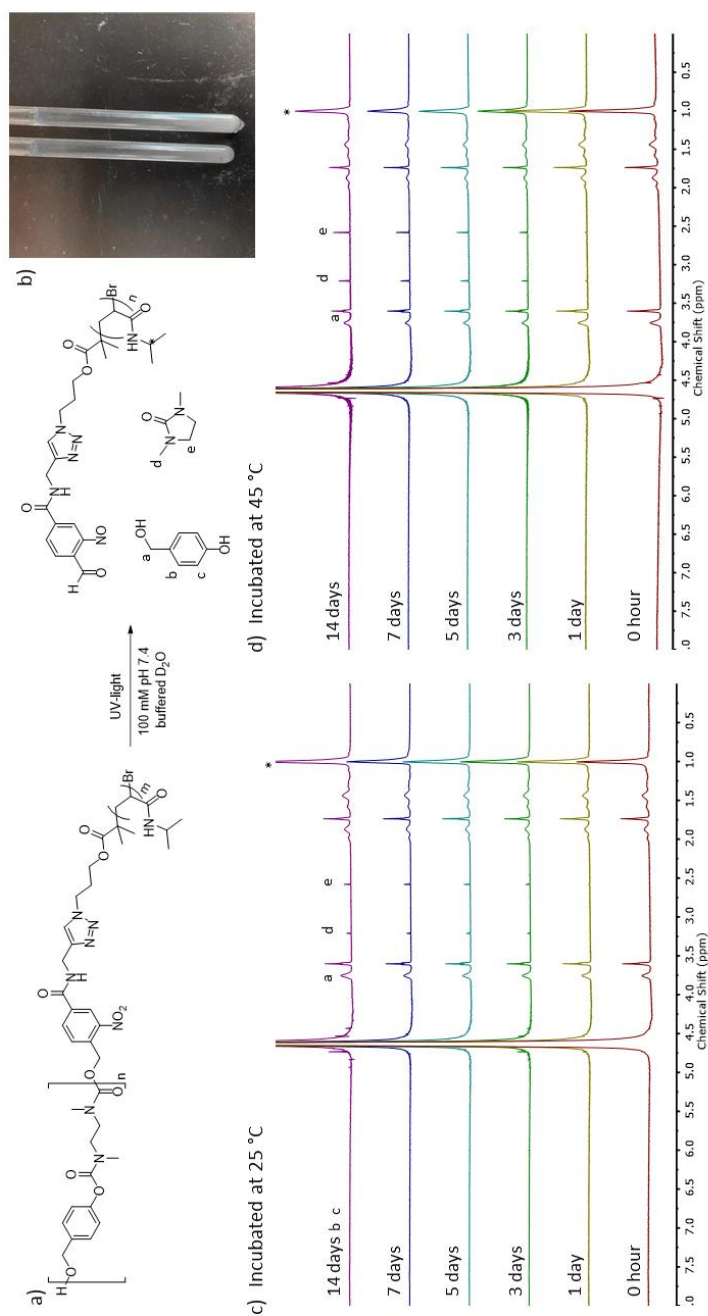


Figure 3.13: a) Depolymerization scheme for the PCB blocks of **PCBUV-PNIPAAm**; b) **PCBUV-PNIPAAm** (left) and **PCB_{CON}-PNIPAAm** (right) ¹H NMR spectroscopy samples incubated at 25 °C after 1 week showing signs of aggregation as the sample precipitated out, coating the NMR tubes; ¹H NMR spectra at different time points for **PCBUV-PNIPAAm** after irradiation and incubation in 100 mM, pH 7.4 sodium phosphate buffered D₂O at c) 25 °C or d) 45 °C showing a small degree of polymer degradation as indicated by peaks d and e corresponding to the cyclic urea degradation product.

After it became apparent that the assemblies were precipitating in the ^1H NMR depolymerization experiment, the methotrexate release experiment was reevaluated to look for evidence of a similar phenomenon. Examining the dialysis bags from the methotrexate study, it was observed that there was evidence of precipitation in the knot of the dialysis bag, which was initially not noticed (**Figure 3.14a**). Furthermore, this behaviour was seen in all bags, regardless of the temperature at which they were incubated. Seeing this in both studies suggested that the micelles were not stable in solution for long periods of time and tended to aggregate, rather than staying as discrete entities in solution. This also explained why in the TEM images the assemblies also appeared in clusters of varying sizes. To further confirm that aggregation was occurring, a sample of **PCB_{UV}-PNIPAAm** nanoassemblies was prepared as described previously. DLS measurements were taken immediately after micelle formation and measurements of the same sample were taken three days later after being kept at room temperature. An increase in nanoparticle size and dispersity of the sample support the conclusion that nanoassemblies were aggregating in solution.

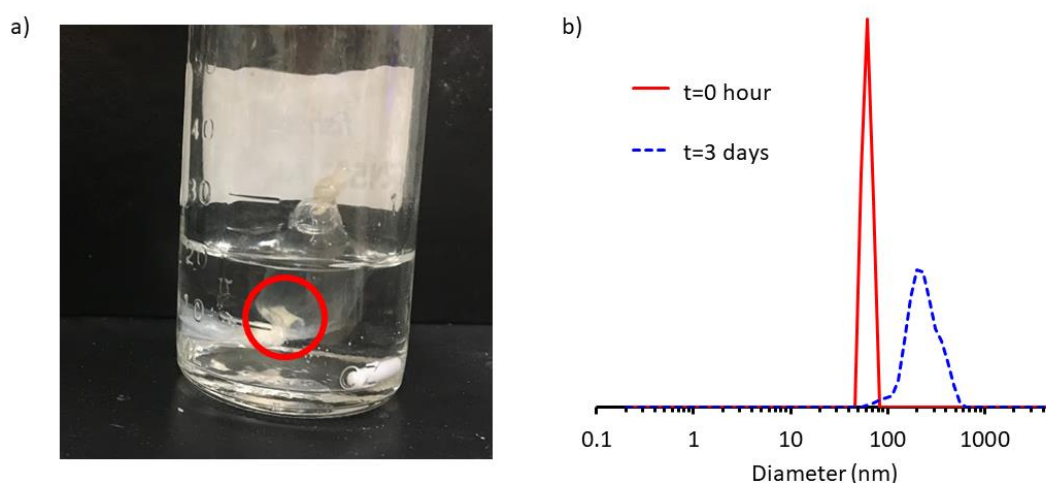


Figure 3.14: a) Methotrexate loaded **PCB_{UV}-PNIPAAm** nanoassemblies incubated at 25 °C after 2 weeks showing signs of aggregation as the sample had precipitated out (red circle) and b) DLS trace of **PCB_{UV}-PNIPAAm** nanoassemblies immediately after preparation and DLS of the same sample after three days at room temperature, showing an increase in particle size and PDI, suggesting particle aggregation.

Although PNIPAAm is a well-known reversible, thermo-responsive polymer, there have been a few reports in the literature of situations where the polymer does not show reversible behavior.³¹ However, the mechanism for the irreversible behaviour is still open to questions. The aggregation behaviour is considered to be concentration dependent. At low concentrations, solutions create a turbid yet consistent solution that exhibits reversible behaviour. At higher concentrations above the cloud point, PNIPAAm tends to flocculate, forming large, visible aggregates that are irreversible. In the current work, the incorporation of PNIPAAm into block copolymers and as part of self-assembled particles complicated the system, increasing the number of variables involved. The local concentrations of PNIPAAm when incorporated into the micelles is suspected to be high enough to create these large aggregates.

3.4 Conclusions

In conclusion, we successfully synthesized PCB-PNIPAAm and PCB-PEG block copolymers containing a hydrophobic SIP block and both thermo-responsive and non-thermo-responsive hydrophilic blocks. Both UV-responsive systems, **PCB_{UV}-PNIPAAm** and **PCB_{UV}-PEG**, and control systems, **PCB_{CON}-PNIPAAm** and **PCB_{CON}-PEG**, were prepared and studied. All four block copolymers were successfully self-assembled using nano-precipitation techniques, resulting in diameters ranging from ~50-90 nm. The PNIPAAm assemblies showed thermo-responsive behaviour, exhibiting cloud points between 36 - 38 °C when in buffered solutions at 0.8 mg/mL, whereas the PEG analogues exhibited no cloud point over the same temperature range and concentrations. Although promising systems were studied, all long-term studies of the PNIPAAm diblock copolymers showed evidence of aggregation over time, suggesting that these systems were not stable in aqueous solutions. Aggregation occurred regardless of whether the samples were incubated above or below their respective cloud points. It is unknown if the higher temperature causes aggregation to occur faster, as this phenomenon was not observed until well after aggregation began.

3.5 References

1. Roth, M. E.; Green, O.; Gnaim, S.; Shabat, D., Dendritic, Oligomeric, and Polymeric Self-Immolative Molecular Amplification. *Chem. Rev.* **2016**, *116*, 1309–1352.
2. Wong, A. D.; DeWit, M. A.; Gillies, E. R., Amplified Release Through the Stimulus-Triggered Degradation of Self-Immolative Oligomers, Dendrimers, and Linear Polymers. *Adv. Drug Deliv. Rev.* **2012**, *64*, 1031–1045.
3. Phillips, S. T.; DiLauro, A. M., Continuous Head-to-Tail Depolymerization: An Emerging Concept for Imparting Amplified Responses to Stimuli-Responsive Materials. *ACS Macro Lett.* **2014**, *3*, 298–304.
4. Fan, B.; Trant, J. F.; Yardley, R. E.; Pickering, A. J.; Laguné-Labarthe, F.; Gillies, E. R., Photocontrolled Degradation of Stimuli-Responsive Poly(ethyl glyoxylate): Differentiating Features and Traceless Ambient Depolymerization. *Macromolecules* **2016**, *49*, 7196–7203.
5. Liu, G.; Wang, X.; Hu, J.; Zhang, G.; Liu, S., Self-Immolative Polymersomes for High-Efficiency Triggered Release and Programmed Enzymatic Reactions. *J. Am. Chem. Soc.* **2014**, *136*, 7492–7497.
6. Dewit, M. A.; Beaton, A.; Gillies, E. R., A Reduction Sensitive Cascade Biodegradable Linear Polymer. *J. Polym. Sci., Part A: Polym. Chem.* **2010**, *48*, 3977–3985.
7. Fan, B.; Gillies, E. R., Poly(ethyl glyoxylate)-Poly(ethylene oxide) Nanoparticles: Stimuli-Responsive Drug Release via End-to-End Polyglyoxylate Depolymerization. *Mol. Pharm.* **2017**, *14*, 2548–2559.
8. Fan, B.; Trant, J. F.; Wong, A. D.; Gillies, E. R., Polyglyoxylates: A Versatile Class of Triggerable Self-Immolative Polymers from Readily Accessible Monomers. *J. Am. Chem. Soc.* **2014**, *136*, 10116–10123.
9. de Gracia Lux, C.; McFearin, C. L.; Joshi-Barr, S.; Sankaranarayanan, J.; Fomina, N.; Almutairi, A., Single UV or Near IR Triggering Event Leads to Polymer Degradation into Small Molecules. *ACS Macro Lett.* **2012**, *1*, 922–926.
10. Sagi, A.; Weinstain, R.; Karton, N.; Shabat, D., Self-Immolative Polymers. *J. Am. Chem. Soc.* **2008**, *130*, 5434–5435.
11. DeWit, M. A.; Gillies, E. R., A Cascade Biodegradable Polymer Based on Alternating Cyclization and Elimination Reactions. *J. Am. Chem. Soc.* **2009**, *131*, 18327–18334.

12. Lewis, G. G.; Robbins, J. S.; Phillips, S. T., Phase-Switching Depolymerizable Poly(carbamate) Oligomers for Signal Amplification in Quantitative Time-Based Assays. *Macromolecules* **2013**, *46*, 5177–5183.
13. McBride, R. A.; Gillies, E. R., Kinetics of Self-Immulative Degradation in a Linear Polymeric System: Demonstrating the Effect of Chain Length. *Macromolecules* **2013**, *46*, 5157–5166.
14. Wong, A. D.; Gungör, T. M.; Gillies, E. R., Multiresponsive Azobenzene End-Cap for Self-Immulative Polymers. *ACS Macro Lett.* **2014**, *3*, 1191–1195.
15. Robbins, J. S.; Schmid, K. M.; Phillips, S. T., Effects of Electronics, Aromaticity, and Solvent Polarity on the Rate of Azaquinone–Methide-Mediated Depolymerization of Aromatic Carbamate Oligomers. *J. Org. Chem.* **2013**, *78*, 3159–3169.
16. Heskins, M.; Guillet, J. E., Solution Properties of Poly(N-isopropylacrylamide). *J. Macromol. Sci. A* **1968**, *2*, 1441–1455.
17. Schild, H. G., Poly(N-isopropylacrylamide): Experiment, Theory and Application. *Prog. Polym. Sci.* **1992**, *17*, 163–249.
18. Plamper, F. A.; Ruppel, M.; Schmalz, A.; Borisov, O.; Ballauff, M.; Müller, A. H. E., Tuning the Thermoresponsive Properties of Weak Polyelectrolytes: Aqueous Solutions of Star-Shaped and Linear Poly(N,N-dimethylaminoethyl Methacrylate). *Macromolecules* **2007**, *40*, 8361–8366.
19. Niskanen, J.; Wu, C.; Ostrowski, M.; Fuller, G. G.; Hietala, S.; Tenhu, H., Thermoresponsiveness of PDMAEMA. Electrostatic and Stereochemical Effects. *Macromolecules* **2013**, *46*, 2331–2340.
20. Hu, Y.; Darcos, V.; Monge, S.; Li, S.; Zhou, Y.; Su, F., Thermo-Responsive Release of Curcumin from Micelles Prepared by Self-Assembly of Amphiphilic P(NIPAAm-co-DMAAm)-b-PLLA-b-P(NIPAAm-co-DMAAm) Triblock Copolymers. *Int. J. Pharm.* **2014**, *476*, 31–40.
21. Mai, Y.; Eisenberg, A., Self-Assembly of Block Copolymers. *Chem. Soc. Rev.* **2012**, *41*, 5969–5985.
22. Yardley, R. E.; Gillies, E. R., Multi-Stimuli-Responsive Self-Immulative Polymer Assemblies. *J. Polym. Sci., Part A: Polym. Chem.* **2018**, *56*, 1868–1877.
23. Wu, L.; Glebe, U.; Böker, A., Synthesis of Polystyrene and Poly(4-vinylpyridine) Mixed Grafted Silica Nanoparticles via a Combination of ATRP and CuI-Catalyzed Azide-Alkyne Click Chemistry. *Macromol. Rapid Commun.* **2017**, *38*, 1600475.

24. Xia, Y.; Yin, X.; Burke, N. A. D.; Stöver, H. D. H., Thermal Response of Narrow-Disperse Poly(N-isopropylacrylamide) Prepared by Atom Transfer Radical Polymerization. *Macromolecules* **2005**, *38*, 5937–5943.
25. Nguyen, P. K.; Snyder, C. G.; Shields, J. D.; Smith, A. W.; Elbert, D. L., Clickable Poly(ethylene glycol)-Microsphere-Based Cell Scaffolds. *Macromol. Chem. Phys.* **2013**, *214*, 948–956.
26. Narumi, A.; Fuchise, K.; Kakuchi, R.; Toda, A.; Satoh, T.; Kawaguchi, S.; Sugiyama, K.; Hirao, A.; Kakuchi, T., A Versatile Method for Adjusting Thermoresponsivity: Synthesis and ‘Click’ Reaction of an Azido End-Functionalized Poly(N-isopropylacrylamide). *Macromol. Rapid Commun.* **2008**, *29*, 1126–1133.
27. Aseyev, V.; Tenhu, H.; Winnik, F. M., Non-ionic Thermoresponsive Polymers in Water. In *Self Organized Nanostructures of Amphiphilic Block Copolymers II*, Müller, A. H. E.; Borisov, O., Eds. Springer Berlin Heidelberg: Berlin, Heidelberg, 2011; p 29–89.
28. Fan, B.; Yardley, R. E.; Trant, J. F.; Borecki, A.; Gillies, E. R., Tuning the Hydrophobic Cores of Self-Immolative Polyglyoxylate Assemblies. *Polym. Chem.* **2018**, *9*, 2601–2610.
29. Martinez, V.; Henary, M., Nile Red and Nile Blue: Applications and Syntheses of Structural Analogues. *Chem. – Eur. J.* **2016**, *22*, 13764–13782.
30. Stuart, M. C. A.; van de Pas, J. C.; Engberts, J. B. F. N., The Use of Nile Red to Monitor the Aggregation Behavior in Ternary Surfactant–Water–Organic Solvent Systems. *J. Phys. Org. Chem.* **2005**, *18*, 929–934.
31. Bischofberger, I.; Trappe, V., New Aspects in the Phase Behaviour of Poly-N-isopropyl Acrylamide: Systematic Temperature Dependent Shrinking of PNiPAM Assemblies Well Beyond the LCST. *Sci. Rep.* **2015**, *5*, 15520.

4 Transesterification of poly(ethyl glyoxylate)s: a simple route towards directly-inaccessible polyglyoxylates

4.1 Introduction

Self-immolative polymers (SIPs) are an important class of smart polymers as they undergo end-to-end depolymerization after the cleavage of their backbones or stimuli-responsive end-caps in response to stimuli including light, redox agents, enzymes, and changes in pH or temperature.¹⁻⁴ This property allows them to exhibit amplified responses to single polymer cleavage events and imparts advantageous properties for various applications including drug delivery systems⁵ and sensors.⁶⁻⁷ Based on their backbones, SIPs can be categorized into polycarbamates,⁸⁻¹¹ polycarbonates,¹² poly(benzyl ether)s,¹³⁻¹⁸ polyphthalaldehydes,¹⁹⁻²⁸ polyglyoxylamides (PGAm)s,²⁹⁻³⁰ and polyglyoxylates (PGs).³¹⁻³² Aside from the unique properties each backbone displays, SIPs can show specific behaviors derived from the nature of their stimuli-responsive end-caps and pendant groups. Hence, synthetic strategies offering SIPs with unprecedented repeating groups and end-caps are extremely valuable.^{29,33}

Poly(methyl glyoxylate)s were the first examples of PGs which were reported decades ago but since they were not equipped with stimuli-responsive end-caps and methanol, a biologically toxic compound, is one of their final degradation products, they did not attract much attention.³⁴⁻³⁶ In contrast, poly(ethyl glyoxylate) (PEtG) has attracted significant attention as it eventually degrades to ethanol and glyoxylic acid hydrate, a metabolic intermediate.³⁷ In addition, we have reported the incorporation of stimuli-responsive end-caps, allowing PEtG to be selectively depolymerized in response to specific stimuli.^{32,38} So far, we have reported the application of PEtGs for drug delivery systems,³⁹⁻⁴⁰ UV-light lithography,⁴¹ smart packaging⁴² as well as their use as precursors to PGAm)s²⁹ which are a different family of SIPs and have different properties from their analogous esters. Besides PEtGs, we also reported the synthesis of poly(benzyl glyoxylate)s,³² poly(*n*-butyl glyoxylate)s,³² and poly(menthyl glyoxylate)s.³⁹ However, our efforts to consistently prepare high molar-mass homopolymers based on benzyl glyoxylate (BnG), menthyl glyoxylate (MenG), or *n*-butyl glyoxylate (*n*-BuG) were not

successful as attaining very high levels of monomer impurity is essential for the synthesis of PGs and our purification methods could not offer those purity levels. To address this limitation, we copolymerized BnG, *n*-BuG, and MenG with ultrapure ethyl glyoxylate (EtG) to afford higher degrees of polymerization.

Recently, we reported the anionic polymerization of EtG and an optimized method for the purification of EtG to levels required for controlled polymerization.⁴³ During this study, we found that for cracking the oligomers and eliminating the hydrate species to yield ultrapure EtG the use of heat and P₂O₅ is inevitable. The optimized working temperature was 165 °C which was only *ca.* 10 °C higher than the boiling temperature of H₃PO₄ which was the byproduct of the reaction of P₂O₅ with hydrate species. EtG boils at *ca.* 110 °C and rapidly starts to degrade at temperatures higher than 220 °C. It is also noteworthy that thermal distillations at temperatures higher than 165 °C or vacuum distillations at lower temperatures tend to result in the contamination of monomers with H₃PO₄ and such monomers produce low molar mass PGs similar to what we originally observed for poly(benzyl glyoxylate)s and poly(*n*-butyl glyoxylate)s. In addition, working at temperatures lower than 155 °C was not practical due to the low monomer distillation yields.

As the applications of PGs have been practically limited to PEGs and we have been interested in the development of new PGs, we decided to reinvestigate the synthesis and purification of glyoxylate monomers in light of this improved knowledge of monomer purification. To directly prepare new PGs from the corresponding monomers, we encountered three problems. First, crude glyoxylate monomers are typically produced by the oxidative cleavage of fumarate diesters with strong agents such as ozone gas.^{32,39} Interesting fumarate diesters like diallyl and dipropargyl fumarate can't preserve their alkyne or alkene groups, under those conditions. Secondly, glyoxylate monomers with functional groups incompatible with P₂O₅ can't be purified to a high level as we employed several drying agents and only P₂O₅ provided ultrapure monomers. In addition, glyoxylate monomers with boiling points similar to or higher than H₃PO₄ (*e.g.*, for BnG and *n*-BuG: bp: *ca.*180 °C) always co-distilled with some H₃PO₄. Multiple distillations typically reduced the H₃PO₄

concentration but they also reduced the yield, and in our hands, never consistently gave high-quality monomers similar to EtG.

At this point, we concluded that, for the preparation of high molar mass PGs, the synthesis of any glyoxylate monomer with a boiling point higher than 130 °C or functional groups incompatible with oxidizing agents, heat, or P₂O₅ is not practical. Hence, we changed our focus to post-polymerization modification methods. Recently, the Sumerlin group published a report regarding the use of 1,5,7-triazabicyclo[4.4.0]dec-5-ene (TBD) as a catalyst for the transesterification reaction of polyacrylates under relatively mild conditions.⁴⁴ Inspired by this finding, we implemented TBD and various alcohols for expanding the PG family. Herein, we report the reactivity of structurally different alcohols towards this reaction, characterization of the resulting new PGs, and the synthesis of functional PGs which can serve for applications including labelling and sensors.

4.2 Experimental

4.2.1 General materials and procedures

All reactions were performed under a N₂ atmosphere using flame or oven-dried glassware. 1,5,7-Triazabicyclo[4.4.0]dec-5-ene, 2-nitrobenzyl alcohol, and 1-(azidomethyl)pyrene were obtained from AK Scientific and used as received. *n*-Pentanol, *n*-hexanol, propargyl alcohol, furfuryl alcohol, *n*-BuLi solution, benzyl chloromethyl ether (technical, ~60%), benzyl chloroformate, CaH₂ (particle size 0-2mm), and (+)-sodium L-ascorbate were obtained from Sigma-Aldrich and used as received. Allyl alcohol, *n*-butanol, and copper (II) sulfate were obtained from Alfa-Aesar and used as received. *n*-Propanol, *i*-propanol, *n*-octanol, pentane, acetone, CDCl₃, chromatography-grade tetrahydrofuran (THF), magnesium sulfate, and hydrochloric acid were obtained from Caledon Laboratories and used as received. Anhydrous ethanol was obtained from Commercial Alcohols and used as received. Toluene was obtained from Caledon Laboratories and distilled over sodium using benzophenone as an indicator. NEt₃ was obtained from Caledon Laboratories and stirred over CaH₂ (particle size 0-2mm) for 16 h before thermal distillation. *N,N*-Dimethyl formamide (DMF) was obtained from a PureSolv MD 5 solvent purification system

equipped with aluminum oxide columns. Column chromatography was performed using silica gel (0.063-0.200 mm particle size, 70-230 mesh) from SiliCycle. Ultrapure deionized water was obtained from a Barnstead EASYpure II system. Dialyses were performed using Spectra/Por regenerated cellulose membranes.

4.2.2 Instrumentation

^1H NMR spectra were obtained at 400 MHz using a Varian INOVA spectrometer. ^{13}C NMR spectra were obtained at 100 MHz using a Varian INOVA spectrometer. NMR spectra were referenced relative using tetramethylsilane (TMS) using the residual solvent signals of CHCl_3 (7.26 ppm), $(\text{CH}_3)_2\text{CO}$ (2.05 ppm), and CH_3CN (1.94 ppm) as internal standards. Size exclusion chromatography (SEC) was conducted using THF solutions of polymers at concentrations of *ca.* 5 mg/mL. The samples were analyzed using a Viscotek GPCmax VE 2001 SEC instrument equipped with an Agilent PolyPore guard column (PL1113-1500) and two sequential Agilent PolyPore SEC columns packed with porous poly(styrene-*co*-divinylbenzene) particles (molar mass range 200 – 2,000,000 g/mol; PL1113-6500) regulated at a temperature of 30 °C. Signal responses were measured using a Viscotek VE 3580 RI detector and molar masses were determined by conventional calibrations using poly(methyl methacrylate) (PMMA) standards purchased from Viscotek. Thermogravimetric analysis (TGA) was performed using a TA Instruments Q50 thermogravimetric analyzer. Samples were placed in a platinum pan and heated at a rate of 10 °C/min from 25 to 1000 °C under a flow of nitrogen (60 mL/min). Differential scanning calorimetry (DSC) thermograms were acquired using a TA Instruments DSC Q20 instrument. The polymer samples were placed in an aluminum Tzero pan and heated from room temperature to maximum temperatures, which were at least 20 °C below the onset of decomposition, at 10 °C/min under a flow of nitrogen (50 mL/min) and cooled to -70 °C at 10 °C/min, before they underwent two additional heating/cooling cycles. Thermal data were obtained from the second heating cycle. Infrared (IR) spectra were obtained on a PerkinElmer Spectrum Two FTIR Spectrometer using the attenuated total reflectance accessory. Fluorescence spectra were obtained using a QM-4 SE spectrometer from Photon

Technology International (PTI) equipped with both excitation and emission monochromators.

4.2.3 Synthetic procedures

Synthesis of PEtG_{carbonate}

In a Schlenk flask, an *n*-BuLi solution (80 μ L, 2.5 M in hexanes, 0.2 mmol) was combined with dry toluene (20 mL), and then freshly distilled EtG (5.0 mL, 50 mmol) was rapidly added at 20 °C. The resulting solution was vigorously stirred for 15 minutes. The resulting solution was then cooled to -20 °C and stirred for 10 minutes before the addition of NEt₃ (0.3 mL, 2 mmol) and stirring for another 10 minutes. Benzyl chloroformate (0.3 mL, 0.2 mmol) was rapidly added, and the resulting mixture was stirred for 3 h at -20 °C before it was allowed to gradually reach 20 °C over 16 hours. The polymerization mixture was precipitated into methanol (250 mL), and then the solvent was decanted and the resulting residue was dried under vacuum. Yield = 4.5 g, 90%. ¹H NMR (400 MHz, CDCl₃, δ): 5.71–5.60 (m, CH, 286 H), 4.20–4.03 (m, CH₂, 577 H), 1.32–1.28 (m, CH₂, 577 H), 0.88 (br s, CH₃, 3 H). Spectral data agreed with those previously reported.⁴³ SEC: M_n = 27.6 kg/mol, M_w = 35.6 kg/mol, *D* = 1.29.

Synthesis of PEtG_{ether}

In a Schlenk flask, an *n*-BuLi solution (100 μ L, 2.5 M in hexanes, 0.25 mmol) was combined with dry toluene (20.0 mL), and then freshly distilled EtG (5.0 mL, 50 mmol) was rapidly added at 20 °C. The resulting solution was vigorously stirred for 15 minutes. The resulting solution was cooled to -20 °C and stirred for 10 minutes before the addition of NEt₃ (0.3 mL, 2 mmol) and stirring for another 10 minutes. Benzyl chloromethyl ether (1.0 mL, 4.3 mmol) was instantly added and the resulting mixture was stirred for 3 h at -20 °C before sealing the flask under N₂ gas and transferring it into a -20 °C freezer where it was kept for 21 hours. The polymerization mixture was precipitated into -20 °C methanol (250 mL), and then the solvent was decanted and the resulting residue was dried under vacuum. Yield = 2.50 g, 50%. ¹H NMR (400 MHz, CDCl₃, δ): 5.70–5.53 (m, CH, 122 H),

4.20–4.03 (m, CH_2 , 247 H), 1.32–1.28 (m, CH_2 , 369 H), 0.89 (br s, CH_3 , 3 H). ^{13}C NMR (100 MHz, $CDCl_3$, δ): 166.0, 165.2, 128.9, 128.3, 128.2, 127.8, 127.7, 152.2, 93.5, 92.9, 92.5, 91.0, 61.9, 13.8. SEC: $M_n = 14.0$ kg/mol, $M_w = 18.1$ kg/mol, $D = 1.29$.

Synthesis of **PEtG_{UV}**

Inside a Schlenk flask and at 20 °C, 2-nitrobenzyl alcohol (153.1 mg, 1.0 mmol) and $(TMS)_2NLi$ (167.3 mg, 1.0 mmol) were combined in dry toluene (80.0 mL) and stirred for 5 seconds, before the instantaneous addition of freshly distilled EtG (20.0 mL, 200 mmol) and then the resulting solution was cooled to –20 °C. After 15 minutes of vigorous stirring, NEt_3 (1.2 mL, 9 mmol) was added and the solution was stirred for another 20 minutes. Benzyl chloromethyl ether (4.0 mL, 17 mmol) was instantly added and the resulting mixture was stirred for 3 h at –20 °C before sealing the flask under N_2 gas and transferring it into a –20 °C freezer where it was kept for 21 hours. The polymerization mixture was then precipitated into methanol (1.0 L). The solvent was decanted, and the resulting residue was dried under vacuum. Yield = 16.0 g, 80%. 1H NMR (400 MHz, $CDCl_3$, δ): 8.10 (s, CH , 1H), 7.87 (d, $J = 16$ Hz, CH , 1 H), 7.67 (d, $J = 8$ Hz, CH , 1H), 7.46 (s, CH , 1 H), 5.70–5.54 (m, CH , 226 H), 5.14 (s, CH_2 , 2 H), 4.99 (s, CH_2 , 2 H), 4.20–4.13 (m, CH_2 , 458 H), 1.37–1.19 (m, CH_3 , 690 H). ^{13}C NMR (100 MHz, $CDCl_3$, δ): 165.9, 165.8, 165.5, 165.2, 128.3, 127.9, 93.6, 92.9, 92.4, 62.0, 13.8. SEC: $M_n = 24.1$ kg/mol, $M_w = 29.9$ kg/mol, $D = 1.24$.

General procedure for transesterification reactions

Note: the transesterification reactions of ethanol, *n*-PrOH, *i*-PrOH, and *n*-BuOH were performed inside pressure tubes prepared/sealed inside a glovebox and heated in a fume hood. The rest of the reactions were carried out using Schlenk flasks using standard Schlenk techniques. Inside a 50 mL flask, **PEtG_{UV}** (200 mg, 1.96 mmol of ethyl ester units, 1.0 equiv.) was combined with an alcohol (10 equiv. or 0.5 equiv) and dry toluene (4.0 mL). The resulting solutions were degassed by bubbling N_2 gas through them for 20 min. Then, TBD (55 mg, 0.39 mmol, 0.2 equiv.) was added and the reaction mixture was heated

to 100 °C for 17 hours under a constant nitrogen flow (*ca.* 5 mL/min) or in a sealed tube depending on the identity of the alcohol. After cooling to 20 °C, the crude products were diluted with CH₂Cl₂ (15 mL) and washed with an HCl solution (pH = 2; 3 × 20 mL). The organic layer was dried with MgSO₄ and concentrated *in vacuo*. The pure PG was isolated by three precipitations of its CH₂Cl₂ solution (1 mL) into pentane (50 mL) or by dialysis against acetone as indicated. The resulting product was dried under vacuum.

PnPrG. From *n*-propanol (1.5 mL, 19.60 mmol, 10 equiv.) and purified by precipitation into pentane. Conversion: >99%. Yield: 57%. ¹H NMR (400 MHz, CDCl₃, δ): 5.70–5.59 (m, CH, 1 H), 4.20–4.03 (m, CH₂, 2 H), 1.69–1.97 (m, CH₂, 2 H), 0.99–0.87 (m, CH₃, 3 H). ¹³C NMR (100 MHz, CDCl₃, δ): 165.8, 128.3, 93.6, 92.6, 67.5, 67.5, 21.6, 10.0. SEC: M_n = 24.1 kg/mol, M_w = 44.3 kg/mol, *D* = 1.77.

PiPrG. From *i*-propanol (1.5 mL, 19.60 mmol, 10 equiv.) and purified by precipitation into pentane. Conversion: 70%. Yield 62%. ¹H NMR (400 MHz, CDCl₃, δ): 5.74–5.44 (m, CH, 1 H), 5.07–5.03 (m, CH, 0.7 H), 4.26–4.15 (m, CH₂, 0.53 H), 1.34–1.21 (m, 3 CH₃, 537 H). ¹³C NMR (100 MHz, CDCl₃, δ): 165.0, 127.8, 93.6, 92.1, 21.4. SEC: M_n = 22.9 kg/mol, M_w = 35.8 kg/mol, *D* = 1.56.

PnBuG. From *n*-butanol (1.8 mL, 19.60 mmol, 10 equiv.) and purified by dialysis (MWCO 6 kg/mol) against acetone. Conversion: >99%. Yield: 70%. ¹H NMR (400 MHz, CDCl₃, δ): 5.74–5.47 (m, CH, 1 H), 4.20–4.06 (m, CH₂, 2 H), 1.69–1.58 (m, CH₂, 2 H), 1.44–1.32 (m, CH₂, 2 H), 0.97–0.86 (m, CH₂, 3 H). ¹³C NMR (100 MHz, CDCl₃, δ): 165.5, 92.3, 92.2, 65.68, 30.2, 18.9, 13.6. SEC: M_n = 22.6 kg/mol, M_w = 35.0 kg/mol, *D* = 1.55.

PPenG. From *n*-pentanol (2.2 mL, 19.60 mmol, 10 equiv.) and purified by dialysis (MWCO 6 kg/mol) against acetone. Conversion: >99%. Yield: 64%. ¹H NMR (400 MHz, CDCl₃, δ): 5.67–5.55 (m, CH, 1 H), 4.20–4.03 (m, CH₂, 2 H), 1.73–1.61 (m, CH₂, 2 H), 1.40–1.25 (m, 2 CH₂, 4 H), 0.94–0.85 (m, CH₂, 3 H). ¹³C NMR (100 MHz, CDCl₃, δ): 165.9, 93.4, 92.4, 66.0, 27.9, 22.3, 13.9. SEC: M_n = 22.6 kg/mol, M_w = 33.2 kg/mol, *D* = 1.46.

PHexG. From *n*-hexanol (2.5 mL, 19.60 mmol, 10 equiv.) and purified by dialysis (MWCO 6 kg/mol) against acetone. Conversion: >99%. Yield: 62%. ^1H NMR (600 MHz, CDCl_3 , δ): 5.71–5.46 (m, *CH*, 1 H), 4.22–4.03 (m, *CH*₂, 2 H), 1.67–1.63 (m, *CH*₂, 2 H), 1.38–1.22 (m, 3 *CH*₂, 6 H), 0.91–0.83 (m, *CH*₃, 3 H). ^{13}C NMR (100 MHz, CDCl_3 , δ): 165.9, 165.5, 93.4, 92.2, 66.0, 31.4, 28.2, 25.3, 22.5, 13.9. SEC: $M_n = 21.8$ kg/mol, $M_w = 37.6$ kg/mol, $D = 1.72$.

POctG. From *n*-octanol (3.1 mL, 19.60 mmol, 10 equiv.) and purified by dialysis (MWCO 6 kg/mol) against acetone. Conversion: >99%. Yield: 61%. ^1H NMR (600 MHz, CDCl_3 , δ): 5.73–5.48 (m, *CH*, 1 H), 4.22–4.07 (m, *CH*₂, 2 H), 1.67–1.58 (m, *CH*₂, 2 H), 1.42–1.22 (m, 5 *CH*₂, 10 H), 0.91–0.88 (m, *CH*₃, 3 H). ^{13}C NMR (100 MHz, CDCl_3 , δ): 165.5, 127.8, 93.5, 92.2, 66.0, 31.8, 29.7, 29., 28.3, 25.67, 22.6, 13.9. SEC: $M_n = 28.9$ kg/mol, $M_w = 54.1$ kg/mol, $D = 1.87$.

PBnG. From benzyl alcohol (2.3 mL, 19.60 mmol, 10 equiv.) and purified by precipitation into pentane. Conversion: >99%. Yield: 67%. ^1H NMR (400 MHz, CDCl_3 , δ): 7.27–7.05 (m, *CH*, 4 H), 5.78–5.47 (m, *CH*, 1 H), 5.05–4.78 (m, *CH*₂, 1 H). Spectral data agreed with those previously reported.³² SEC: $M_n = 18.8$ kg/mol, $M_w = 29.4$ kg/mol, $D = 1.57$.

PFuG. From furfuryl alcohol (0.22 mL, 2.45 mmol, 0.5 equiv.) and purified by precipitation into pentane. Conversion: 15%. Yield: 59%. ^1H NMR (400 MHz, CDCl_3 , δ): 7.43–7.38 (m, *CH*, 0.16 H), 6.50–6.43 (m, *CH*, 0.15 H), 6.35–6.29 (m, *CH*, 0.15 H), 5.70–5.51 (m, *CH*, 1 H), 5.16 (m, *CH*₂, 0.3 H), 4.29–4.14 (m, *CH*₂, 1.69 H), 1.33–1.27 (m, *CH*₃, 2.64 H). SEC: $M_n = 21.7$ kg/mol, $M_w = 35.8$ kg/mol, $D = 1.65$.

PAIG. From allyl alcohol (0.17 mL, 2.45 mmol, 0.5 equiv.) and purified by precipitation into pentane. Conversion: 25%. Yield: 71%. ^1H NMR (400 MHz, CDCl_3 , δ): 5.98–5.89 (m, *-CH=CH*₂, 0.26), 5.70–5.54 (m, *CH*, 1 H), 5.36–5.32 (m, *-CH=CHH*, 0.25 H), 5.24–5.22 (m, *-CH=CHH*, 0.25 H), 4.70–4.62 (m, *CH*₂, 0.54 H), 4.27–4.17 (m, *CH*₂, 1.57 H), 1.32–1.35 (m, *CH*₃, 2.38 H). SEC: $M_n = 20.2$ kg/mol, $M_w = 33.4$ kg/mol, $D = 1.51$.

PPG. From propargyl alcohol (0.15 mL, 2.45 mmol, 0.5 equiv.) and purified by precipitation into pentane. Conversion: 26%. Yield: 60%. $^1\text{H NMR}$ (400 MHz, CDCl_3 , δ): 5.71–5.56 (m, CH , 1 H), 4.82–4.76 (m, CH_2 , 0.18 H), 4.27–4.18 (m, CH_2 , 1.83 H), 2.62–2.47 (m, CH , 0.07 H), 1.29 (m, CH_3 , 1.57 H). SEC: $M_n = 20.2$ kg/mol, $M_w = 35.8$ kg/mol, $D = 1.65$.

PPG_{pyr}. Inside a Schlenk flask, **PPG** (50 mg, 0.12 mmol propargyl group, 1.0 equiv.), 1-(azidomethyl)pyrene (47 mg, 0.18 mmol, 1.5 equiv.), CuSO_4 (3.9 mg, 0.025 mmol, 0.2 equiv.) and (+)-sodium L-ascorbate ascorbate (5.0 mg, 0.02 mmol, 0.2 equiv.) were combined. After the addition of DMF (5.0 mL), the flask was heated at 40 °C for 17 hours. The crude product was then cooled to 20 °C and passed through a silica plug to remove excess copper. The pure product was isolated after dialysis against DMF (MWCO = 6 kg/mol; 2 cycles) and ultrapure water (2 cycles). Yield: 53%. $^1\text{H NMR}$ (400 MHz, CDCl_3 , δ): 8.33–7.34 (m, 9 CH , 2 H), 5.71–5.56 (m, CH , 1 H), 5.31–4.82 (m, CH_2 , 0.31 H) 4.32–3.86 (m, CH_2 , 1.3 H), 1.33–0.76 (m, CH_3 , 2.58 H). SEC

4.2.4 SEC depolymerization study for **PEtG_{carbonate}** (general procedure)

In a Schlenk flask, **PEtG_{carbonate}**, (150 mg, 1.47 mmol of ethyl ester units, 1.0 equiv.) toluene (5 mL), ethanol (0.87 mL, 14.7 mmol, 10 equiv.), and TBD (44 mg, 0.29 mmol, 0.2 equiv.) were combined and degassed for 15 minutes. The solution was then divided between five pressure tubes in a glovebox, and heated at 100 °C outside the glovebox for 0, 1, 3, 6, or 24 hours. After cooling to 20 °C, the crude samples were dried *in vacuo* and analyzed by SEC.

4.2.5 $^1\text{H NMR}$ depolymerization studies of **PEtG_{UV}** (general procedure)

A PG (20 mg) was dissolved in a $\text{CD}_3\text{CN}/\text{D}_2\text{O}$ mixture (9/1; 1.2 mL) at 21 °C. The solution was then transferred into two quartz NMR tubes, and the tubes were promptly sealed. One tube was exposed to UV light (450 W bulb, 2.8 mW/cm^2 of UVA radiation) to initiate the removal of the photolabile end-cap. The other NMR tube was kept in dark and was

analyzed as a control sample for measuring the background polymer degradation. ^1H NMR spectra were recorded at defined intervals (0, 1, 3, 5, and 24 hours) to monitor the depolymerization.

4.2.6 Florescence of pyrene

In a 10 mL volumetric flask, 1.5 mg of **PPG_{pyr}** was dissolved in a 9/1: MeCN/water solvent mixture. After being degassed by bubbling N_2 for 10 min, it was placed inside a quartz cuvette for analysis. The emission spectrum was recorded using an excitation wavelength of 341 nm, emission range of 351–800 nm, and a slit width of 5 nm. The sample was then irradiated with a UV light (450 W bulb, 2.8 mW/cm^2 of UVA radiation) for 30 minutes and incubated for 24 h before recording the emission spectrum of the depolymerized sample.

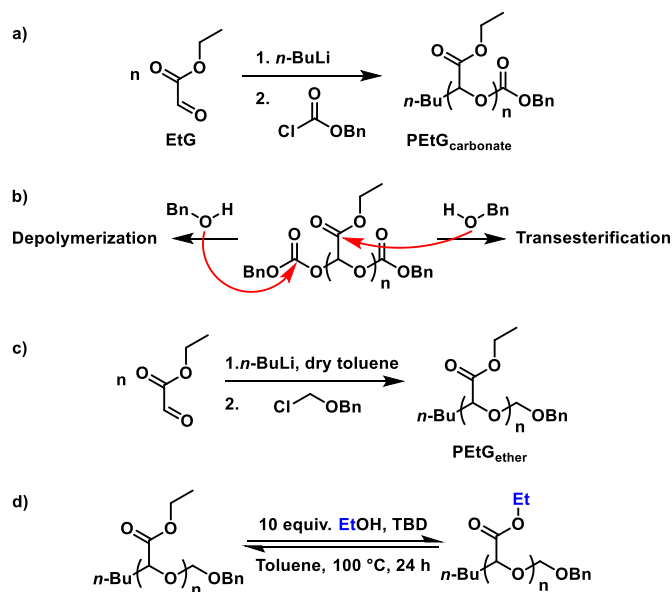
4.3 Results and discussion

4.3.1 Optimizing the PEtG design for transesterification reactions

A typical transesterification reaction included combining a PEtG with an excess amount of an alcohol, *i.e.*, 10 equiv., and a catalytic amount of TBD, *i.e.*, 0.2 equiv., in dry toluene. The resulting solutions were then purged with N_2 gas and heated at 100 °C for 17 – 24 h under an active flow of N_2 gas, *i.e.*, *ca.* 5 mL/min, to remove the released ethanol and push the equilibrium from the starting PEtG towards the formation of the targeted PG. After cooling to 20 °C, the solutions were diluted with CH_2Cl_2 and washed with an HCl solution (pH = 2) to remove TBD. Depending on the solubility of the alcohols and resulting PGs, pure PGs were isolated by dissolving the residues in CH_2Cl_2 and precipitation from pentane or alternatively *via* dialysis against acetone.

So far, self-immolative PEtGs have been reported with acid-sensitive end-caps, which cannot tolerate the mentioned workup,⁴² or carbonate-containing end-groups which originate from chloroformate end-caps.^{38, 45} Hence, we started our study by using a benzyl carbonate-end-capped PEtG (**PEtG_{carbonate}**) as a representative example of a PEtG with a carbonate-containing end-cap. **PEtG_{carbonate}** was prepared following a literature procedure

and its purity was confirmed by ^1H NMR spectroscopy (**Figure A4.1**).⁴³ **PEtG_{carbonate}** was isolated in 90% yield with an M_n of 27.6 kg/mol, $M_w = 35.6$ kg/mol, and $D = 1.29$ (**Scheme 4.1a**). For the first experiment, a combination of **PEtG_{carbonate}** with benzyl alcohol and TBD was heated at 100 °C for 48 h to probe the reactivity of PEtG. We chose benzyl alcohol for several reasons. First, its relatively high boiling point allowed it to remain mostly inside the reaction medium rather than residing in the headspace or even leaving the reaction flask along with ethanol. Using it also facilitated the interpretation of the product ^1H NMR spectra as poly(benzyl glyoxylate)'s (**PBnG**) aromatic peaks do not overlap with the aliphatic peaks of PEtG and released ethanol. ^1H NMR spectroscopy of the resulting crude reaction mixture showed no trace of the targeted **PBnG** or even starting **PEtG_{carbonate}**. This suggested that **PEtG_{carbonate}** did not survive the transesterification reaction. Hence, optimization experiments using different PEtG/BnOH/TBD ratios, temperatures, and solvents were conducted. Preliminary experiments showed that heating at 100 °C was essential for reaching high conversions but it also promoted the depolymerization.



Scheme 4.1: (a) Preparation of **PEtG_{carbonate}** using benzyl chloroformate (b) possible pathways for the reaction of alcohols with **PEtG_{carbonate}**, (c) preparation of **PEtG_{ether}** and (d) testing the stability of **PEtG_{ether}** under the transesterification reaction conditions.

To investigate the depolymerization kinetics, stability tests were carried out using SEC. First, a degassed solution of **PEtG_{carbonate}**, toluene, ethanol, and TBD was prepared, and then it was divided between five flasks and heated at 100 °C for 0, 1, 3, 6, or 24 hours. After cooling to 20 °C, the crude samples were analyzed by SEC. Ethanol was used for two reasons. First, this experiment was intended to provide information regarding the stability of **PEtG_{carbonate}** rather than the efficiency of the transesterification reaction. Secondly, using a different alcohol would give a substituted PG with a different molar mass, and make the analysis unnecessarily complicated. The comparison of the SEC traces revealed that the intensity of the PEtG peak (elution time: *ca.* 15 min) gradually decreased over time and lost most of its intensity after 24 h (**Figure 4.1a**). These experiments confirmed that **PEtG_{carbonate}** rapidly degrades under the reaction conditions.

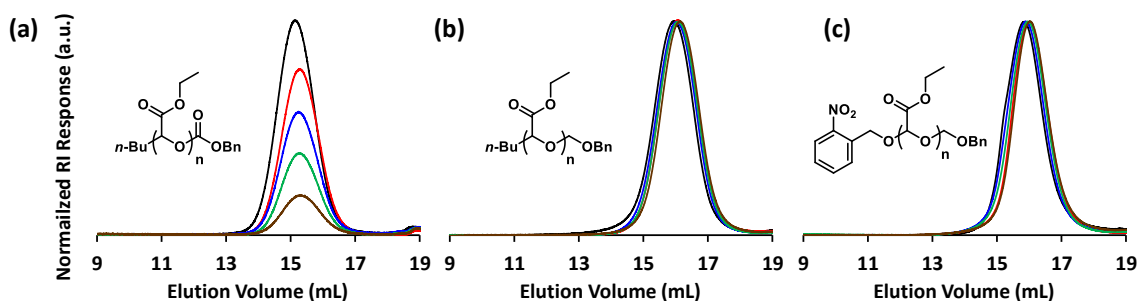


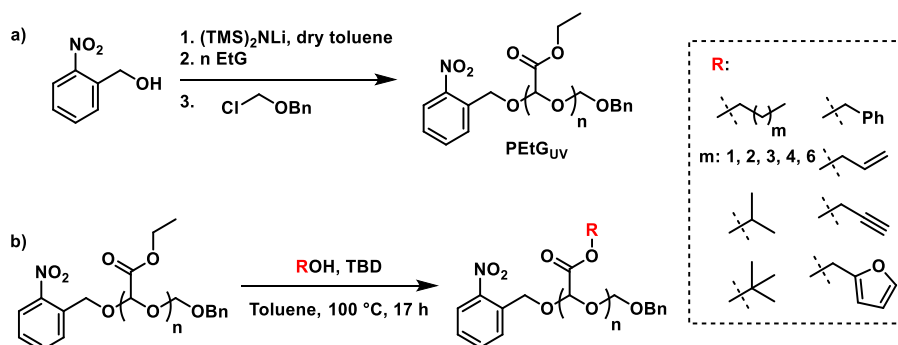
Figure 4.1: SEC traces recorded during the stability tests of (a) **PEtG_{carbonate}**, (b) **PEtG_{ether}**, and (c) **PEtG_{UV}**. Black, red, blue, green, and brown colors were used for depicting traces recorded at 0, 1, 3, 6, and 24 h, respectively.

Theoretically, carbonate linkers are the weakest points of the polymer backbone because their electrophilic carbonyl groups are susceptible to nucleophilic attacks, specifically when activating TBD catalysts are present (**Scheme 4.1b**). Hence, we decided to use chloromethyl benzyl ether (BOMCl) as an end-cap to prepare a PEtG with a very similar structure but carbonate-free backbone (**Scheme 4.1c**). The anionic polymerization was conducted following our published method⁴³ and initiated with *n*-BuLi in toluene. BOMCl was added to the polymerization mixture at -20 °C and the resulting mixture was kept at -

20 °C for 24 h to ensure a good end-capping efficiency was reached. Then, a methanol precipitation gave an acid-stable PEtG which was equipped with a carbonate-free end cap, *i.e.*, **PEtG_{ether}**. The polymerization success and purity of **PEtG_{ether}** were confirmed by ¹H NMR spectroscopy as **PEtG_{ether}** gave rise to 3 main peaks at *ca.* 1.3, 4.2, and 5.6 ppm due to the repeating units, *i.e.*, CH₃, CH₂, and CH, respectively, as well as the CH₃ group of *n*-Bu group which appeared at 0.89 ppm (**Figure A4.3**). In addition, **PEtG_{ether}** had an M_n of 13.9 kg/mol, M_w = 18.1 kg/mol, Đ = 1.29, and DP_n = 136 which was consistent with DP_n calculated by ¹H NMR end-group analysis, *i.e.*, DP_n = 122. This close accordance confirmed the high quality of the starting EtG and the fact that all the polymer chains initiated from *n*-BuLi. However, the experimental DP_n was lower than the targeted value DP_n, *i.e.*, 200, probably because BOMCl was not very reactive at –20 °C and it started the end-capping at a higher temperature when the polymerization mixture was gradually warming up to 20 °C and partial depolymerization had occurred. This hypothesis was supported by observing considerable traces of EtG (1.5 mol% at 9.39 ppm) and EtGH (22 mol% at 5.06 ppm) in the ¹H NMR spectrum of the concentrated crude polymerization mixture (**Figure A4.2**). EtGH was observed as the NMR solvent was not dry and EtG rapidly reacts with water to form EtGH. The end-capping limitation at –20 °C can be easily resolved by using more reactive end-caps such as MOMBr but as **PEtG_{ether}** was isolated with a satisfactory yield/molar mass, its end-group was a carbonate-free version of **PEtG_{carbonate}**, and our goal was to see the effect of carbonate group on the stability, we continued our studies with **PEtG_{ether}**.

To test the stability of **PEtG_{ether}** to the transesterification reaction, the stability tests performed on **PEtG_{carbonate}** were repeated for **PEtG_{ether}** (**Scheme 4.1d**). As shown in **Figure 4.1b**, the main peak corresponding to **PEtG_{ether}** retained its intensity even after 24 h of heating at 100 °C. This finding supported our hypothesis that the carbonate linkers were responsible for the low stability of **PEtG_{carbonate}** and that PEtGs with carbonate-free end-caps can tolerate the transesterification reaction conditions.

BOMCl is an inexpensive reagent that conveniently yielded **PEtG_{ether}**. However, as **PEtG_{ether}** was not stimuli-responsive, we targeted a UV-responsive PEtG with carbonate-free end-caps to continue this study. In this regard, 2-nitrobenzyl alcohol was lithiated using lithium bis(trimethylsilyl)amide [(TMS)₂NLi] which is a strong non-nucleophilic base. Using the resulting anionic alkoxide as an initiator and BOMCl as an end-cap, **PEtG_{UV}** with an asymmetric design including UV-responsive and non-responsive end-caps (*i.e.*, 2-nitrobenzyl and benzyl ether groups, respectively) was prepared (**Scheme 4.2a**).



Scheme 4.2: (a) Preparation of **PEtG_{UV}** and (b) transesterification of **PEtG_{ether}** using different alcohols.

PEtG_{UV} was purified similarly to **PEtG_{ether}** and then analyzed by ¹H NMR spectroscopy and SEC. For end-group analysis, the integration of aromatic peaks of the 2-nitrobenzyl group were compared with that of the peak at 5.6 ppm (*CH* of the backbone) (**Figure A4.5**). This analysis suggested DP_n = 226, which is comparable with the DP_n value recorded by SEC, *i.e.*, DP_n = 236. The stability test of **PEtG_{UV}** under the similar conditions revealed that **PEtG_{UV}** had a stability comparable with **PEtG_{ether}** and suggested that its backbone can tolerate the transesterification reaction (**Scheme 4.1** **Figure 4.1c**).

4.3.2 Transesterification reactions

To study the structure-reactivity relationships of alcohols for this reaction, **PEtG_{UV}** was combined with TBD and structurally different alcohols, including *n*-propanol, *i*-propanol, *n*-butanol, *t*-butanol, *n*-pentanol, *n*-hexanol, *n*-octanol, or benzyl alcohol before heating at 100 °C (**Scheme 4.2b**). The success of the transesterification reaction was confirmed when

PnPrG, PiPrG, PnBuG, PPenG, PHexG, POctG, and PBnG were isolated in good yields 61-70% and gave rise to peaks associated with the newly introduced ester groups in the ^1H NMR spectra of the products (**Figures A4.7– A4.19**). To calculate the conversion percentages, *CH* peaks from the backbone were used as NMR handles because their chemical shifts did not change by altering the pendant ester groups in this study. In contrast, by increasing the conversion, the intensity of CH_3 peaks corresponding to the ethyl ester groups (*ca.* 1.3 ppm) decreased because the CH_3 groups of the resulting alkyl esters appeared upfield (*ca.* 0.9 ppm) and did not overlap with the starting CH_3 peaks. The integration of the backbone *CH* peak, which represents both converted/unreacted repeating units and appears at *ca.* 5.6 ppm, was assigned as 1.0. Then, the intensity of CH_3 peaks from the resulting alkyl ester groups were measured and conversion percentages were calculated using **equation 1**. The conversion of the benzyl alcohol was calculated by determining the intensity of the CH_3 peaks from the unreacted ethyl alcohol and was calculated using **equation 2**.

$$\text{Conversion\%} = 100 \times \frac{(\text{intensity of } \text{CH}_3 \text{ peaks from alkyl ester groups})}{3} \quad (\text{equation 4.1})$$

$$\text{Conversion\%} = 100 \times \frac{(3 - \text{intensity of } \text{CH}_3 \text{ peaks from ethyl ester groups})}{3} \quad (\text{equation 4.2})$$

For the series of primary alcohols including *n*-propanol, *n*-butanol, 1-pentanol, 1-hexanol, 1-octanol, and benzyl alcohol, high conversions, *i.e.*, 96–100%, were observed (**Table 4.1**). While, *i*-propanol, a secondary alcohol, showed a 70 conversion% and *t*-butanol did not react under the transesterification reaction conditions. This drastic difference in the conversion values revealed the large impact of the steric bulk surrounding the hydroxyl group on its reactivity.

Table 4.1: SEC characterization data and reaction conversions for PGs.

Polymer	Conversion (%) ^a	M _n (kg/mol) ^b	M _w (kg/mol) ^b	<i>D</i> ^b	T _g (°C) ^d	T _o (°C) ^e
PEtG _{carbonate}	-	27.6	35.6	1.29	-4	211
PEtG _{ether}	-	14.0	18.1	1.29	-10	224
PEtG _{UV}	-	24.1	29.9	1.24	-12	223
PnPrG	>95	23.0	35.8	1.56	-21	121
PiPrG	70	15.8	28.0	1.77	3	136
PnBuG	>95	22.6	35.0	1.55	-33	162
PtBuG	No reaction	-	-	-	-	-
PPenG	>95	22.6	33.2	1.46	-41	158
PHexG	>95	26.4	44.1	1.67	-46	169
POctG	>95	28.9	54.1	1.87	-47	158
PBnG	>95	18.8	29.4	1.57	2	142
PAIG	25	20.2	31.3	1.55	-7	168
PFuG	17	21.7	35.8	1.65	4	169
PPG	26	20.2	33.4	1.65	2	166
PPG _{pyr}	100 ^c	10.6	35.2	3.31	N/A ^f	N/A ^f

^aCalculated using ¹H NMR spectra of the purified PGs. ^bObtained in THF and conventionally calibrated vs. PMMA standards. ^cRelative to the parent **PPG**. ^dCalculated using DSC. ^eCalculated using TGA. ^fNot measured.

After confirming the conversion by ¹H NMR spectroscopy, the resulting pure polymers were analyzed by SEC (**Figure 2a**). The fact that all PGs demonstrated elution times associated with high molar mass polymers confirmed that they preserved their macromolecular nature during the reaction and purification steps. SEC also revealed that most recorded DP_n values were in a close agreement but were not exactly the same probably because they differently fractionated during the purification step. However, **PiPrG** and **PBnG** appeared with noticeably lower DP_ns than the parent **PEtG_{UV}** suggesting that **PiPrG** and **PBnG** had smaller hydrodynamic volumes in the SEC eluent compared to the rest of PGs due to their non-linear structures. This SEC phenomenon has been reported for other

polyacetals such as PGAMs with non-linear pendant groups.²⁹ It is also worth to note that by increasing the length of the pendant groups from ethyl to octyl, the solubility in THF (the SEC eluent) drastically decreased. Therefore, higher D values were recorded, and the molar-mass distributions were skewed towards the lower elution-time ends.

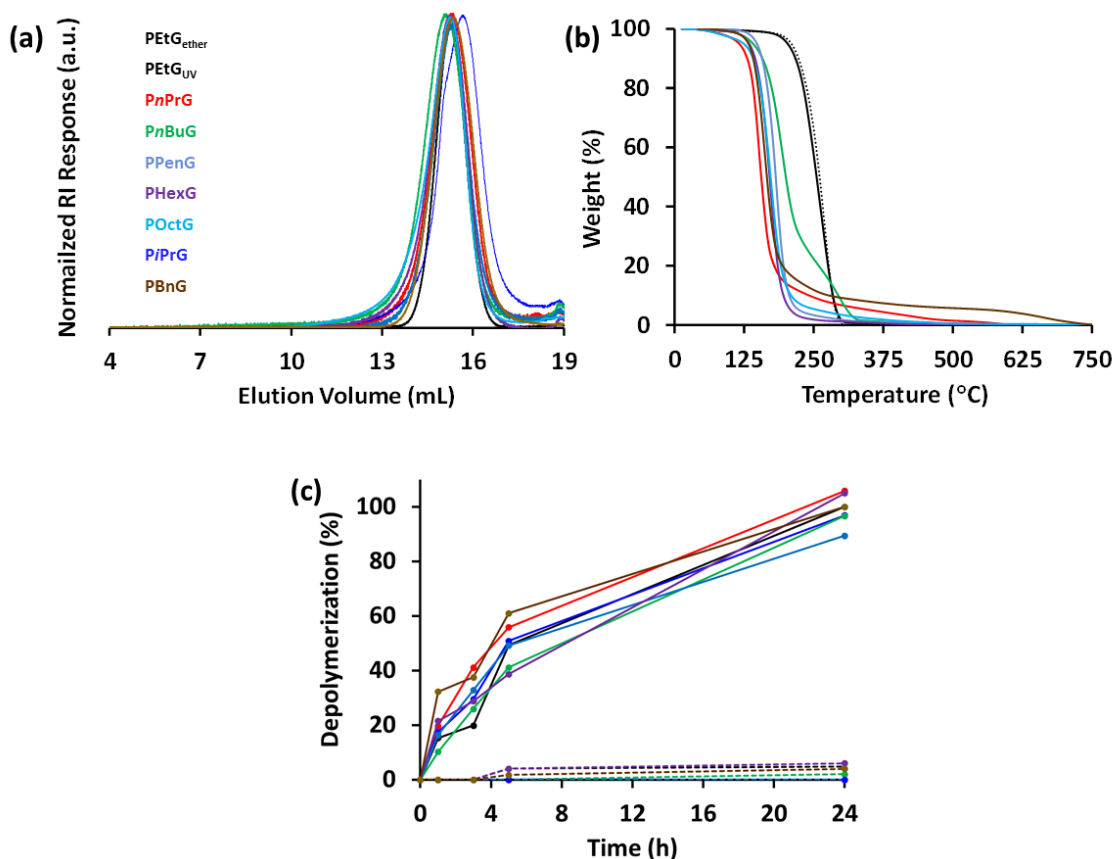


Figure 4.2: (a) SEC, (b) TGA, and (c) UV-degradation study results for **PnPrG**, **PiPrG**, **PnBuG**, **PPenG**, **PHexG**, **POctG**, and **PBnG**, results for UV-light exposed and kept in dark samples are depicted using solid and broken lines, respectively. Note: depolymerization% were calculated relative to the depolymerization amount observed for the parent PEtG_{UV} in 24 h, **PnPrG**, **PiPrG**, **PnBuG**, **PPenG**, and **PBnG** were studied in a 9/1 mixture of $\text{CD}_3\text{CN}/\text{D}_2\text{O}$ and **PHexG** and **POctG** were studied in a 9/1 mixture of acetone- $d_6/\text{D}_2\text{O}$.

As most **PGs** generated in this study are unprecedented, they were analyzed using DSC and TGA to investigate their structure-property relationships. The boiling point of EtG is *ca.* 110 $^{\circ}\text{C}$. TGA analysis showed that PEtG_{UV} and $\text{PEtG}_{\text{ether}}$ had very similar onset of

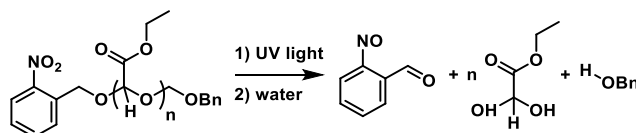
decomposition temperatures (T_o), which were about 13 °C higher than that of the **PEtG_{carbonate}**, *i.e.*, 211 °C. This difference can be attributed to the higher thermal stability of ether-type end-caps compared to their carbonate-type alternatives and implies that the overall stability of the PEtGs is dominated by the end-caps. The new pendant ester derivative PGs exhibited lower T_o s, *ca.* 150 °C (**Figure 4.2b**). Considering that their end-caps were all the same as **PEtG_{UV}** but they showed lower thermal stabilities, we postulate that the thermal degradation behavior of the new PGs was governed by their electronics, as their backbones are more electron-rich compared to the parent **PEtG_{UV}**. This is consistent with the fact that electron-withdrawing groups improve the thermal stability of polyphthalaldehydes. For example, poly(4,5-dichlorophthalaldehyde)s are more thermally stable compared to polyphthalaldehydes.⁴⁶

DSC revealed that the glass transition temperature (T_g) of PGs, derived from the linear alcohols, decreased with increasing number of carbons of the parent alcohol, *i.e.*, from -4 to -47 °C (**Figures A4.24–A4.32** and **Table 4.1**). This is the translation of the fact that the increasing segmental motion of the linear pendant groups decreases the strength of the interactions between the polymer chains in the solid-state. In contrast, PGs derived from non-linear alcohols exhibited T_g s with higher values, *i.e.*, 3 and 2 °C for **PiPrG** and **PBnG**, respectively, as the rigidity and steric hindrance of the pendant groups can inhibit segmental motion. It is also worth to note that the recorded T_g for **PnBuG** (-33 °C) was consistent with what was previously reported, *i.e.*, $T_g = -30$ °C, for poly(butyl glyoxylate) homopolymer which was directly synthesized from the monomer.³² As the only reported example of poly(benzyl glyoxylate) homopolymer had a very low molar mass (*i.e.*, $M_n = 2.1$ kg/mol) and thermal properties of oligomers and polymers are typically different, a similar comparison was not possible for **PBnG**.

4.3.3 Depolymerization studies

2-Nitrobenzyl is a UV-responsive group which was incorporated as an end-group for **PEtG_{UV}** to introduce a self-immolative behaviour (**Scheme 4.3**). **PEtG_{UV}** was expected to be UV-responsive as having one responsive end group is sufficient for an SIP. To assess

whether the parent **PEtG_{UV}** and resulting PGs show a UV-responsive depolymerization behaviour, ¹H NMR depolymerization studies were carried out, except for **POctG** due to its poor solubility. PGs were dissolved in a 9/1 mixture of CD₃CN/D₂O or acetone-*d*₆/D₂O, depending on their solubility. The resulting solutions were then split into 2 samples. One sample was irradiated for 30 minutes with a UV light and the other one was kept in dark (control sample). Over 24 h, the samples were analyzed by ¹H NMR spectroscopy, at different time intervals (**Figure 4.2c** and **A4.36– A4.55**). The percent depolymerization was quantified based on the relative integrations of the peak corresponding to the backbone methine *CH*, at *ca.* 5.6 ppm, and the peak corresponding to the methine *CH* group of the depolymerization product (corresponding glyoxylate hydrate), at *ca.* 5 ppm. **PEtG_{UV}** reached a 30% degradation in 24 h and this amount was used as a benchmark for evaluating the depolymerization performance of the resulting PGs. The UV-light-exposed samples demonstrated a *ca.* 50% depolymerization, after 5 h, and a full depolymerization relative to **PEtG_{UV}** in *ca.* 24 hours. In contrast, the non-irradiated (control) samples showed negligible depolymerization amounts (< 5%). These results showed that our synthetic strategy for installing a UV-responsive group was successful and that the amount of depolymerization was determined by the nature of the backbone/end-group and not the pendant groups (**Figure 4.2c**).



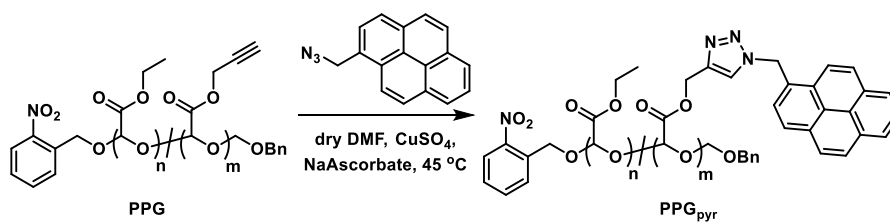
Scheme 4.3: UV-light depolymerization of **PEtG_{UV}**.

4.3.4 Synthesis and characterization of PGs with functional groups

To further prove the versatility of this method and show how it has opened a door towards the synthesis of a variety SIPs with a PG backbone and desired pendant groups, we employed several functional alcohols including allyl, propargyl and furfuryl alcohol, which gave PGs suitable for click chemistry and applications such as labeling, sensing, and network formation. In this regard, we only employed 0.5 equivalents of the corresponding

alcohols as typically for such applications a small percentage of functional groups is sufficient. These reactions were conducted inside pressure tubes which allowed the starting alcohols remain inside the reaction media. This method gave the targeted partially-converted **PAIG**, **PPG**, and **PFuG** with 21, 23, and 17% conversion respectively. They were also analyzed by SEC and appeared as polymers with molar masses similar to that of the **PEtG_{UV}** (**Figure A4.56**). TGA studies showed that these PGs had T_o s lower than that of the **PEtG_{UV}** (**Figure A4.57**). Considering the fact that they were only partially converted but showed T_o similar to the fully converted PGs, we believe that the thermal stability of these PGs was limited by the stability of repeating units. The breaking a PG chain at places where those repeating units are located triggers the full depolymerization and the higher thermal stability of the rest of repeating units can not prevent that. DSC thermograms demonstrated that the T_g s of these random copolymers were slightly higher than that of the parent **PEtG_{UV}** probably due to the higher rigidity of the newly introduced ester groups compared to the original ethyl ester groups (**Figures S33–S35** and **Table 4.1**).

As not all functional groups are compatible with conditions required for this transesterification reaction/purification method, we decided to prove the concept that this strategy can be exploited for the preparation of many SIPs with PG backbones and such groups. We chose **PPG** as a precursor and conducted a copper assisted azide-alkyne click (CuACC) reaction to install pyrene as a fluorescent group. In theory, pyrene alcohol could be added directly, but it was used as a fluorescent group to demonstrate the principle of another round of post polymerization modification. For the click reaction, **PPG** was combined with CuSO_4 , sodium ascorbate, and an excess amount of 1-(azidomethyl)pyrene (**Py-N₃**), in dry DMF (**Scheme 4.4**).



Scheme 4.4: Click reaction of **PPG** with **Pyr-N₃**.

The crude product was then dialyzed against DMF and also water to remove excess pyrene moieties and any residual copper species. Pure **PPG_{pyr}** was analyzed by ¹H NMR, FTIR, and fluorescence emission spectroscopies, as well as SEC. In the ¹H NMR spectrum, the aromatic protons of pyrene gave rise to a broad peak at *ca.* 7.9 ppm in addition to its methylene peak which appeared at *ca.* 5.1 ppm. This conversion was also confirmed by FTIR spectroscopy as the C-H stretch of the alkyne groups of **PPG** led to an absorption band at 3300 cm⁻¹. This band was absent in the FTIR spectrum of **PPG_{pyr}** as the alkyne groups of **PPG** transformed to the triazole ring and were not present in the structure of **PPG_{pyr}** (**Figure 4.3a**). Furthermore, SEC confirmed that **PPG** did not degrade during the process and **PPG_{pyr}** preserved the macromolecular character. However, **PPG_{pyr}** exhibited a SEC trace skewed towards low elution-volumes due to its poor solubility in THF (**Figure 4.3b**). This can be attributed to the strong interactions between the pendant pyrene groups which limited the solubility.

Pyrene is a chromophore sensitive to its medium, especially when pyrene units are bound in a close proximity, because pyrene can form an excimer state.⁴⁷ An excimer is defined as a dimer which is associated in an excited electronic state, but dissociative in its ground state. When an electronically excited pyrene encounters a pyrene in its ground state, they create an excimer.⁴⁷ A pyrene excimer emits at *ca.* 475 nm, while a single pyrene (“locally excited” or monomer) emits with two maxima at *ca.* 360 and 375 nm.⁴⁸ Taking advantage of this phenomenon, we decided to test the capability of **PPG_{pyr}** as a sensor because it was expected that the pyrene units would change their behavior by changing the ratio of excimers to monomers after the triggered depolymerization.

In this regard, a dilute solution (3.6×10^{-4} M pyrene moieties in MeCN/H₂O: 9/1) of **PPG_{pyr}** was prepared and degassed and its emission spectrum was obtained using an excitation wavelength of 341 nm. A broad peak at 475 nm confirmed that the pyrene groups of **PPG_{pyr}** were preferentially in an excimer form as the integrity of **PPG_{pyr}** kept them in a close proximity although the overall concentration of **PPG_{pyr}** was very low (**Figure 4.3c**). The sample was then irradiated with a UV-light and allowed to depolymerize for 24 hours.

The sample was again excited at 341 nm to obtain an emission spectrum which showed a dramatic decrease in the intensity of the excimer peak while the released pyrene units gave rise to peaks at 360 and 375 nm. This example confirms the capability of **PPG_{pyr}** to serve as a sensor and highlights the fact that many PGs with functional groups, such as drug or dye moieties, which cannot be directly synthesized from a glyoxylate monomer or tolerate the transesterification reaction can be accessible using our strategy.

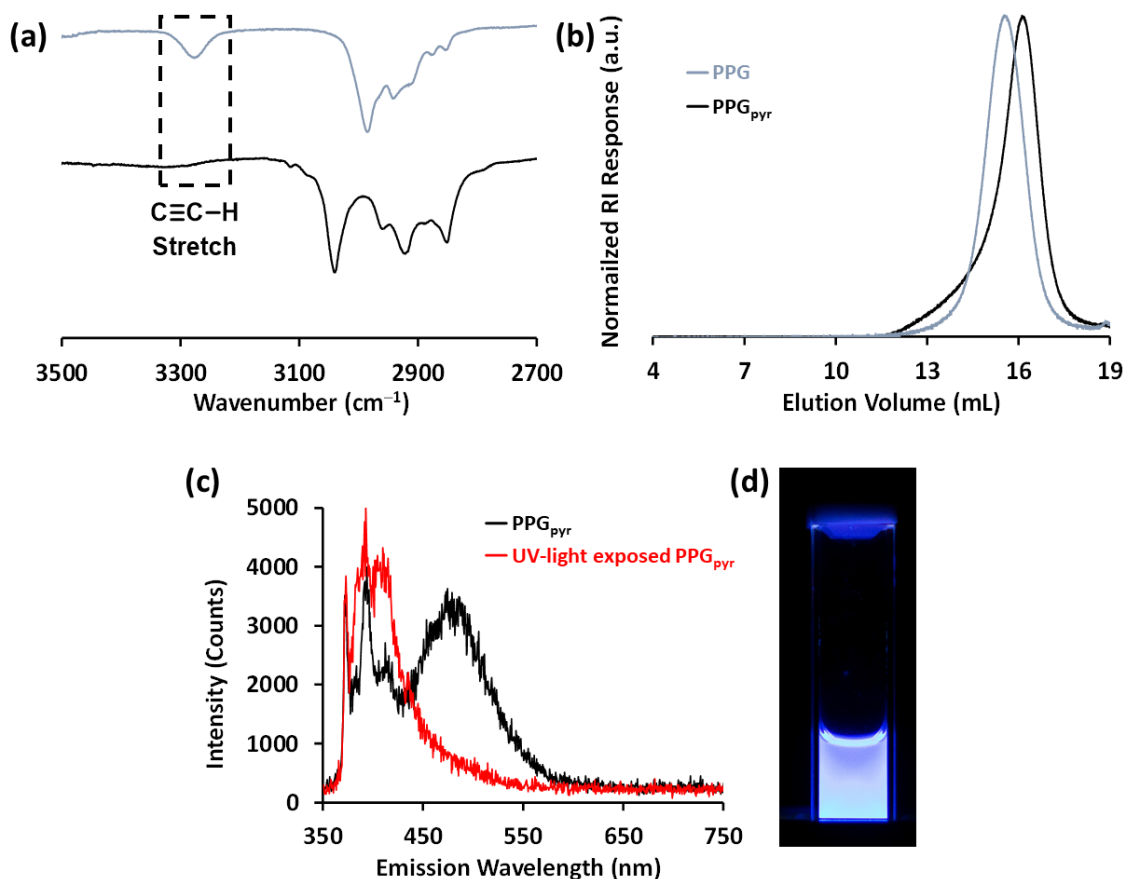


Figure 4.3: (a) Alkyne region of the FTIR spectra recorded for **PPG** and **PPG_{pyr}** showing the loss of a **H-C≡C** stretch after CuAAC reaction (b) SEC traces for **PPG** and **PPG_{pyr}**, (c) emission spectra of **PPG_{pyr}** before/after UV-light exposure recorded in MeCN/H₂O: 9/1 (irradiation at 341 nm), and (d) **PPG_{pyr}** sample used for emission spectroscopy.

4.4 Conclusions

In conclusion, as **PEtG_{carbonate}**, representing the previous generations of PEtGs with carbonyl-containing end-groups, did not survive the TBD-mediated transesterification

reaction, new end-caps were successfully employed to create **PEtG_{ether}** and **PEtG_{UV}** compatible with this method. Reactions of **PEtG_{UV}** with *n*-propanol, *i*-propanol, *n*-butanol, *t*-butanol, *n*-pentanol, *n*-hexanol, *n*-octanol, or benzyl alcohol, in the presence of catalytic amounts of TBD, showed that, while primary alcohols successfully gave the corresponding PGs with conversion > 95%, the steric hindrance surrounding the hydroxyl groups of non-linear alcohols can lower the conversion. ¹H NMR spectroscopy confirmed the structure of the newly introduced ester groups and SEC showed that all PGs preserved the macromolecular nature of the parent **PEtG_{UV}**. Depolymerization studies revealed that all PGs mirrored the self-immolative behavior of **PEtG_{UV}** and changing the pendant ester groups did not have a noticeable effect on the depolymerization behavior. TGA showed that replacing ethyl ester groups with more electron-donating groups can lower the onset of decomposition temperature from *ca.* 230 to 160 °C, even at low conversion%. In addition, DSC demonstrated that changing the pendant groups can be utilized for tuning the mechanical properties as PGs with *T_g*s ranging from -47 to 3 °C were prepared. To prove that the number of PGs accessible *via* this strategy can go beyond what is shown in this study, allyl, propargyl and furfuryl alcohols were used to prepare PGs suitable for click chemistry. The CuAAC reaction of **PPG** with **Pyr-N₃** gave **PPG_{pyr}** with potential for sensing applications, as successfully confirmed *via* fluorescence emission spectroscopy.

4.5 Acknowledgments

The authors thank Mr. Quinton Sirianni for performing the polymer thermal analysis and the Natural Sciences and Engineering Research Council of Canada (Discovery Grant 2016-04636 and Canada Graduate Scholarship for REY) for funding this work.

4.6 References

1. Yardley, R. E.; Rabiee Kenaree, A.; Gillies, E. R., Triggering Depolymerization: Progress and Opportunities for Self-Immolative Polymers. *Macromolecules* **2019**, DOI: 10.1021/acs.macromol.1029b00965.

2. Roth, M. E.; Green, O.; Gnam, S.; Shabat, D., Dendritic, Oligomeric, and Polymeric Self-Immulative Molecular Amplification. *Chem. Rev.* **2016**, *116*, 1309–1352.
3. Phillips, S. T.; DiLauro, A. M., Continuous Head-to-Tail Depolymerization: An Emerging Concept for Imparting Amplified Responses to Stimuli-Responsive Materials. *ACS Macro Lett.* **2014**, *3*, 298–304.
4. Wong, A. D.; DeWit, M. A.; Gillies, E. R., Amplified release through the stimulus triggered degradation of self-immulative oligomers, dendrimers, and linear polymers. *Adv. Drug Delivery Rev.* **2012**, *64*, 1031–1045.
5. Esser-Kahn, A. P.; Sottos, N. R.; White, S. R.; Moore, J. S., Programmable Microcapsules from Self-Immulative Polymers. *J. Am. Chem. Soc.* **2010**, *132*, 10266–10268.
6. Lewis, G. G.; Robbins, J. S.; Phillips, S. T., A Prototype Point-of-use Assay for Measuring Heavy Metal Contamination in Water Using Time as a Quantitative Readout. *Chem. Commun.* **2014**, *50*, 5352–5354.
7. Lewis, G. G.; Robbins, J. S.; Phillips, S. T., Phase-Switching Depolymerizable Poly(carbamate) Oligomers for Signal Amplification in Quantitative Time-Based Assays. *Macromolecules* **2013**, *46*, 5177–5183.
8. Yardley, R. E.; Gillies, E. R., Multi-Stimuli-Responsive Self-Immulative Polymer Assemblies. *J. Polym. Sci., Part A: Polym. Chem.* **2018**, *56*, 1868–1877.
9. Liu, G.; Wang, X.; Hu, J.; Zhang, G.; Liu, S., Self-Immulative Polymersomes for High-Efficiency Triggered Release and Programmed Enzymatic Reactions. *J. Am. Chem. Soc.* **2014**, *136*, 7492–7497.
10. McBride, R. A.; Gillies, E. R., Kinetics of Self-Immulative Degradation in a Linear Polymeric System: Demonstrating the Effect of Chain Length. *Macromolecules* **2013**, *46*, 5157–5166.
11. DeWit, M. A.; Gillies, E. R., A Cascade Biodegradable Polymer Based on Alternating Cyclization and Elimination Reactions. *J. Am. Chem. Soc.* **2009**, *131*, 18327–18334.
12. Sagi, A.; Weinstain, R.; Karton, N.; Shabat, D., Self-Immulative Polymers. *J. Am. Chem. Soc.* **2008**, *130*, 5434–5435.
13. Palermo, E. F.; Lienkamp, K.; Gillies, E. R.; Ragona, P. J., Antibacterial Activity of Polymers: Discussions on the Nature of Amphiphilic Balance. *Angew. Chem.* **2019**, *131*, 3728–3731.

14. Xiao, Y.; Li, H.; Zhang, B.; Cheng, Z.; Li, Y.; Tan, X.; Zhang, K., Modulating the Depolymerization of Self-Immolative Brush Polymers with Poly(benzyl ether) Backbones. *Macromolecules* **2018**, *51*, 2899–2905.
15. Ergene, C.; Palermo, E. F., Cationic Poly(benzyl ether)s as Self-Immolative Antimicrobial Polymers. *Biomacromolecules* **2017**, *18*, 3400–3409.
16. Baker, M. S.; Kim, H.; Olah, M. G.; Lewis, G. G.; Phillips, S. T., Depolymerizable Poly(benzyl ether)-Based Materials for Selective Room Temperature Recycling. *Green Chem.* **2015**, *17*, 4541–4545.
17. Yeung, K.; Kim, H.; Mohapatra, H.; Phillips, S. T., Surface-Accessible Detection Units in Self-Immolative Polymers Enable Translation of Selective Molecular Detection Events into Amplified Responses in Macroscopic, Solid-State Plastics. *J. Am. Chem. Soc.* **2015**, *137*, 5324–5327.
18. Olah, M. G.; Robbins, J. S.; Baker, M. S.; Phillips, S. T., End-Capped Poly(benzyl ethers): Acid and Base Stable Polymers That Depolymerize Rapidly from Head-to-Tail in Response to Specific Applied Signals. *Macromolecules* **2013**, *46*, 5924–5928.
19. Schwartz, J. M.; Gourdin, G.; Phillips, O.; Engler, A.; Lee, J.; Abdulkadir, N. R.; Miller, R. C.; Sutlief, A.; Kohl, P. A., Cationic Polymerization of High-Molecular-Weight Phthalaldehyde-Butanal Copolymer. *J. Appl. Polym. Sci.* **2019**, *136*, 46921.
20. Lopez Hernandez, H.; Takekuma, S. K.; Mejia, E. B.; Plantz, C. L.; Sottos, N. R.; Moore, J. S.; White, S. R., Processing-Dependent Mechanical Properties of Solvent Cast Cyclic Polyphthalaldehyde. *Polymer* **2019**, *162*, 29–34.
21. Lloyd, E. M.; Lopez Hernandez, H.; Feinberg, A. M.; Yourdkhani, M.; Zen, E. K.; Mejia, E. B.; Sottos, N. R.; Moore, J. S.; White, S. R., Fully Recyclable Metastable Polymers and Composites. *Chem. Mater.* **2019**, *31*, 398–406.
22. Lopez Hernandez, H.; Lee, O. P.; Possanza Casey, C. M.; Kaitz, J. A.; Park, C. W.; Plantz, C. L.; Moore, J. S.; White, S. R., Accelerated Thermal Depolymerization of Cyclic Polyphthalaldehyde with a Polymeric Thermoacid Generator. *Macromol. Rapid Commun.* **2018**, *39*, 1800046.
23. Park, C. W.; Kang, S.-K.; Lopez Hernandez, H.; Kaitz, J. A.; Wie, D. S.; Shin, J.; Lee, O. P.; Sottos, N. R.; Moore, J. S.; Rogers, J. A.; White, S. R., Thermally Triggered Degradation of Transient Electronic Devices. *Adv. Mater.* **2015**, *27*, 3783–3788.
24. Kaitz, J. A.; Moore, J. S., Copolymerization of *o*-Phthalaldehyde and Ethyl Glyoxylate: Cyclic Macromolecules with Alternating Sequence and Tunable Thermal Properties. *Macromolecules* **2014**, *47*, 5509–5513.

25. Kaitz, J. A.; Diesendruck, C. E.; Moore, J. S., End Group Characterization of Poly(phthalaldehyde): Surprising Discovery of a Reversible, Cationic Macrocyclization Mechanism. *J. Am. Chem. Soc.* **2013**, *135*, 12755–12761.
26. Kaitz, J. A.; Diesendruck, C. E.; Moore, J. S., Divergent Macrocyclization Mechanisms in the Cationic Initiated Polymerization of Ethyl Glyoxylate. *Macromolecules* **2014**, *47*, 3603–3607.
27. Kaitz, J. A.; Moore, J. S., Functional Phthalaldehyde Polymers by Copolymerization with Substituted Benzaldehydes. *Macromolecules* **2013**, *46*, 608–612.
28. Chen, E. K. Y.; McBride, R. A.; Gillies, E. R., Self-Immolative Polymers Containing Rapidly Cyclizing Spacers: Toward Rapid Depolymerization Rates. *Macromolecules* **2012**, *45*, 7364–7374.
29. Sirianni, Q. E. A.; Rabiee Kenaree, A.; Gillies, E. R., Polyglyoxylamides: Tuning Structure and Properties of Self-Immolative Polymers. *Macromolecules* **2019**, *52*, 262–270.
30. Ree, L. H. S.; Sirianni, Q. E. A.; Gillies, E. R.; Kelland, M. A., Systematic Study of Polyglyoxylamides as Powerful, High-Cloud-Point Kinetic Hydrate Inhibitors. *Energy Fuels* **2019**, *33*, 2067–2075.
31. Fan, B.; Gillies, E. R., Poly(ethyl glyoxylate)-Poly(ethylene oxide) Nanoparticles: Stimuli-Responsive Drug Release via End-to-End Polyglyoxylate Depolymerization. *Mol. Pharmaceutics* **2017**, *14*, 2548–2559.
32. Fan, B.; Trant, J. F.; Wong, A. D.; Gillies, E. R., Polyglyoxylates: A Versatile Class of Triggerable Self-Immolative Polymers from Readily Accessible Monomers. *J. Am. Chem. Soc.* **2014**, *136*, 10116–10123.
33. Kaitz, J. A.; Diesendruck, C. E.; Moore, J. S., Dynamic Covalent Macrocyclic Poly(phthalaldehyde)s: Scrambling Cyclic Homopolymer Mixtures Produces Multi-Block and Random Cyclic Copolymers. *Macromolecules* **2013**, *46*, 8121–8128.
34. Brachais, C. H.; Duclos, R.; Vaugelade, C.; Huguet, J.; Capelle-Hue, M. L.; Bunel, C., Poly(methylglyoxylate), a Biodegradable Polymeric Material for New Drug Delivery Systems. *Int. J. Pharm.* **1998**, *169*, 23–31.
35. Brachais, C. H.; Huguet, J.; Bunel, C.; Brachais, L., In Vitro Degradation of Poly(methyl glyoxylate) in Water. *Polymer* **1998**, *39*, 883–890.
36. Brachais, C. H.; Huguet, J.; Bunel, C., Synthesis, Characterization and Stabilization of Poly(methyl glyoxylate). *Polymer* **1997**, *38*, 4959–4964.

37. Belloncle, B.; Bunel, C.; Menu-Bouaouiche, L.; Lesouhaitier, O.; Burel, F., Study of the Degradation of Poly(ethyl glyoxylate): Biodegradation, Toxicity and Ecotoxicity Assays. *J. Polym. Environ.* **2012**, *20*, 726–731.
38. Fan, B.; Trant, J. F.; Gillies, E. R., End-Capping Strategies for Triggering End-to-End Depolymerization of Polyglyoxylates. *Macromolecules* **2016**, *49*, 9309–9319.
39. Fan, B.; Yardley, R. E.; Trant, J. F.; Borecki, A.; Gillies, E. R., Tuning the Hydrophobic Cores of Self-Immolative Polyglyoxylate Assemblies. *Polym. Chem.* **2018**, *9*, 2601–2610.
40. Gambles, M. T.; Fan, B.; Borecki, A.; Gillies, E. R., Hybrid Polyester Self-Immolative Polymer Nanoparticles for Controlled Drug Release. *ACS Omega* **2018**, *3*, 5002–5011.
41. Fan, B.; Trant, J. F.; Yardley, R. E.; Pickering, A. J.; Lagurné-Labarhet, F.; Gillies, E. R., Photocontrolled Degradation of Stimuli-Responsive Poly(ethyl glyoxylate): Differentiating Features and Traceless Ambient Depolymerization. *Macromolecules* **2016**, *49*, 7196–7203.
42. Fan, B.; Salazar, R.; Gillies, E. R., Depolymerization of Trityl End-Capped Poly(Ethyl Glyoxylate): Potential Applications in Smart Packaging. *Macromol. Rapid Commun.* **2018**, *39*, 1800173.
43. Rabiee Kenaree, A.; Gillies, E. R., Controlled Polymerization of Ethyl Glyoxylate Using Alkylolithium and Alkoxide Initiators. *Macromolecules* **2018**, *51*, 5501–5510.
44. Easterling, C. P.; Kubo, T.; Orr, Zachary M.; Fanucci, G. E.; Sumerlin, B. S., Synthetic Upcycling of Polyacrylates Through Organocatalyzed Post-Polymerization Modification. *Chem. Sci.* **2017**, *8*, 7705–7709.
45. Fan, B.; Trant, J. F.; Hemery, G.; Sandre, O.; Gillies, E. R., Thermo-Responsive Self-Immolative Nanoassemblies: Direct and Indirect triggering. *Chem. Commun.* **2017**, *53*, 12068–12071.
46. Ito, H.; Schwalm, R., Thermally Developable, Positive Resist Systems with High Sensitivity. *J. Electrochem. Soc.* **1989**, *136*, 241–245.
47. Winnik, F. M., Photophysics of Preassociated Pyrenes in Aqueous Polymer Solutions and in Other Organized Media. *Chem. Rev.* **1993**, *93*, 587–614.
48. Casier, R.; Gauthier, M.; Duhamel, J., Using Pyrene Excimer Fluorescence To Probe Polymer Diffusion in Latex Films. *Macromolecules* **2017**, *50*, 1635–1644.

5 Conclusion and future work

The work presented throughout this thesis describes the significant expansion to two different self-immolative polymer systems: polycarbamates and polyglyoxylates.

5.1 Polycarbamates

5.1.1 Conclusions

The work described in chapter 2 dealt with the incorporation of polycarbamate SIPs into amphiphilic block copolymers and their use to prepare nanoassemblies. This was attempted because these SIPs are known to have depolymerization rates that depend on environmental factors such as solvent and pH. In previous work, hydrophobic SIPs have been incorporated into amphiphilic block copolymers.¹⁻³ However, stimuli-responsive hydrophilic blocks have not previously been incorporated into these polymers. I synthesized amphiphilic copolymers composed of a hydrophobic polycarbamate SIP block and a hydrophilic PDMAEMA block connected by a UV light-responsive linker end-cap. It was hypothesized that after assembly of the block copolymers into nanoparticles, chain collapse of the PDMAEMA above its LCST might change the environment of the SIP block, thereby altering its depolymerization rate. Self-assembly of the block copolymers was performed, and the depolymerization of the resulting assemblies was studied by fluorescence spectroscopy, dynamic light scattering, and NMR spectroscopy. At 20 °C, the system exhibited a selective response to UV light. At 65 °C, above the LCST of PDMAEMA, the systems underwent a more rapid depolymerization, suggesting that the increase in depolymerization arising from the higher temperature dominated over environmental effects arising from chain collapse (**Figure 5.1**).

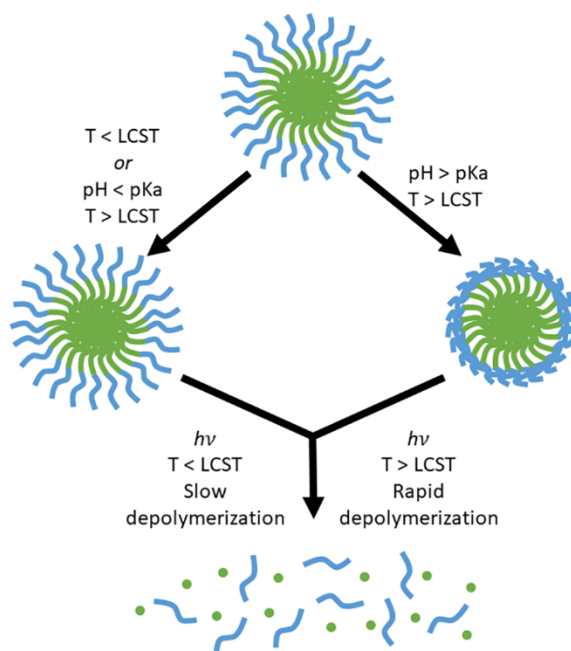


Figure 5.1: Graphical summary of Chapter 2. Out of the three stimuli investigated (pH, UV, and temperature) the elevated temperature dominated the depolymerization behaviour, masking any other environmental factors.

The main limitation of the Chapter 2 study was the high temperature necessary to induce chain collapse in the PDMAEMA, which masked any possible environmental effects on the SIP depolymerization. To mitigate this, a polymer with a lower LCST, PNIPAAm, was selected to be incorporated into the amphiphilic block copolymers, via a connection with a UV-responsive linker. These polymers were synthesized and demonstrated self-assembly behaviour enabling the formation of nanoparticles. Depolymerization behaviour was monitored via small molecule release and NMR spectroscopy with results that were not in agreement with each other. The self-assembled nanoparticles were aggregating into larger particles over time, regardless of the incubation temperature, as noticed in DLS studies and TEM images. During the NMR study, it was also noted that the polymers were precipitating out of solution. This suggested that the nanoparticles were unstable in the buffered environment.

The reversible thermo-responsive behavior of the PDMAEMA and PNIPAAm blocks of the amphiphilic block copolymers was the main issue with the system. For PDMAEMA,

the high temperature masked any environmental effects arising from chain collapse, although the micelles were stable throughout the tests. For PNIPAAm, the transition from the solvated to the de-solvated state led to instability in the micelles, and precipitation of the block copolymers out of solution. The reasons PNIPAAm experienced this and PDMAEMA did not may be attributed to the relative hydrophilicity of the two polymers, with PDMAEMA being more hydrophilic and therefore creating more stable nanoparticles.

5.1.2 Future work

Both above studies were aimed at determining how a change in local environment would affect the amount of depolymerization of the SIP block. By collapsing the corona reversibly, these systems could potentially have had the ability to turn on and off this behaviour. Since neither study produced conclusive evidence of this effect due to the high temperatures needed in Chapter 2 and the micelle aggregation in Chapter 3, an alternative is to create crosslinked micelles. Although, this may lack the desired multi-stimuli responsive behavior, it should provide insight into the depolymerization behaviour.

Crosslinked polymeric micelles can be made via core-crosslinked (CCPM)⁴ or shell-crosslinked polymeric micelles (SCPM).⁵ CCPMs have been extensively studied for drug release and show an increased *in vivo* stability and prolonged drug release. SCMP were first demonstrated by Wooley and coworker in 1996,⁶ and have since been studied for biomedical applications. They can hold the nanostructure of the assemblies in blood, avoid burst release in the first few hours, and do not aggregate in solution.

The crosslinked nature of the micelles would allow retention of the depolymerization products, similar to drug retention, resulting in higher local concentrations of the depolymerization products. To avoid chemical modification to the hydrophobic SIP block, which could change the amount of depolymerization, the hydrophilic block will be switched to a polymer that can undergo crosslinking. To avoid inter-micellar crosslinking, a tri-block copolymer will be synthesized, allowing for the crosslinking to only occur on the inner shell (**Figure 5.2**).

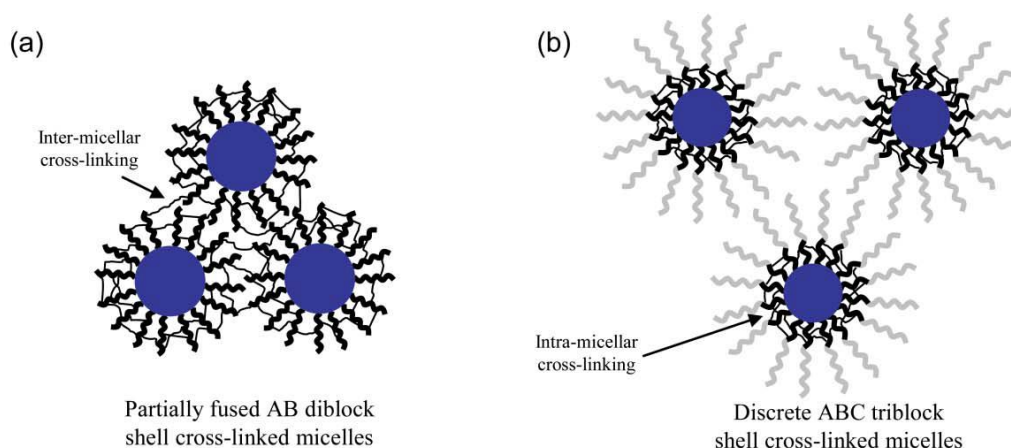
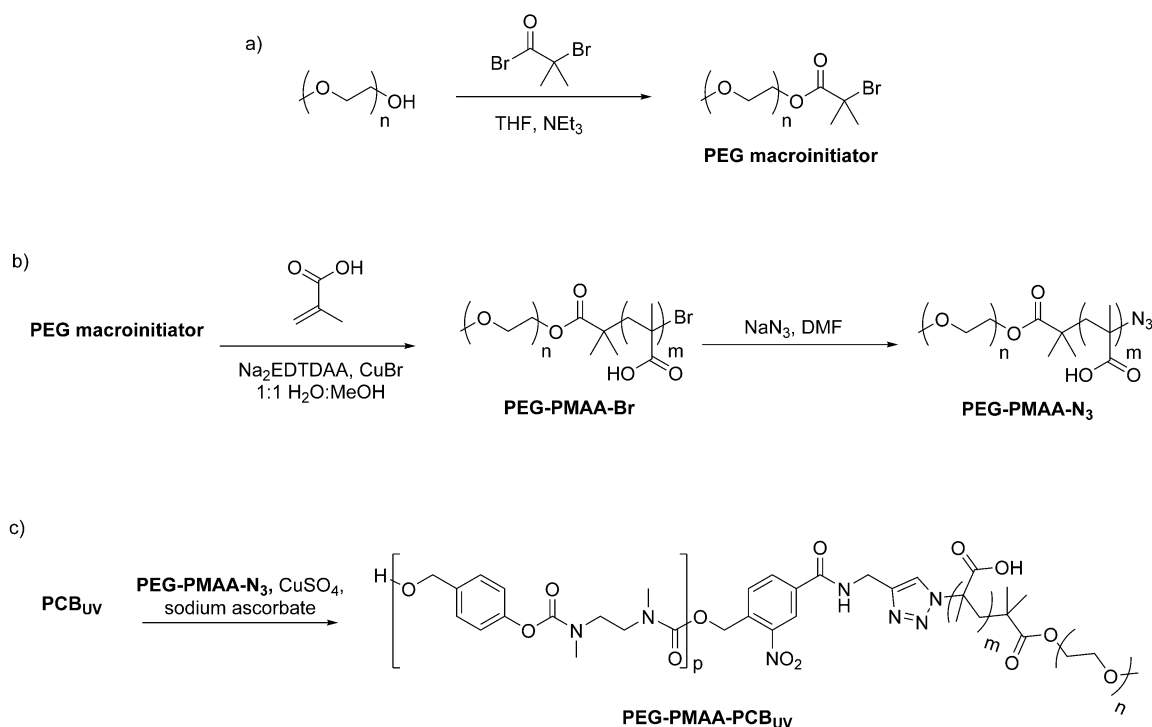


Figure 5.2: Schematic representation of the inter-micellar and intra-micellar crosslinking for a) AB diblock copolymer and (b) ABC triblock copolymer micelles at high copolymer concentrations. Reproduced with permission from reference 5. Copyright 2007 the Royal Society of Chemistry

PEG macroinitiators for ATRP can be synthesized by reacting poly(ethylene oxide) monomethyl ether with α -bromoisobutyryl bromide (**Scheme 5.1a**).⁷ The macroinitiator can then undergo ATRP with any compatible monomer. Since this block will be used to crosslink, methyl acrylic acid can be used, which possesses carboxylic acid groups capable of crosslinking via an EDC coupling. This will yield a hydrophilic polymer, **PEG-PMAA-Br**, with a short PMAA block (~10 units), where the terminal bromine can be easily converted to an azide, **PEG-PMAA-N₃** (**Scheme 5.1b**).⁸ Having an azide will allow for the use of the same UV-responsive end-cap as used in Chapters 2 and 3 on the **PCB_{UV}**. The hydrophobic SIP (**PCB_{UV}**) and the hydrophilic **PEG-PMAA-N₃** can be conjugated via CuAAC, to create a tri-block copolymer, **PEG-PMAA-PCB_{UV}**. (**Scheme 5.1c**).



Scheme 5.1: a) Synthesis of PEG macroinitiator for ATRP; b) synthesis of diblock copolymer **PEG-PMAA-Br** via ATRP and the subsequent conversion of the bromine end-group to an azide, **PEG-PMAA-N₃**; and c) the synthesis of ABC triblock copolymer **PEG-PMAA-PCB_{UV}** by CuAAC.

This amphiphilic block copolymer can then be self-assembled to form nanoparticles in solution and the inner shell can be crosslinked via an EDC coupling using 2,2-(ethylenedioxy)bis(ethylamine) as the crosslinker (**Figure 5.3**). The crosslinked layer will provide stability and slow the release of the depolymerization products. If the SIP block cannot tolerate the EDC conditions, which have not been tried to date, the carboxylic acid group can be converted to a different functional group (*e.g.* EDC coupling with allyl amine) prior to the CuAAC.

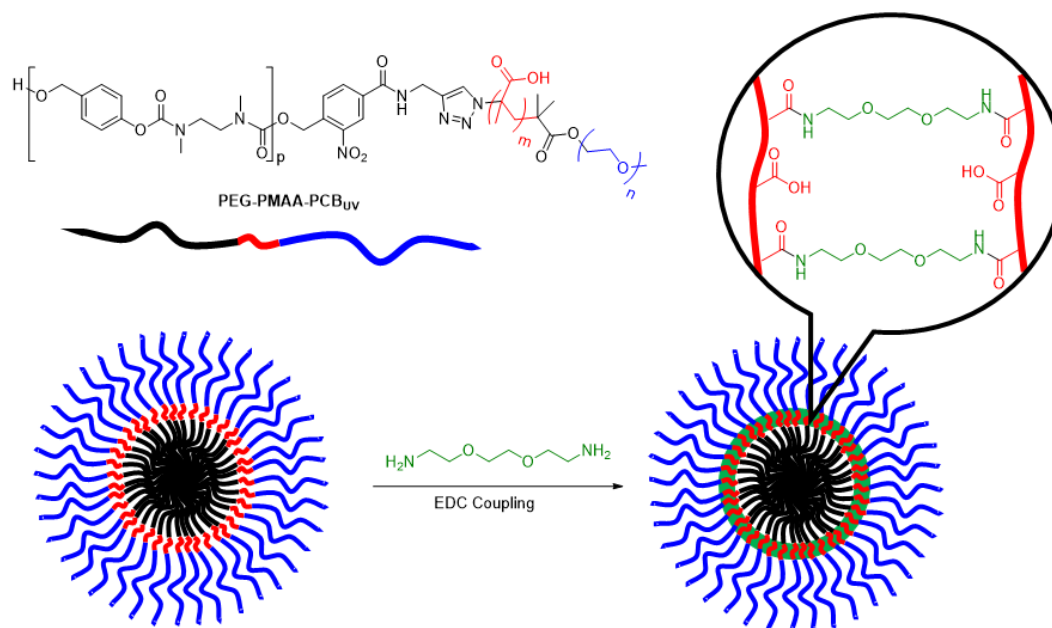


Figure 5.3: Schematic of the self-assembly of ABC triblock copolymer **PEG-PMAA-PCBUV** and subsequent crosslinking by EDC coupling with 2,2-(ethylenedioxy)bis(ethylamine) to yield SCMPs.

When the inner SIP is cleaved upon irradiation with UV light, the shell structure should be maintained in the crosslinked structure, allowing for a high concentration of depolymerizing SIPs in the core. Monitoring the evolution of depolymerization products of the SIP blocks in both the crosslinked and un-crosslinked micelles will illustrate a relationship between concentration and depolymerization behaviour. This study could also be expanded to look at other environmental conditions, including pH and temperature.

5.2 Polyglyoxylates

5.2.1 Conclusions

Until this work, many glyoxylates were previously inaccessible because of problems synthesizing the monomers or achieving large volumes of sufficiently pure monomers for polymerization. This resulted in only a few new monomers (*i.e.* butyl-, benzyl-, and menthyl glyoxylate) which often only yielded short homopolymers (*ca.* $DP_n = 20$ units)

compared to the larger PEtG homopolymers ($DP_n > 200$).^{1, 9} This limited the possible applications of PGs. Further to this, previous attempts at achieving new glyoxylates through transesterification reactions had resulted in complete depolymerization of the starting polymers.

Through work presented in this thesis, it was determined that the carbonate linker present in many previously reported end-caps of the PEtG system could not tolerate the transesterification conditions of TBD. This prompted the development of a new end-capping system based on the more stable ether linkages, including a UV-responsive end-cap based on 2-nitrobenzyl alcohol.

A series of new PGs was created by the complete conversions of **PEtG_{UV}** using the TBD catalyst, including **PnPrG**, **PiPrG**, **PnBuG**, **PPenG**, **PHexG**, **POctG**, and **PBnG** (**Figure 5.4**). These polymers maintained their macromolecular nature, as well as their ability to depolymerize. An inverse relationship between the number of carbons on the parent alcohol and T_g was observed from -4 to -47 °C, which will allow for tuning of the properties in low temperature applications such as outdoor adhesives in winter months. To further demonstrate the versatility of this method, alcohols with functional groups were incorporated into polymers creating **PAIG**, **PFuG**, and **PPG**. This post-transesterification modification of these groups will increase future possibilities of this work. To demonstrate the possibility for applying such modifications, **PPG** underwent a CuAAC reaction to conjugate it to a 1-(azidomethyl)pyrene, a fluorescent probe.

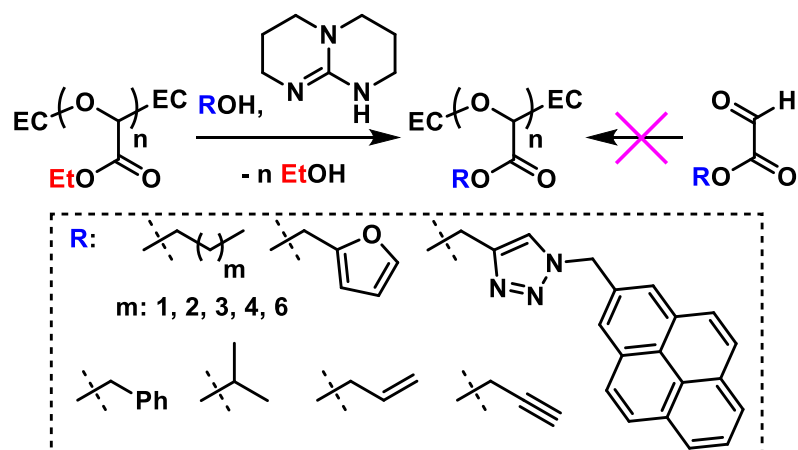


Figure 5.4: Graphical summary of Chapter 4. The transesterification reaction of PETG with TBD has led to the development of previously inaccessible PGs.

5.2.2 Future work

The ability to achieve polyglyoxylates that were previously inaccessible can allow the field of polyglyoxylates to rapidly grow and expand. Taking advantage of the functional handles that have already been attached, various reactions can be used to append groups, including CuAAC and Sonogashira cross-couplings on the propargyl moieties, thiol-ene click chemistry on the allyl groups, and cycloaddition reactions to the furans (**Figure 5.5**). This can be used to attach several moieties including drugs and dyes, or crosslinking agents to create gels.

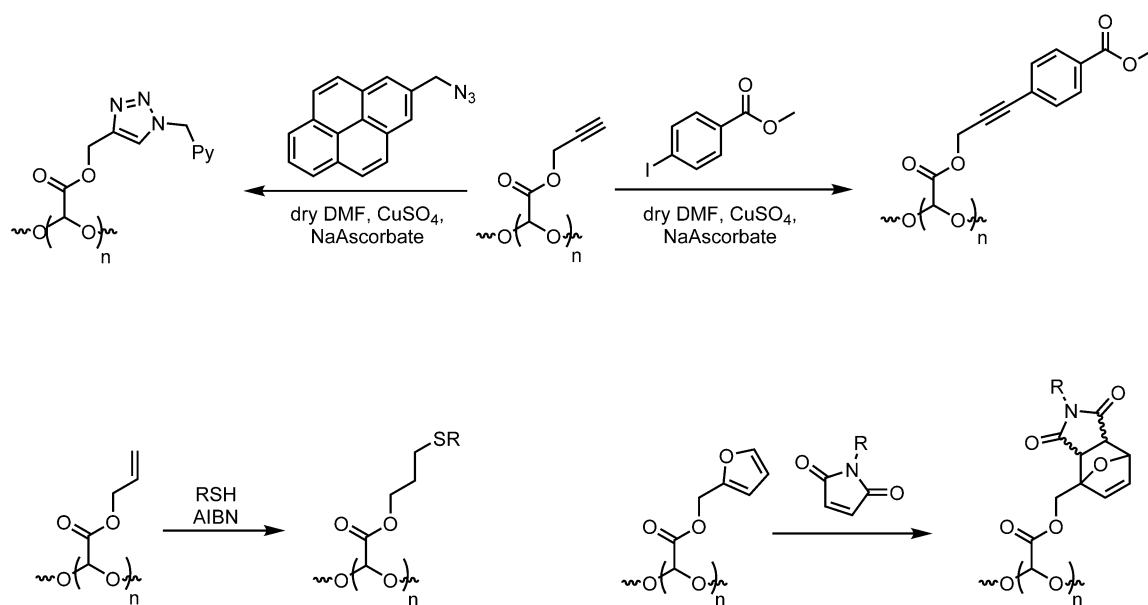


Figure 5.5: Possible reactions that could be performed on the available functional handles including CuAAC and Sonogashira cross-couplings on the propargyl, thiolene click chemistry on the allyl, and cycloaddition reactions to the furan.

To date, there has been no water-soluble PGs synthesized, which, if synthesized could enable several applications, including hydrogels or completely degradable amphiphilic block copolymers. The PEtG could be made water soluble by the incorporation of 2-methoxyethanol. Combining 2-methoxyethanol with a small amount 5-methylfurfuryl alcohol during the transesterification will yield a methylfuran-functionalized, a water-soluble PG which could be used to create hydrogels. The Shoichet and Trant groups created injectable hydrogels using a methylfuran-modified hyaluronan and bismaleimide PEG.¹⁰ The advantage of this system is that rapid gelation will occur when the two polymers are in an aqueous environment at pH 7.4, allowing for the *in situ* formation of hydrogels in the human body. By creating an analogous system with a PG backbone, there is the potential to create injectable hydrogels, that can be triggered to degrade, which can be used for drug delivery of 3D cell culture (**Figure 5.6**).

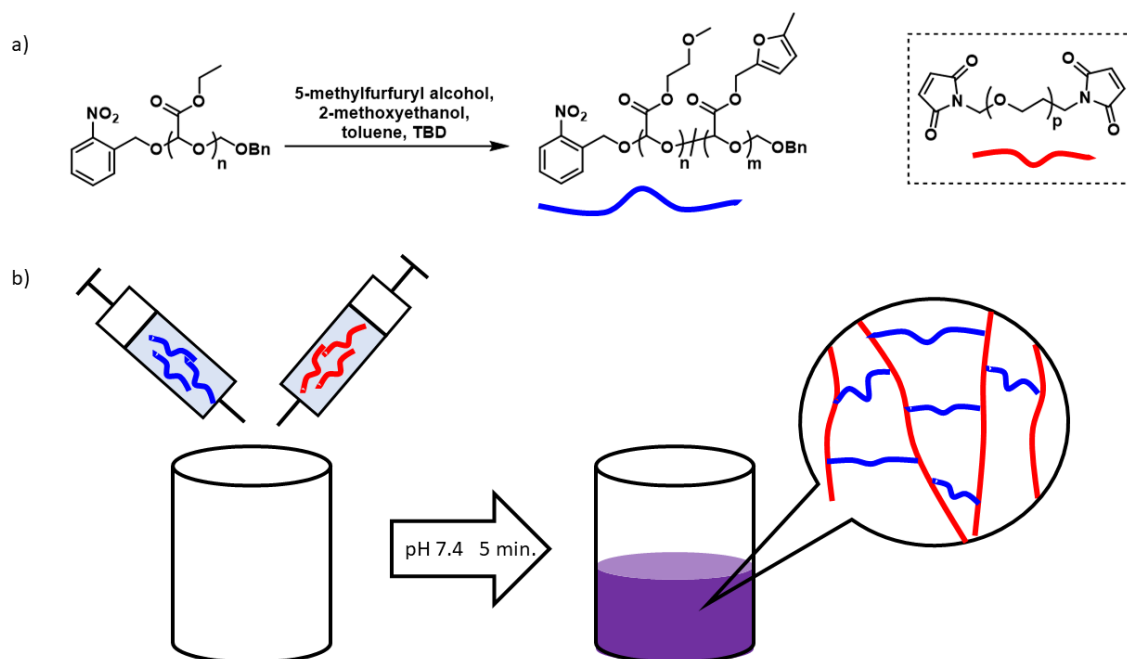


Figure 5.6: a) synthetic strategy for making water-soluble, crosslinkable PGs and b) schematic representing their use as fast-gelling injectable-hydrogels at pH 7.4.

5.3 References

1. Fan, B.; Trant, J. F.; Wong, A. D.; Gillies, E. R., Polyglyoxylates: A Versatile Class of Triggerable Self-Immolative Polymers from Readily Accessible Monomers. *J. Am. Chem. Soc.* **2014**, *136*, 10116–10123.
2. Fan, B.; Yardley, R. E.; Trant, J. F.; Borecki, A.; Gillies, E. R., Tuning the Hydrophobic Cores of Self-Immolative Polyglyoxylate Assemblies. *Polym. Chem.* **2018**, *9*, 2601–2610.
3. DeWit, M. A.; Gillies, E. R., A Cascade Biodegradable Polymer Based on Alternating Cyclization and Elimination Reactions. *J. Am. Chem. Soc.* **2009**, *131*, 18327–18334.
4. Talelli, M.; Barz, M.; Rijcken, C. J. F.; Kiessling, F.; Hennink, W. E.; Lammers, T., Core-Crosslinked Polymeric Micelles: Principles, Preparation, Biomedical Applications and Clinical Translation. *Nano Today* **2015**, *10*, 93–117.
5. Read, E. S.; Armes, S. P., Recent Advances in Shell Cross-Linked Micelles. *Chem. Commun.* **2007**, 3021–3035.

6. Thurmond, K. B.; Kowalewski, T.; Wooley, K. L., Water-Soluble Knedel-like Structures: The Preparation of Shell-Cross-Linked Small Particles. *J. Am. Chem. Soc.* **1996**, *118*, 7239–7240.
7. Zhang, Q.; Tang, X.; Wang, T.; Yu, F.; Guo, W.; Pei, M., Thermo-Sensitive Zwitterionic Block Copolymers via ATRP. *RSC Adv.* **2014**, *4*, 24240–24247.
8. Coessens, V.; Nakagawa, Y.; Matyjaszewski, K., Synthesis of Azido End-Functionalized Polyacrylates via Atom Transfer Radical Polymerization. *Polym. Bull.* **1998**, *40*, 135–142.
9. Rabiee Kenaree, A.; Gillies, E. R., Controlled Polymerization of Ethyl Glyoxylate Using Alkylolithium and Alkoxide Initiators. *Macromolecules* **2018**, *51*, 5501–5510.
10. Smith, L. J.; Taimoory, S. M.; Tam, R. Y.; Baker, A. E. G.; Bintah Mohammad, N.; Trant, J. F.; Shoichet, M. S., Diels–Alder Click-Cross-Linked Hydrogels with Increased Reactivity Enable 3D Cell Encapsulation. *Biomacromolecules* **2018**, *19*, 926–935.

Appendices

Appendix 1 – Permission to reuse copyrighted material



Copyright Clearance Center



[Home](#)
[Account Info](#)
[Help](#)




ACS Publications
Most Trusted. Most Cited. Most Read.

Title: Efficient Colorimetric pH Sensor Based on Responsive Polymer-Quantum Dot Integrated Graphene Oxide

Author: Kwanyeol Paek, Hyunseung Yang, Junhyuk Lee, et al

Publication: ACS Nano

Publisher: American Chemical Society

Date: Mar 1, 2014

Copyright © 2014, American Chemical Society

Logged in as:
Rebecca Yardley
Western University
Account #:
3001449083

[LOGOUT](#)

PERMISSION/LICENSE IS GRANTED FOR YOUR ORDER AT NO CHARGE

This type of permission/license, instead of the standard Terms & Conditions, is sent to you because no fee is being charged for your order. Please note the following:

- Permission is granted for your request in both print and electronic formats, and translations.
- If figures and/or tables were requested, they may be adapted or used in part.
- Please print this page for your records and send a copy of it to your publisher/graduate school.
- Appropriate credit for the requested material should be given as follows: "Reprinted (adapted) with permission from (COMPLETE REFERENCE CITATION). Copyright (YEAR) American Chemical Society." Insert appropriate information in place of the capitalized words.
- One-time permission is granted only for the use specified in your request. No additional uses are granted (such as derivative works or other editions). For any other uses, please submit a new request.

If credit is given to another source for the material you requested, permission must be obtained from that source.

[BACK](#)
[CLOSE WINDOW](#)

Copyright © 2019 Copyright Clearance Center, Inc. All Rights Reserved. [Privacy statement](#). [Terms and Conditions](#).
Comments? We would like to hear from you. E-mail us at customercare@copyright.com

**Royal Society of Chemistry LICENSE
TERMS AND CONDITIONS**

Aug 30, 2019

This is a License Agreement between Western University -- Rebecca Yardley ("You") and Royal Society of Chemistry ("Royal Society of Chemistry") provided by Copyright Clearance Center ("CCC"). The license consists of your order details, the terms and conditions provided by Royal Society of Chemistry, and the payment terms and conditions.

All payments must be made in full to CCC. For payment instructions, please see information listed at the bottom of this form.

License Number	4659070243155
License date	Aug 30, 2019
Licensed content publisher	Royal Society of Chemistry
Licensed content title	RSC advances
Licensed content date	Jan 1, 2011
Type of Use	Thesis/Dissertation
Requestor type	Academic institution
Format	Print, Electronic
Portion	image/photo
Number of images/photos requested	1
The requesting person/organization is:	Rebecca Yardley
Title or numeric reference of the portion(s)	Figure 1
Title of the article or chapter the portion is from	Unusual thermogelling behaviour of poly[2- (dimethylamino)ethyl methacrylate] (PDMAEMA)- based polymers polymerized in bulk
Editor of portion(s)	N/A
Author of portion(s)	N/A
Volume of serial or monograph.	N/A
Page range of the portion	62315
Publication date of portion	01 September 2019
Rights for	Main product
Duration of use	Life of current edition
Creation of copies for the disabled	no
With minor editing privileges	no
For distribution to	Worldwide
In the following language(s)	Original language of publication
With incidental promotional use	no
The lifetime unit quantity of new product	More than 2,000,000
Title	Synthesis of Polycarbamate-Based Nanoassemblies and Previously Inaccessible Polyglyoxylates
Institution name	n/a
Expected presentation date	Sep 2019
Total (may include CCC user fee)	0.00 USD
Terms and Conditions	



RightsLink®

Home

Account
Info

Help



ACS Publications
Most Trusted. Most Cited. Most Read.

Title: Spiropyran-Conjugated
Thermoresponsive Copolymer as
a Colorimetric Thermometer
with Linear and Reversible Color
Change

Author: Yasuhiro Shiraishi, Ryo
Miyamoto, Takayuki Hirai

Publication: Organic Letters

Publisher: American Chemical Society

Date: Apr 1, 2009

Copyright © 2009, American Chemical Society

Logged in as:

Rebecca Yardley
Western University
Account #: 3001449083

LOGOUT

PERMISSION/LICENSE IS GRANTED FOR YOUR ORDER AT NO CHARGE

This type of permission/license, instead of the standard Terms & Conditions, is sent to you because no fee is being charged for your order. Please note the following:

- Permission is granted for your request in both print and electronic formats, and translations.
- If figures and/or tables were requested, they may be adapted or used in part.
- Please print this page for your records and send a copy of it to your publisher/graduate school.
- Appropriate credit for the requested material should be given as follows: "Reprinted (adapted) with permission from (COMPLETE REFERENCE CITATION). Copyright (YEAR) American Chemical Society." Insert appropriate information in place of the capitalized words.
- One-time permission is granted only for the use specified in your request. No additional uses are granted (such as derivative works or other editions). For any other uses, please submit a new request.

If credit is given to another source for the material you requested, permission must be obtained from that source.

BACK

CLOSE WINDOW

Copyright © 2019 Copyright Clearance Center, Inc. All Rights Reserved. [Privacy statement](#). [Terms and Conditions](#).
Comments? We would like to hear from you. E-mail us at customercare@copyright.com

**RightsLink**[®][Home](#)[Account Info](#)[Help](#)**ACS Publications**
Most Trusted. Most Cited. Most Read.

Title: CO2-Responsive Cellulose Nanofibers Aerogels for Switchable Oil-Water Separation
Author: Yingzhan Li, Liqian Zhu, Nathan Grishkewich, et al
Publication: Applied Materials
Publisher: American Chemical Society
Date: Mar 1, 2019

Logged in as:
Rebecca Yardley
Western University
Account #:
3001449083

[LOGOUT](#)

Copyright © 2019, American Chemical Society

PERMISSION/LICENSE IS GRANTED FOR YOUR ORDER AT NO CHARGE

This type of permission/license, instead of the standard Terms & Conditions, is sent to you because no fee is being charged for your order. Please note the following:

- Permission is granted for your request in both print and electronic formats, and translations.
- If figures and/or tables were requested, they may be adapted or used in part.
- Please print this page for your records and send a copy of it to your publisher/graduate school.
- Appropriate credit for the requested material should be given as follows: "Reprinted (adapted) with permission from (COMPLETE REFERENCE CITATION). Copyright (YEAR) American Chemical Society." Insert appropriate information in place of the capitalized words.
- One-time permission is granted only for the use specified in your request. No additional uses are granted (such as derivative works or other editions). For any other uses, please submit a new request.

If credit is given to another source for the material you requested, permission must be obtained from that source.

[BACK](#)[CLOSE WINDOW](#)

Copyright © 2019 [Copyright Clearance Center, Inc.](#) All Rights Reserved. [Privacy statement.](#) [Terms and Conditions.](#) Comments? We would like to hear from you. E-mail us at customercare@copyright.com



RightsLink®

Home

Account
Info

Help



ACS Publications
Most Trusted. Most Cited. Most Read.

Title: Extended Release of Native Drug
Conjugated in Polyketal
Microparticles

Author: Shutao Guo, Yoshiyuki
Nakagawa, Aoune Barhoumi, et
al

Publication: Journal of the American
Chemical Society

Publisher: American Chemical Society

Date: May 1, 2016

Logged in as:
Rebecca Yardley
Western University
Account #:
3001449083

LOGOUT

Copyright © 2016, American Chemical Society

PERMISSION/LICENSE IS GRANTED FOR YOUR ORDER AT NO CHARGE

This type of permission/license, instead of the standard Terms & Conditions, is sent to you because no fee is being charged for your order. Please note the following:

- Permission is granted for your request in both print and electronic formats, and translations.
- If figures and/or tables were requested, they may be adapted or used in part.
- Please print this page for your records and send a copy of it to your publisher/graduate school.
- Appropriate credit for the requested material should be given as follows: "Reprinted (adapted) with permission from (COMPLETE REFERENCE CITATION). Copyright (YEAR) American Chemical Society." Insert appropriate information in place of the capitalized words.
- One-time permission is granted only for the use specified in your request. No additional uses are granted (such as derivative works or other editions). For any other uses, please submit a new request.

If credit is given to another source for the material you requested, permission must be obtained from that source.

BACK

CLOSE WINDOW

Copyright © 2019 Copyright Clearance Center, Inc. All Rights Reserved. [Privacy statement](#). [Terms and Conditions](#).
Comments? We would like to hear from you. E-mail us at customer@copyright.com



RightsLink®

[Home](#)
[Account Info](#)
[Help](#)


Title: Hydrophobic Cysteine Poly(disulfide)-based Redox-Hypersensitive Nanoparticle Platform for Cancer Theranostics

Author: Omid C. Farokhzad, James L. MacLean, Matthew Mulvale, et al

Publication: Angewandte Chemie International Edition

Publisher: John Wiley and Sons

Date: Jun 26, 2015

© 2015 WILEY-VCH Verlag GmbH & Co. KGaA, Weinheim

Logged in as:
Rebecca Yardley
Western University
Account #:
3001449083

[LOGOUT](#)

Order Completed

Thank you for your order.

This Agreement between Western University -- Rebecca Yardley ("You") and John Wiley and Sons ("John Wiley and Sons") consists of your license details and the terms and conditions provided by John Wiley and Sons and Copyright Clearance Center.

Your confirmation email will contain your order number for future reference.

[printable details](#)

License Number	4659071086494
License date	Aug 30, 2019
Licensed Content Publisher	John Wiley and Sons
Licensed Content Publication	Angewandte Chemie International Edition
Licensed Content Title	Hydrophobic Cysteine Poly(disulfide)-based Redox-Hypersensitive Nanoparticle Platform for Cancer Theranostics
Licensed Content Author	Omid C. Farokhzad, James L. MacLean, Matthew Mulvale, et al
Licensed Content Date	Jun 26, 2015
Licensed Content Volume	54
Licensed Content Issue	32
Licensed Content Pages	6
Type of use	Dissertation/Thesis
Requestor type	University/Academic
Format	Print and electronic
Portion	Figure/table
Number of figures/tables	1
Original Wiley figure/table number(s)	Scheme 1
Will you be translating?	No
Title of your thesis / dissertation	Synthesis of Polycarbamate-Based Nanoassemblies and Previously Inaccessible Polyglyoxylates
Expected completion date	Sep 2019
Expected size (number of pages)	250
Requestor Location	Western University 1151 Richmond Street London, ON N6A 3K7 Canada Attn: Western University
Publisher Tax ID	EUB26007151
Total	0.00 CAD



RightsLink®

Home

Account Info

Help



ACS Publications
Most Trusted. Most Cited. Most Read.

Title: Light-Triggered Intramolecular Cyclization in Poly(lactic-co-glycolic acid)-Based Polymers for Controlled Degradation
Author: Jason Olejniczak, Minnie Chan, Adah Almutairi

Publication: Macromolecules
Publisher: American Chemical Society
Date: May 1, 2015

Copyright © 2015, American Chemical Society

Logged in as:
Rebecca Yardley
Western University
Account #:
3001449083

LOGOUT

PERMISSION/LICENSE IS GRANTED FOR YOUR ORDER AT NO CHARGE

This type of permission/license, instead of the standard Terms & Conditions, is sent to you because no fee is being charged for your order. Please note the following:

- Permission is granted for your request in both print and electronic formats, and translations.
- If figures and/or tables were requested, they may be adapted or used in part.
- Please print this page for your records and send a copy of it to your publisher/graduate school.
- Appropriate credit for the requested material should be given as follows: "Reprinted (adapted) with permission from (COMPLETE REFERENCE CITATION). Copyright (YEAR) American Chemical Society." Insert appropriate information in place of the capitalized words.
- One-time permission is granted only for the use specified in your request. No additional uses are granted (such as derivative works or other editions). For any other uses, please submit a new request.

If credit is given to another source for the material you requested, permission must be obtained from that source.

BACK

CLOSE WINDOW

Copyright © 2019 Copyright Clearance Center, Inc. All Rights Reserved. [Privacy statement](#). [Terms and Conditions](#).
Comments? We would like to hear from you. E-mail us at customercare@copyright.com

**Royal Society of Chemistry LICENSE
TERMS AND CONDITIONS**

Aug 30, 2019

This is a License Agreement between Western University -- Rebecca Yardley ("You") and CCC Reproduction ("CCC Reproduction") provided by Copyright Clearance Center ("CCC"). The license consists of your order details, the terms and conditions provided by CCC Reproduction, and the payment terms and conditions.

All payments must be made in full to CCC. For payment instructions, please see information listed at the bottom of this form.

License Number	4659061062878
License date	Aug 30, 2019
Licensed content publisher	CCC Reproduction
Licensed content title	Green chemistry
Licensed content date	Jan 1, 1999
Type of Use	Thesis/Dissertation
Requestor type	Academic institution
Format	Print, Electronic
Portion	image/photo
Number of images/photos requested	1
The requesting person/organization is:	Rebecca Yardley
Title or numeric reference of the portion(s)	Figure 3
Title of the article or chapter the portion is from	Depolymerizable poly(benzyl ether)-based materials for selective room temperature recycling
Editor of portion(s)	N/A
Author of portion(s)	N/A
Volume of serial or monograph.	N/A
Page range of the portion	4543
Publication date of portion	01 September 2019
Rights for	Main product
Duration of use	Life of current edition
Creation of copies for the disabled	no
With minor editing privileges	no
For distribution to	Worldwide
In the following language(s)	Original language of publication
With incidental promotional use	no
The lifetime unit quantity of new product	More than 2,000,000
Title	Synthesis of Polycarbamate-Based Nanoassemblies and Previously Inaccessible Polyglyoxylates
Institution name	n/a
Expected presentation date	Sep 2019
Total (may include CCC user fee)	0.00 USD
Terms and Conditions	



RightsLink®

Home

Account
Info

Help



ACS Publications
Most Trusted. Most Cited. Most Read.

Title: Dynamic Covalent Macrocyclic Poly(phthalaldehyde)s: Scrambling Cyclic Homopolymer Mixtures Produces Multi-Block and Random Cyclic Copolymers

Author: Joshua A. Kaitz, Charles E. Diesendruck, Jeffrey S. Moore

Publication: Macromolecules

Publisher: American Chemical Society

Date: Oct 1, 2013

Copyright © 2013, American Chemical Society

Logged in as:

Rebecca Yardley
Western University

Account #:
3001449083

LOGOUT

PERMISSION/LICENSE IS GRANTED FOR YOUR ORDER AT NO CHARGE

This type of permission/license, instead of the standard Terms & Conditions, is sent to you because no fee is being charged for your order. Please note the following:

- Permission is granted for your request in both print and electronic formats, and translations.
- If figures and/or tables were requested, they may be adapted or used in part.
- Please print this page for your records and send a copy of it to your publisher/graduate school.
- Appropriate credit for the requested material should be given as follows: "Reprinted (adapted) with permission from (COMPLETE REFERENCE CITATION). Copyright (YEAR) American Chemical Society." Insert appropriate information in place of the capitalized words.
- One-time permission is granted only for the use specified in your request. No additional uses are granted (such as derivative works or other editions). For any other uses, please submit a new request.

If credit is given to another source for the material you requested, permission must be obtained from that source.

BACK

CLOSE WINDOW

Copyright © 2019 Copyright Clearance Center, Inc. All Rights Reserved. [Privacy statement](#). [Terms and Conditions](#).
Comments? We would like to hear from you. E-mail us at customercare@copyright.com



RightsLink®

[Home](#)
[Account Info](#)
[Help](#)


Title: Triggered Transience of Metastable Poly(phthalaldehyde) for Transient Electronics

Author: Scott R. White, John A. Rogers, Jeffrey S. Moore, et al

Publication: Advanced Materials

Publisher: John Wiley and Sons

Date: Oct 20, 2014

© 2014 WILEY-VCH Verlag GmbH & Co. KGaA, Weinheim

Logged in as:
Rebecca Yardley
Western University
Account #:
3001449083

[LOGOUT](#)

Order Completed

Thank you for your order.

This Agreement between Western University -- Rebecca Yardley ("You") and John Wiley and Sons ("John Wiley and Sons") consists of your license details and the terms and conditions provided by John Wiley and Sons and Copyright Clearance Center.

Your confirmation email will contain your order number for future reference.

[printable details](#)

License Number	4659041229548
License date	Aug 30, 2019
Licensed Content Publisher	John Wiley and Sons
Licensed Content Publication	Advanced Materials
Licensed Content Title	Triggered Transience of Metastable Poly(phthalaldehyde) for Transient Electronics
Licensed Content Author	Scott R. White, John A. Rogers, Jeffrey S. Moore, et al
Licensed Content Date	Oct 20, 2014
Licensed Content Volume	26
Licensed Content Issue	45
Licensed Content Pages	6
Type of use	Dissertation/Thesis
Requestor type	University/Academic
Format	Print and electronic
Portion	Figure/table
Number of figures/tables	1
Original Wiley figure/table number(s)	TOC
Will you be translating?	No
Title of your thesis / dissertation	Synthesis of Polycarbamate-Based Nanoassemblies and Previously Inaccessible Polyglyoxylates
Expected completion date	Sep 2019
Expected size (number of pages)	250
Requestor Location	Western University 1151 Richmond Street London, ON N6A 3K7 Canada Attn: Western University
Publisher Tax ID	EU826007151
Total	0.00 CAD

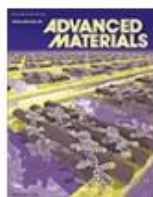
Would you like to purchase the full text of this article? If so, please continue on to the content ordering system located here: [Purchase PDF](#)

If you click on the buttons below or close this window, you will not be able to return to the content ordering system.

[ORDER MORE](#)
[CLOSE WINDOW](#)



RightsLink®

[Home](#)
[Account Info](#)
[Help](#)


Title: Thermally Triggered Degradation of Transient Electronic Devices
Author: Scott R. White, John A. Rogers, Jeffrey S. Moore, et al
Publication: Advanced Materials
Publisher: John Wiley and Sons
Date: May 20, 2015
 © 2015 WILEY-VCH Verlag GmbH & Co. KGaA, Weinheim

Logged in as:
 Rebecca Yardley
 Western University
 Account #:
 3001449083

[LOGOUT](#)

Order Completed

Thank you for your order.

This Agreement between Western University -- Rebecca Yardley ("You") and John Wiley and Sons ("John Wiley and Sons") consists of your license details and the terms and conditions provided by John Wiley and Sons and Copyright Clearance Center.

Your confirmation email will contain your order number for future reference.

[printable details](#)

License Number	4659060422291
License date	Aug 30, 2019
Licensed Content Publisher	John Wiley and Sons
Licensed Content Publication	Advanced Materials
Licensed Content Title	Thermally Triggered Degradation of Transient Electronic Devices
Licensed Content Author	Scott R. White, John A. Rogers, Jeffrey S. Moore, et al
Licensed Content Date	May 20, 2015
Licensed Content Volume	27
Licensed Content Issue	25
Licensed Content Pages	6
Type of use	Dissertation/Thesis
Requestor type	University/Academic
Format	Print and electronic
Portion	Figure/table
Number of figures/tables	1
Original Wiley figure/table number(s)	TOC
Will you be translating?	No
Title of your thesis / dissertation	Synthesis of Polycarbamate-Based Nanoassemblies and Previously Inaccessible Polyglyoxylates
Expected completion date	Sep 2019
Expected size (number of pages)	250
Requestor Location	Western University 1151 Richmond Street London, ON N6A 3K7 Canada Attn: Western University
Publisher Tax ID	EUB26007151
Total	0.00 CAD

Would you like to purchase the full text of this article? If so, please continue on to the content ordering system located here: [Purchase PDF](#)

If you click on the buttons below or close this window, you will not be able to return to the content ordering system.

[ORDER MORE](#)
[CLOSE WINDOW](#)



RightsLink®

Home

Account
Info

Help



ACS Publications
Most Trusted. Most Cited. Most Read.

Title: Fully Recyclable Metastable Polymers and Composites
Author: Evan M. Lloyd, Hector Lopez Hernandez, Adam M. Feinberg, et al

Publication: Chemistry of Materials
Publisher: American Chemical Society
Date: Jan 1, 2019

Copyright © 2019, American Chemical Society

Logged in as:
Rebecca Yardley
Western University
Account #: 3001449083

LOGOUT

PERMISSION/LICENSE IS GRANTED FOR YOUR ORDER AT NO CHARGE

This type of permission/license, instead of the standard Terms & Conditions, is sent to you because no fee is being charged for your order. Please note the following:

- Permission is granted for your request in both print and electronic formats, and translations.
- If figures and/or tables were requested, they may be adapted or used in part.
- Please print this page for your records and send a copy of it to your publisher/graduate school.
- Appropriate credit for the requested material should be given as follows: "Reprinted (adapted) with permission from (COMPLETE REFERENCE CITATION). Copyright (YEAR) American Chemical Society." Insert appropriate information in place of the capitalized words.
- One-time permission is granted only for the use specified in your request. No additional uses are granted (such as derivative works or other editions). For any other uses, please submit a new request.

If credit is given to another source for the material you requested, permission must be obtained from that source.

BACK

CLOSE WINDOW

Copyright © 2019 Copyright Clearance Center, Inc. All Rights Reserved. [Privacy statement](#). [Terms and Conditions](#).
Comments? We would like to hear from you. E-mail us at customercare@copyright.com



RightsLink®

Home

Account
Info

Help



Title: Self-Immolative Poly(4,5-dichlorophthalaldehyde) and its Applications in Multi-Stimuli-Responsive Macroscopic Plastics

Author: Scott T. Phillips, Gregory G. Lewis, Anthony M. DiLauro

Publication: Angewandte Chemie International Edition

Publisher: John Wiley and Sons

Date: Mar 30, 2015

© 2015 WILEY-VCH Verlag GmbH & Co. KGaA, Weinheim

Logged in as:

Rebecca Yardley
Western UniversityAccount #:
3001449083

LOGOUT

Order Completed

Thank you for your order.

This Agreement between Western University -- Rebecca Yardley ("You") and John Wiley and Sons ("John Wiley and Sons") consists of your license details and the terms and conditions provided by John Wiley and Sons and Copyright Clearance Center.

Your confirmation email will contain your order number for future reference.

[printable details](#)

License Number	4659070601384
License date	Aug 30, 2019
Licensed Content Publisher	John Wiley and Sons
Licensed Content Publication	Angewandte Chemie International Edition
Licensed Content Title	Self-Immolative Poly(4,5-dichlorophthalaldehyde) and its Applications in Multi-Stimuli-Responsive Macroscopic Plastics
Licensed Content Author	Scott T. Phillips, Gregory G. Lewis, Anthony M. DiLauro
Licensed Content Date	Mar 30, 2015
Licensed Content Volume	54
Licensed Content Issue	21
Licensed Content Pages	6
Type of use	Dissertation/Thesis
Requestor type	University/Academic
Format	Print and electronic
Portion	Figure/table
Number of figures/tables	1
Original Wiley figure/table number(s)	Figure 3
Will you be translating?	No
Title of your thesis / dissertation	Synthesis of Polycarbonate-Based Nanoassemblies and Previously Inaccessible Polyglyoxylates
Expected completion date	Sep 2019
Expected size (number of pages)	250
Requestor Location	Western University 1151 Richmond Street London, ON N6A 3K7 Canada Attn: Western University
Publisher Tax ID	EU826007151
Total	0.00 CAD



RightsLink®

[Home](#)
[Account Info](#)
[Help](#)


Title: Probe-Based 3-D Nanolithography Using Self-Amplified Depolymerization Polymers

Author: Urs Duerig, Jane Frommer, James L. Hedrick, et al

Publication: Advanced Materials

Publisher: John Wiley and Sons

Date: Aug 4, 2010

Copyright © 2010 WILEY-VCH Verlag GmbH & Co. KGaA, Weinheim

Logged in as:
Rebecca Yardley
Western University
Account #:
3001449083

[LOGOUT](#)

Order Completed

Thank you for your order.

This Agreement between Western University -- Rebecca Yardley ("You") and John Wiley and Sons ("John Wiley and Sons") consists of your license details and the terms and conditions provided by John Wiley and Sons and Copyright Clearance Center.

Your confirmation email will contain your order number for future reference.

[printable details](#)

License Number	4659050297699
License date	Aug 30, 2019
Licensed Content Publisher	John Wiley and Sons
Licensed Content Publication	Advanced Materials
Licensed Content Title	Probe-Based 3-D Nanolithography Using Self-Amplified Depolymerization Polymers
Licensed Content Author	Urs Duerig, Jane Frommer, James L. Hedrick, et al
Licensed Content Date	Aug 4, 2010
Licensed Content Volume	22
Licensed Content Issue	31
Licensed Content Pages	5
Type of use	Dissertation/Thesis
Requestor type	University/Academic
Format	Print and electronic
Portion	Figure/table
Number of figures/tables	1
Original Wiley figure/table number(s)	Figure 2C
Will you be translating?	No
Title of your thesis / dissertation	Synthesis of Polycarbonate-Based Nanoassemblies and Previously Inaccessible Polyglyoxylates
Expected completion date	Sep 2019
Expected size (number of pages)	250
Requestor Location	Western University 1151 Richmond Street London, ON N6A 3K7 Canada Attn: Western University
Publisher Tax ID	EU826007151
Total	0.00 CAD

Would you like to purchase the full text of this article? If so, please continue on to the content ordering system located here: [Purchase PDF](#)

If you click on the buttons below or close this window, you will not be able to return to the content ordering system.

**Royal Society of Chemistry LICENSE
TERMS AND CONDITIONS**

Aug 30, 2019

This is a License Agreement between Western University -- Rebecca Yardley ("You") and CCC Republication ("CCC Republication") provided by Copyright Clearance Center ("CCC"). The license consists of your order details, the terms and conditions provided by CCC Republication, and the payment terms and conditions.

All payments must be made in full to CCC. For payment instructions, please see information listed at the bottom of this form.

License Number	4659070870276
License date	Aug 30, 2019
Licensed content publisher	CCC Republication
Licensed content title	Chemical communications
Licensed content date	Jan 1, 1996
Type of Use	Thesis/Dissertation
Requestor type	Academic institution
Format	Print, Electronic
Portion	image/photo
Number of images/photos requested	1
The requesting person/organization is:	Rebecca Yardley
Title or numeric reference of the portion(s)	Figure 3
Title of the article or chapter the portion is from	Thermo-responsive self-immolative nanoassemblies: direct and indirect triggering
Editor of portion(s)	N/A
Author of portion(s)	N/A
Volume of serial or monograph.	N/A
Page range of the portion	12070
Publication date of portion	01 September 2019
Rights for	Main product
Duration of use	Life of current edition
Creation of copies for the disabled	no
With minor editing privileges	no
For distribution to	Worldwide
In the following language(s)	Original language of publication
With incidental promotional use	no
The lifetime unit quantity of new product	More than 2,000,000
Title	Synthesis of Polycarbamate-Based Nanoassemblies and Previously Inaccessible Polyglyoxylates
Institution name	n/a
Expected presentation date	Sep 2019
Total (may include CCC user fee)	0.00 USD
Terms and Conditions	

**Royal Society of Chemistry LICENSE
TERMS AND CONDITIONS**

Aug 30, 2019

This is a License Agreement between Western University -- Rebecca Yardley ("You") and Royal Society of Chemistry ("Royal Society of Chemistry") provided by Copyright Clearance Center ("CCC"). The license consists of your order details, the terms and conditions provided by Royal Society of Chemistry, and the payment terms and conditions.

All payments must be made in full to CCC. For payment instructions, please see information listed at the bottom of this form.

License Number	4659040908408
License date	Aug 30, 2019
Licensed content publisher	Royal Society of Chemistry
Licensed content title	Chemical communications
Licensed content date	Jan 1, 1996
Type of Use	Thesis/Dissertation
Requestor type	Academic institution
Format	Print, Electronic
Portion	image/photo
Number of images/photos requested	1
The requesting person/organization is:	Rebecca Yardley
Title or numeric reference of the portion(s)	Fig. 3 Schematic representation of the inter-micellar and intra-micellar cross-linking for (a) AB diblock copolymer and (b) ABC triblock copolymer micelles at high copolymer concentrations (.1% solids)
Title of the article or chapter the portion is from	N/A
Editor of portion(s)	N/A
Author of portion(s)	N/A
Volume of serial or monograph.	N/A
Page range of the portion	3022
Publication date of portion	01 September 2019
Rights for	Main product
Duration of use	Life of current edition
Creation of copies for the disabled	no
With minor editing privileges	no
For distribution to	Worldwide
In the following language(s)	Original language of publication
With incidental promotional use	no
The lifetime unit quantity of new product	More than 2,000,000
Title	Synthesis of Polycarbamate-Based Nanoassemblies and Previously Inaccessible Polyglyoxylates
Institution name	n/a
Expected presentation date	Sep 2019
Total (may include CCC user fee)	0.00 USD
Terms and Conditions	

TERMS AND CONDITIONS

The following terms are individual to this publisher:

None

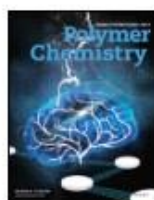


RightsLink®

Home

Account
Info

Help



Title: Multi-stimuli-responsive self-immolative polymer assemblies
Author: Elizabeth R. Gillies, Rebecca E. Yardley
Publication: Journal of Polymer Science Part A: Polymer Chemistry
Publisher: John Wiley and Sons
Date: Aug 24, 2018
 © 2018 Wiley Periodicals, Inc.

Logged in as:
 Rebecca Yardley
 Western University
 Account #:
 3001449083

[LOGOUT](#)

Order Completed

Thank you for your order.

This Agreement between Western University -- Rebecca Yardley ("You") and John Wiley and Sons ("John Wiley and Sons") consists of your license details and the terms and conditions provided by John Wiley and Sons and Copyright Clearance Center.

Your confirmation email will contain your order number for future reference.

[printable details](#)

License Number	4659040166479
License date	Aug 30, 2019
Licensed Content Publisher	John Wiley and Sons
Licensed Content Publication	Journal of Polymer Science Part A: Polymer Chemistry
Licensed Content Title	Multi-stimuli-responsive self-immolative polymer assemblies
Licensed Content Author	Elizabeth R. Gillies, Rebecca E. Yardley
Licensed Content Date	Aug 24, 2018
Licensed Content Volume	56
Licensed Content Issue	16
Licensed Content Pages	11
Type of use	Dissertation/Thesis
Requestor type	Author of this Wiley article
Format	Print and electronic
Portion	Full article
Will you be translating?	No
Title of your thesis / dissertation	Synthesis of Polycarbamate-Based Nanoassemblies and Previously Inaccessible Polyglyoxylates
Expected completion date	Sep 2019
Expected size (number of pages)	250
Requestor Location	Western University 1151 Richmond Street London, ON N6A 3K7 Canada Attn: Western University
Publisher Tax ID	EU826007151
Total	0.00 CAD

Would you like to purchase the full text of this article? If so, please continue on to the content ordering system located here: [Purchase PDF](#)

If you click on the buttons below or close this window, you will not be able to return to the content ordering system.

[ORDER MORE](#)
[CLOSE WINDOW](#)

Copyright © 2019 Copyright Clearance Center, Inc. All Rights Reserved. [Privacy statement](#). [Terms and Conditions](#).
 Comments? We would like to hear from you. E-mail us at customer@copyright.com



RightsLink®

Home

Account
Info

Help



ACS Publications
Most Trusted. Most Cited. Most Read.

Title: Triggering Depolymerization: Progress and Opportunities for Self-Immolative Polymers
Author: Rebecca E. Yardley, Amir Rabiee Kenaree, Elizabeth R. Gillies
Publication: Macromolecules
Publisher: American Chemical Society
Date: Aug 1, 2019

Logged in as:
Rebecca Yardley
Western University
Account #:
3001449083

LOGOUT

Copyright © 2019, American Chemical Society

PERMISSION/LICENSE IS GRANTED FOR YOUR ORDER AT NO CHARGE

This type of permission/license, instead of the standard Terms & Conditions, is sent to you because no fee is being charged for your order. Please note the following:

- Permission is granted for your request in both print and electronic formats, and translations.
- If figures and/or tables were requested, they may be adapted or used in part.
- Please print this page for your records and send a copy of it to your publisher/graduate school.
- Appropriate credit for the requested material should be given as follows: "Reprinted (adapted) with permission from (COMPLETE REFERENCE CITATION). Copyright (YEAR) American Chemical Society." Insert appropriate information in place of the capitalized words.
- One-time permission is granted only for the use specified in your request. No additional uses are granted (such as derivative works or other editions). For any other uses, please submit a new request.

BACK

CLOSE WINDOW

Copyright © 2019 Copyright Clearance Center, Inc. All Rights Reserved. [Privacy statement](#). [Terms and Conditions](#).
Comments? We would like to hear from you. E-mail us at customer@copyright.com

Appendix 2 – Supporting information for Chapter 2

NMR Spectra

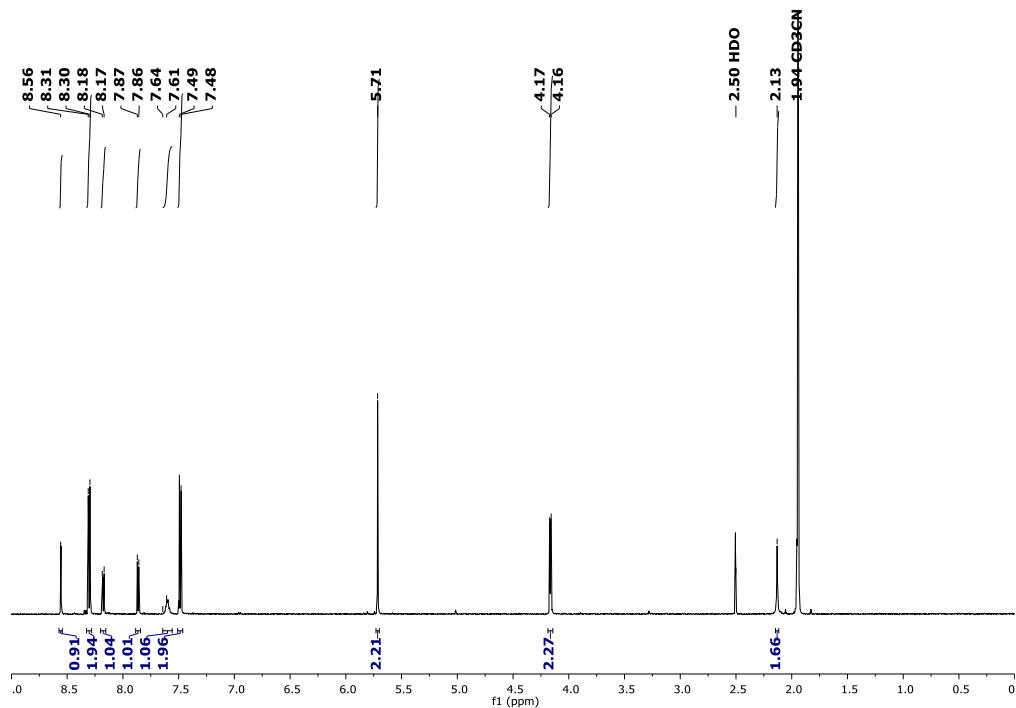


Figure A2.1: ^1H NMR spectrum of compound **2.2** (600 MHz, CD_3CN).

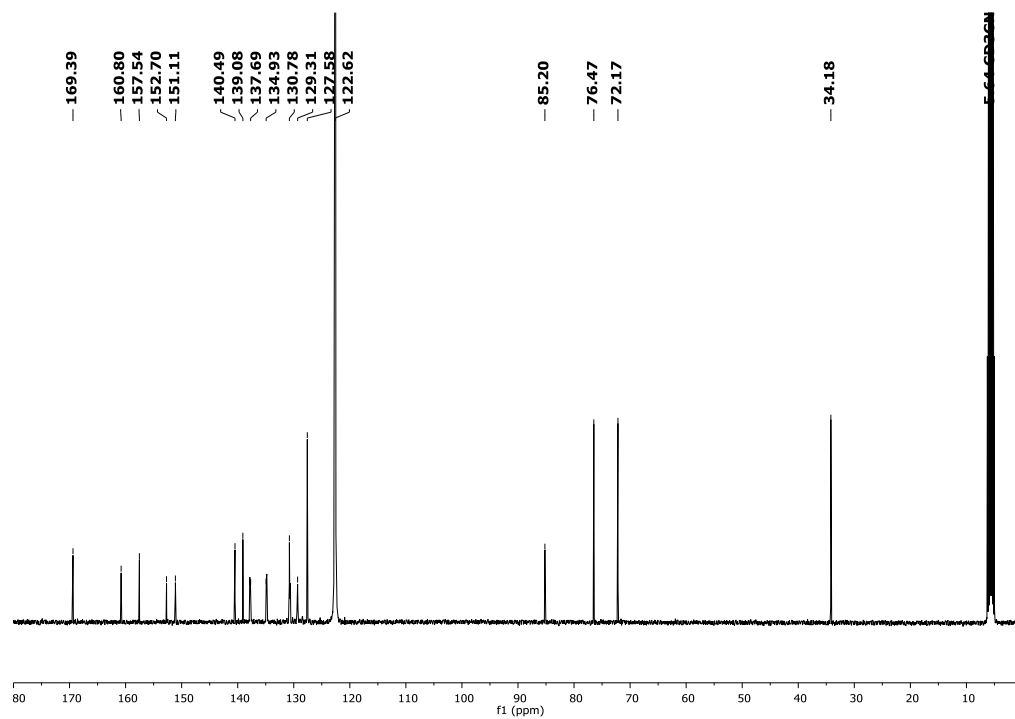


Figure A2.2: ^{13}C NMR spectrum of compound **2.2** (150 MHz, CD_3CN).

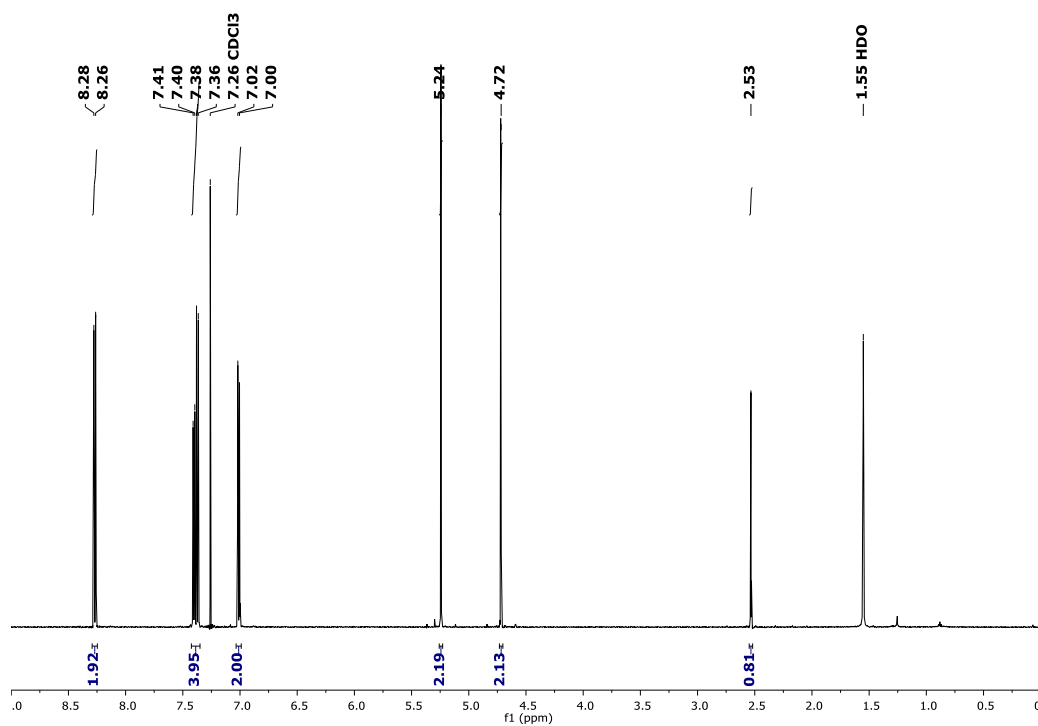


Figure A2.3: ^1H NMR spectrum of compound **2.4** (600 MHz, CDCl_3).

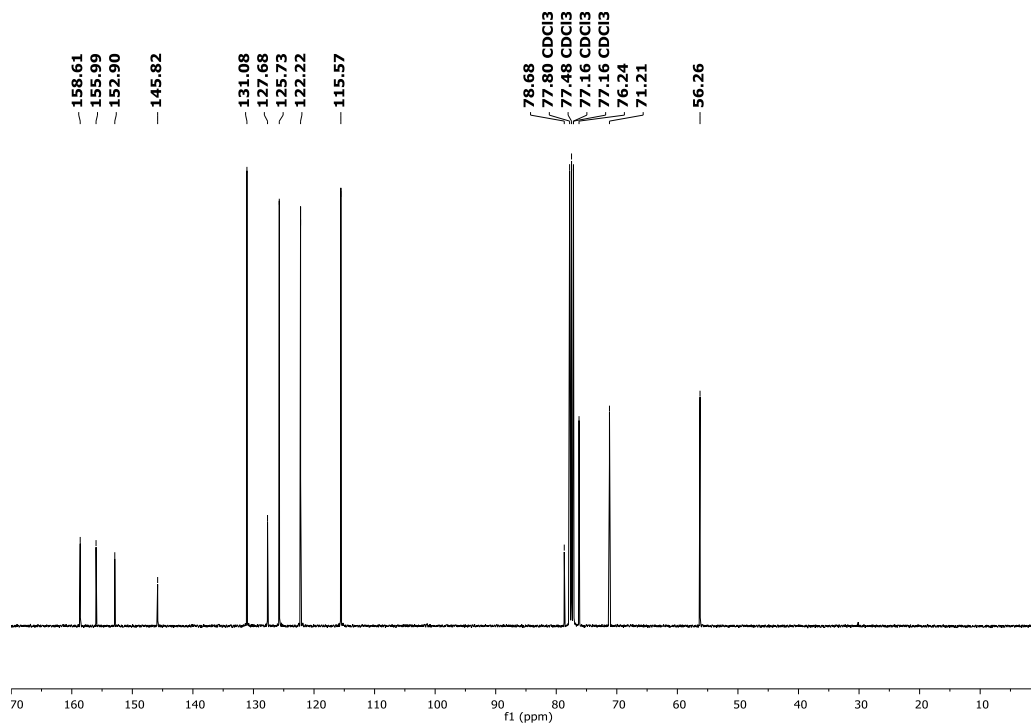


Figure A2.4: ¹³C NMR spectrum of compound **2.4** (600 MHz, CDCl₃).

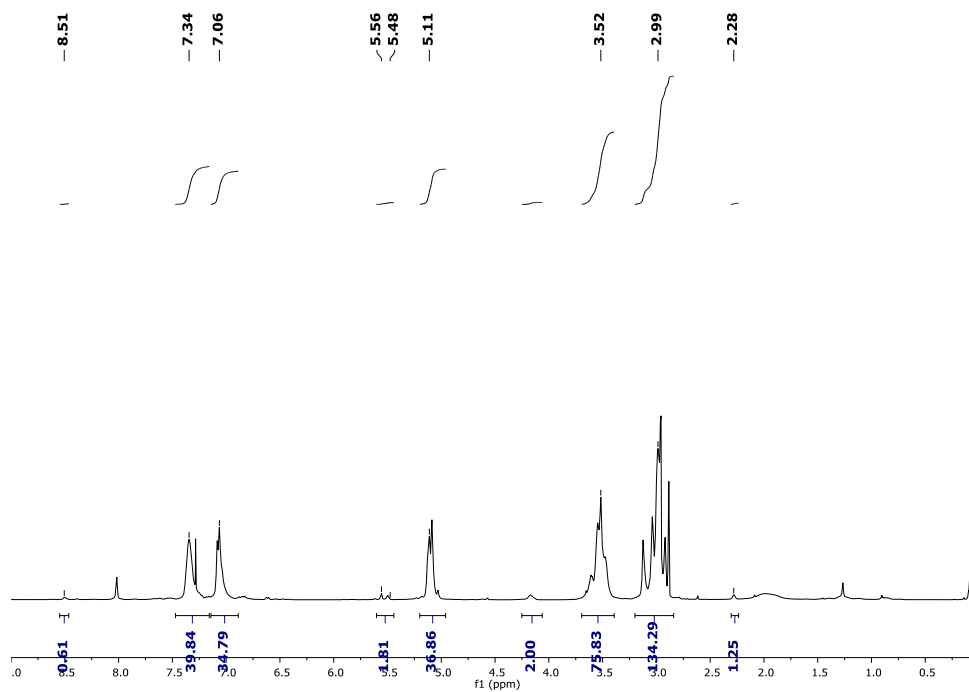


Figure A2.5: ¹H NMR spectrum of **PCB_{UV}** (600 MHz, CDCl₃).

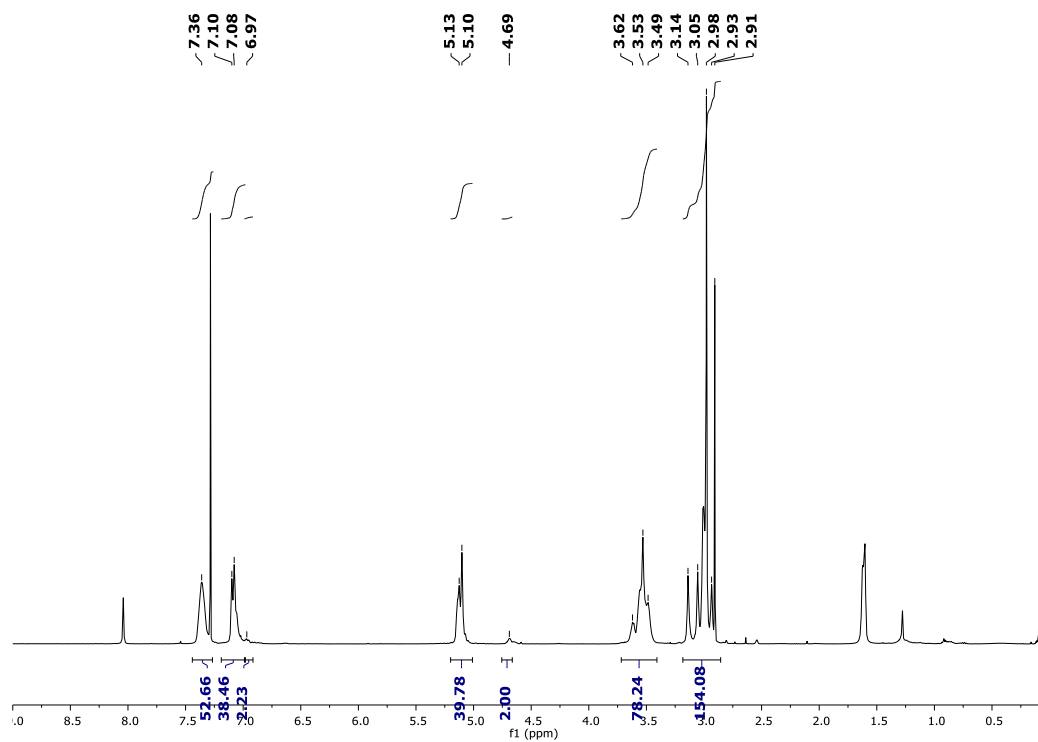


Figure A2.6: ^1H NMR spectrum of **PCB_{CON}** (600 MHz, CDCl_3).

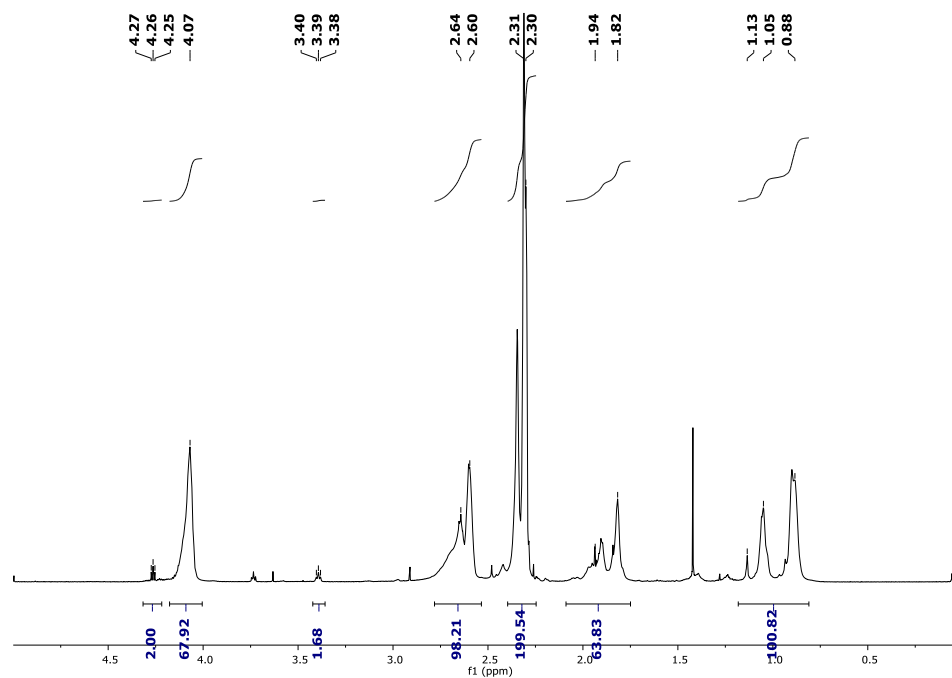


Figure A2.7: ^1H NMR spectrum of **PDMAEMA-N₃** (600 MHz, CDCl_3).

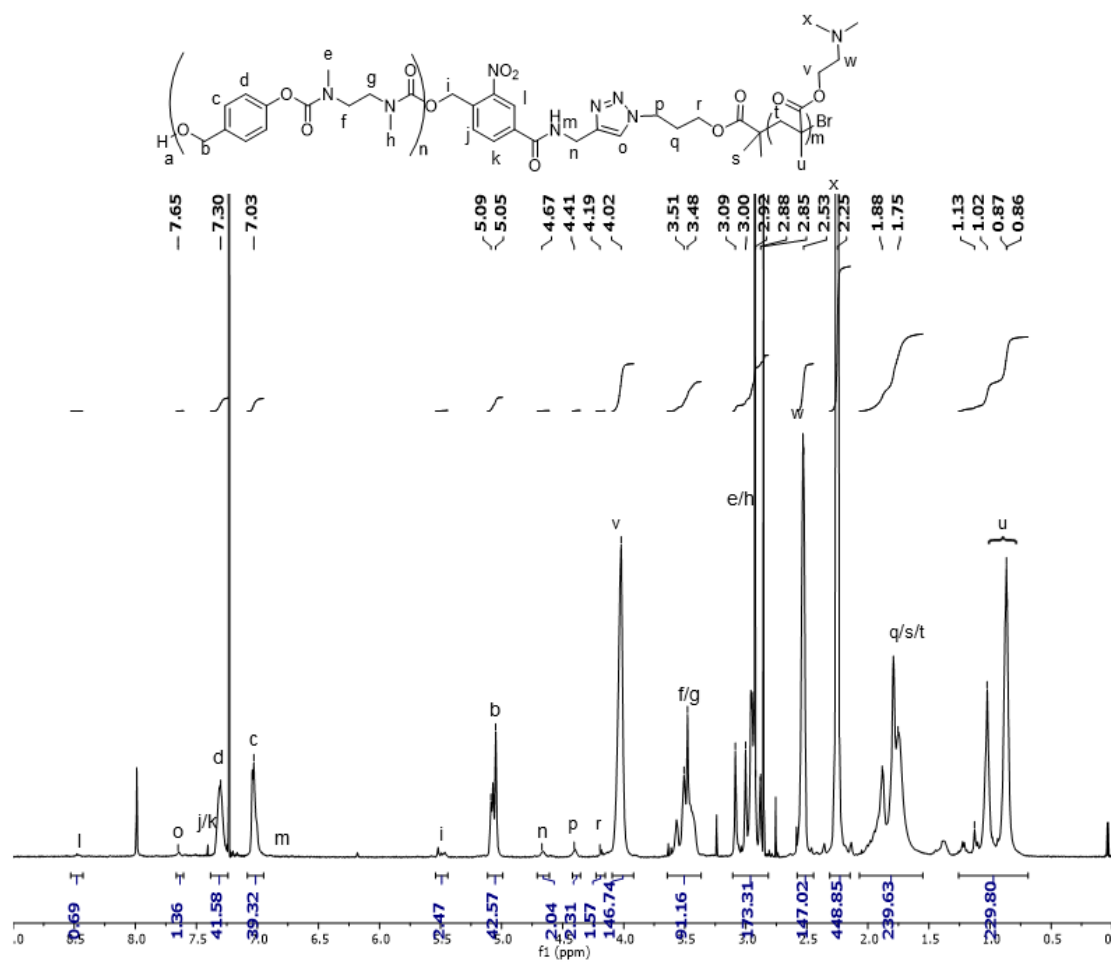


Figure A2.8: ^1H NMR spectrum of PCB_{UV}-PDMAEMA (600 MHz, CDCl_3).

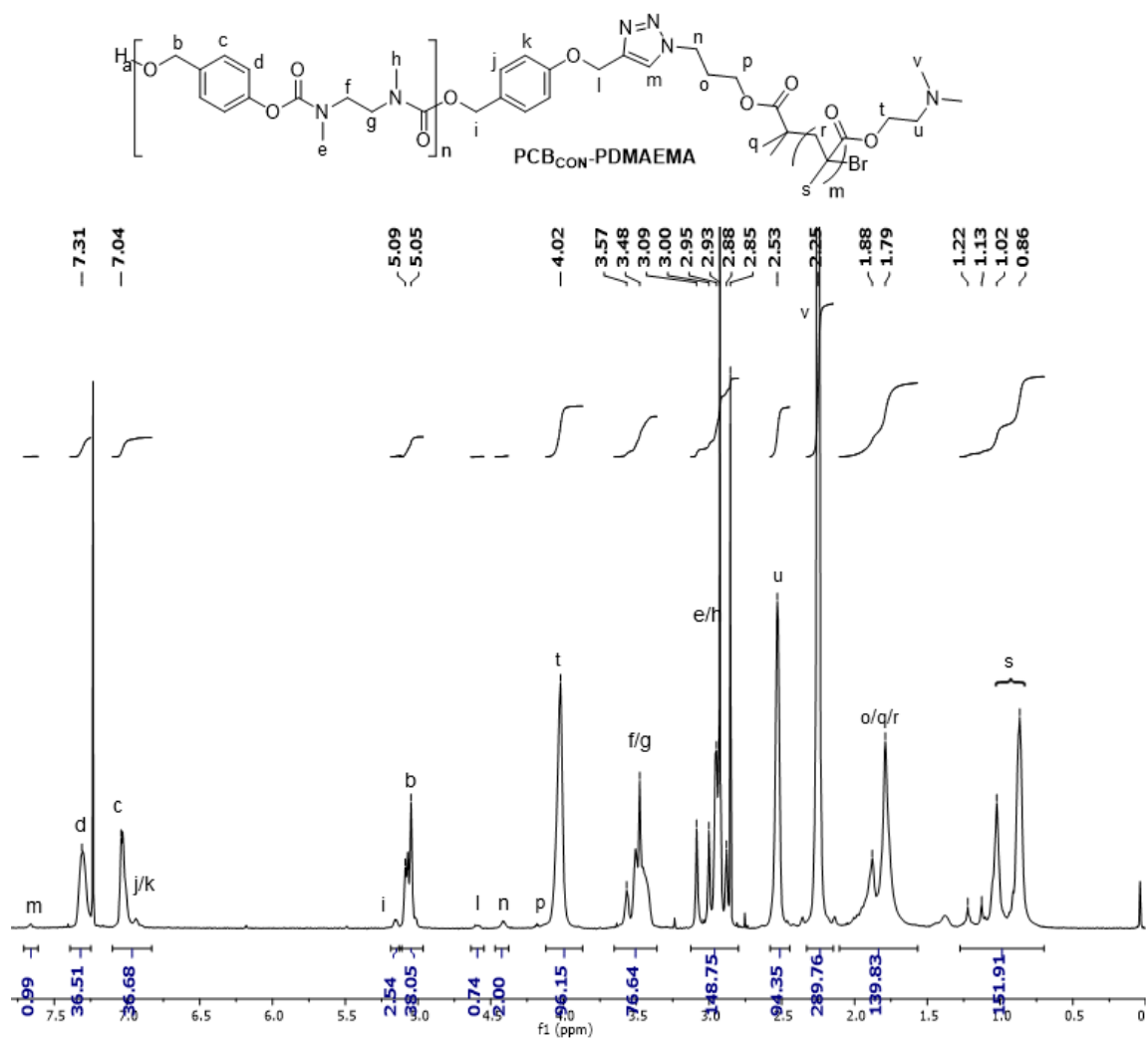
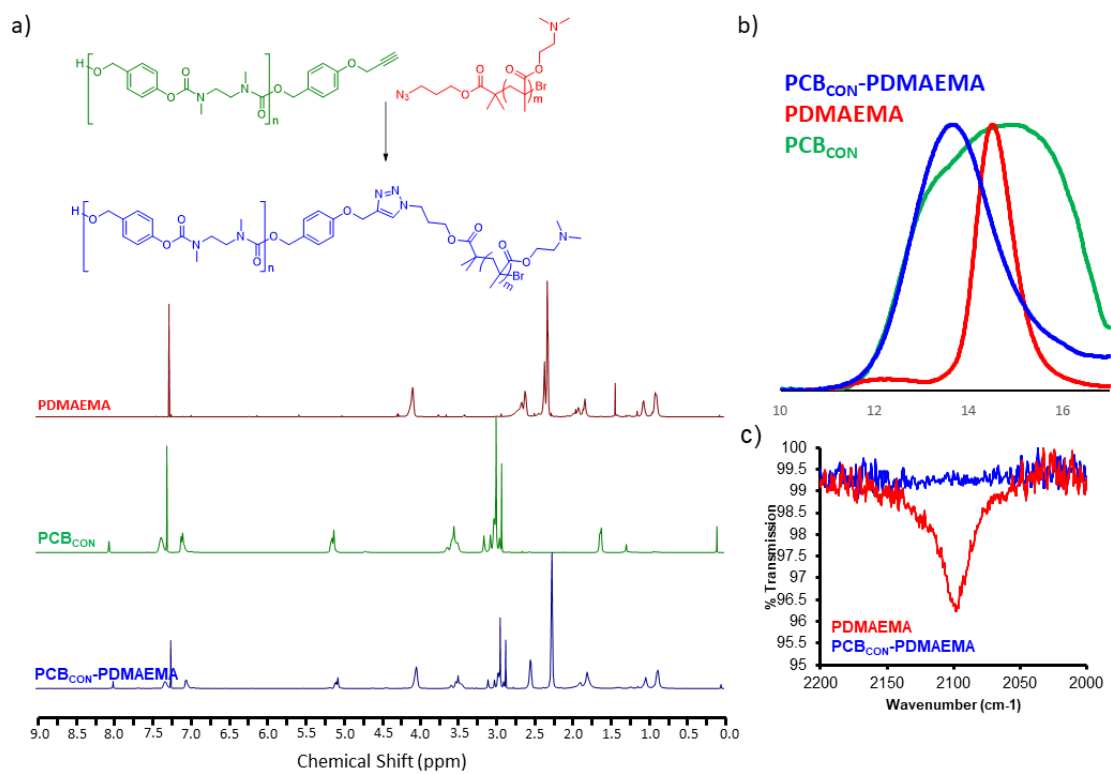


Figure A2.9: ^1H NMR spectrum of $\text{PCB}_{\text{CON}}\text{-PDMAEMA}$ (600 MHz, CDCl_3).



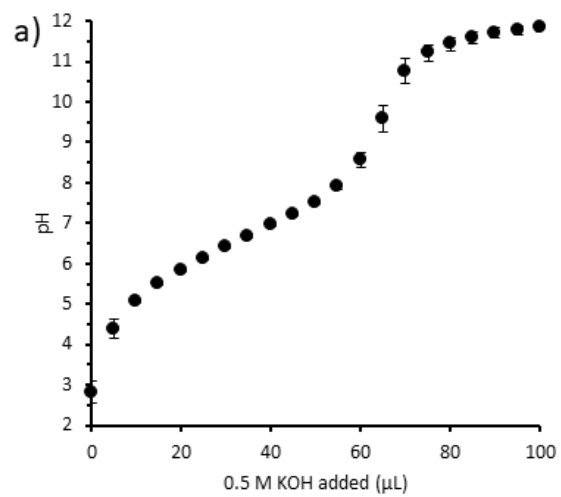


Figure A2.11: pK_a determination of PDMAEMA. The pK_a was determined as the pH at high end of the equivalence point.

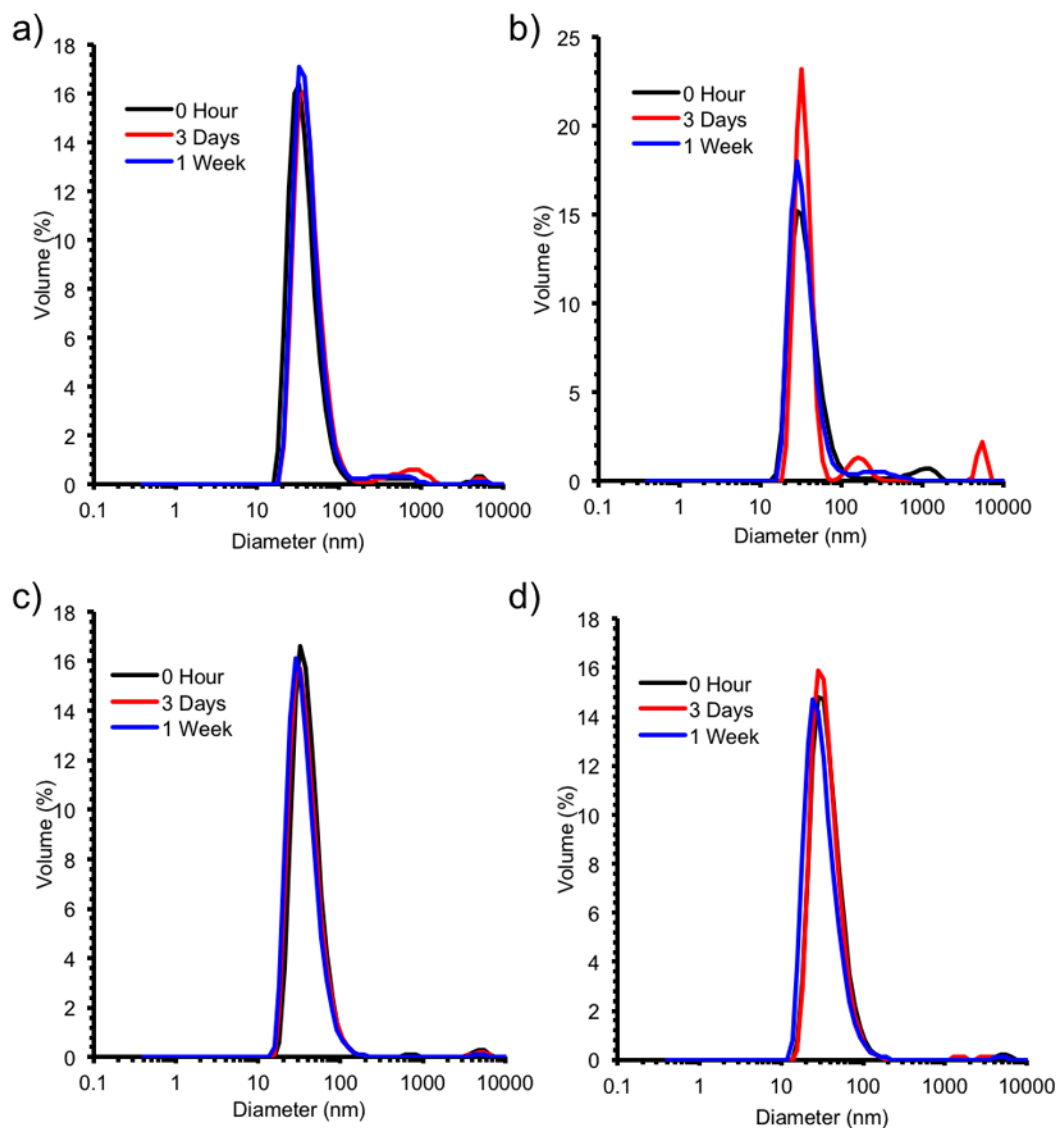


Figure A2.12: Representative Dynamic Light Scattering (DLS) volume traces of a) **PCB_{UV}-PDMAEMA** in 100 mM, pH 7.0 phosphate buffer incubated at 20 °C; b) **PCB_{UV}-PDMAEMA** in 100 mM, pH 7.0 phosphate buffer incubated at 65 °C; c) **PCB_{CON}-PDMAEMA** in 100 mM, pH 7.0 phosphate buffer incubated at 20 °C; d) **PCB_{CON}-PDMAEMA** in 100 mM, pH 7.0 phosphate buffer incubated at 65 °C.

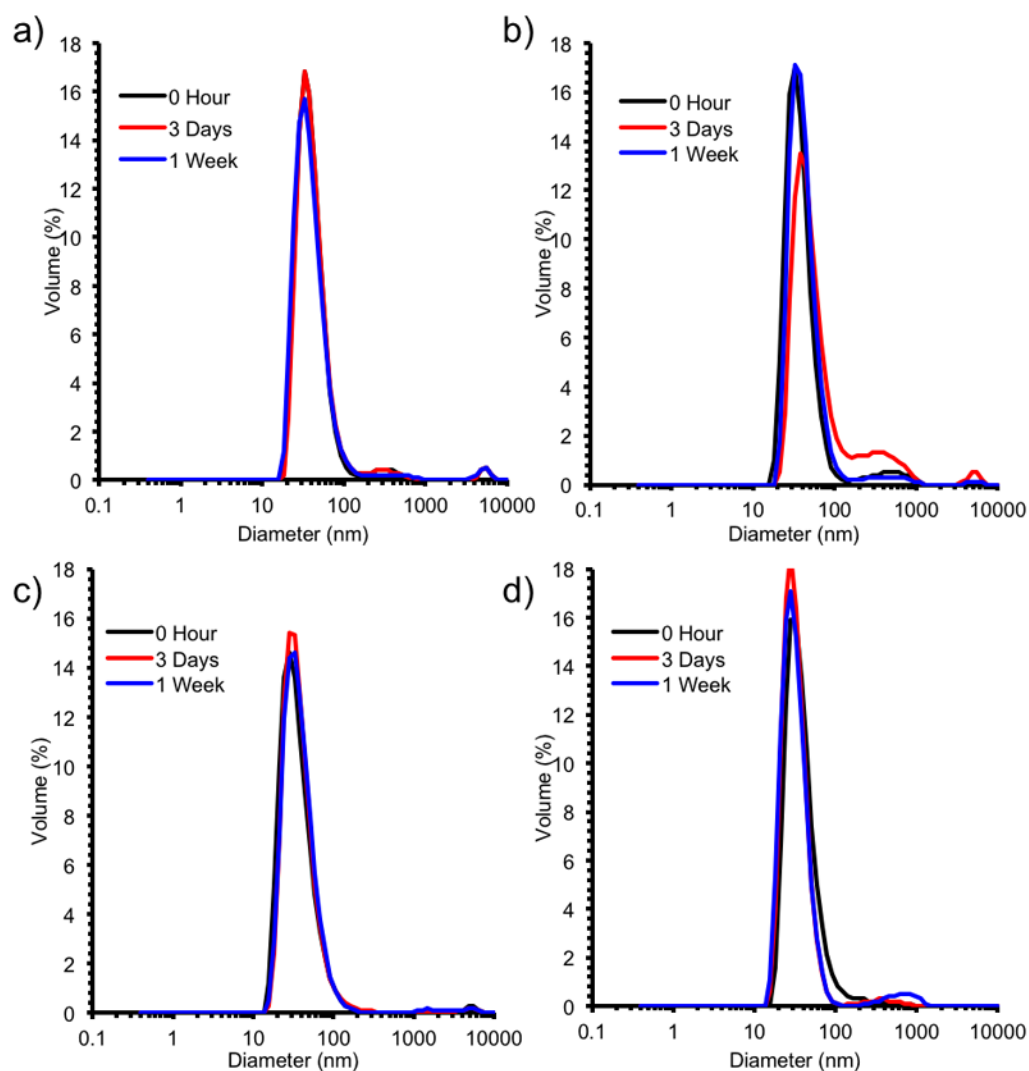


Figure A2.13: Representative Dynamic Light Scattering (DLS) volume traces of a) PCB_{UV}-PDMAEMA in 100 mM, pH 8.0 phosphate buffer incubated at 20 °C; b) PCB_{UV}-PDMAEMA in 100 mM, pH 8.0 phosphate buffer incubated at 65 °C; c) PCB_{CON}-PDMAEMA in 100 mM, pH 8.0 phosphate buffer incubated at 20 °C; d) PCB_{CON}-PDMAEMA in 100 mM, pH 8.0 phosphate buffer incubated at 65 °C.

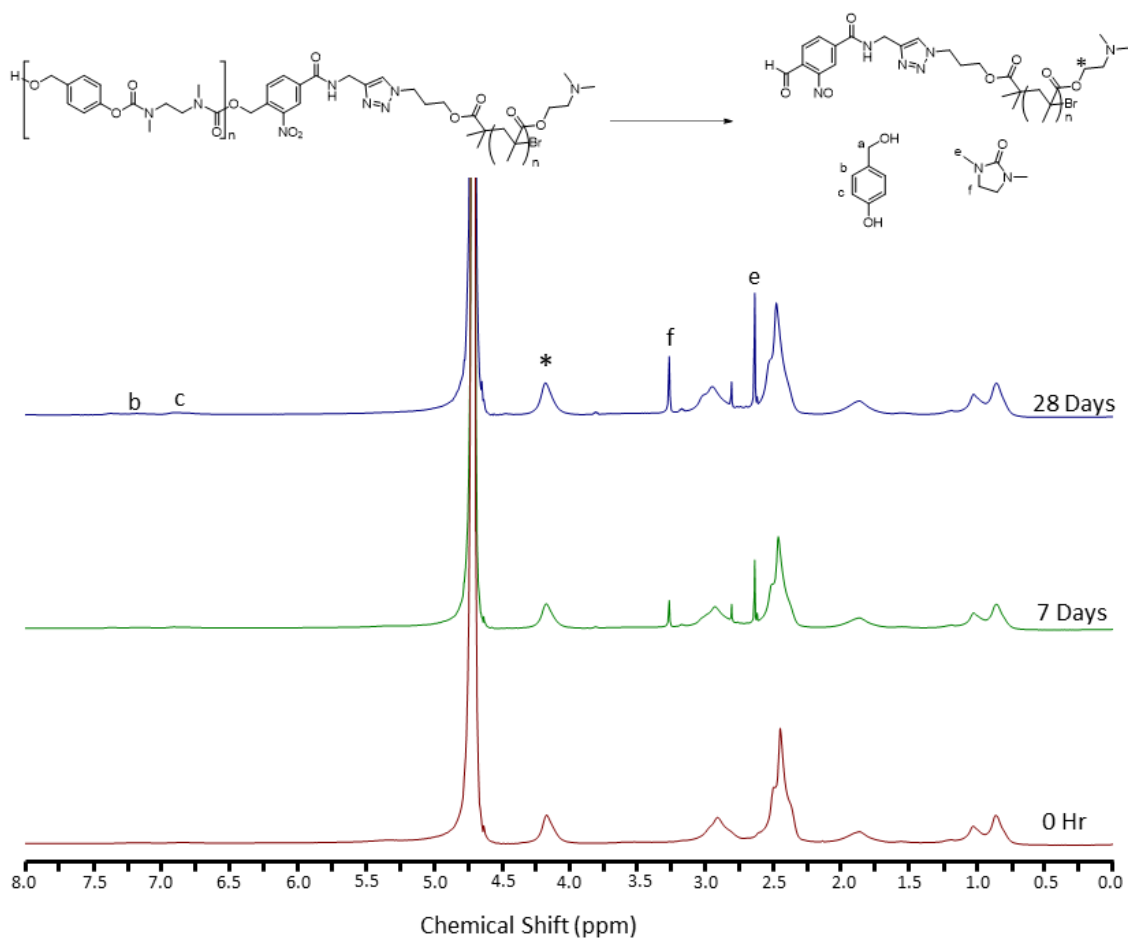


Figure A2.14: Representative ^1H NMR spectra (400 MHz) of **PCB_{UV}-PDMAEMA** and its depolymerization products following incubation in 100 mM, pH 8.0 phosphate buffered D_2O at 20 °C for varying time periods. The peak labeled **f** was used to quantify the extent of depolymerization based on its integration relative to that of the distinct peak at 4.17 ppm (*****) from the PDMAEMA.

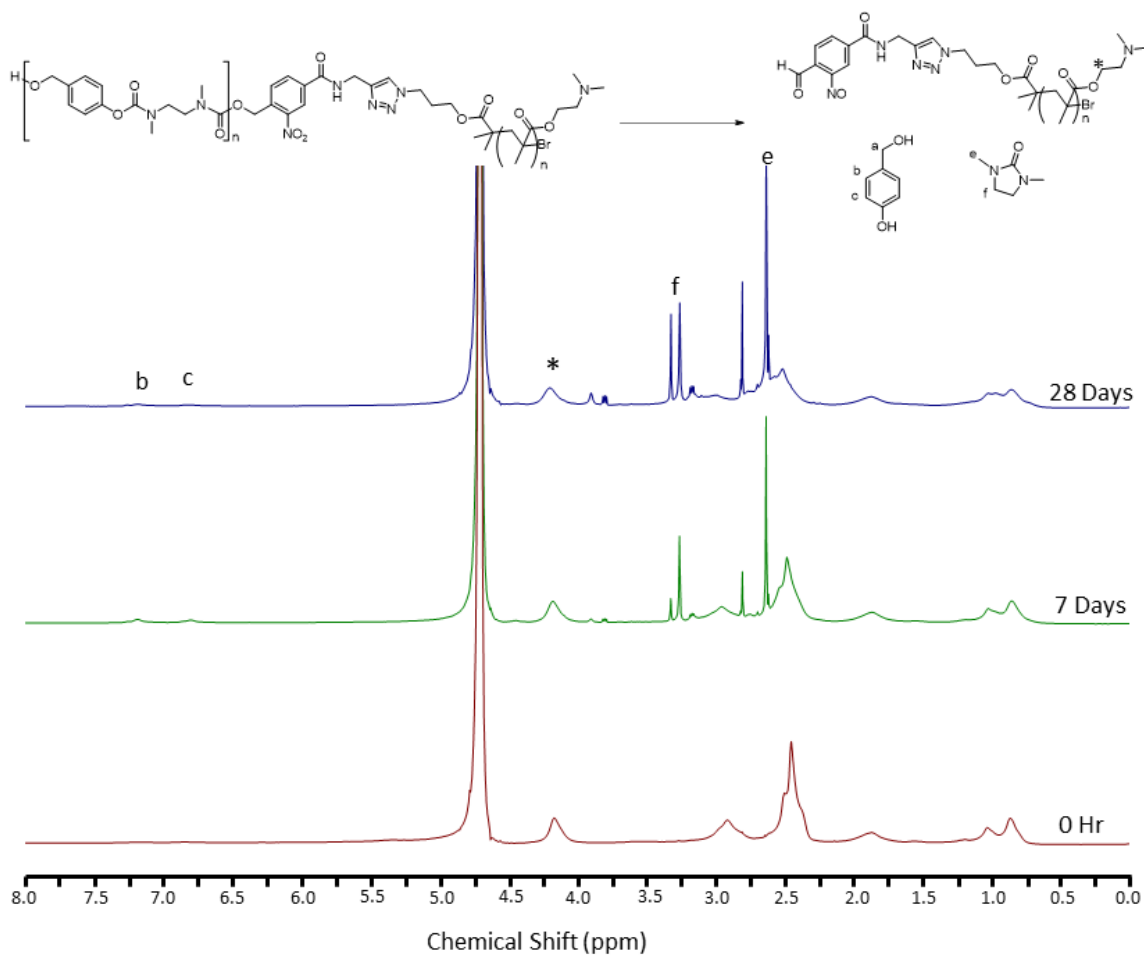


Figure A2.15: Representative ^1H NMR spectra (400 MHz) of **PCB_{UV}-PDMAEMA** and its depolymerization products following incubation in 100 mM, pH 8.0 phosphate buffered D_2O at 65 °C for varying time periods. The peak labeled f was used to quantify the extent of depolymerization based on its integration relative to that of the distinct peak at 4.17 ppm (*) from the PDMAEMA.

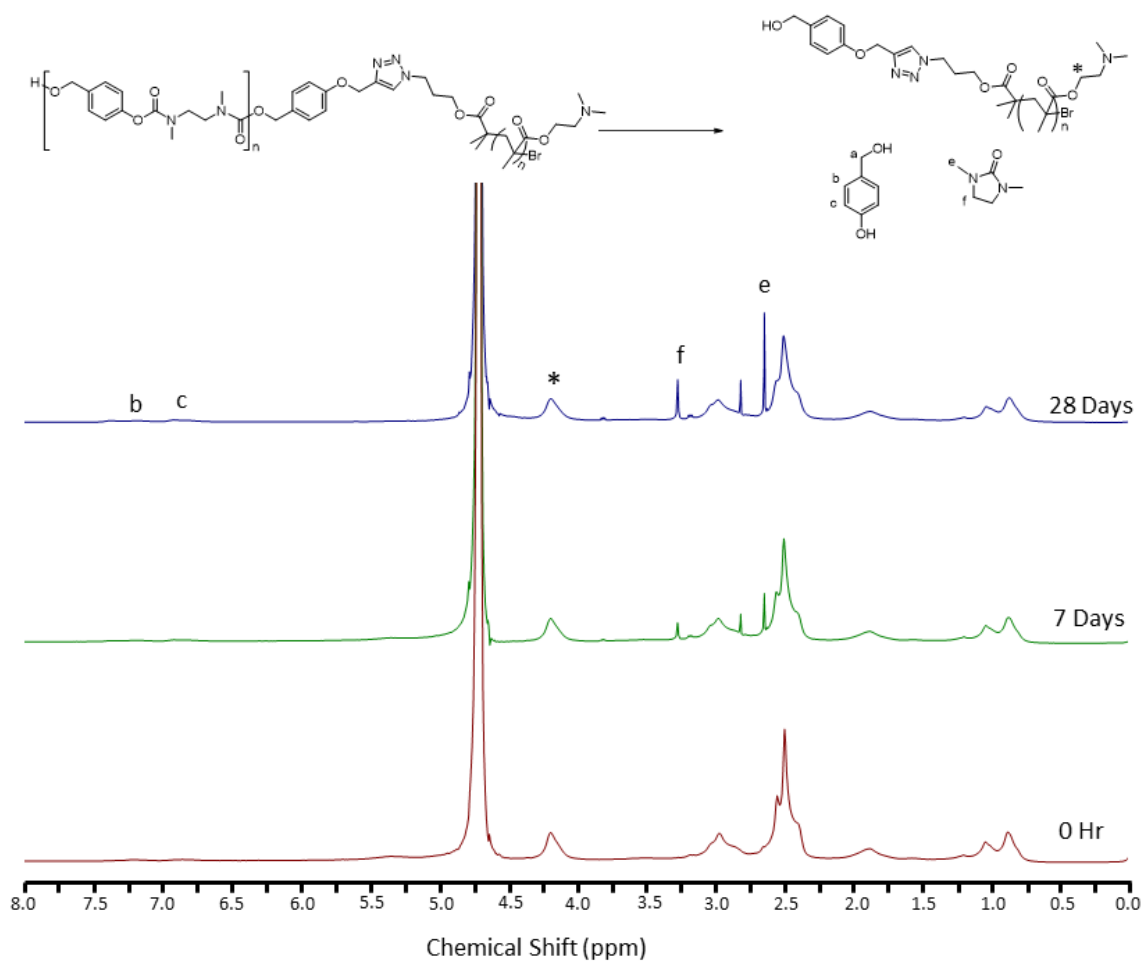


Figure A2.16: Representative ^1H NMR spectra (400 MHz) of $\text{PCB}_{\text{CON}}\text{-PDMAEMA}$ and its depolymerization products following incubation in 100 mM, pH 8.0 phosphate buffered D_2O at 20 $^\circ\text{C}$ for varying time periods. The peak labeled f was used to quantify the extent of depolymerization based on its integration relative to that of the distinct peak at 4.17 ppm (*) from the PDMAEMA.

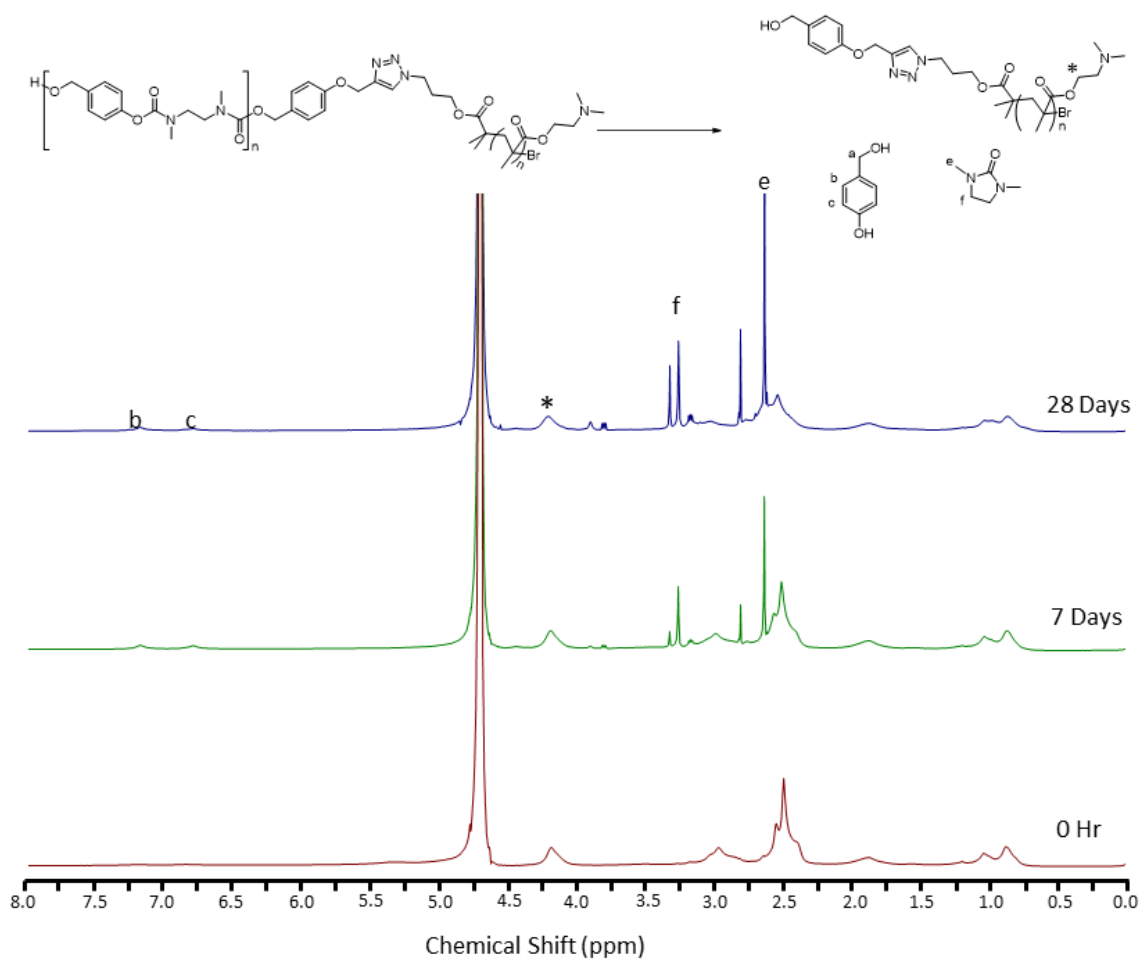


Figure A2.17: Representative ^1H NMR spectra (400 MHz) of **PCB_{CON}-PDMAEMA** and its depolymerization products following incubation in 100 mM, pH 8.0 phosphate buffered D_2O at 65 °C for varying time periods. The peak labeled f was used to quantify the extent of depolymerization based on its integration relative to that of the distinct peak at 4.17 ppm (*) from the PDMAEMA.

Appendix 3 – Supporting Information for Chapter 3

NMR Spectra

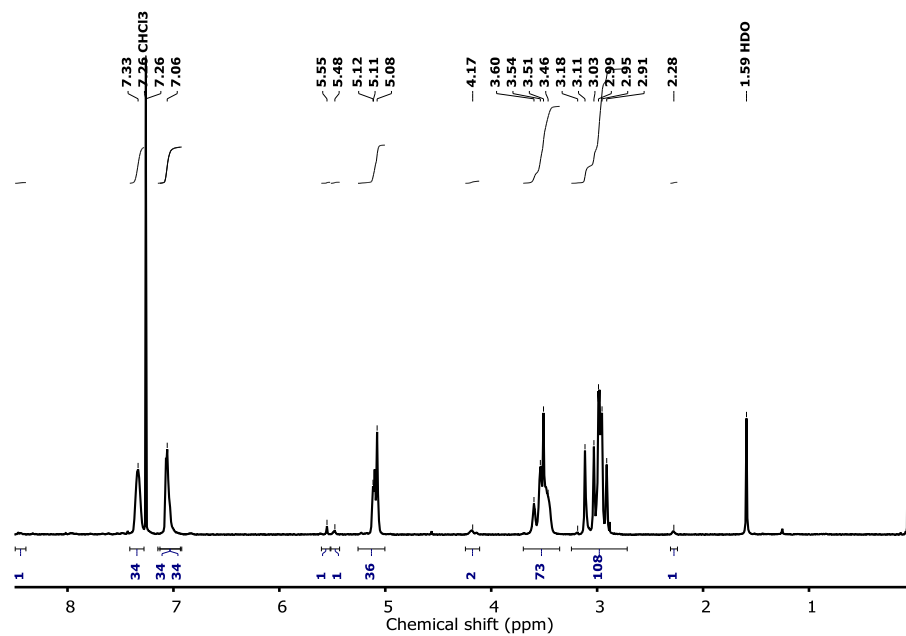


Figure A3.1: ^1H NMR spectrum of PCB_{UV} (CDCl_3 , 600 MHz). Asterisks denote residual solvent signals.

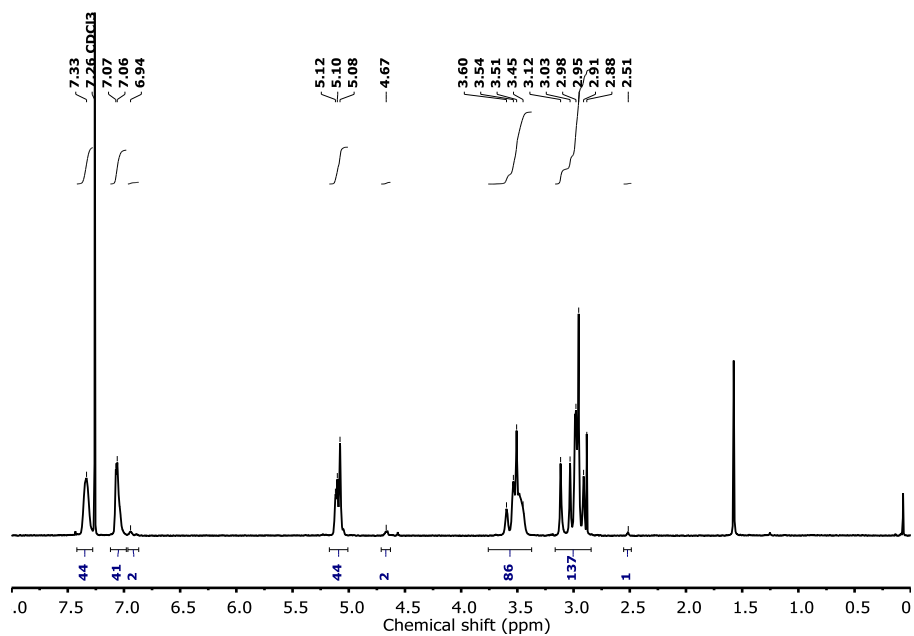


Figure A3.2: ^1H NMR spectrum of **PCB_{CON}** (CDCl_3 , 600 MHz). Asterisks denote residual solvent signals.

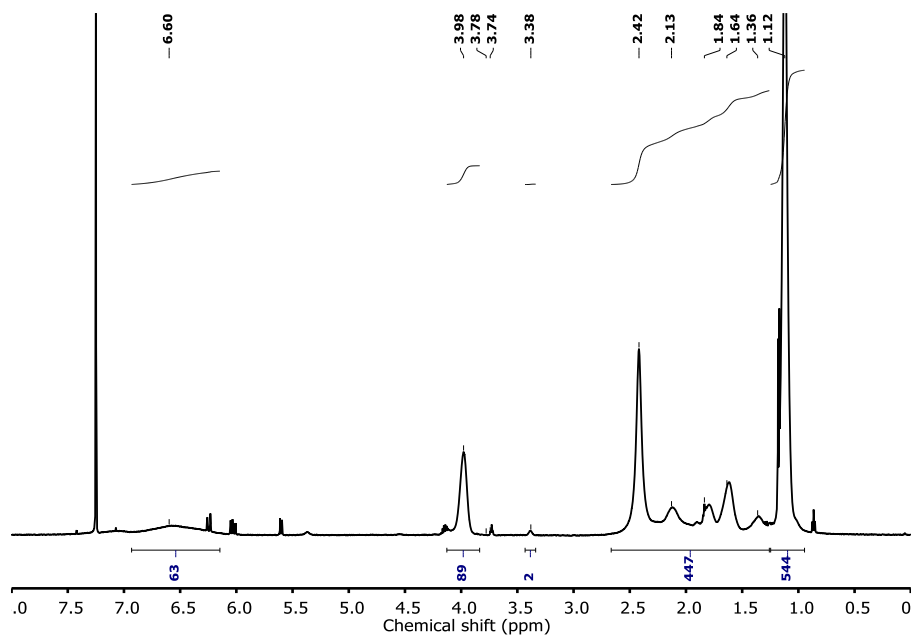


Figure A3.3: ^1H NMR spectrum of **PNIPAAm- N_3** (CDCl_3 , 600 MHz). Asterisks denote residual solvent signals.

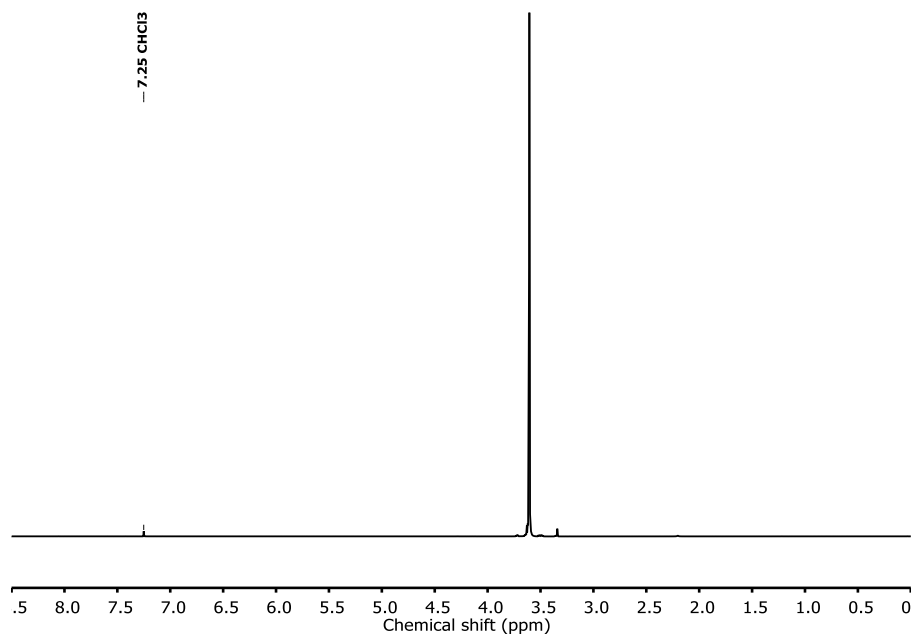


Figure A3.4: ^1H NMR spectrum of **PEG-N₃** (CDCl_3 , 600 MHz). Asterisks denote residual solvent signals.

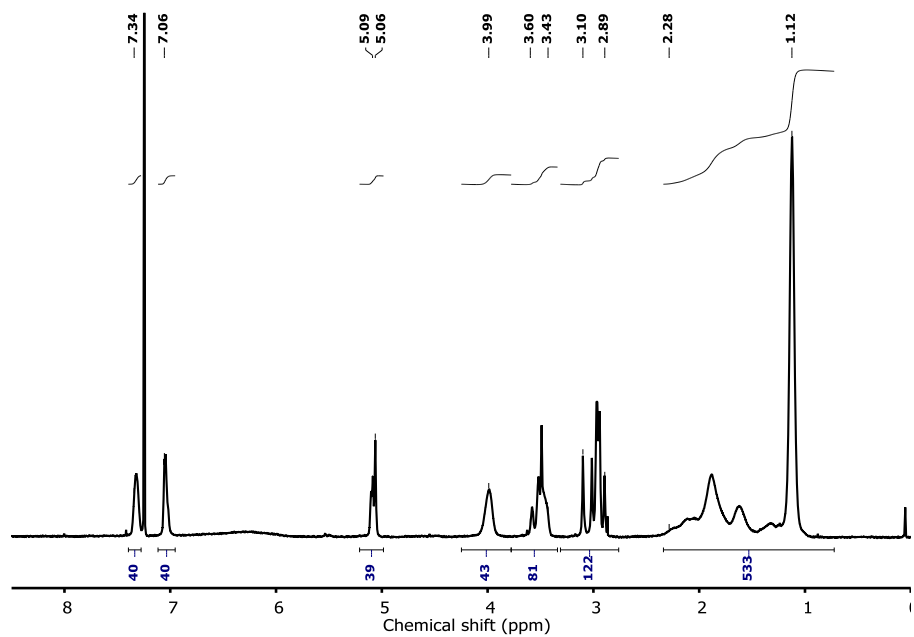


Figure A3.5: ^1H NMR spectrum of **PCB_{uv}-PNIPAAm** (CDCl_3 , 600 MHz). Asterisks denote residual solvent signals.

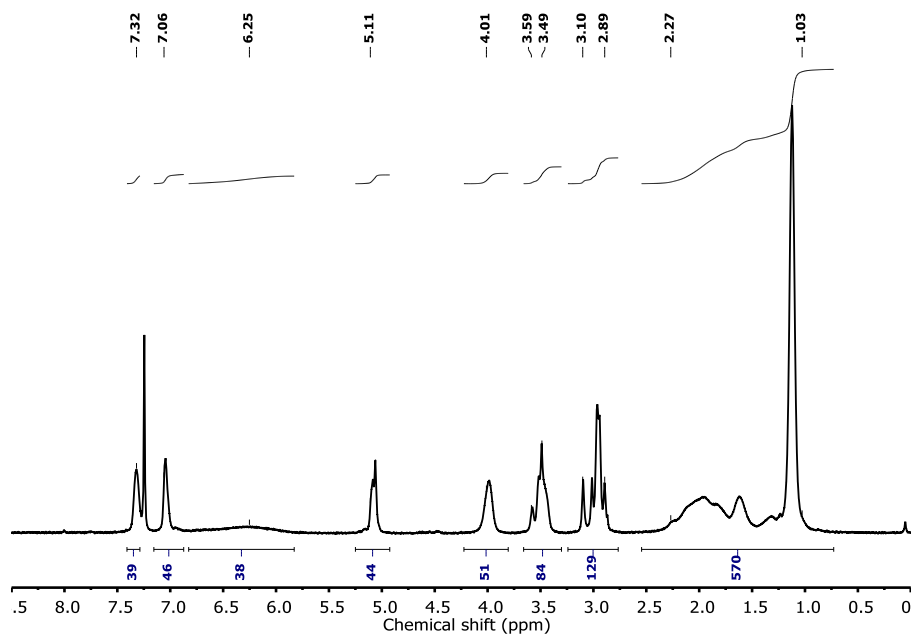


Figure A3.6: ^1H NMR spectrum of $\text{PCB}_{\text{CON}}\text{-PNIPAAm}$ (CDCl_3 , 600 MHz). Asterisks denote residual solvent signals.

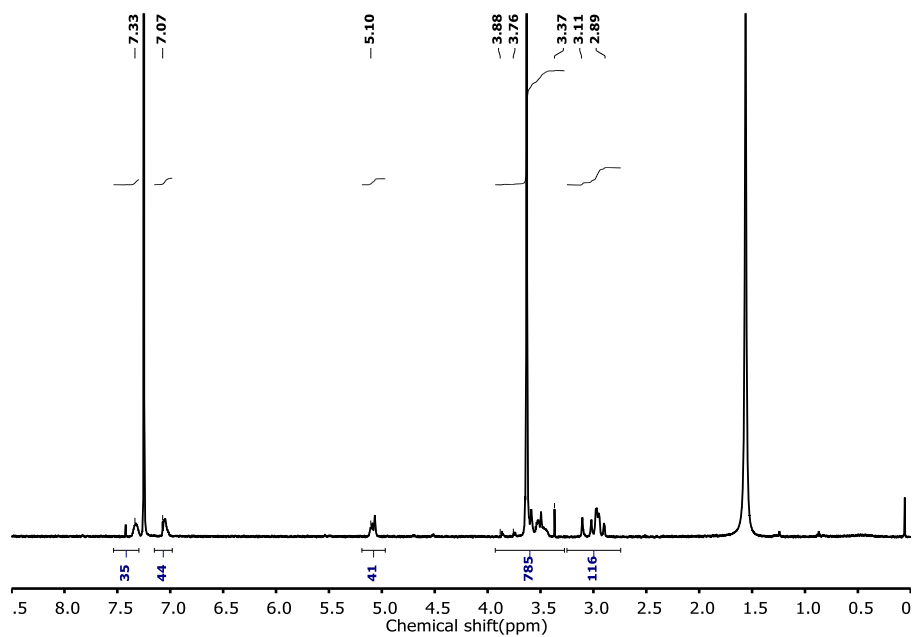


Figure A3.7: ^1H NMR spectrum of $\text{PCB}_{\text{UV}}\text{-PEG}$ (CDCl_3 , 600 MHz). Asterisks denote residual solvent signals.

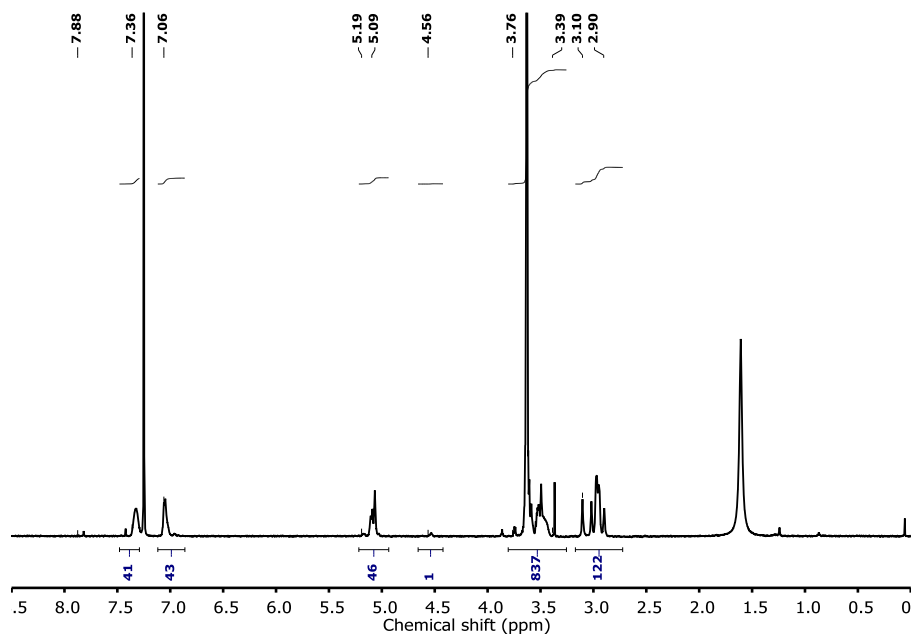


Figure A3.8: ^1H NMR spectrum of **PCBcon-PEG** (CDCl_3 , 600 MHz). Asterisks denote residual solvent signals.

Characterization overlays

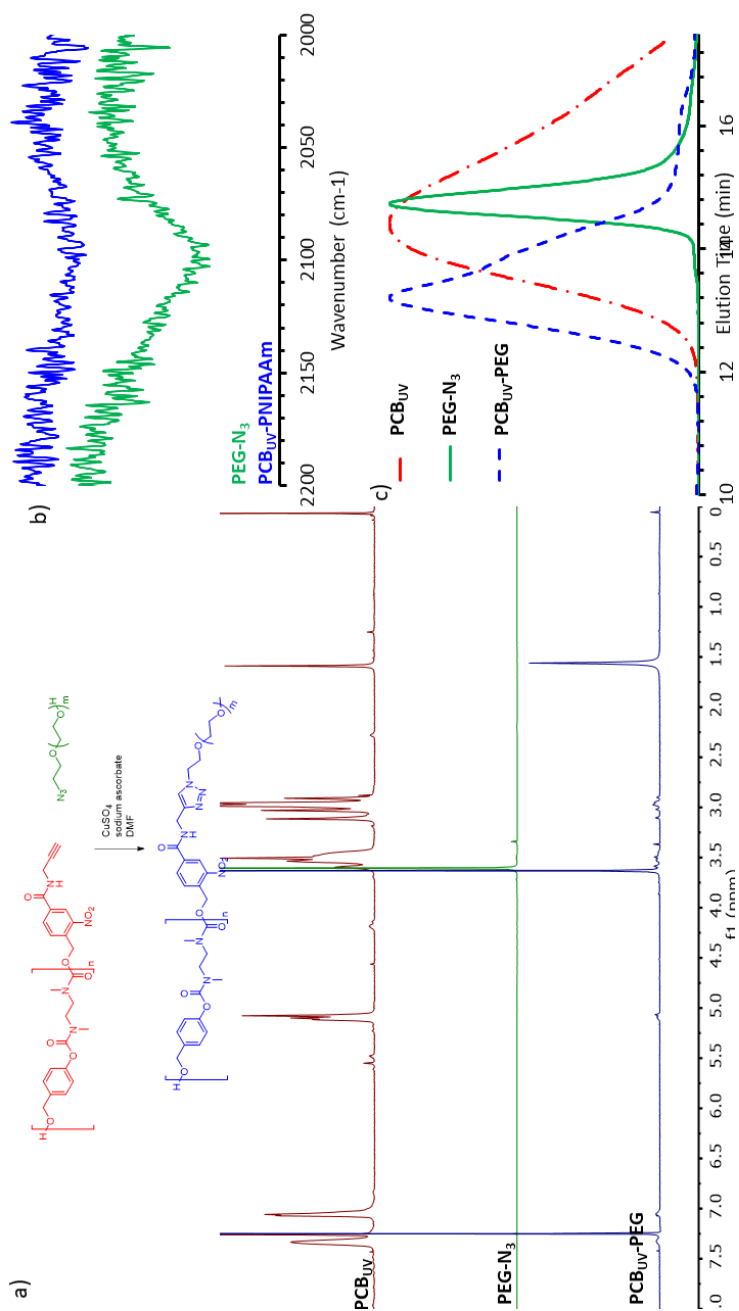


Figure A3.9: Characterization of **PCB_{UV}-PEG**: a) ^1H NMR spectra (600 MHz, CDCl_3); b) DMF SEC traces (refractive index detection); c) IR Spectra. The ^1H NMR spectra of **PCB_{UV}-PEG** has peaks from both blocks after purification and the SEC trace of **PCB_{UV}-PEG** has a decreased retention time, indicating an increase in molecular peaks as well as no peaks corresponding to the original homopolymers. The azide stretch at 2100 cm^{-1} is absent post CuAAC, indicating no free **PEG-N₃** is present.

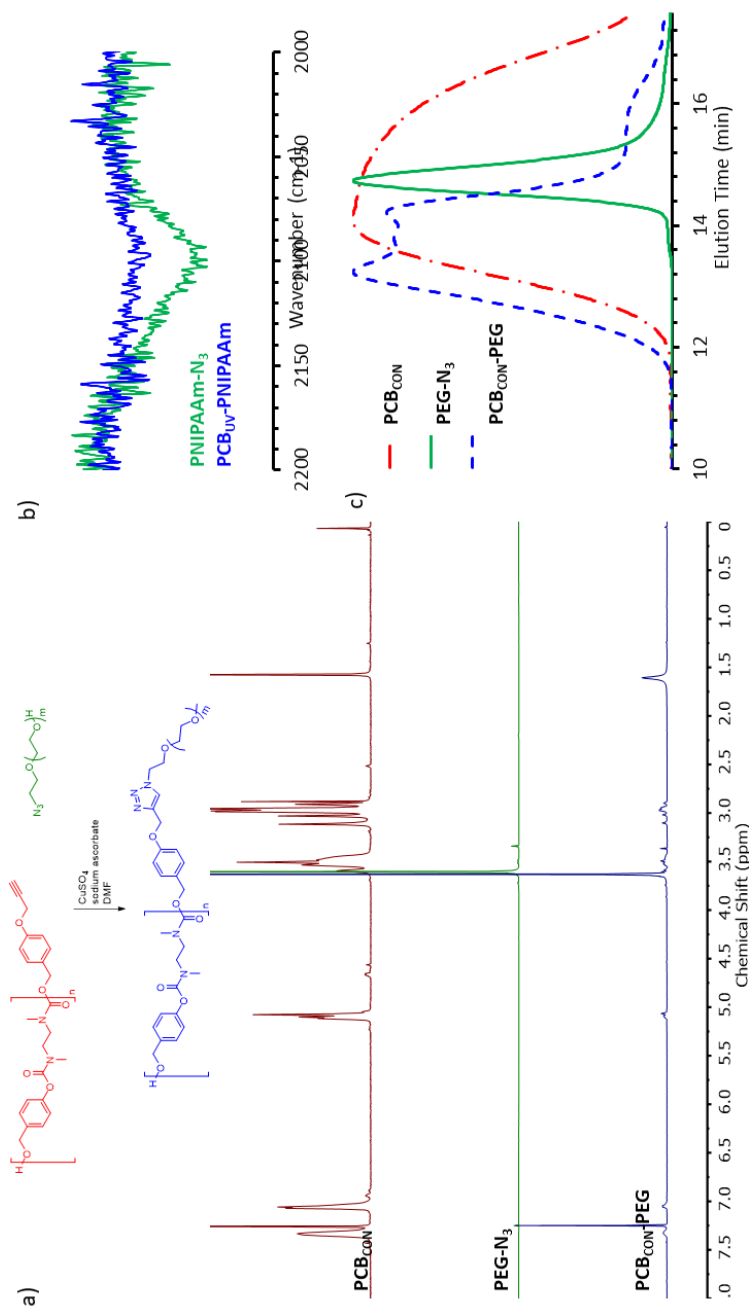


Figure A3.10: Characterization of $\text{PCB}_{\text{CON}}\text{-PEG}$: a) ^1H NMR spectra (600 MHz, CDCl_3); b) DMF SEC traces (refractive index detection); c) IR Spectra. The ^1H NMR spectra of $\text{PCB}_{\text{UV}}\text{-PEG}$ has peaks from both blocks after purification and the SEC trace of $\text{PCB}_{\text{UV}}\text{-PEG}$ has a decreased retention time, indicating an increase in molecular peaks as well as no peaks corresponding to the original homopolymers. The azide stretch at 2100 cm^{-1} is absent post CuAAC, indicating no free PEG-N_3 is present.

Drug loading and calibration curve

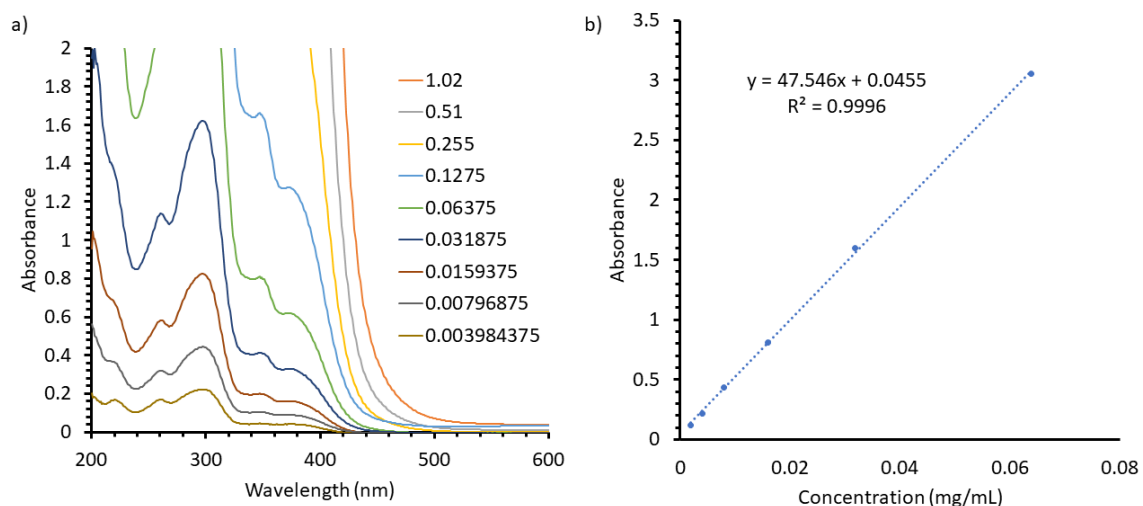


Figure A3.11: a) UV-absorbance of methotrexate in MeOH at varying concentrations (mg/mL) and b) the calibration curve for methotrexate absorbance at 302 nm versus concentration.

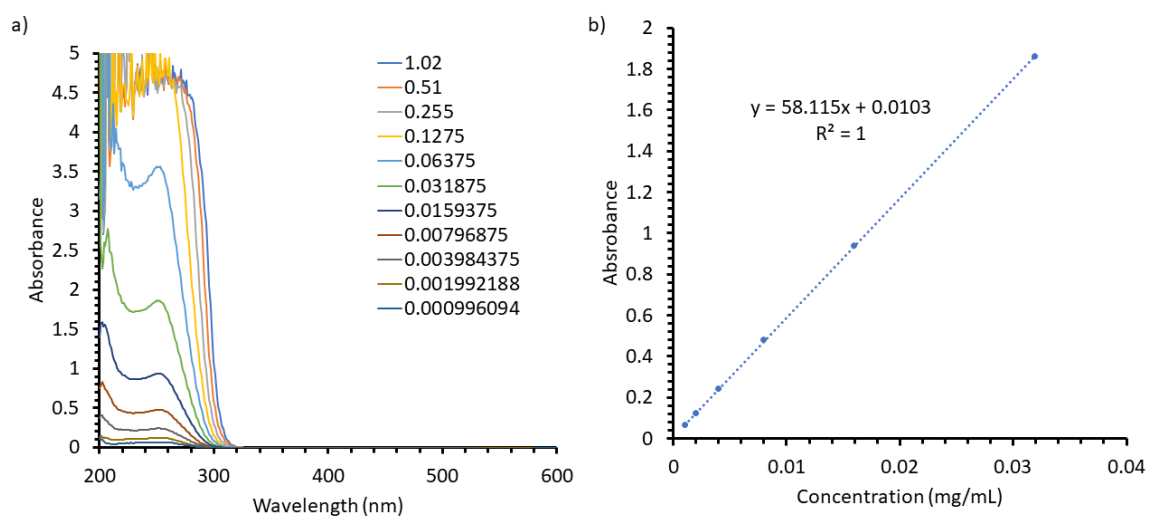


Figure A3.12: a) UV-absorbance of celecoxib in MeOH at varying concentrations (mg/mL) and b) the calibration curve for celecoxib absorbance at 252 nm versus concentration.

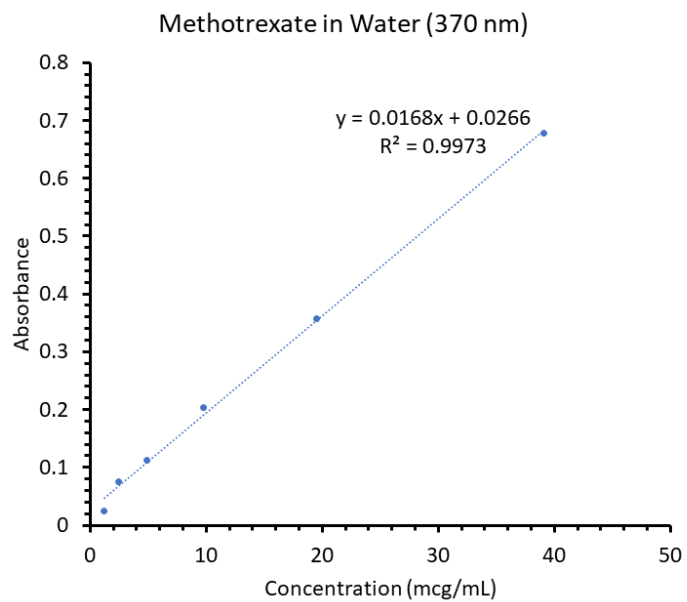


Figure A3.13: The calibration curve for methotrexate in water absorbance at 370 nm versus concentration (mcg/mL).

Appendix 4 – Supporting information for Chapter 4

NMR spectra

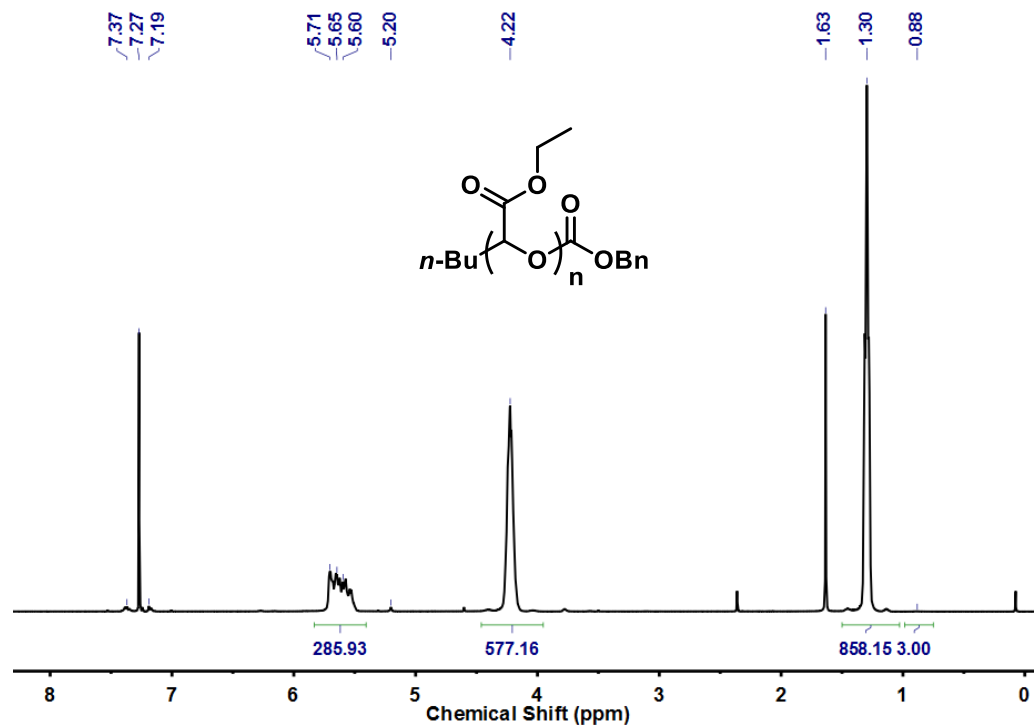


Figure A4.1. ^1H NMR spectrum of PETG carbonate (CDCl_3 , 400 MHz). Asterisks denote residual solvent signals.

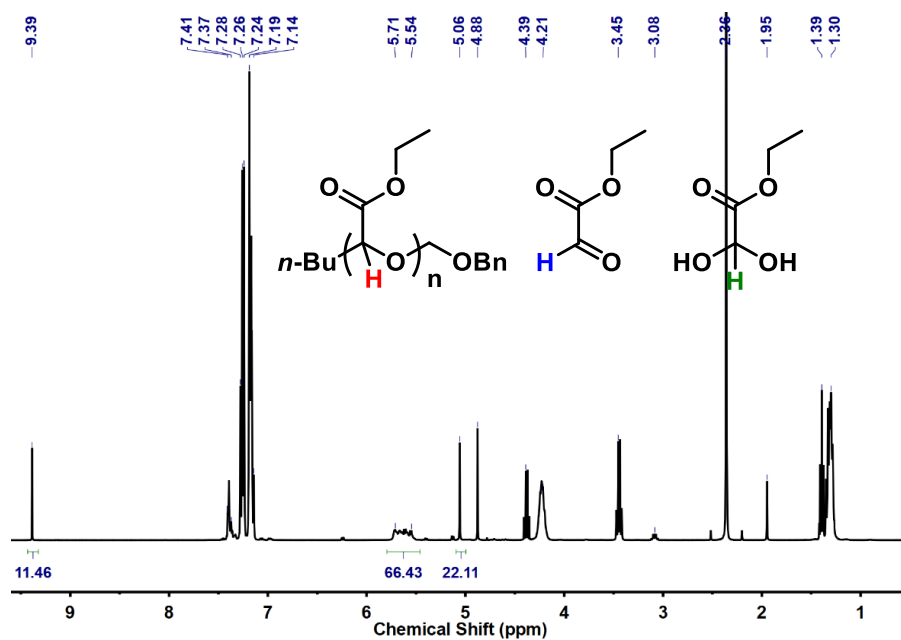


Figure A4.2. ^1H NMR spectrum of the crude reaction mixture of **PEtG_{ether}** (CDCl_3 , 400 MHz). Red, blue, and green circles denote traces of PETG, EtG, and EtGH.

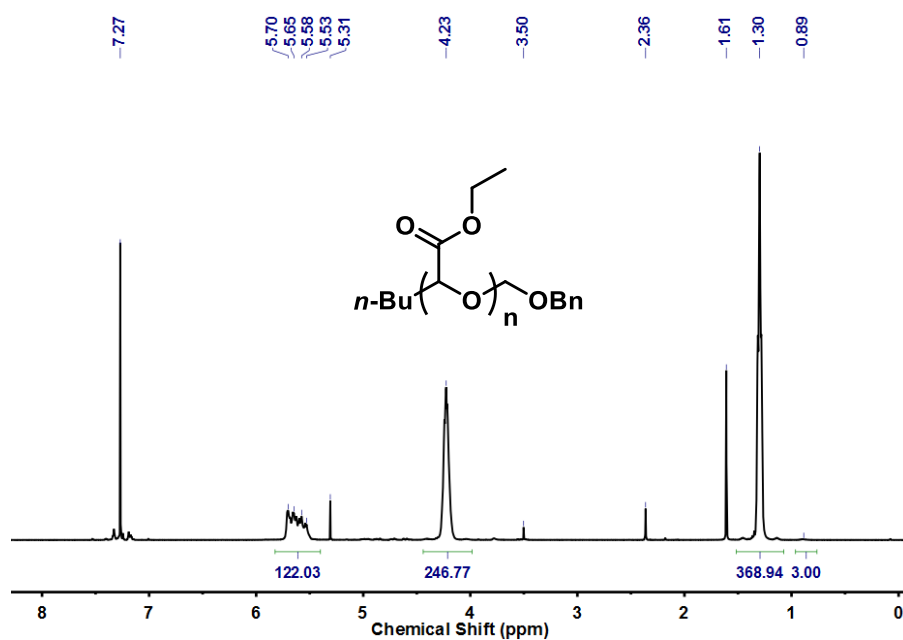


Figure A4.3. ^1H NMR spectrum of **PEtG_{ether}** (CDCl_3 , 400 MHz). Asterisks denote a residual solvent signals.

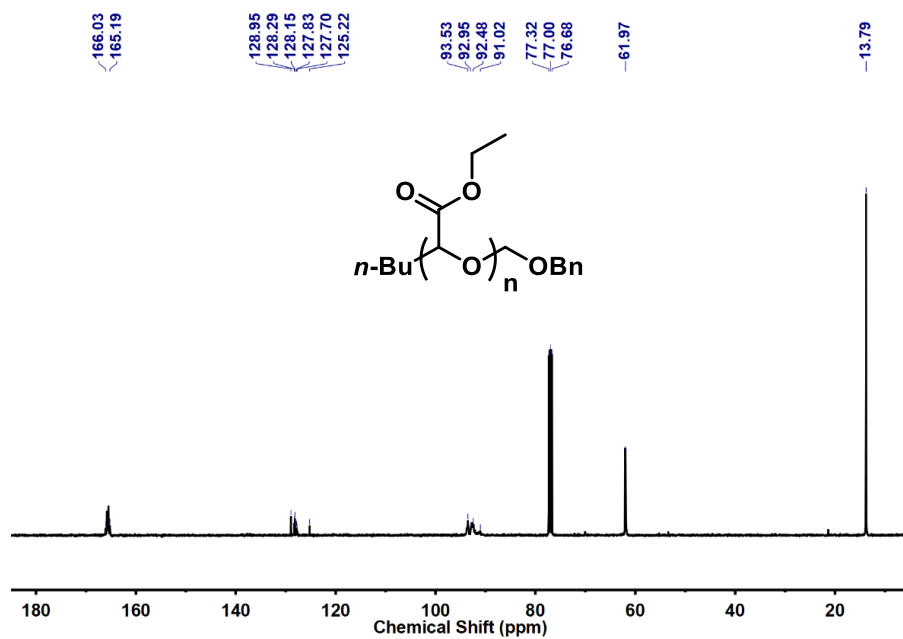


Figure A4.4. ^{13}C NMR spectrum of **PEtG_{ether}** (CDCl_3 , 100 MHz). Asterisk denotes residual solvent signal.

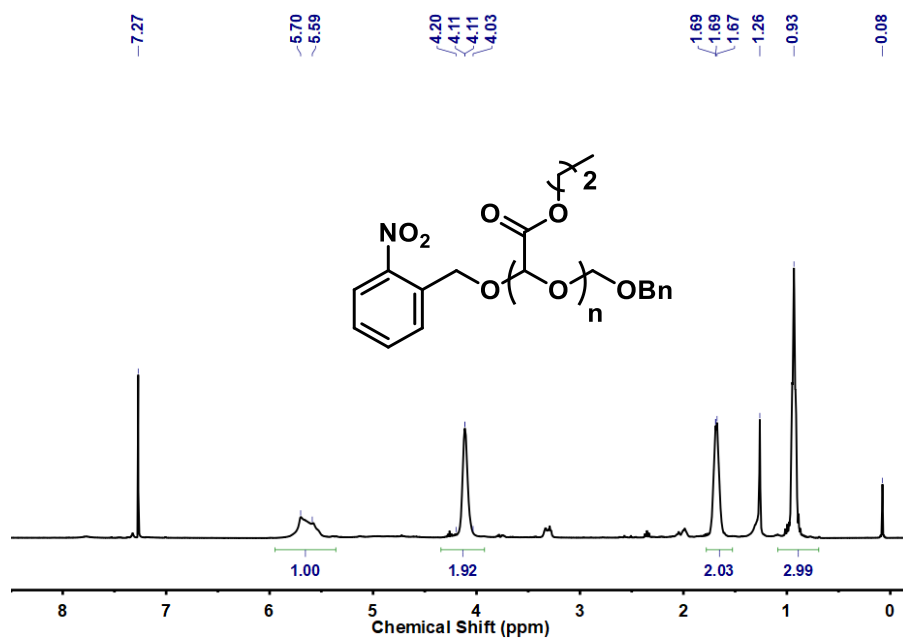


Figure A4.7. ^1H NMR spectrum of P_nPrG (CDCl_3 , 400 MHz). Asterisks denote residual solvent and silicone grease signals.

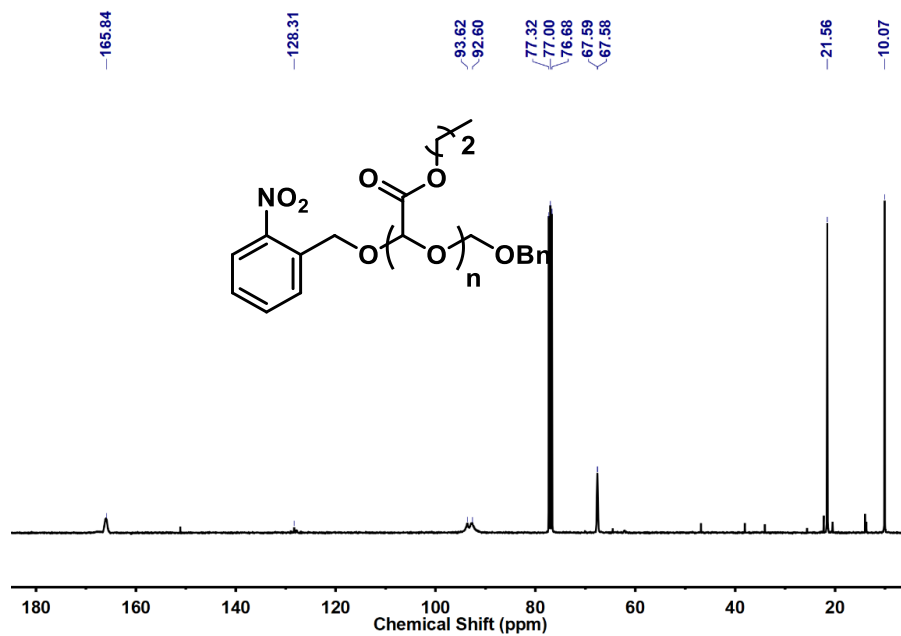


Figure A4.8. ^{13}C NMR spectrum of P_nPrG (CDCl_3 , 100 MHz). Asterisk denotes a residual solvent signal.

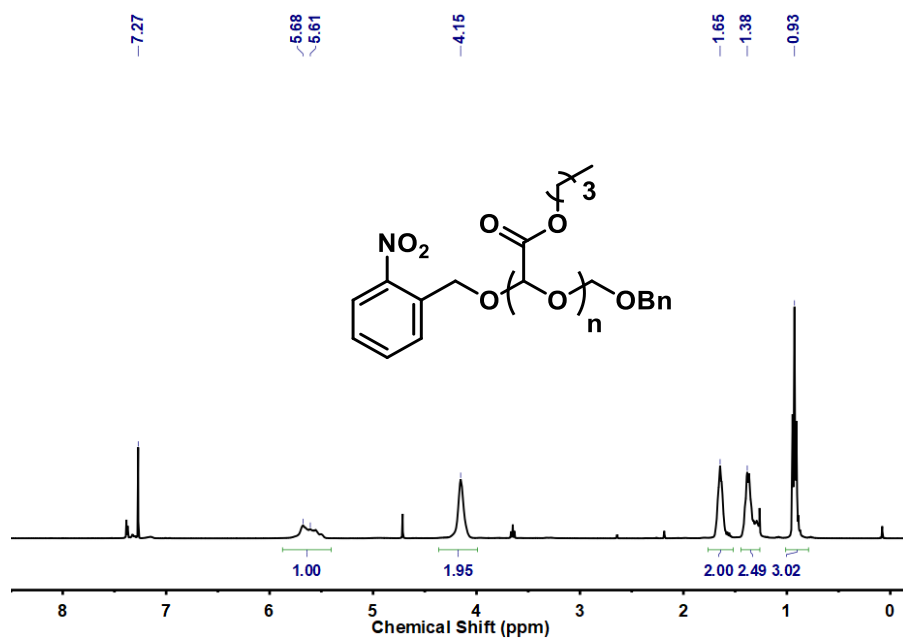


Figure A4.9. 1H NMR spectrum of P_nBuG ($CDCl_3$, 400 MHz). Asterisks denote residual solvent signals.

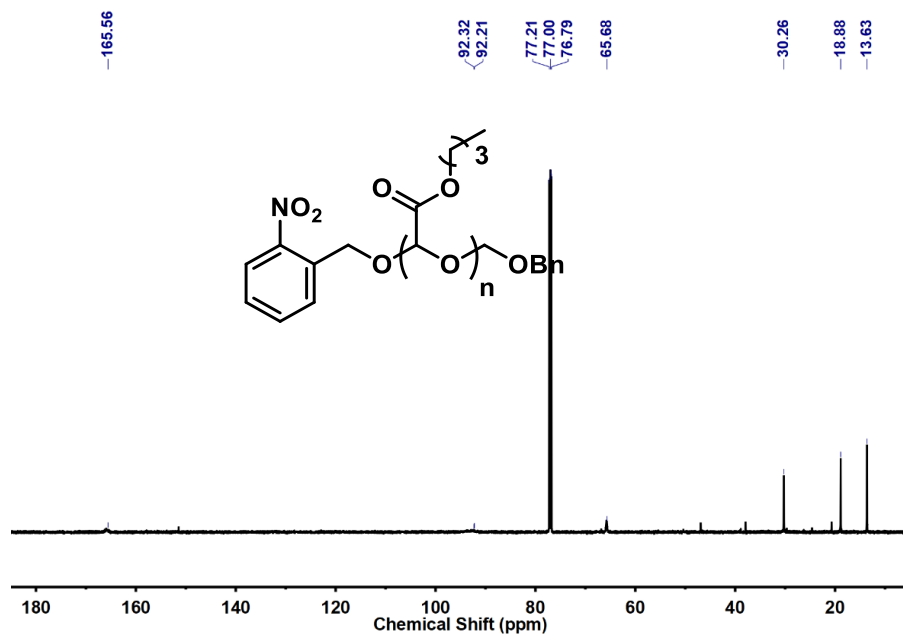


Figure A4.10. ^{13}C NMR spectrum of P_nBuG ($CDCl_3$, 100 MHz). Asterisk denotes a residual solvent signal.

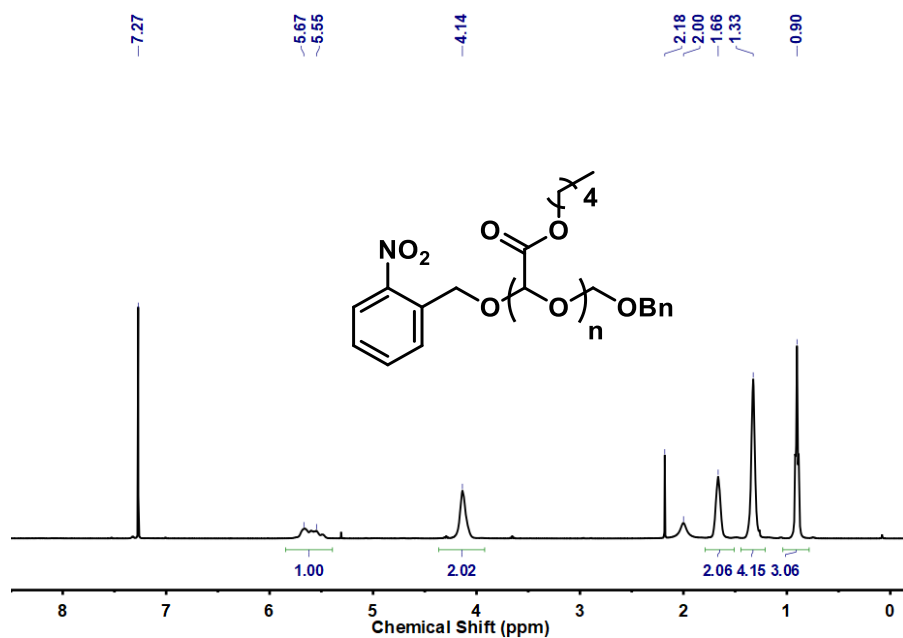


Figure A4.11. 1H NMR spectrum of P_nPenG ($CDCl_3$, 400 MHz). Asterisks denote residual solvent signals.

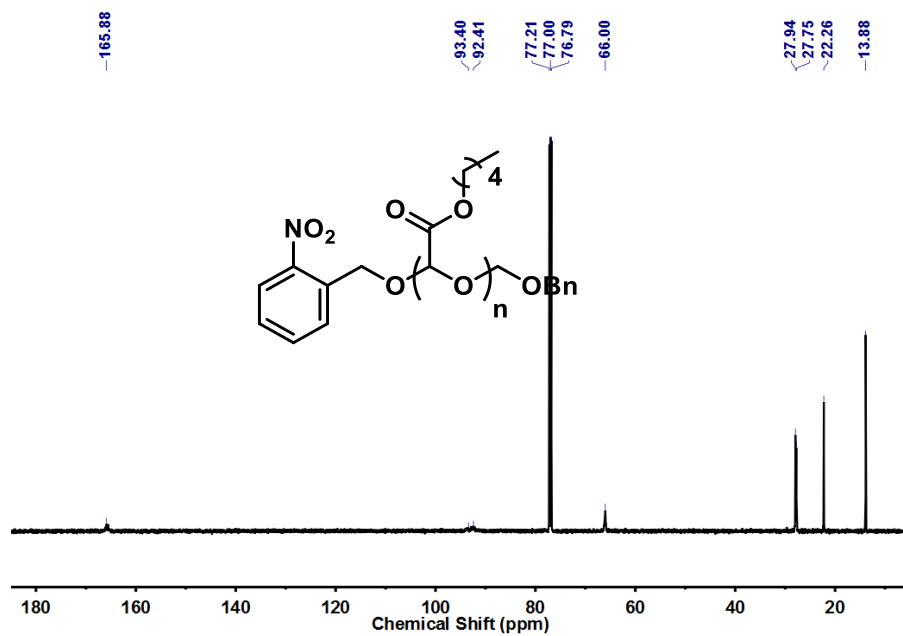


Figure A4.12. ^{13}C NMR spectrum of P_nPenG ($CDCl_3$, 100 MHz). Asterisk denotes a residual solvent signal.

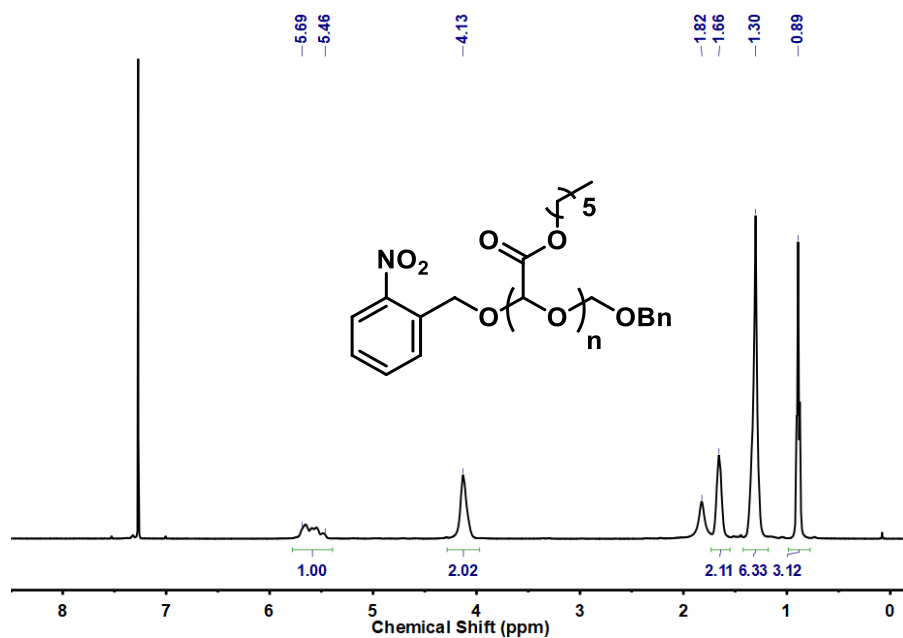


Figure A4.13. ¹H NMR spectrum of **PHexG** (CDCl₃, 400 MHz). Asterisks denote residual solvent and silicone grease signals.

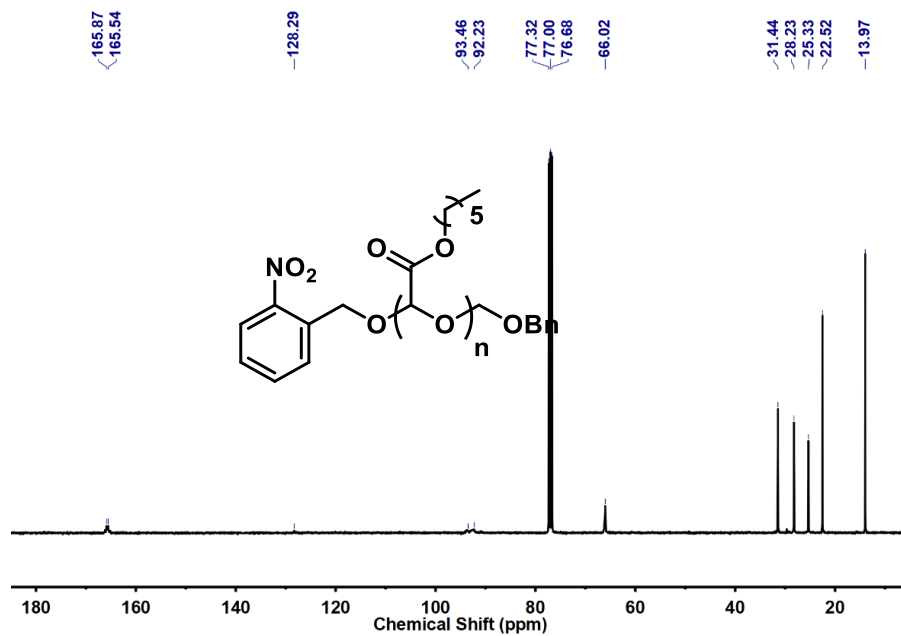


Figure A4.14. ¹³C NMR spectrum of **PHexG** (CDCl₃, 100 MHz). Asterisk denotes a residual solvent signal.

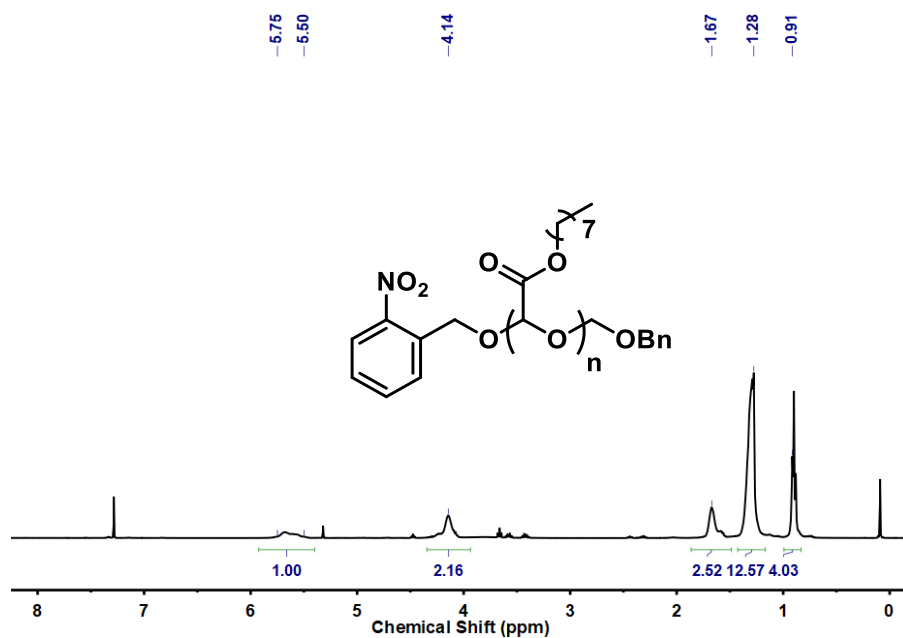


Figure A4.15. ¹H NMR spectrum of **POctG** (CDCl₃, 400 MHz). Asterisk denote residual solvent signals.

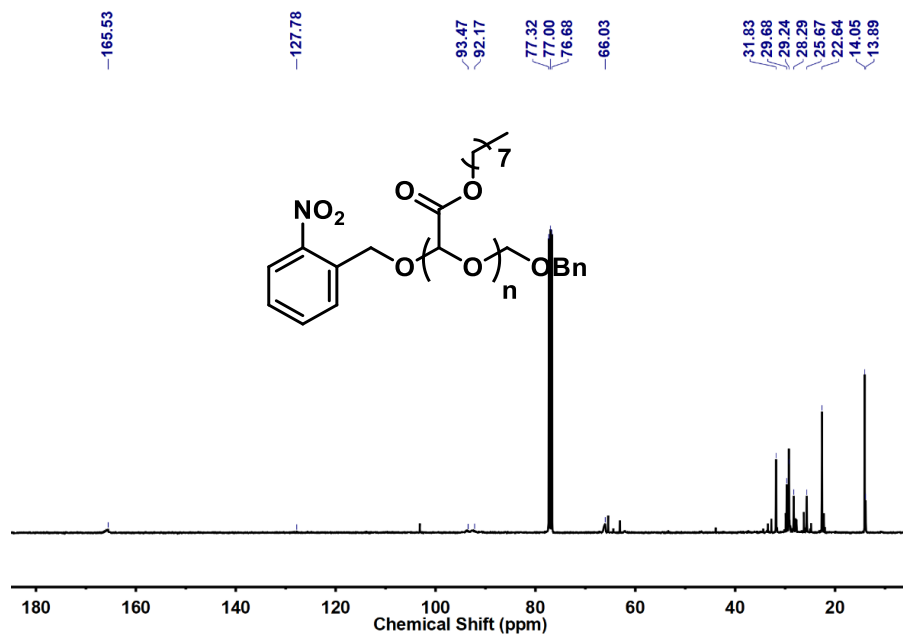


Figure A4.16. ¹³C NMR spectrum of **POctG** (CDCl₃, 100 MHz). Asterisk denotes a residual solvent signal.

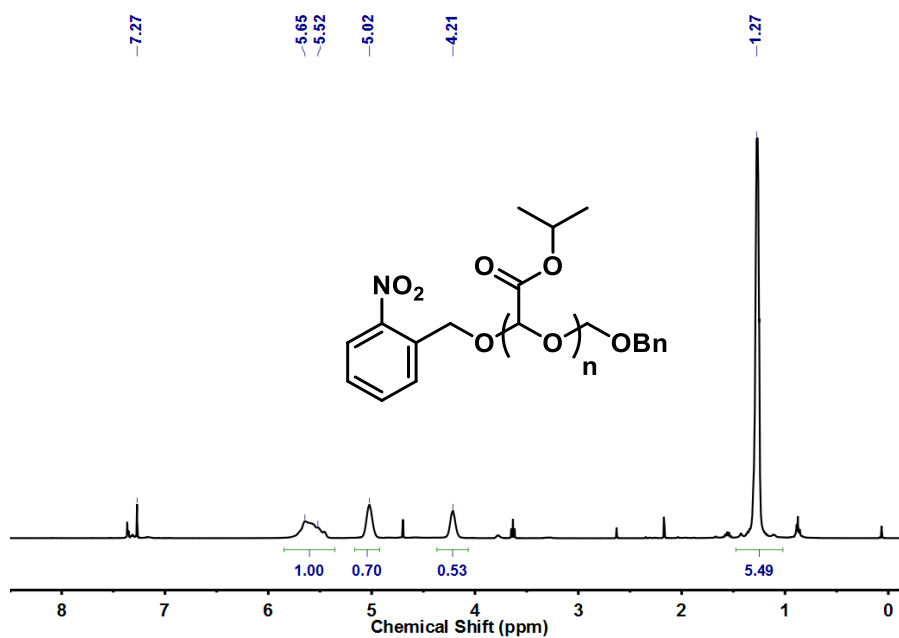


Figure A4.17. 1H NMR spectrum of P_iPrG ($CDCl_3$, 400 MHz). Asterisks denote residual solvent signals.

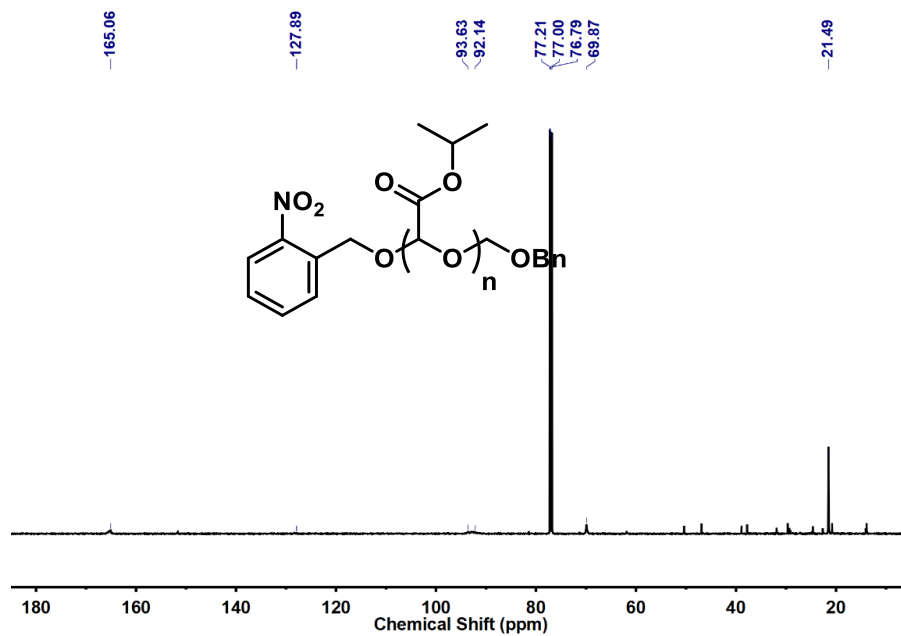


Figure A4.18. ^{13}C NMR spectrum of P_iPrG ($CDCl_3$, 100 MHz). Asterisk denotes a residual solvent signal.

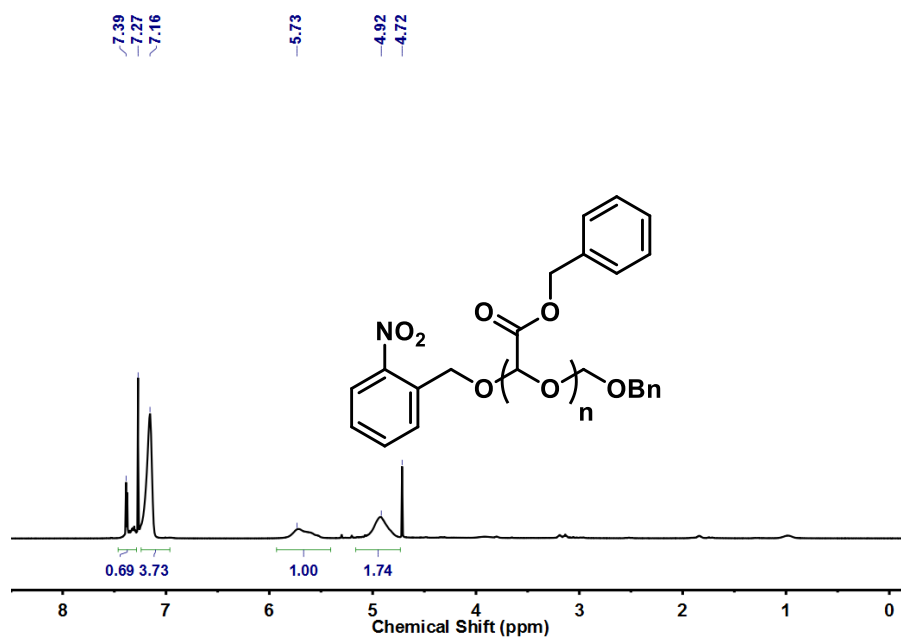


Figure A4.19. ¹H NMR spectrum of PBnG (CDCl₃, 400 MHz). Asterisks denote residual solvent signals.

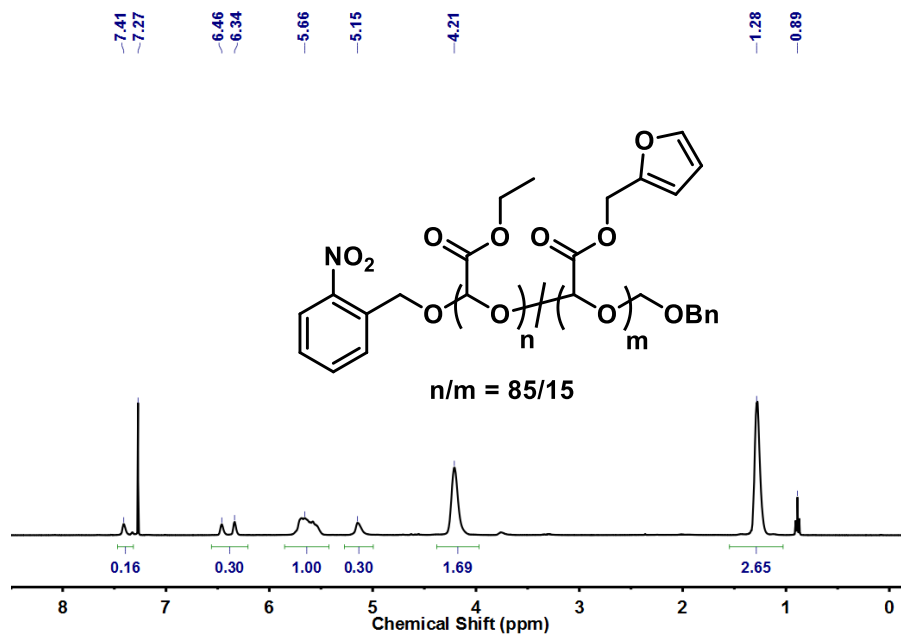


Figure A4.20. ¹H NMR spectrum of PAIG (CDCl₃, 400 MHz). Asterisks denote residual solvent signals.

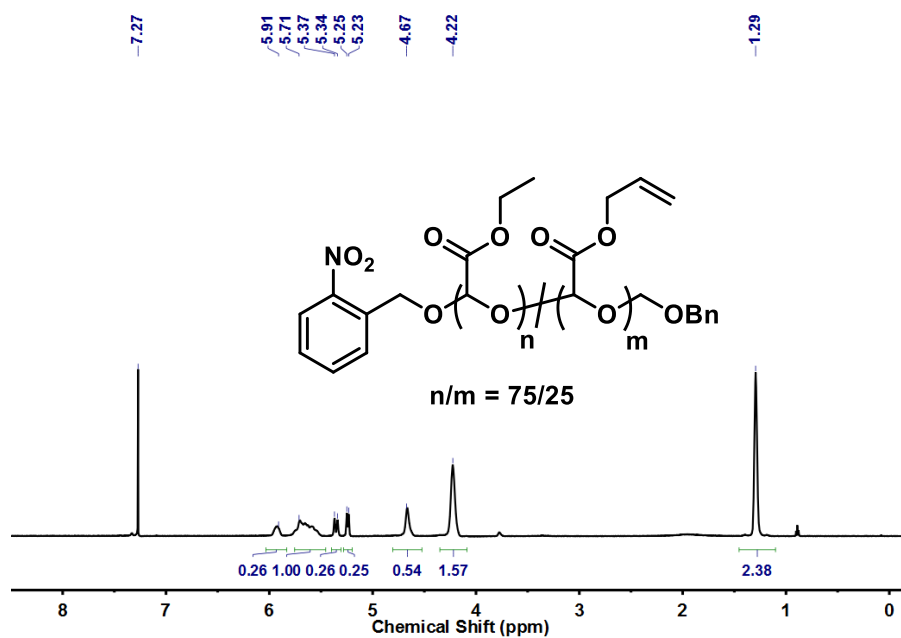


Figure A4.21. ^1H NMR spectrum of **PFuG** (CDCl_3 , 400 MHz). Asterisk denotes a residual solvent signal.

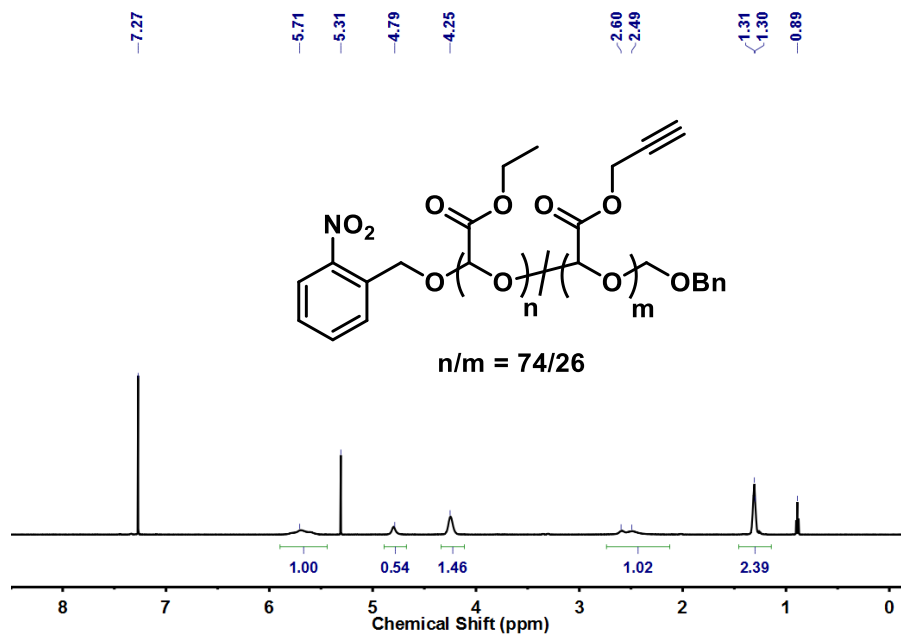


Figure A4.22. ^1H NMR spectrum of **PPG** (CDCl_3 , 400 MHz). Asterisks denote residual solvent signals.

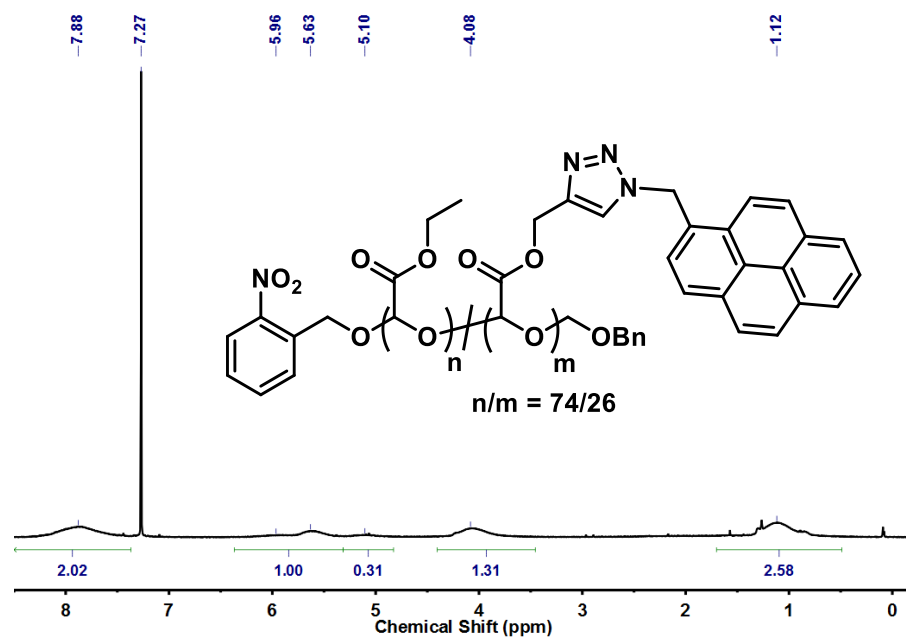


Figure A4.23. ¹H NMR spectrum of PPG_{Pyr} (CDCl₃, 400 MHz). Asterisk denotes residual solvent signal.

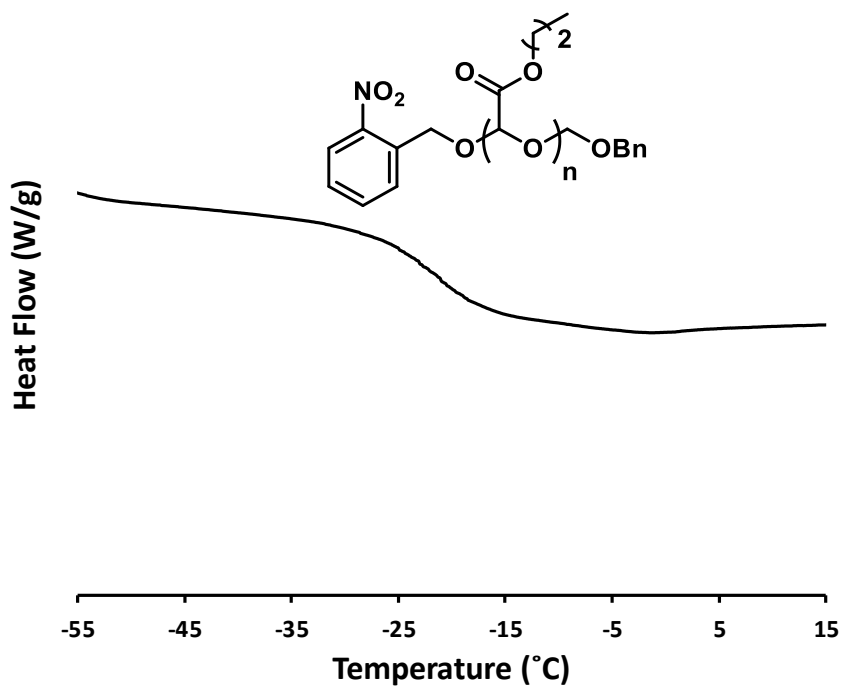


Figure A4.26. DSC thermogram recorded for P_nPrG .

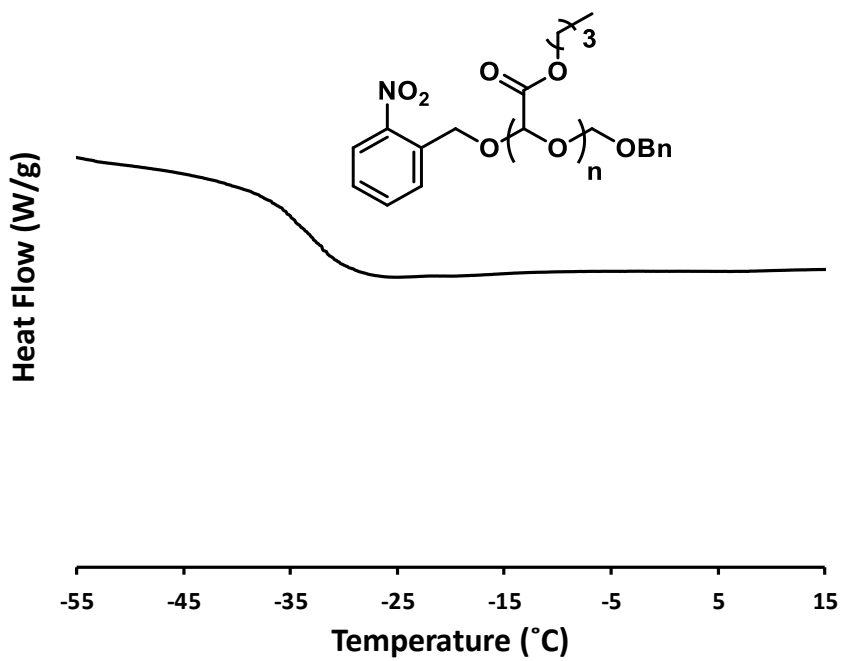


Figure A4.27. DSC thermogram recorded for P_nBuG .

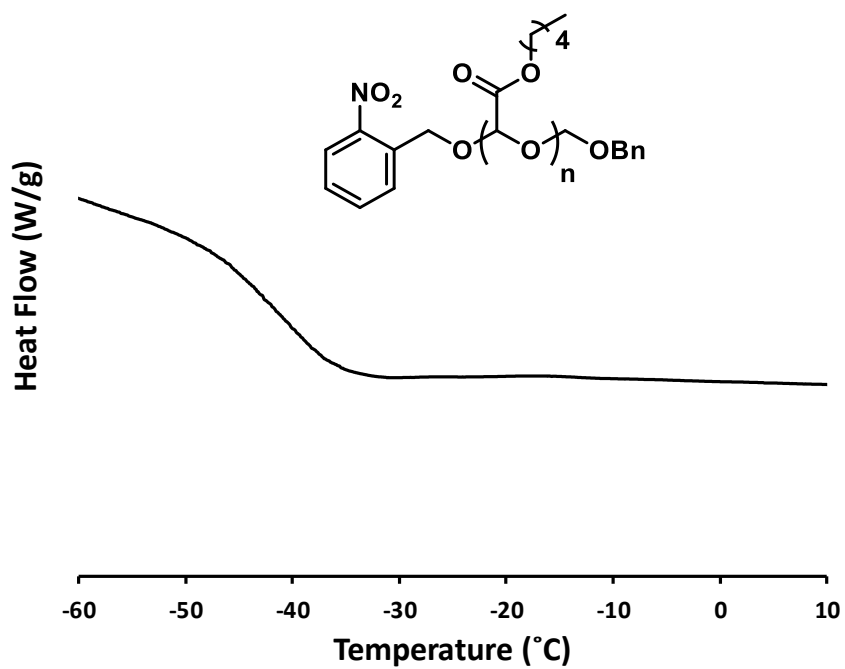


Figure A4.28. DSC thermogram recorded for P_nPenG.

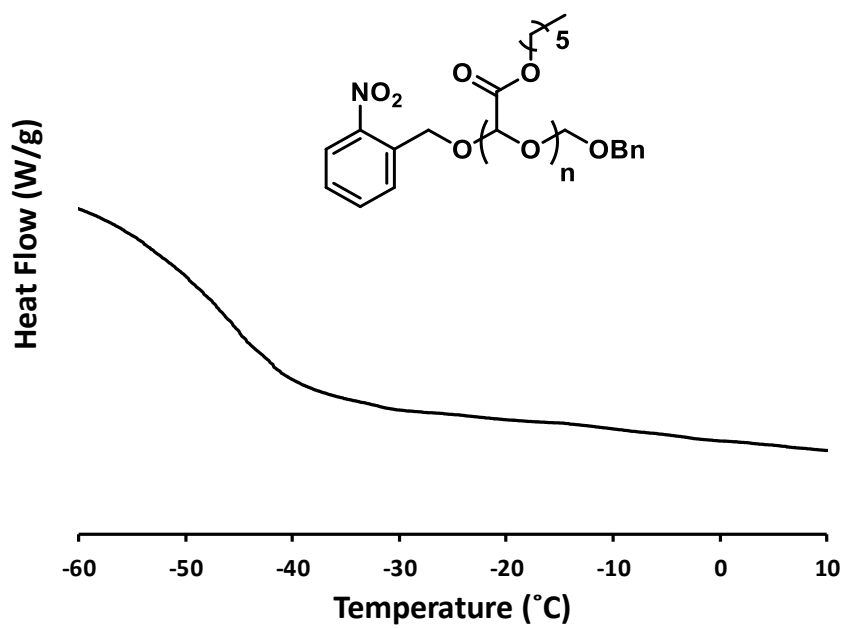


Figure A4.29. DSC thermogram recorded for PHexG.

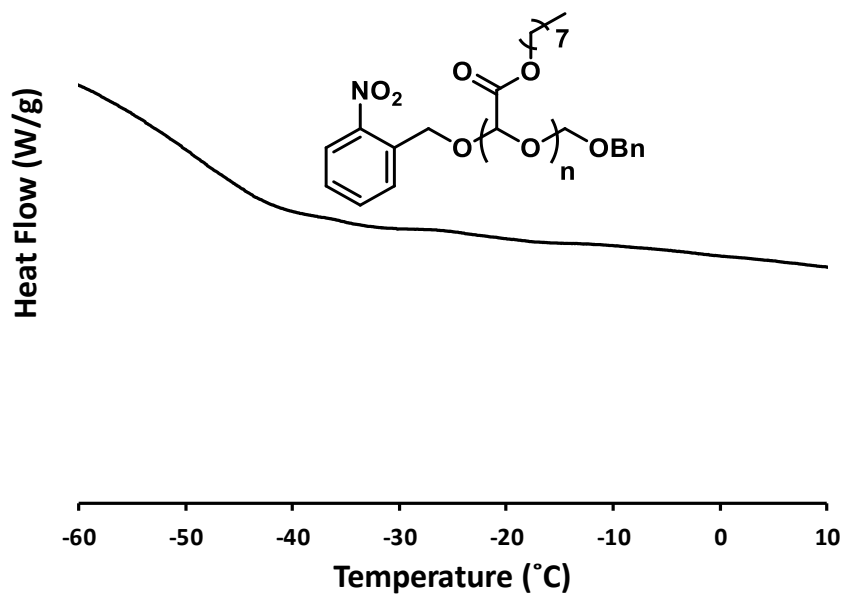


Figure A4.30. DSC thermogram recorded for POctG.

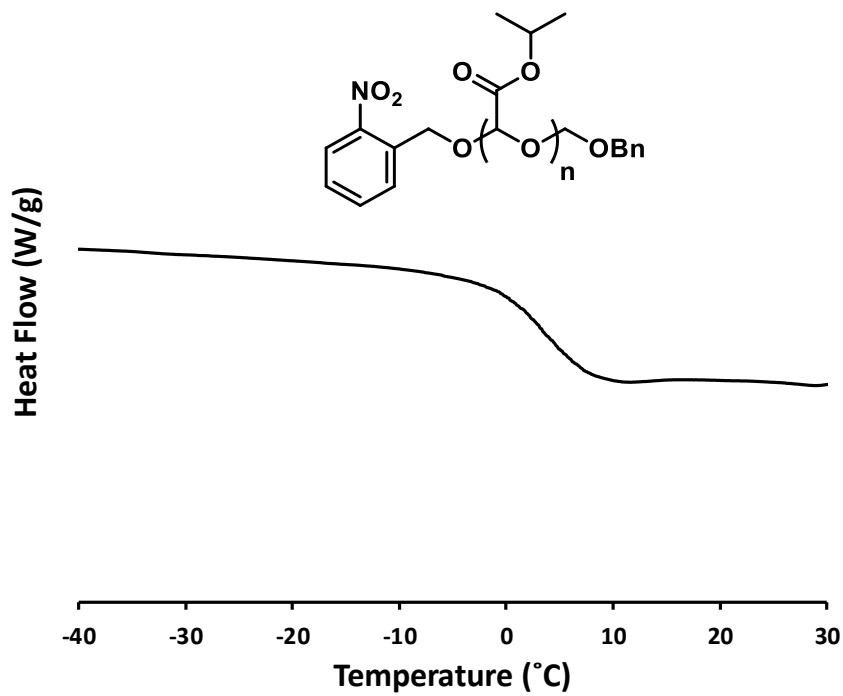


Figure A4.31. DSC thermogram recorded for PiPrG.

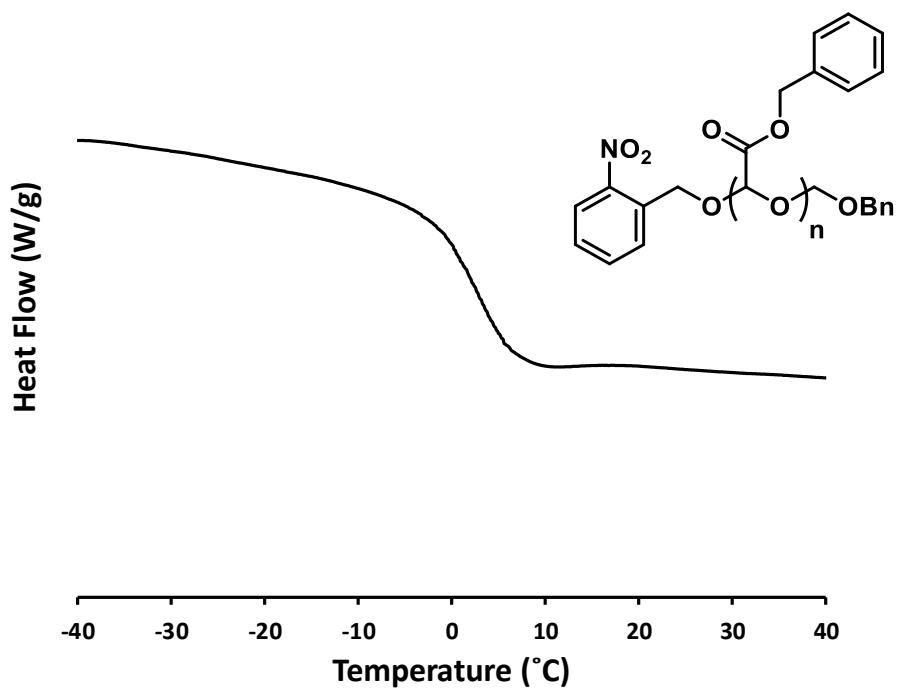


Figure A4.32. DSC thermogram recorded for PBnG.

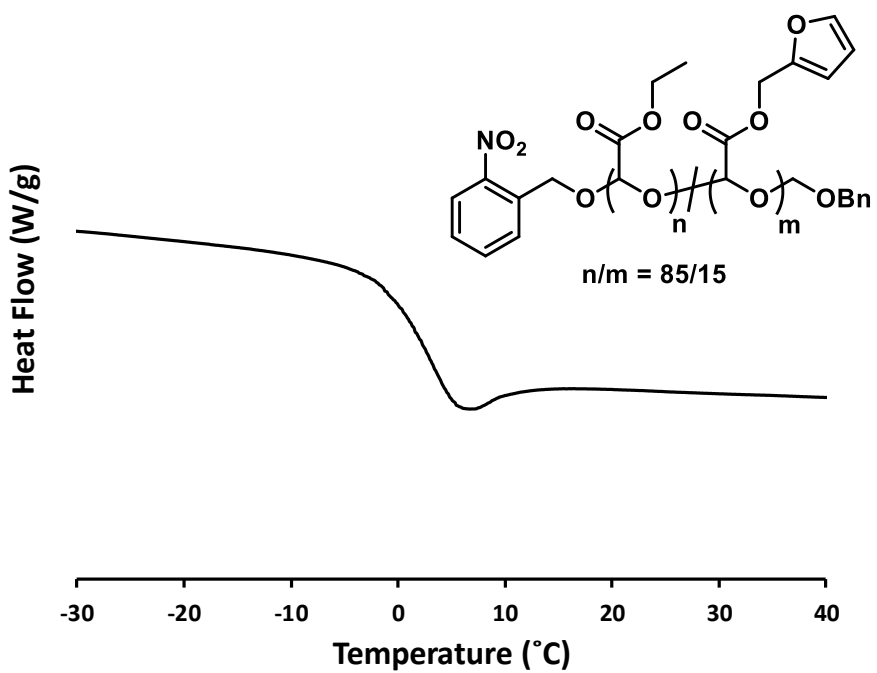


Figure A4.33. DSC thermogram recorded for PFuG.

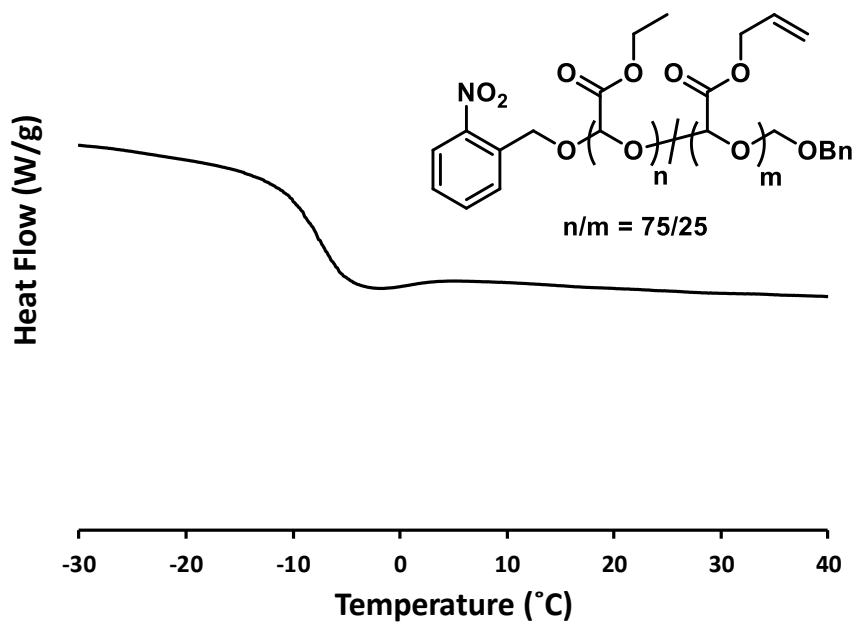


Figure A4.34. DSC thermogram recorded for PAIG.

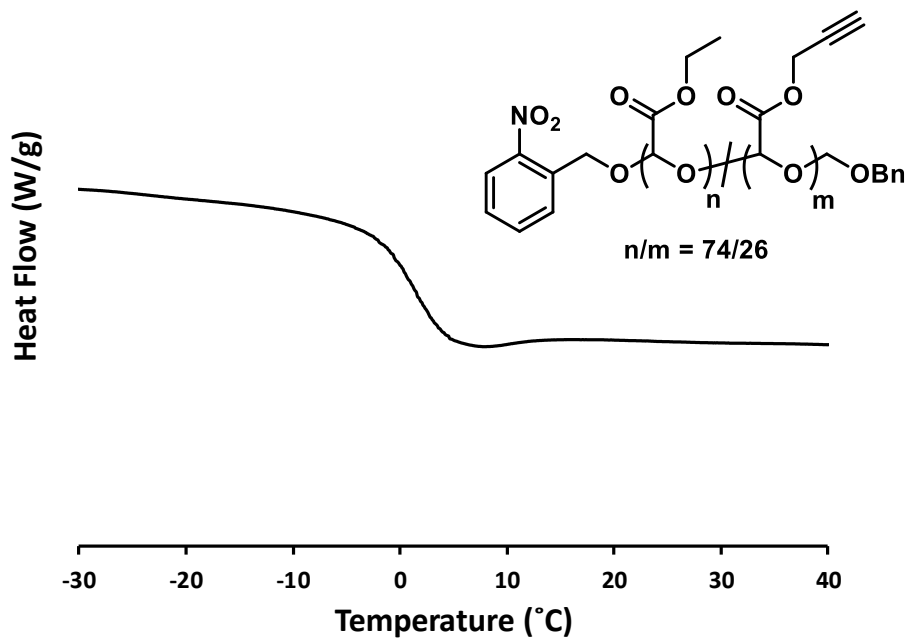


Figure A4.35. DSC thermogram recorded for PPG.

Degradation studies

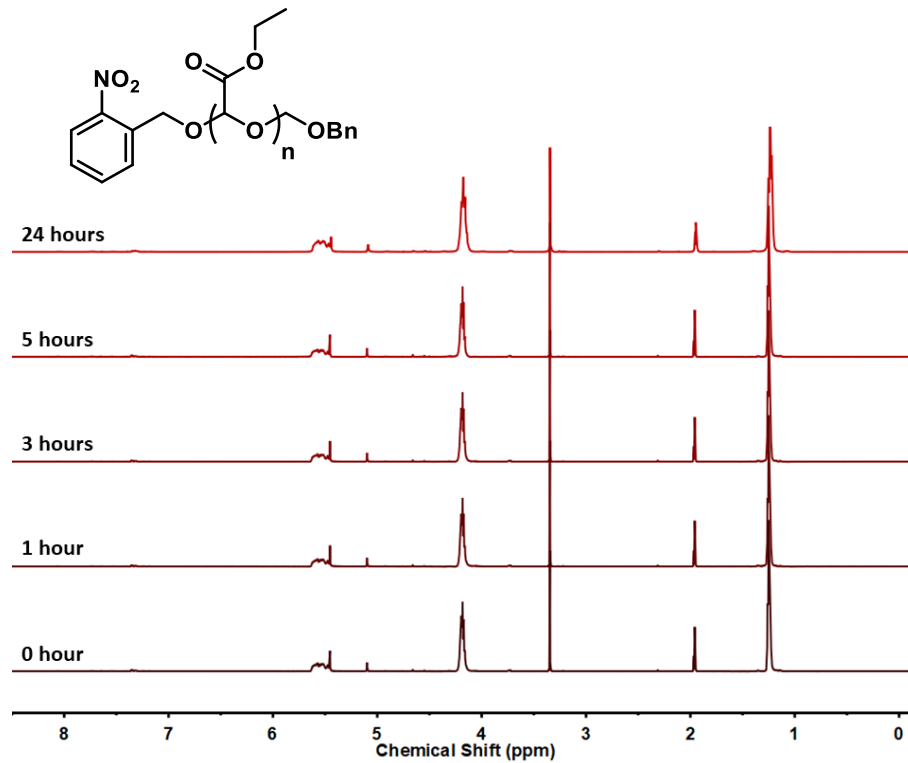


Figure A4.36. ¹H NMR spectra recorded for PETG_{uv} kept in dark at different time intervals (9/1: CD₃CN/D₂O, 400 MHz). Asterisks denote residual solvent signals.

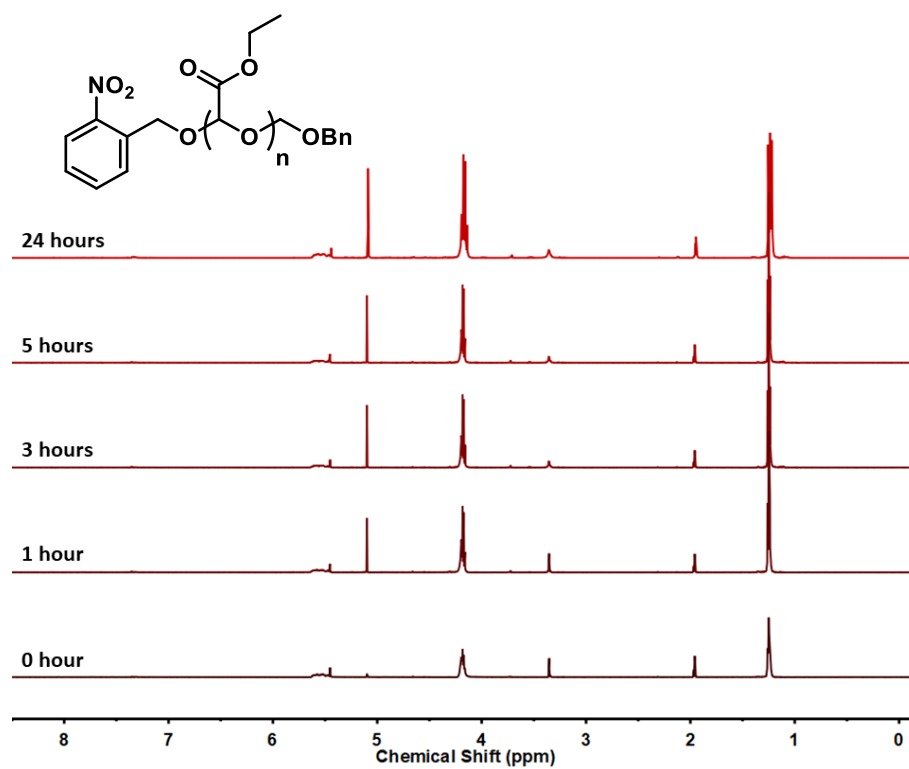


Figure A4.37. ¹H NMR spectra recorded for **PETG_{UV}** exposed to a UV light at different time intervals (9/1: CD₃CN/D₂O, 400 MHz). Asterisks denote residual solvent signals.

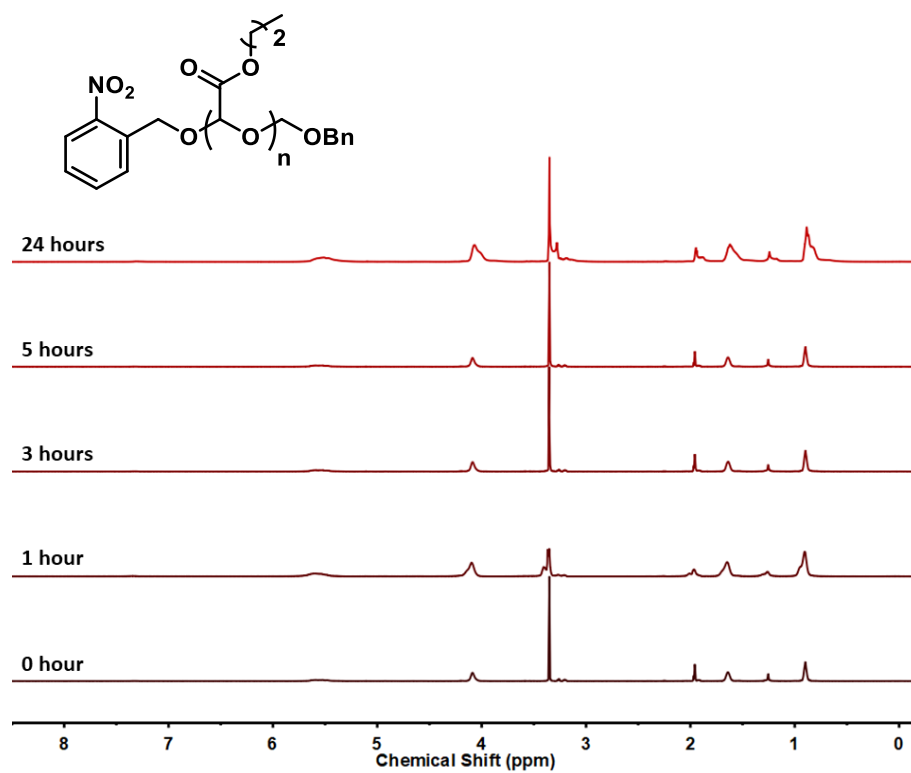


Figure A4.38. 1H NMR spectra recorded for P_nPrG kept in dark at different time intervals (9/1: CD₃CN/D₂O, 400 MHz). Asterisks denote residual solvent signals.

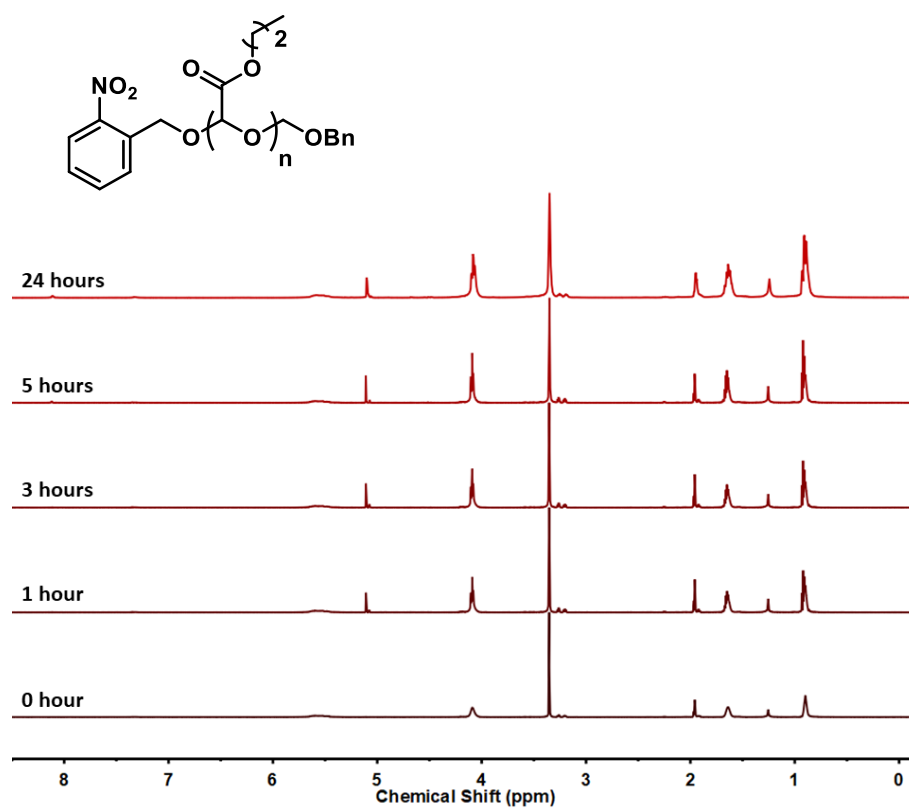


Figure A4.39. 1H NMR spectra recorded for P_nPrG exposed to a UV light at different time intervals (9/1: CD_3CN/D_2O , 400 MHz). Asterisks denote residual solvent signals.

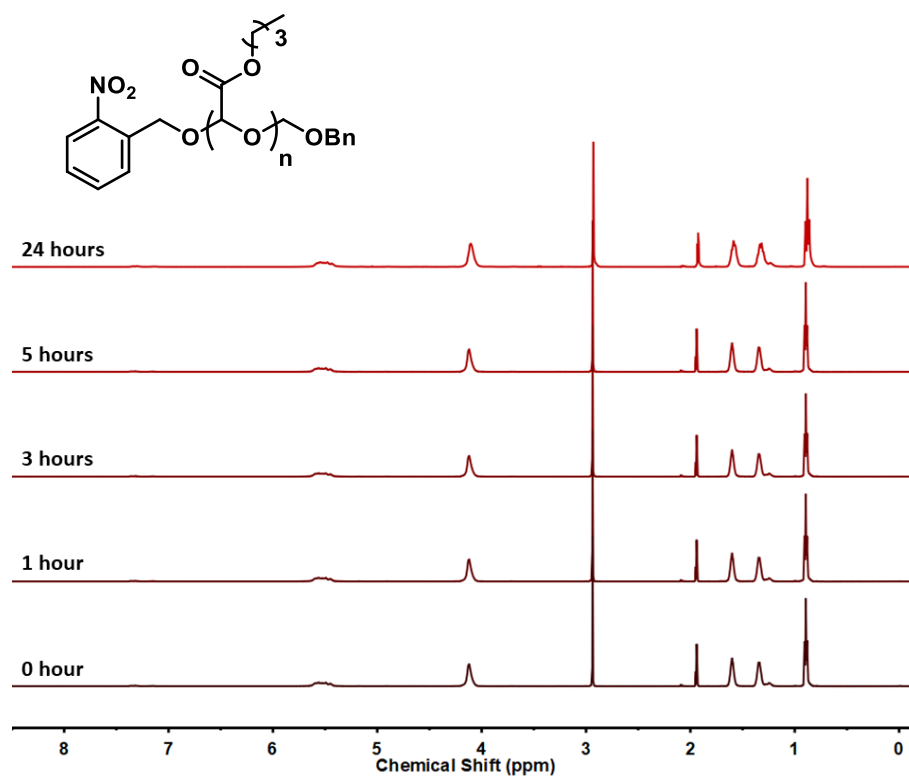


Figure A4.40. ¹H NMR spectra recorded for **P_nBuG** kept in dark at different time intervals (9/1: CD₃CN/D₂O, 400 MHz). Asterisks denote residual solvent signals.

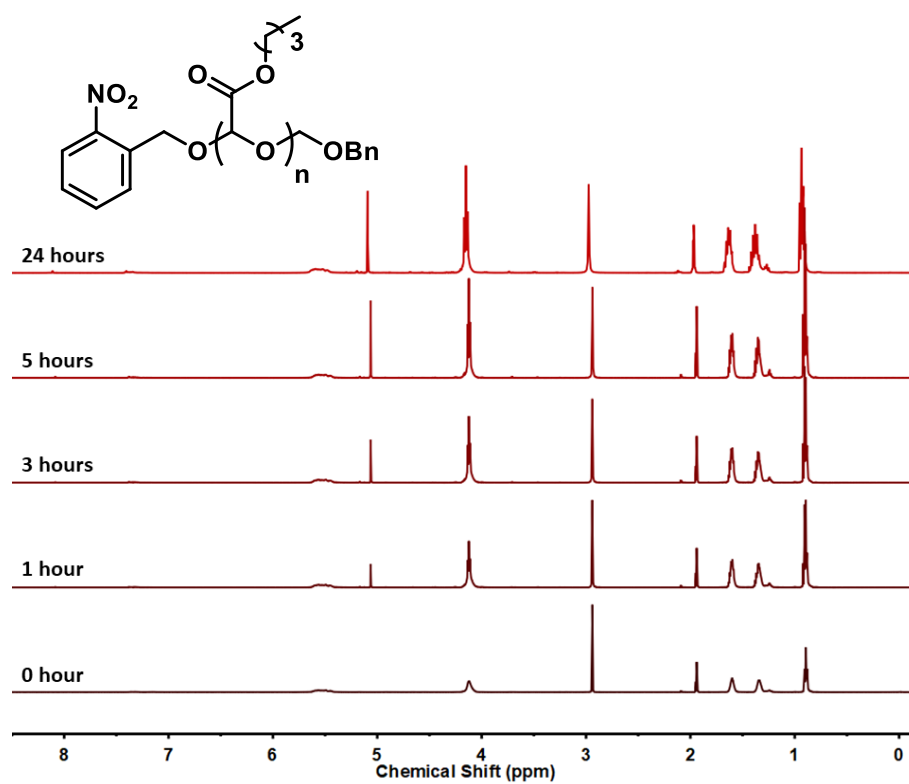


Figure A4.41. 1H NMR spectra recorded for P_nBuG exposed to a UV light at different time intervals (9/1: CD_3CN/D_2O , 400 MHz). Asterisks denote residual solvent signals.

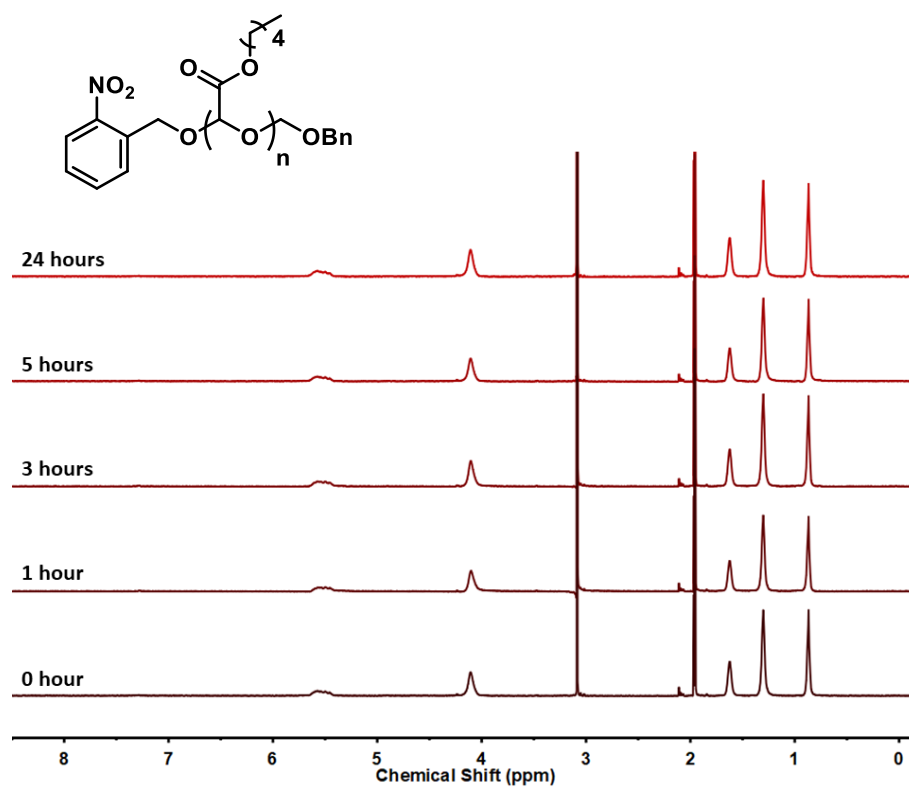


Figure A4.42. 1H NMR spectra recorded for P_nPenG kept in dark at different time intervals (9/1: CD_3CN/D_2O , 400 MHz). Asterisks denote residual solvent signals.

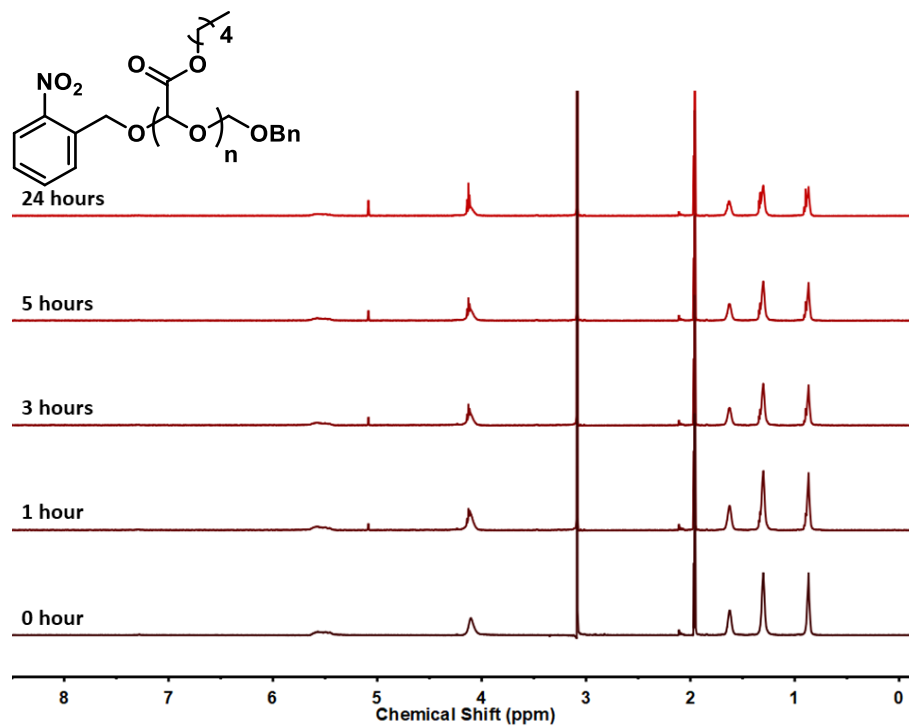


Figure A4.43. ¹H NMR spectra recorded for P_nPenG exposed to a UV light at different time intervals (9/1: CD₃CN/D₂O, 400 MHz). Asterisks denote residual solvent signals.

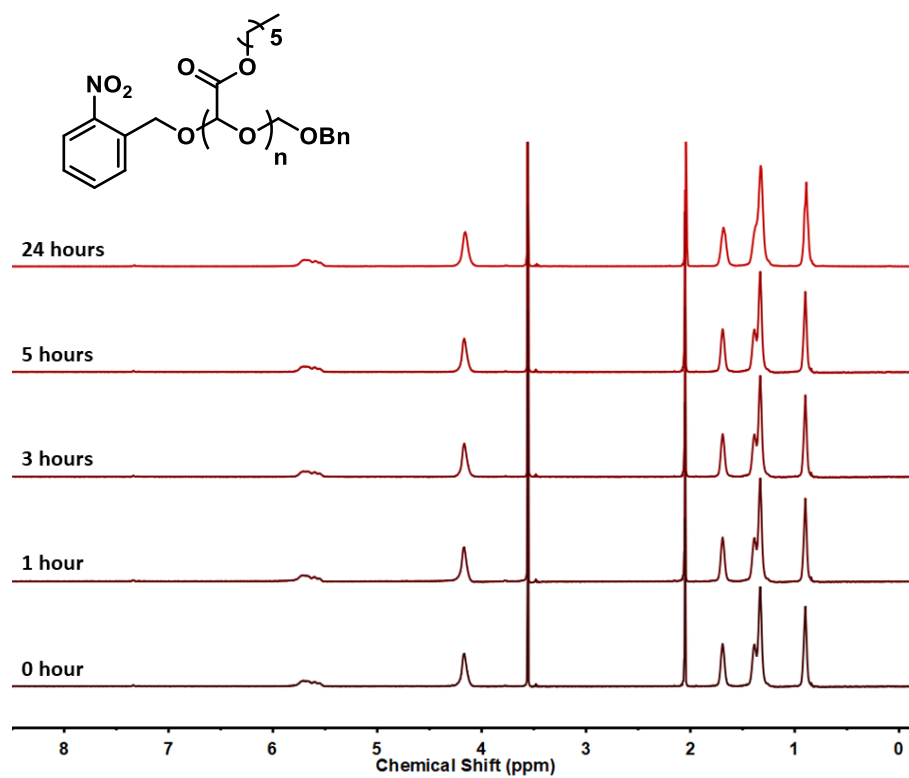


Figure A4.44. ¹H NMR spectra recorded for **PHexG** kept in dark at different time intervals (9/1: CD₃CN/D₂O, 400 MHz). Asterisks denote residual solvent signals.

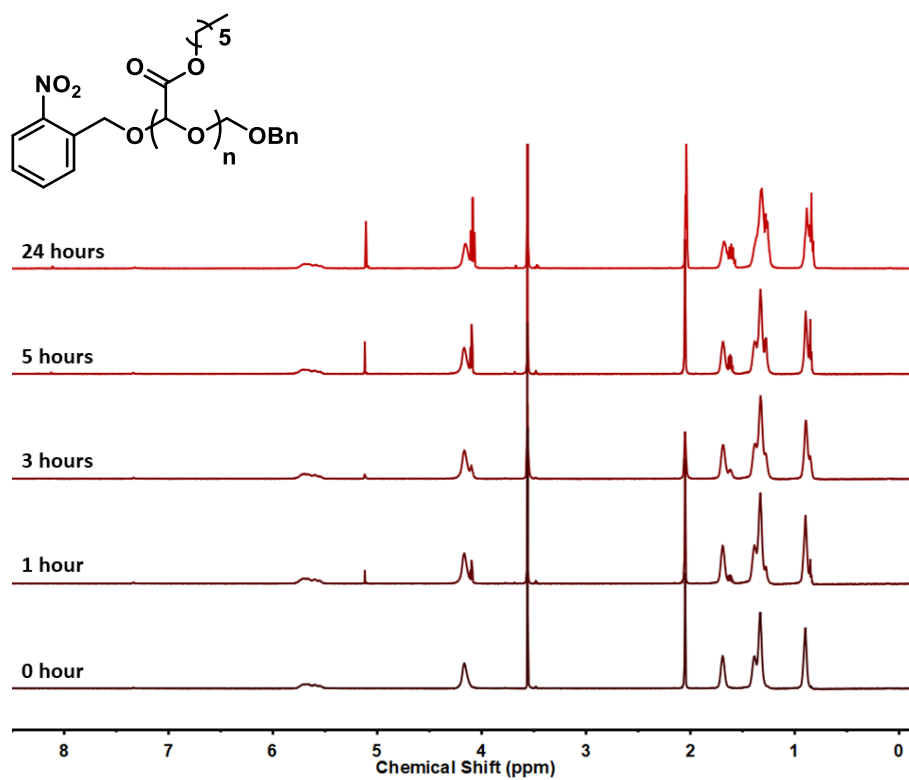


Figure A4.45. ¹H NMR spectra recorded for **PHexG** exposed to a UV light at different time intervals (9/1: CD₃CN/D₂O, 400 MHz). Asterisks denote residual solvent signals.

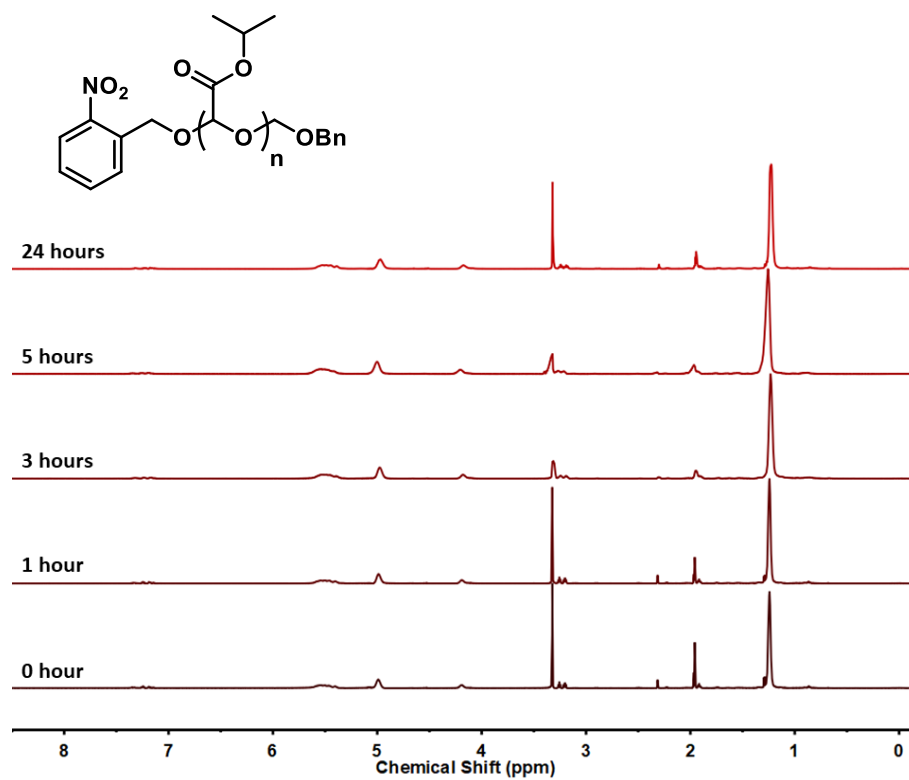


Figure A4.46. ¹H NMR spectra recorded for P_iPrG kept in dark at different time intervals (9/1: CD₃CN/D₂O, 400 MHz). Asterisks denote residual solvent signals.

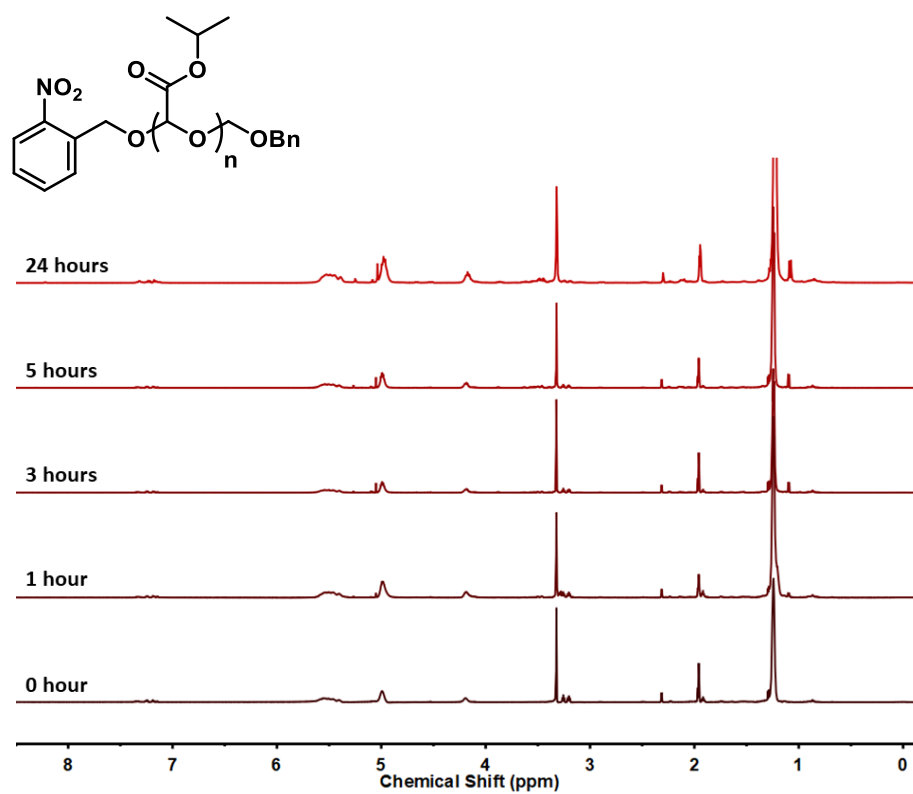


Figure A4.47. ¹H NMR spectra recorded for **P_iPrG** exposed to a UV light at different time intervals (9/1: CD₃CN/D₂O, 400 MHz). Asterisks denote residual solvent signals.

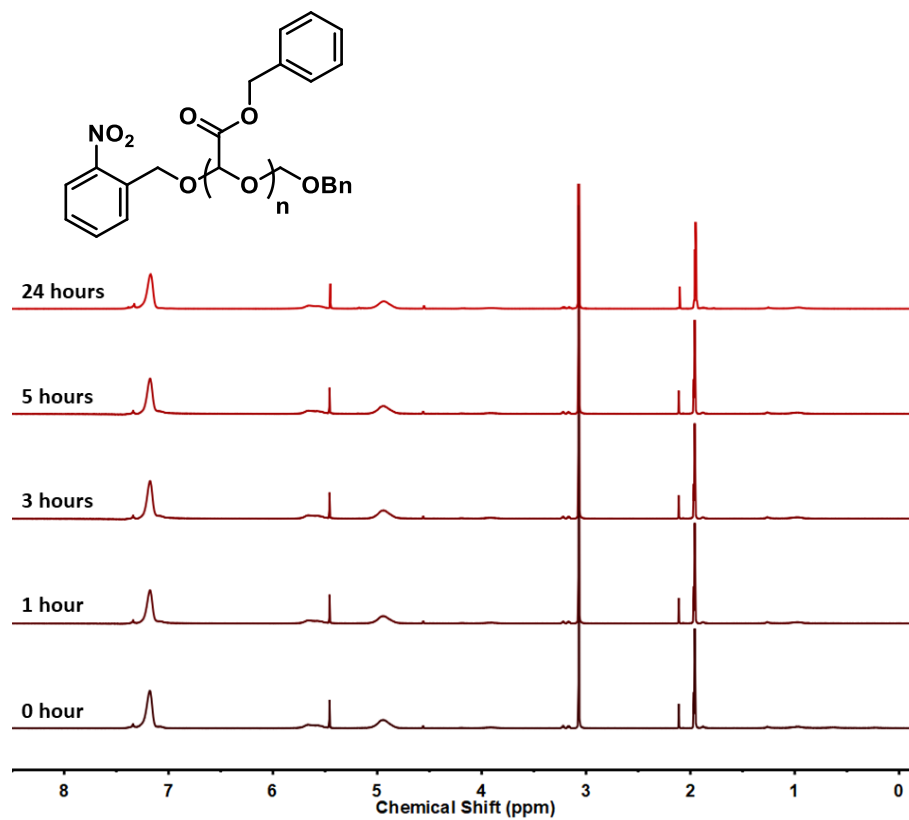


Figure A4.48. ¹H NMR spectra recorded for **PBN-G** kept in dark at different time intervals (9/1: CD₃CN/D₂O, 400 MHz). Asterisks denote residual solvent signals.

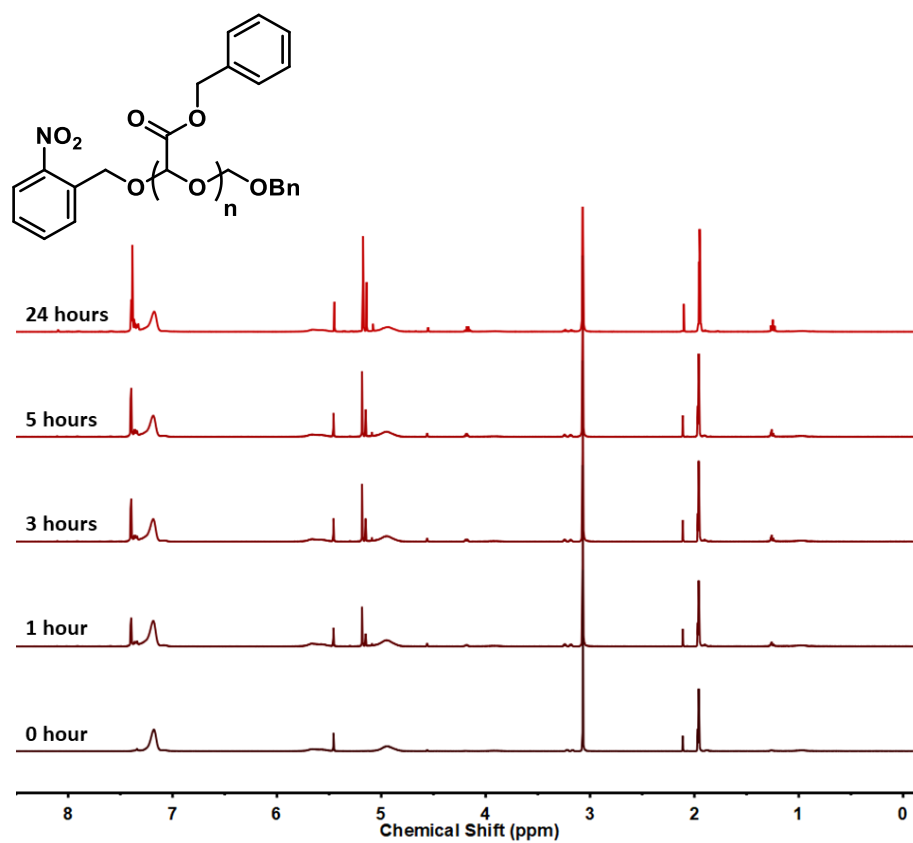


Figure A4.49. ¹H NMR spectra recorded for **PBnG** exposed to a UV light at different time intervals (9/1: CD₃CN/D₂O, 400 MHz). Asterisks denote residual solvent signals.

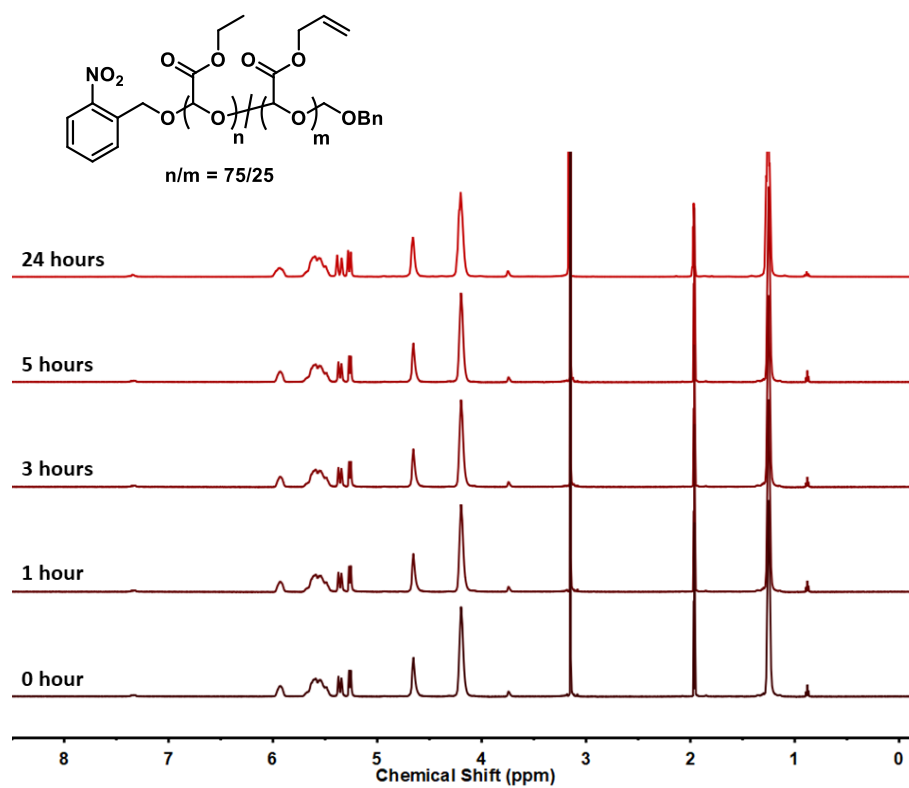


Figure A4.50. ¹H NMR spectra recorded for **PAIG** kept in dark at different time intervals (9/1: CD₃CN/D₂O, 400 MHz). Asterisks denote residual solvent signals.

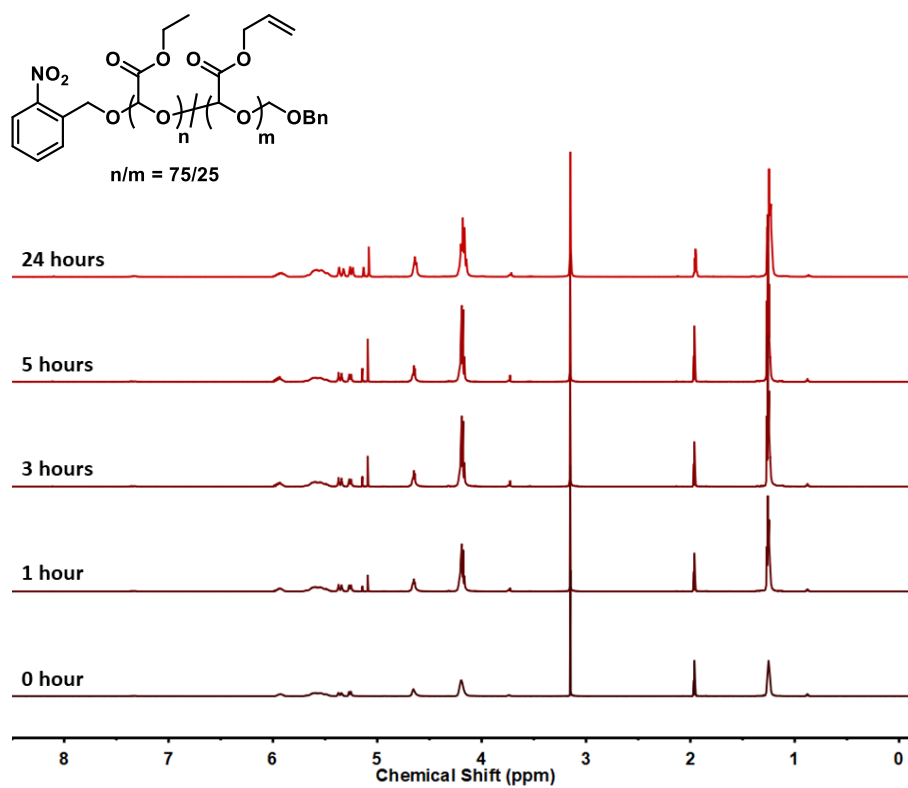


Figure A4.51. ¹H NMR spectra recorded for PAIG exposed to a UV light at different time intervals (9/1: CD₃CN/D₂O, 400 MHz). Asterisks denote residual solvent signals.

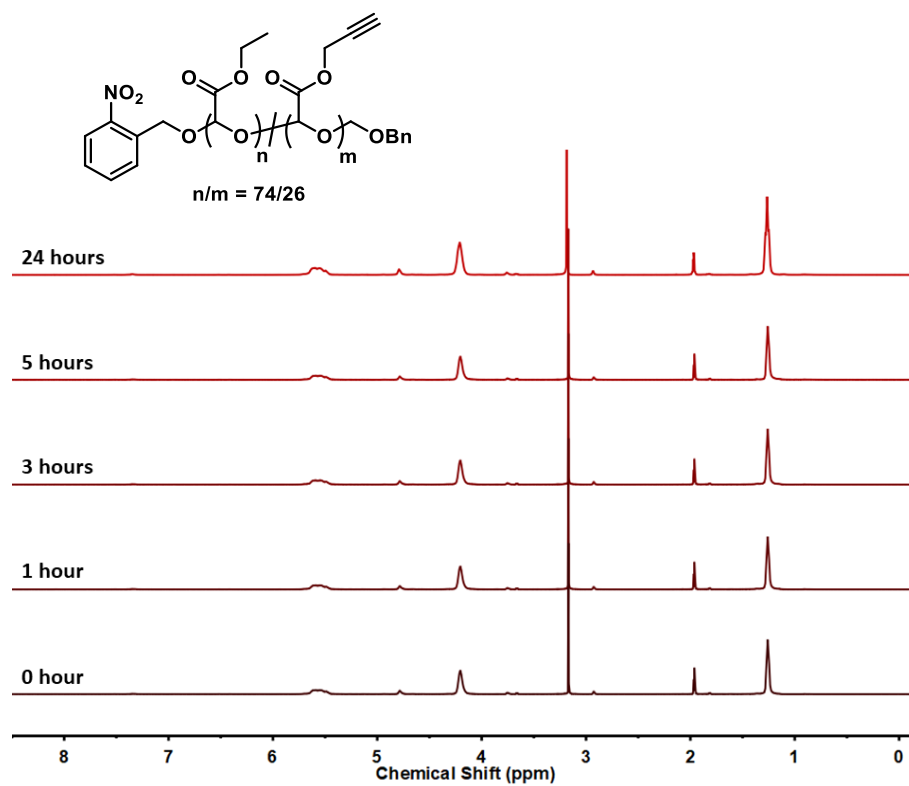


Figure A4.52. ^1H NMR spectra recorded for **PPG** kept in dark at different time intervals (9/1: $\text{CD}_3\text{CN}/\text{D}_2\text{O}$, 400 MHz). Asterisks denote residual solvent signals.

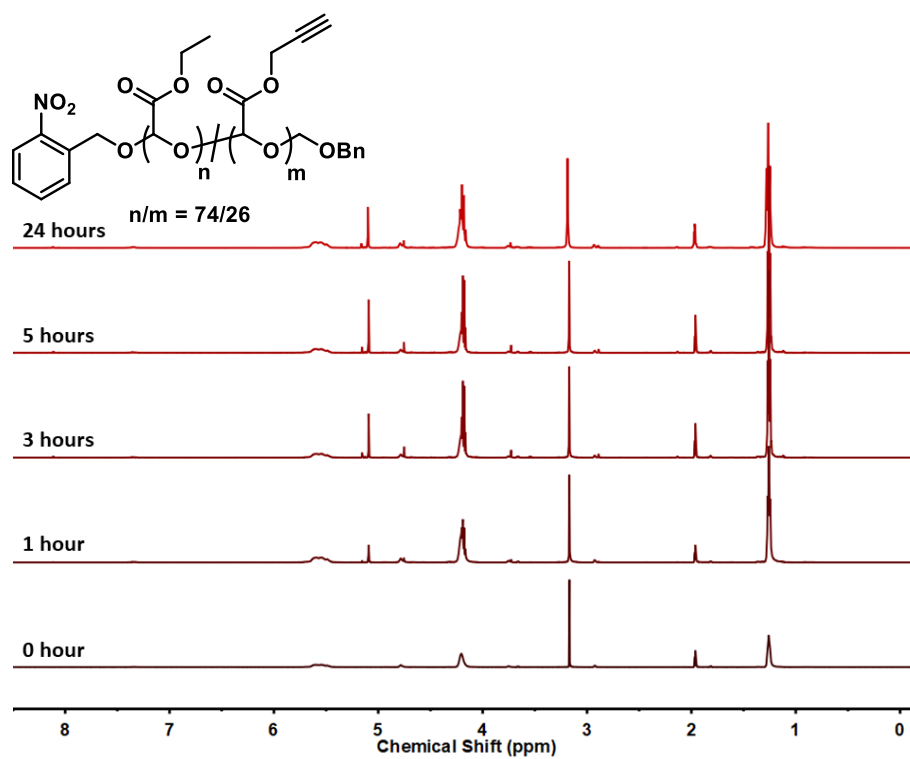


Figure A4.53. ^1H NMR spectra recorded for **PPG** exposed to a UV light at different time intervals (9/1: $\text{CD}_3\text{CN}/\text{D}_2\text{O}$, 400 MHz). Asterisks denote residual solvent signals.

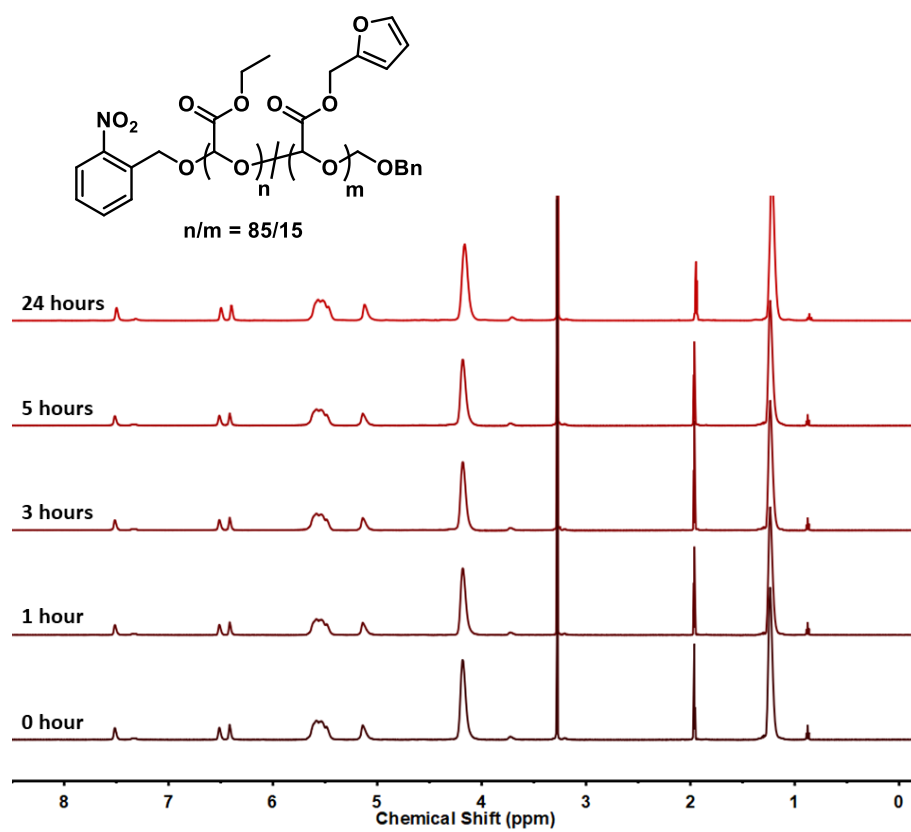


Figure A4.54. ^1H NMR spectra recorded for **PFuG** kept in dark at different time intervals (9/1: $\text{CD}_3\text{CN}/\text{D}_2\text{O}$, 400 MHz). Asterisks denote residual solvent signals.

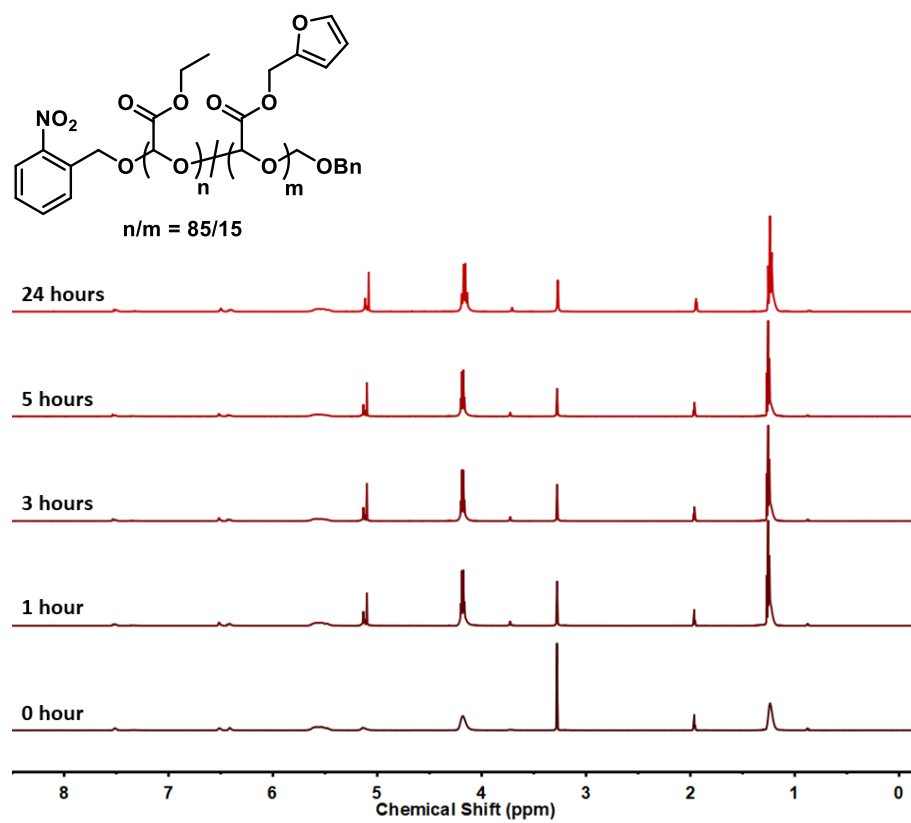


Figure A4.55. ^1H NMR spectra recorded for **PFuG** exposed to a UV light at different time intervals (9/1: $\text{CD}_3\text{CN}/\text{D}_2\text{O}$, 400 MHz). Asterisks denote residual solvent signals.

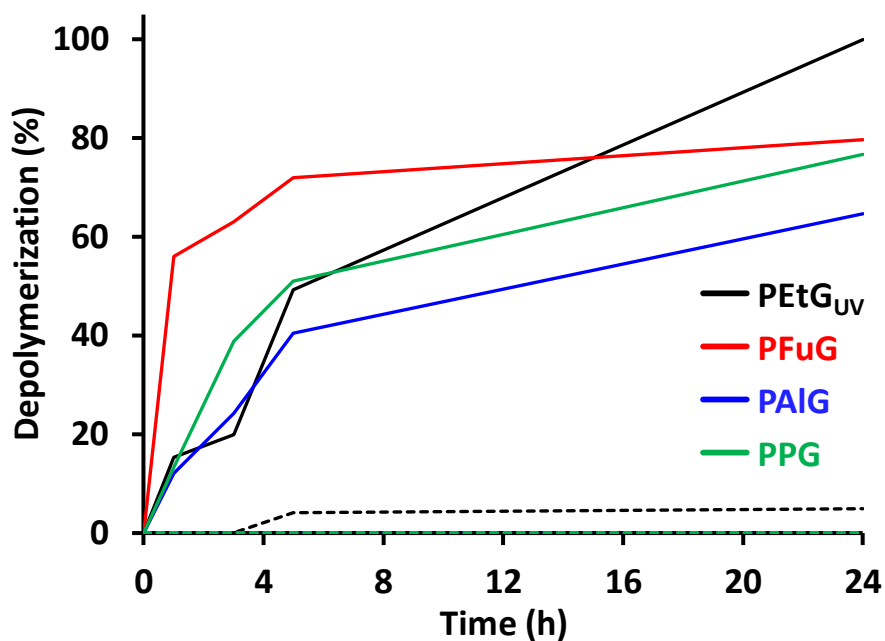


Figure A4.56. UV-degradation study of **PFuG**, **PAIG**, **PPG**, vs. **PETG_{UV}** at different time intervals. Results for UV-light exposed and kept in dark samples are depicted using solid and broken lines, respectively. Note: depolymerization% were calculated relative to the depolymerization amount observed for the parent **PETG_{UV}** in 24 hours.

SEC data

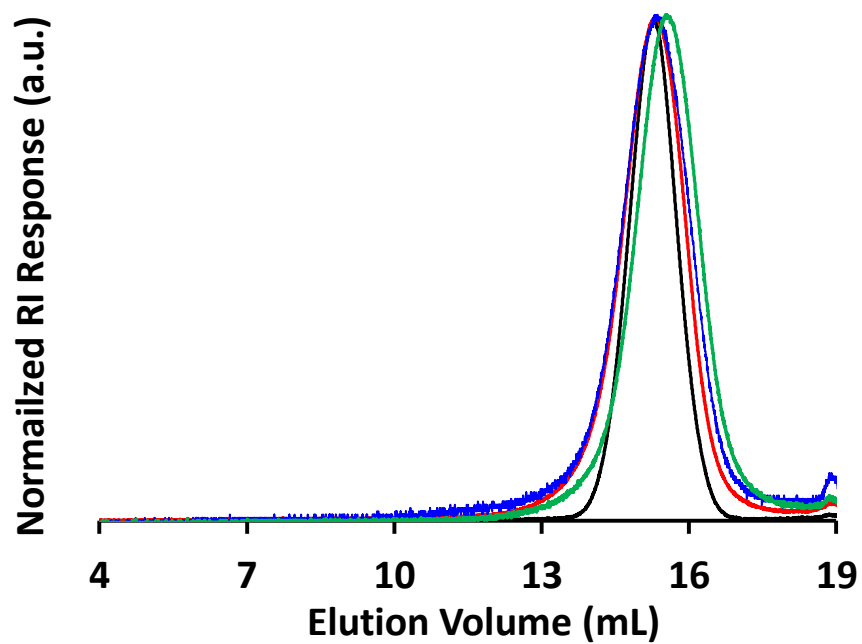


Figure A4.57. SEC traces of **PFuG** (blue), **PAIG** (red), and **PPG**, (green) vs. **PETGUV** (black).

TGA results

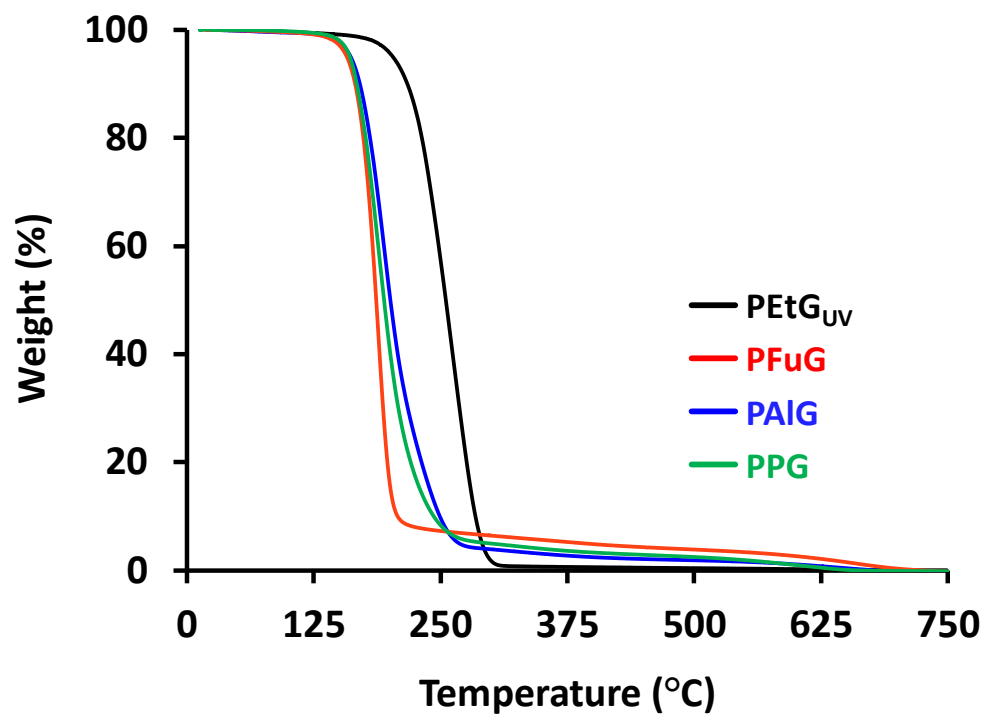


Figure A4.58. TGA traces recorded for PFuG, PAIG, and PPG, vs. PEtGUv.

FTIR spectra

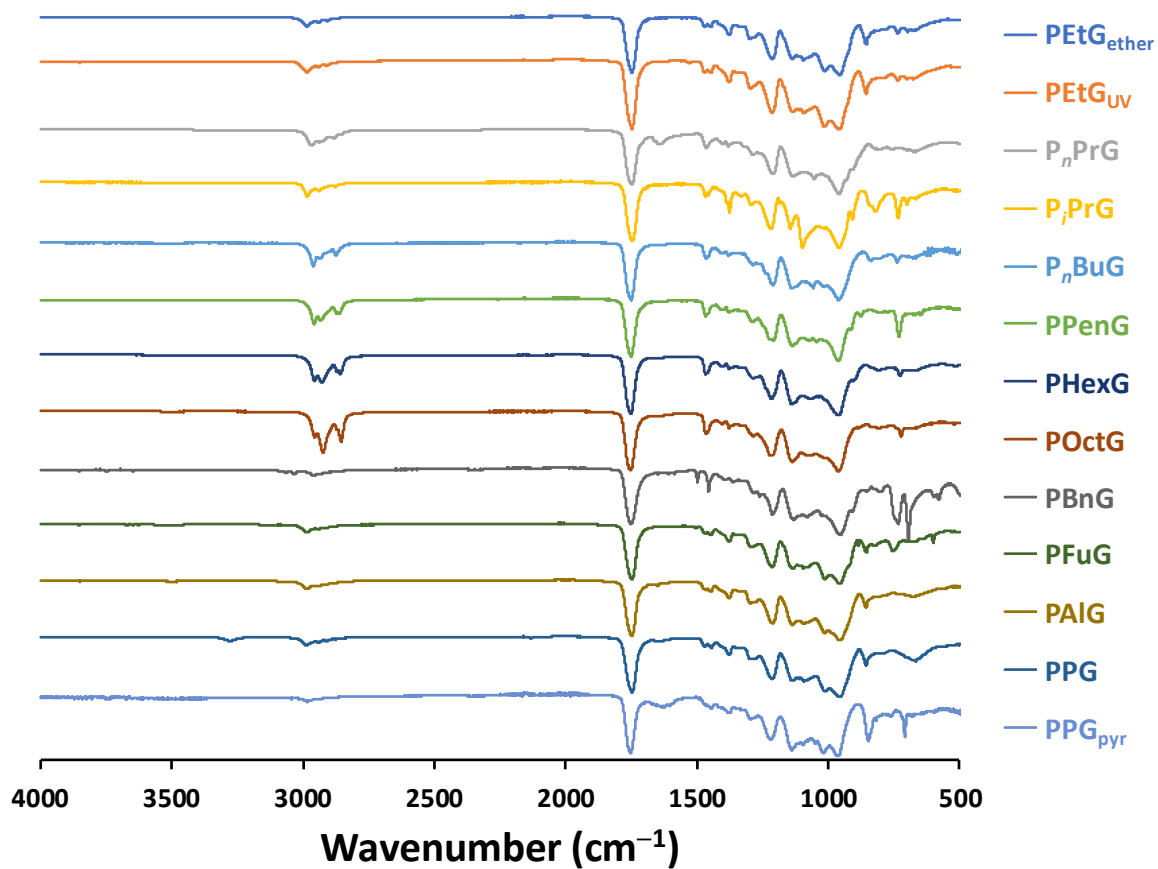


Figure A4.59. FTIR spectra recorded for PGs.

Curriculum vitae

Name:	Rebecca E. Yardley	
Post-secondary education and degrees:	Wilfrid Laurier University Waterloo, Ontario, Canada 2010-2014 B.Sc. (Chemistry)	
	The University of Western Ontario London, Ontario, Canada 2014-2019 Ph.D. (Chemistry)	
Honours and awards:	NSERC Science, Action! Winner 2019	
	Three Minute Thesis (3MT) Western Finalist (Top 20) 2019	
	Alexander Graham Bell Canada Graduate Scholarship (CGS-D) Doctoral Fellowship 2016-2019	\$105,000
	Doctoral Excellence Research Award for Tri-Agency Recipients 2016-2016	\$15,000
	Ontario Graduate Scholarship (OGS) 2016-2017 (declined)	
	Ontario Graduate Scholarship (OGS) 2015-2016	\$15,000
	National Science and Engineering Research Council (NSERC) Masters Fellowship 2014-2015	\$17,500
	Ontario Graduate Scholarship (OGS) 2015-2016 (declined)	
Related work experience	Preliminary Program Lecturer – Chemistry Brescia University College May–August 2019	

Lead Tutor for CH1301a and CH1302b
Brescia University College
September 2018-April 2019

Teaching Assistant – CH1302b, CH2003b, CH2213a
The University of Western Ontario
September 2014–April 2016

Publications:

7. **Yardley, R. E.**, Rabiee Kenaree, A., Gillies, E. R.* Transesterification of Poly(ethyl glyoxylate)s: A Simple Route Towards Directly-inaccessible Polyglyoxylates. *Manuscript in preparation*.
6. **Yardley, R. E.**; Paquette, J. A.; Taking, H.; Gaebler, H. M.; Eichhorn, S. H.; Hamilton, I. P.; Maly, K. E.* Stabilization of Columnar Liquid Crystal Phases via Arene-Perfluoroarene Interactions. *Org. Lett.* **2019**, DOI: 10.1021/acs.orglett.9b04091
5. **Yardley, R. E.**, Rabiee Kenaree, A., Gillies, E. R.* Triggering Depolymerization: Progress and Opportunities for Self-Immolative Polymers. *Macromolecules*, **2019**, *52*, 6342-6360.
4. **Yardley, R. E.**, Gillies, E. R.* Multi-Stimuli-Responsive Self-Immolative Polymer Assemblies. *Journal of Polymer Science Part A: Polymer Chemistry*, **2018**, *16*, 1868-1877.
3. Fan, B., **Yardley, R. E.**, Trant, J. F., Borecki, A., Gillies, E. R.* Tuning the hydrophobic cores of self-immolative polyglyoxylates assemblies. *Polymer Chemistry*, **2018**, *9*, 2601-2610.

2. Fan, B., Trant, J. F., **Yardley, R. E.**, Pickering, A. J., Lagugne-Labarthe, F., Gillies, E. R.* Photocontrolled Degradation of Stimuli-Responsive Poly(ethyl glyoxylate): Differentiating Features and Traceless Ambient Depolymerization. *Macromolecules*, **2016**, *49*, 7196-7203.
1. Paquette, J. A., **Yardley, R. E.**, Yu, J., Eichhorn, S. H., Maly, K. E.* Anthra- and Pentacenequinone Derivatives: Influence of Structure on the Formation of Columnar Liquid Crystal Phases. *New Journal of Chemistry*, **2016**, *40*, 5985-5988.

Selected conferences:

8. **R. E. Yardley**, A. Rabiee Kenaree, E. R. Gillies, “Functional Self-immolative Polyglyoxylates via Simple Transesterification Reactions.” Oral Presentation delivered at the 102nd Canadian Chemistry Conference and Exhibition, Quebec, QC, June 2019.
7. **R. E. Yardley**, E. R. Gillies, “Multi-Stimuli-Responsive Self-Immolative Polymer Assemblies.” Oral Presentation delivered at the 38th High Polymer Forum, Gananoque, ON, July 2018.
6. **R. E. Yardley**, E. R. Gillies, “*The Effects of PDMAEMA on the Depolymerization of Block Copolymers in Solution.*” Oral Presentation delivered at the 100th Canadian Chemistry Conference and Exhibition, Toronto, ON, May 2017.

5. **R. E. Yardley**, B. Fan, J. F. Trant, A. D. Wong, T. M. Gungor E. R. Gillies, “*Stimuli-responsive supramolecular assemblies of amphiphilic self-immolative polymers.*” Poster Presentation delivered at The International Chemical Congress of Pacific Basin Societies 2015, Honolulu, HI, December 15–20.
4. **R. E. Yardley**, B. Fan, J. F. Trant, E. R. Gillies, “*Synthesis and self-assembly of polyglyoxylate based tri-block copolymers.*” Poster Presentation delivered at 98th Canadian Chemistry Conference and Exhibition, Ottawa, ON, June 13–18.
3. **R. E. Yardley**, J. A. Paquette, K. E. Maly, “*Synthesis and Characterization of Novel Liquid Crystalline Dibenzo[a,c]pentacenequinones.*” Oral Presentation delivered at the 42nd Southern Ontario Undergraduate Student Chemistry Conference, Windsor, ON, March 29.
2. **R. E. Yardley**, J. A. Paquette, K. E. Maly, “*Synthesis and Characterization of Novel Liquid Crystalline Dibenzo[a,c]pentacenequinones.*” Poster presentation delivered at the 41st Physical Organic Mini-symposia, Montreal, QC, November 2013.
1. **R.E. Yardley**, J. A. Paquette, K. E. Maly, “*Synthesis and Characterization of Novel Liquid Crystalline Acenequinones.*” Poster presentation delivered at the 96th Canadian Chemistry Conference and Exhibition, Quebec, QC, May 26–30.